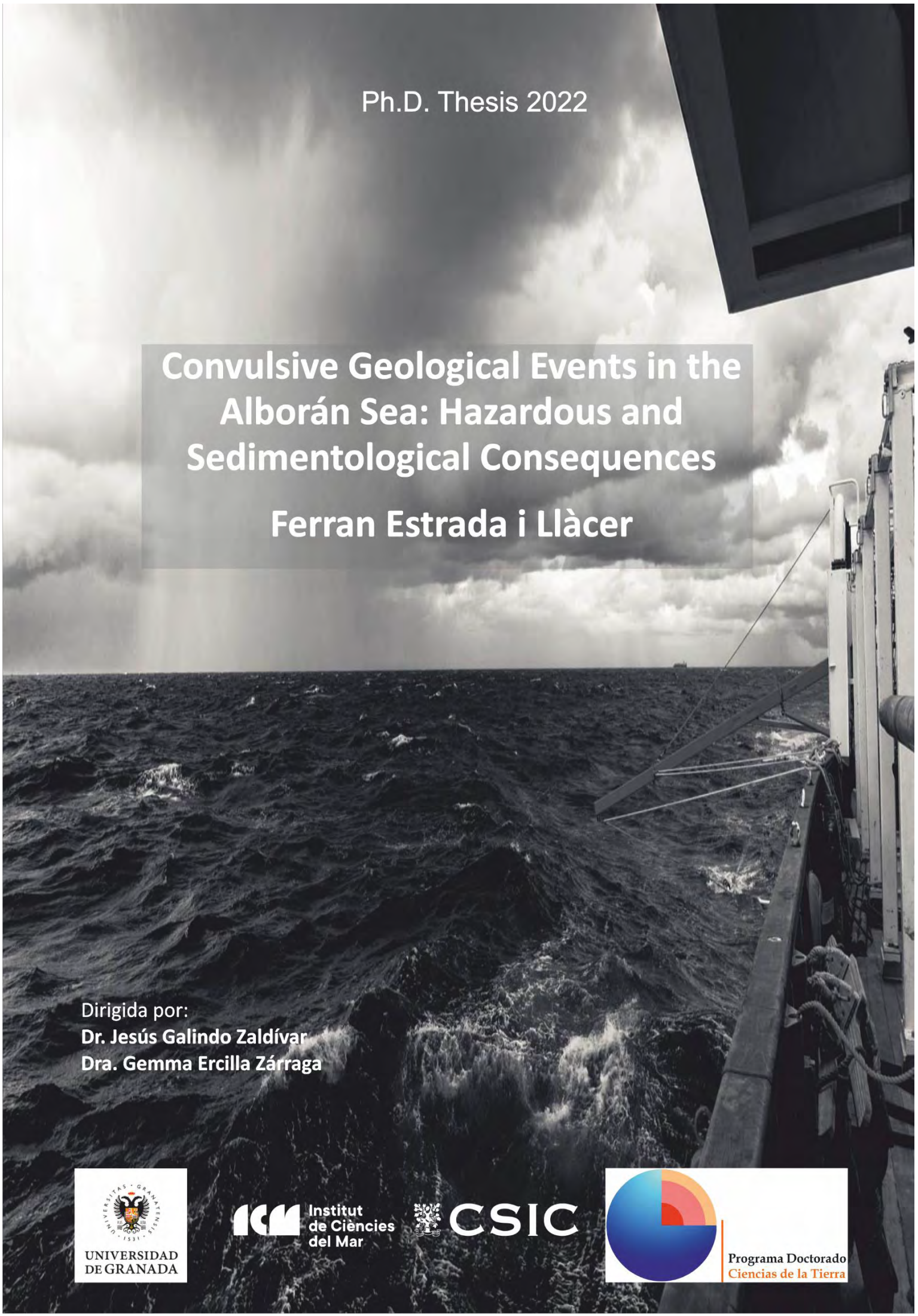

Ph.D. Thesis 2022

Convulsive Geological Events in the Alborán Sea: Hazardous and Sedimentological Consequences

Ferran Estrada i Llàcer

Dirigida por:
Dr. Jesús Galindo Zaldívar
Dra. Gemma Ercilla Zárraga

UNIVERSIDAD DE GRANADA

Institut de Ciències del Mar

CSIC

Programa Doctorado Ciencias de la Tierra

UNIVERSIDAD DE GRANADA

Programa official de doctorado de ciencias de la tierra

TESIS DOCTORAL

Convulsive Geological Events in the Alborán Sea: Hazardous and Sedimentological Consequences

Tesis doctoral presentada por:

Ferran Estrada i Llàcer

Dirigida por:

Dr. Jesús Galindo Zaldívar

Dra. Gemma Ercilla Zárraga

Granada, Julio de 2022

Editor: Universidad de Granada. Tesis Doctorales
Autor: Ferran Estrada i Llàcer
ISBN: 978-84-1117-435-0
URI: http://hdl.handle.net/10481/75967

Als pares, Alvar (al cel sia) i Nuri,

a la meva filla Amèlia i a

la lluna Irene

AGRADECIMIENTOS

Mucha gente a quien agradecer, de una forma u otra todos los que nos rodean contribuyen consciente o inconscientemente, pero empezaré por mi directora y director de tesis. Gracias a ambos por depositar vuestra confianza y conocimiento en mí, creo que sois los directores de tesis ideales. Gemma, no se me ocurre como simplificarlo, pero me viene a la mente amistad incondicional y tenacidad, mucho conocimiento de la geología marina y debate, tú ya me entiendes. Jesús, gracias por abrirme tu "casa" me refiero a las dos, la física y la de tu saber geológico, haces que todo parezca fácil, siempre disfruto aprendiendo contigo, gracias.

A todos los compañeros y compañeras del departamento, de los cuales me he enriquecido con su saber y amistad. Belén Alonso, cuantos años compartiendo vicisitudes, risas, campañas y amistad. David Casas, un compañero ideal con quien compartir amistad e ideas, gracias por la foto de la portada. Marcel·lí Farran, de ti he aprendido todos los intríngulis que subyacen en el tratamiento de datos de todo tipo, un artista, un amigo y un andador nato. Pere Puig y Jorge Guillén, por achucharme todos estos años a presentar la tesis, al final lo habéis conseguido. Con ellos me una amistad de muchos años. A Rafael Bartolomé, por compartir todos esos ratos en el ICM y muchos más que espero compartir. A Albert Palanques, que en su momento confió en mí. A todos aquellos que vinieron y se fueron, especialmente a Jesús Baraza. A Fernando Pérez-Belzuz, juntos nos iniciamos en esto con nuestras locuras incluidas.

Quiero agradecer y hacer mención especial a todo el personal técnico que ha contribuido con mucho más de lo que se les reconoce. A todos los del departamento, sin su trabajo nada funcionaría. A todo el personal de la UTM que hacen posible que los barcos funcionen y podamos obtener los datos en las campañas: Pedro Jornet, Pablo Rodríguez, Manu, Camilo, Roberto, Iván y muchos otros más, a todos gracias. Así mismo, a todas las tripulaciones de marineros y marineras que nos hacen la vida a bordo más fácil, mención especial a los que nos dan de comer.

A todos con los que he trabajado, de ellos siempre he aprendido algo más, especialmente los que han contribuido en esta tesis como coautores de varios artículos, Daniel García-Castellanos, con él comparto una megainundación. A los colegas de la

Universidad de Málaga, José Manuel González Vida, Jorge Macías, Sergio Ortega; de la Universidad de Jaén, José Antonio Peláez; IEO de Málaga, Juan Tomás Vázquez, gracias por tu amistad, y al resto de la gente de Fuengirola incluida Yuki. A Carlos Sanz de Galdeano por su sabiduría y por compartirla.

À mon cher ami Christian Gorini, por hacerme sentir como en casa cada vez que he visitado la Sorbonne Université de París, merci beaucoup al resto del equipo de París. Así mismo, quiero agradecer la colaboración de todos los colegas de Marruecos.

A mi compañera de la vida Irene Alejo Flores, por la paciencia en los tramos finales de esta tesis y por otras muchas cosas que aquí no puedo decir y por tus enseñanzas del medio costero. A Amèlia y su universo, nada de lo que diga puede expresar lo que significas para mí. A Desmond Barton y Teri Navarro, gracias por vuestro ánimo, amistad y copas de cava. A Guillermo Francés y Mamen gracias por existir y compartir tantos buenos ratos. A Miguel Nombela, un fenómeno de la naturaleza, gracias por tu buen humor y a Marta.

Que me perdonen los que se han quedado en el tintero, pero ya son muchos años y gente a quien agradecer.

Este trabajo ha sido posible gracias a una serie de proyectos de investigación que han dado respaldo científico y económico: TOPOMED (ESF-CGL2008-03474-E/BTE), SAGASbis (Ref. CTM2009/07893-E/MAR), CONTOURIBER (CTM2008-06399-C04-04/MAR) y MONTERA (Ref. CTM-14157-C02-02/MAR), FAUCES CMT2015-65461-C2-R (MINECO/FEDER), DAMAGE (AEI/FEDER CGL2016-80687-R) y RNM148. INCRISIS, DAMAGE (CGL2016-80687-R AEI/FEDER), RNM 148 - Junta de Andalucía, y a las campañas Marlboro. Al programa francés Actions Marges, al programa de la Comunidad Europea EUROFLEETS. Al proyecto SARAS (FP7/2007-2013; 228344). A los proyectos B-RNM-301-UGR18 y AGORA P18-RT-3275 de la Junta de Andalucía. El autor agradece a IHS-Kingdom por la concesión de una licencia académica de su software.

ABSTRACT

Convulsive geological events are natural processes of a destructive nature characterized by a sudden, highly energetic release of regional or global extent. These processes are extraordinary in nature and their impact, although it may be significant, is not well known in the geological record, especially in the marine environment. In this Ph. D. Thesis, two cases of convulsive events in the Alborán Sea, a geodynamic active area located at the Eurasian-African plate boundary have been analysed, one of a tsunamigenic type associated with faults and the other the controversial Zanclean megaflood that put an end to the Messinian Salinity Crisis. The central question of this thesis comprises several research questions: given the historical and sedimentary evidence of tsunamis in the Alborán Sea, what is their genesis; being most of the faults in this area strike-slip, can they generate tsunamis; and in relation to the megaflood, what is the evidence in the sedimentary record that shows that it existed? To address these research questions, geological analysis through seismic profiles of different resolutions, commercial and scientific wells, and multibeam bathymetry with mathematical modelling have been combined. This approach allows to identify, characterize and map, as well as better understand the geological evidences in order to improve the interpretation of convulsive processes.

In order to determine a potential tsunamigenic fault, the tectonic context of the central area of the Alborán Sea has been studied, which indicates that a tectonic indentation process is currently taking place due to the NW approach of the African plate with respect to the Eurasian plate. This indenting block of African crust is the cause of most of the recent seismic and tectonic activity in the area. Two strike-slip fault systems bound this block, the WNW-ESE Yusuf dextral fault and the NNE-SSW Al-Idrisi sinistral fault. The indentation front coincides with a large antiform, the Alborán Ridge. As a consequence of the indentation process, a conjugate system of strike-slip faults develops to the north, forming a 75º angle characteristic of indented zones. Several of these conjugate faults, despite being strike-slip faults, have significant vertical offsets at their ends, such as the Averroes fault (5.4 m), which has been selected to mathematically model its tsunamigenic potential. The NW-SE dextral Averroes fault has

been active since the early Pliocene. In the last 124,000 years up to 4 events have been identified, the last one deforming the seafloor.

Currently one of the most active faults in the studied area is the NNE-SSW Al-Idrisi fault near the Moroccan coast of Al Hoceima and the Incrisis fault, about 10 km west of the previous one and crossing sea-land. The Incrisis fault seems to have been the trigger for several recent seismic shocks (1993-1994, 2004 and 2016-2017), even affecting the Al-Idrisi fault as well. Recent landslides have also been identified in this area where both faults develop. This fact warns, from a geological risk point of view, of a potentially dangerous area.

Mathematical modelling of the Averroes fault indicates that for a fault offset of 5.4 m an earthquake of magnitude 7 was produced, generating a tsunami with waves up to 6 m high, with an arrival time at the nearest coast of Balerma (Almeria) of 21 minutes. Other areas affected by the tsunami are the coast of Malaga and the Moroccan coast west of Nador, respectively, with waves of 2 m and 1 m, and times of 35 and 27 minutes. These short arrival times warn of the need to develop an early warning system that considers the short time elapsed between the earthquake and the arrival of the tsunami to the coast. Particularly since the Alborán Sea is an area with densely populated beaches, during the summer. Likewise, this modelling highlights the need to review early warning systems in similar geological contexts where strike-slip faults predominate, since these are not normally associated with tsunamis because they are not considered to produce significant fault offsets.

The sismostratigraphic analysis of the Messinian-Pliocene transition in the Alborán Sea shows the scarce development or absence of the typical units of the Messinian Salinity Crisis (MSC) identified in other areas of the Mediterranean, the trilogy formed by the Lower (LU), Mobile (MU) and Upper (UU) Units. The saline unit (MU) has not been identified throughout the basin and in its place a chaotic unit is developed that was formed by erosion of the LU, during the 1500 m sea level lowering that characterizes the MSC. Remnants of the UU have only been identified in the eastern end of the basin. The existence of several erosional structures in the Alborán Sea basin, such as terraces, hanging canyons, large erosional surfaces on the continental slope and in the deep basin, suggest that this area during the MSC was in subaerial exposure at some time.

The most remarkable erosional element is a large erosional channel that crosses the entire basin from west to east along its deepest part, unlike other areas of the Mediterranean where the main erosion is observed on the continental slope. The age of this channel is stratigraphically constrained by the erosion of the UU which closes the cycle of the MSC trilogy. Apart from the erosion caused by the Zanclean megaflood, chaotic wedge-shaped deposits have been observed to be associated with products of the megaflood. Similarly, equivalent deposits have been found at the Sicily sill. Further evidence supporting the existence of the megaflood is the lack of contourite deposits during the MSC. This absence contrasts, however, with their omnipresence from the Pliocene onwards, when the Mediterranean was already connected to the Atlantic Ocean.

Mathematical modelling of the Zanclean megaflood indicates that this convulsive event occurred in five phases. Phase 0 corresponds to a period of relatively longer duration where the reduced inflow of Atlantic water generates little significant erosion. In phase 1, the Strait of Gibraltar becomes deeper and wider, exponentially increasing its rate of erosion and Atlantic water flow. In phase 2, there is a reduction in the hydrological gradient between the Atlantic Ocean and the western Mediterranean, resulting in a decrease in the flow velocity and discharge of water, as well as a decrease in the rate of erosion. During this phase, all the Atlantic water entering through the Strait of Gibraltar is reversed to refill the Western Mediterranean Basin. In phase 3, the sea level reaches the Sicily threshold. The hydrologic gradient remains constant in the Western Basin, as the water entering through the Strait of Gibraltar is transferred to the Eastern Basin, producing a rapid rise in sea level in the Eastern Basin, resulting in the chaotic deposits identified in Sicily. Finally, in phase 4, the sea level rises synchronously in both Mediterranean basins until it levels with the Atlantic Ocean. The estimated time to transfer 90% of the water to the Mediterranean basin is two years, causing a sea level rise of 10 m per day. Due to the enormous flow generated at the peak of the megaflood (10^8 m^3 s^{-1}) and the high velocities reached (v=40 m s^{-1}) it is very likely that the cascade image widely used in the literature for the filling of the Mediterranean basin is not correct and was probably produced by a flood ramp. The confirmation of the existence of the Zanclean megaflood settles the current debate on the models of the MSC, deep

desiccated basin, deep non- desiccated basin and mixed, in favour of the desiccated or mixed basin model.

The results of the study of these convulsive processes of different nature show that one of the challenges in future research in marine geosciences includes the need to identify them, characterize them and analyse their impacts. These impacts affect marine geological hazards and the paleogeographic evolution of marine basins with palaeoceanographic and paleoclimatic implications.

RESUMEN

Los eventos geológicos convulsivos son procesos naturales de carácter destructivo que se caracterizan por una liberación súbita, altamente energética, y de carácter regional o global. Estos procesos son extraordinarios en la naturaleza y su impacto, aunque importante, poco conocido en el registro geológico, especialmente en el medio marino. En esta Tesis se analizan dos casos de eventos convulsivos en el Mar de Alborán, situado en la zona geodinámica activa del límite entre las placas euroasiatica y africana. Un evento es de tipo tsunamigénico asociado a fallas y el otro la controvertida megainundación del Zancliense que puso fin a la Crisis de Salinidad Messiniense. El planteamiento central de esta tesis comprende varias cuestiones que requieren investigación: dadas las evidencias históricas y sedimentarias de tsunamis en el Mar de Alborán ¿cuál es su génesis?; la mayoría de las fallas en esta zona son de dirección ¿pueden éstas generar tsunamis?; y en relación a la megainundación ¿cuáles son las evidencias en el registro sedimentario que demuestren que existió?. Para abordar estas cuestiones se ha combinado el análisis geológico mediante perfiles sísmicos de distinta resolución, sondeos comerciales y científicos, y batimetrías de multihaz en combinación con la modelización matemática. Esta aproximación permite identificar, caracterizar y cartografiar y comprender mejor las evidencias geológicas y mejorar la interpretación de los procesos convulsivos.

Con el objetivo de determinar una falla potencialmente tsunamigénica se ha estudiado el contexto tectónico de la zona central del Mar de Alborán, el cual revela que actualmente se está produciendo un proceso de indentación tectónica que obedece a la aproximación hacia el NO de la placa africana respecto la euroasiática. Este bloque indentador de corteza africana es el causante de la mayoría de la actividad sísmica y tectónica reciente de la zona. Dos sistemas de falla de dirección limitan este bloque, la falla dextra ONO-ESE de Yusuf y la falla sinistra NNE-SSO de Al-Idrisi. El frente de indentación coincide con un gran antiforme, la Dorsal de Alborán. Como consecuencia del proceso de indentación se desarrolla al norte un sistema conjugado de fallas de dirección que forman un ángulo de 75º característico de zonas de indentación. Varias de estas fallas conjugadas, a pesar de ser fallas de dirección, presentan saltos verticales importantes en sus extremos, como la falla de Averroes (5,4 m), la cual se ha

seleccionado para modelizar matemáticamente su potencial tsunamigénico. La falla dextra NO-SE de Averroes es activa desde el Plioceno temprano. En los últimos 124000 años se han identificado hasta 4 eventos, el último de los cuales deforma el fondo marino.

Actualmente, una de las fallas más activas de la zona estudiada es la falla NNE-SSO de Al-Idrisi, cerca de la costa marroquí de Alhucemas, y la falla de Incrisis a unos 10 km al oeste de la anterior y que atraviesa mar-tierra. La falla Incrisis parece haber sido la detonante de varias crisis sísmicas recientes (1993-1994, 2004 y 2016-2017), llegando también a afectar a la falla de Al-Idrisi. En esta zona, donde se desarrollan ambas fallas, también se han identificado deslizamientos recientes. Este hecho advierte desde un punto de vista de los riesgos geológicos de la existencia de una zona potencialmente peligrosa.

La modelización matemática de la falla de Averroes indica que para un salto de falla de 5,4 m se produjo un terremoto de magnitud 7 que generó un tsunami con olas de hasta 6 m de altura, con un tiempo de llegada a la costa más próxima de Balerma (Almería) de 21 minutos. Otras zonas afectadas por el tsunami son la costa de Málaga y la marroquí al oeste de Nador, respectivamente, con olas de 2 m y 1 m y tiempos de llegada de 35 y 27 minutos. Estos tiempos de llegada tan cortos advierten de la necesidad de elaborar para el Mar de Alborán, una zona con playas densamente pobladas en verano, un plan de alerta temprana que tenga en cuenta el poco tiempo transcurrido entre el terremoto y la llegada del tsunami a la costa. Así mismo, esta modelización pone de manifiesto la necesidad de revisar los planes de alerta temprana en contextos geológicos similares donde predominan las fallas de dirección, ya que normalmente éstas no se asocian a tsunamis pues se considera que no producen saltos de falla significativos.

El análisis sismoestratigráfico de la transición Messiniense-Plioceno en el Mar de Alborán pone de manifiesto el escaso desarrollo o ausencia de las unidades típicas de la Crisis de Salinidad Messiniense identificadas en otras zonas del Mediterráneo, la trilogía formada por la Lower (LU), Mobile (MU) y Upper (UU) Units. La unidad salina (MU) no se ha identificado en toda la cuenca y en su lugar se desarrolla una unidad caótica que se formó por la erosión de la LU, durante la bajada del nivel del mar de 1500 m que

caracteriza la MSC. De la UU solo se han identificado remanentes en el extremo oriental de la cuenca. La existencia de varias estructuras erosivas, como terrazas, cañones colgados, grandes superficies erosivas en el talud y en la cuenca profunda, sugieren que la cuenca de Alborán estuvo en exposición subaérea en algún momento durante la MSC. El elemento erosivo más destacable es un gran canal erosivo que cruza toda la cuenca de oeste a este por su parte más profunda, a diferencia de otras zonas del Mediterráneo donde la erosión principal se observa en el talud continental. La edad de este canal queda constreñida estratigráficamente por la erosión de la UU la cual cierra el ciclo de la trilogía de la MSC. Aparte de la erosión provocada por la megainundación Zancliense, se han observado depósitos caóticos en forma de cuña que se asocian a productos de la megainundación. De igual forma, se han hallado depósitos equivalentes en el umbral de Sicilia. Otra evidencia que apoya la existencia de la megainundación es la falta de depósitos contorníticos durante la MSC. Esta ausencia contrasta, sin embargo, con la omnipresencia de los mismos a partir del Plioceno, cuando el Mediterráneo ya estaba conectado al océano Atlántico.

La modelización matemática de la megainundación del Zancliense indica que este evento convulsivo ocurrió en cinco fases. La fase 0 corresponde a un periodo de relativa mayor duración donde la reducida entrada de agua atlántica genera una erosión poco significativa. En la fase 1, el Estrecho de Gibraltar se hace más profundo y ancho, aumentando de forma exponencial su tasa de erosión y de flujo de agua atlántica. En la fase 2, se produce una reducción del gradiente hidrológico entre el Océano Atlántico y el Mediterráneo Occidental que resulta en una disminución de la velocidad del flujo y de la descarga de agua, así como de la tasa de erosión. Durante esta fase, toda el agua atlántica que entra por el Estrecho de Gibraltar se invierte en rellenar la Cuenca Mediterránea Occidental. En la fase 3, el nivel del mar alcanza el umbral de Sicilia y el gradiente hidrológico se mantiene constante en la Cuenca Occidental, ya que el agua que entra por el Estrecho de Gibraltar es transferida a la Cuenca Oriental, produciendo en ésta un ascenso rápido del nivel del mar que da lugar a los depósitos caóticos identificados en Sicilia. Finalmente, en la fase 4, el nivel del mar asciende sincrónicamente en ambas cuencas mediterráneas hasta nivelarse con el Océano Atlántico. El tiempo estimado para transferir el 90% del agua a la cuenca mediterránea

es de dos años, provocando un ascenso del nivel del mar de 10 m por día. Debido al enorme caudal generado en el pico de la megainundación (10^8 m^3 s^{-1}) y las altas velocidades alcanzadas (v=40 m s^{-1}) es muy probable que la imagen de cascada ampliamente empleada en la literatura para el relleno la cuenca mediterránea no sea correcta y probablemente se produjo mediante una rampa de inundación.

La constatación de la existencia de la megainundación zancliense dirime el debate actual sobre los modelos de la MSC, de cuenca profunda desecada, de cuenca profunda no desecada y mixta, a favor del modelo de cuenca desecada o mixta.

Los resultados del estudio de estos procesos convulsivos de diferente naturaleza ponen de manifiesto que uno de los retos en la investigación futura en geociencias marinas comprende la necesidad de identificarlos, caracterizarlos y analizar sus impactos. Estos impactos afectan a los riesgos geológicos marinos y a la evolución paleogeográfica de cuencas marinas con implicaciones paleoceanográficas y paleoclimáticas.

TABLE OF CONTENTS

PART I

Chapter 1

1 INTRODUCTION

1.1 Convulsive geological events

Convulsive (catastrophic) geological events are violent disturbances of regional and sometimes global scale (Clifton, 1985, 1988). These events are rare in nature and for this reason, they remain almost unknown, although their impact on the environment is generally extreme and instantaneous on a geological scale. Several types of convulsive events are recognised in nature, most of them described on land. In the following, we will focus mainly on events occurring in the marine environment, although, due to their uniqueness and for comparative purposes, some examples occurring on land are also shown. The most common in literature are, earthquakes, tsunamis, megafloods, volcanic eruptions and extraterrestrial bolide impacts.

Convulsive events related to strong *earthquakes* are common in both the geological and historical record and occur in both marine and terrestrial areas. When the earthquake occurs under the sea, it can generate tsunamis and large landslides. Generally, earthquakes with significant magnitude values occur in subduction zones such as the Pacific Ring of Fire or in areas of tectonic indentation, such as in the Himalayas (Fig. 1-1). Some examples of historical convulsive earthquakes in these contexts are: Valdivia earthquake (Chile) with a magnitude 9.5, occurred in 1960; Prince William Sound (Alaska) with a magnitude 9.2, in 1964; Sumatra-Andaman with a magnitude 9.1, in 2004; or Tohoku (Japan) magnitude 9, occurred in 2011. The Altantic and Mediterranean Sea are also areas with significant seismic activity, but of comparatively lower magnitude. Some historical examples are: Lisbon earthquake in 1755; Karpathos (Greece) earthquake in 1948 (Dimova et al., 2021). Large earthquakes are also identified in the geological record through the study of palaeoseisms (Goldfinger et al., 2012; Ratzov et al., 2015).

Tsunamigenic convulsive events are caused by sudden offsets of the seabed that displace the water column. These displacements are mainly caused by seismic faults

(96% of events), landslides and volcanic processes. To a lesser extent, by extraterrestrial bolide impacts, by sudden release of gas pockets and by sudden variations in atmospheric pressure (meteotsunamis). Examples of large tsunamis are: from extraterrestrial bolide impact, the Chicxulub crater (65 my) which generated a 1.6 km wave (Range et al., 2018); from seismic origin the Lisbon tsunami earthquake (1755) with a wave height of 20 m (Mader, 2001), or the Okushiri Island (Sea of Japan) tsunami (1993) with a tsunami height of up to 31.7 m (Bryant, 2008).

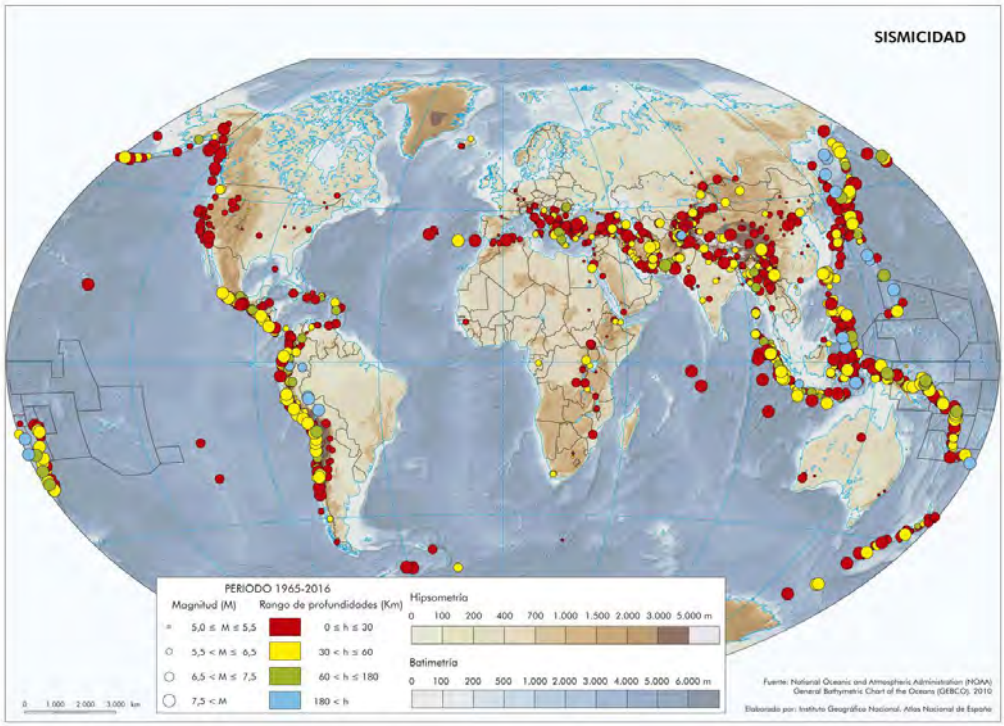

Figure 1-1 World seismicity map (source IGN).

Megafloods are mainly related to glacial lakes and to a lesser extent to sea level variations. Currently, there are several examples of megafloods associated with sudden glacial lake outbursts caused by natural ice dam breaks due to waning ice sheets, (Fig. 1-2): Channeled Scablands associated with Lake Missoula Washington (USA) (Waitt et al., 2021), Lake Missoula Montana (USA) (O'connor et al., 2020); Lake Bonneville Wisconsin (USA) (O'connor et al., 2020) and Altai megaflood in Siberia (Herget et al., 2020). Examples of megafloods related to sea level variations are known from the Strait of Dover, in the English Channel (Gupta et al., 2007), and in the Black Sea by flooding of

Mediterranean water into this sea, which at that time was a freshwater lake (Ryan et al., 1999); and the controversial Zanclean megaflood that ended the Messinian Salinity Crisis (MSC) (Hsü et al., 1973; Blanc, 2002), which is part of the study of this Thesis.

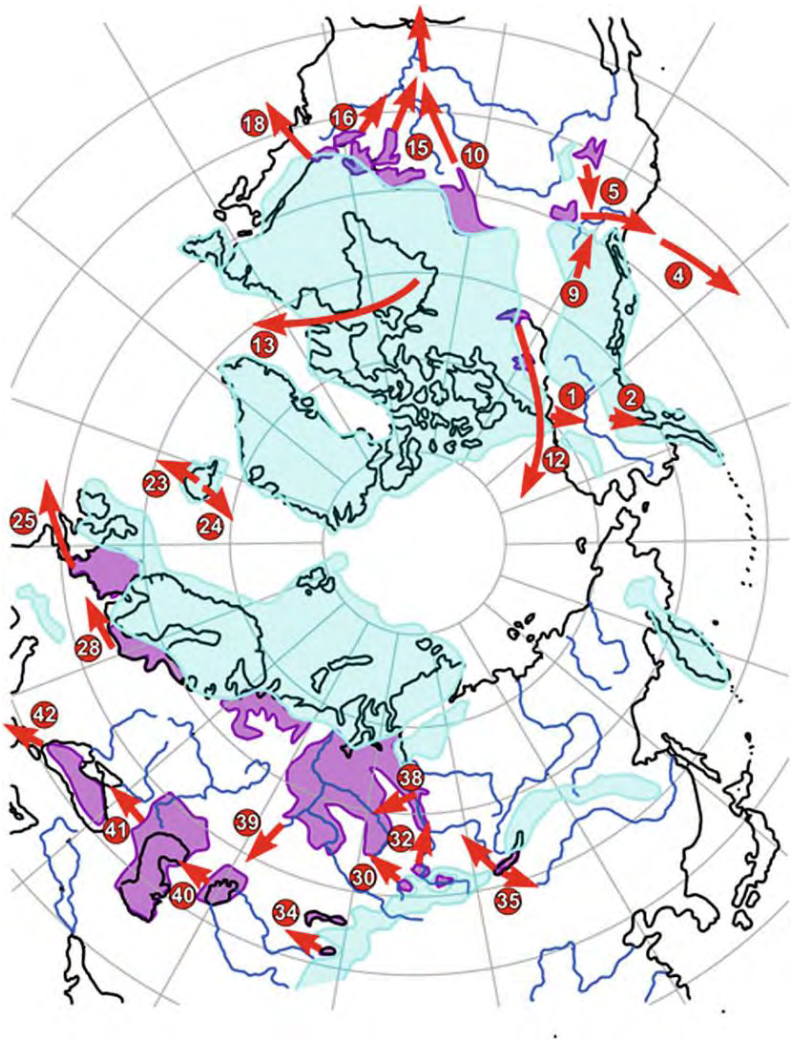

Figure 1-2 Hypothetical location of several megaflood events associated with the Late Pleistocene glaciation in the Northern Hemisphere and their path (Baker, 2020).

Both *submarine and coastal landslides* can trigger tsunamis (Fig. 1-3) (Bryant, 2008). The largest landslide-associated runup occurred at Lituya Bay (Alaska) in 1958 as a result of an earthquake-triggered rockfall, with wave heights of 30-50 m (Miller, 1960). Another important event was the Grand Banks (Canada) in 1929 with runup heights of up to 13 m (Piper 1999). Moreover, an important tsunamigenic source in the marine environment is found on volcanic islands. Due to the steep slopes and the volcanic

activity itself, submarine debris avalanches capable of generating tsunamis occur on volcanic islands, such as in Hawaii (Satake et al., 2002) or in the Canary Islands (Pérez-Torrado et al., 2006).

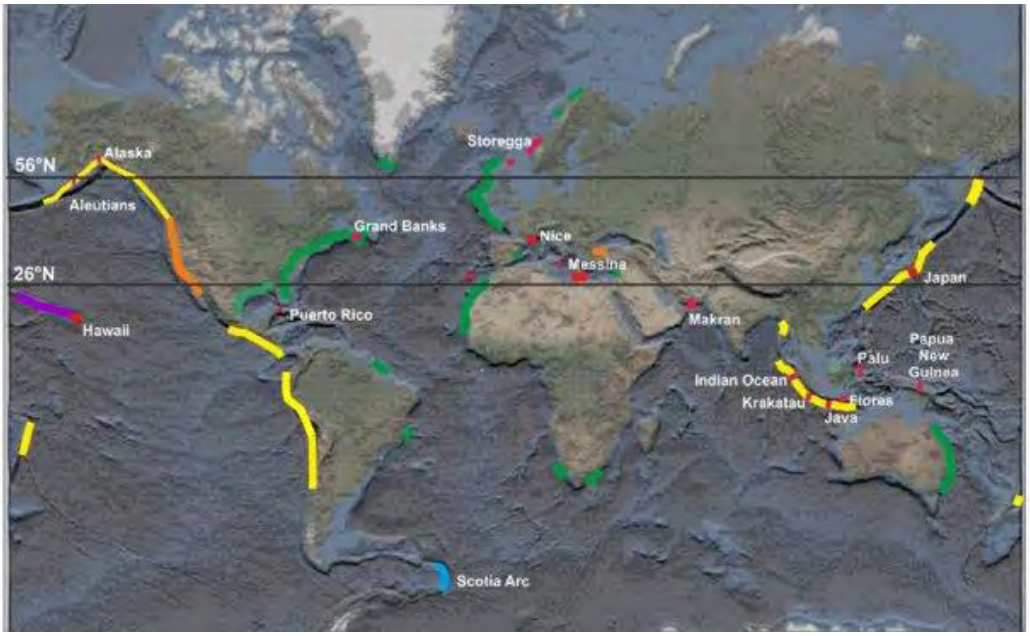

Figure 1-3. Global distribution of mapped submarine landslides (SLs): green, SLs on passive margins; yellow, SLs located along convergent margins; orange, SLs on strike-slip margins; purple, volcanoes; red, tsunamis associated with SLs. Submarine landslide tsunamis (in red) are mainly located along convergent margins, but also along passive and strike-slip margins and on flanks of volcanoes (Sassa et al., 2022).

Volcanism can generate tsunamis by various mechanisms (Latter, 1981), the most notable of which are due to submarine eruptions or explosions, pyroclastic flows or caldera collapse. The eruption of Thera in the Aegean Sea (1630-1550 B.C.E.) caused a tsunami (McCoy and Heiken, 2000) that contributed to the disappearance of the Minoan culture. More recently, in 1883, the eruption of Krakatau had a global impact and generated tsunami of more than 10 m (Bryant, 2008). From a marine point of view, volcanic eruptions affecting the water column can be grouped into four basic typologies whose main effects are summarised by Ercilla et al. (2021) (Fig. 1-4): near-shore sub-area eruptions; shallow water eruptions (<200 m); intermediate eruptions (300-600 m) and deep eruptions (>600 m).

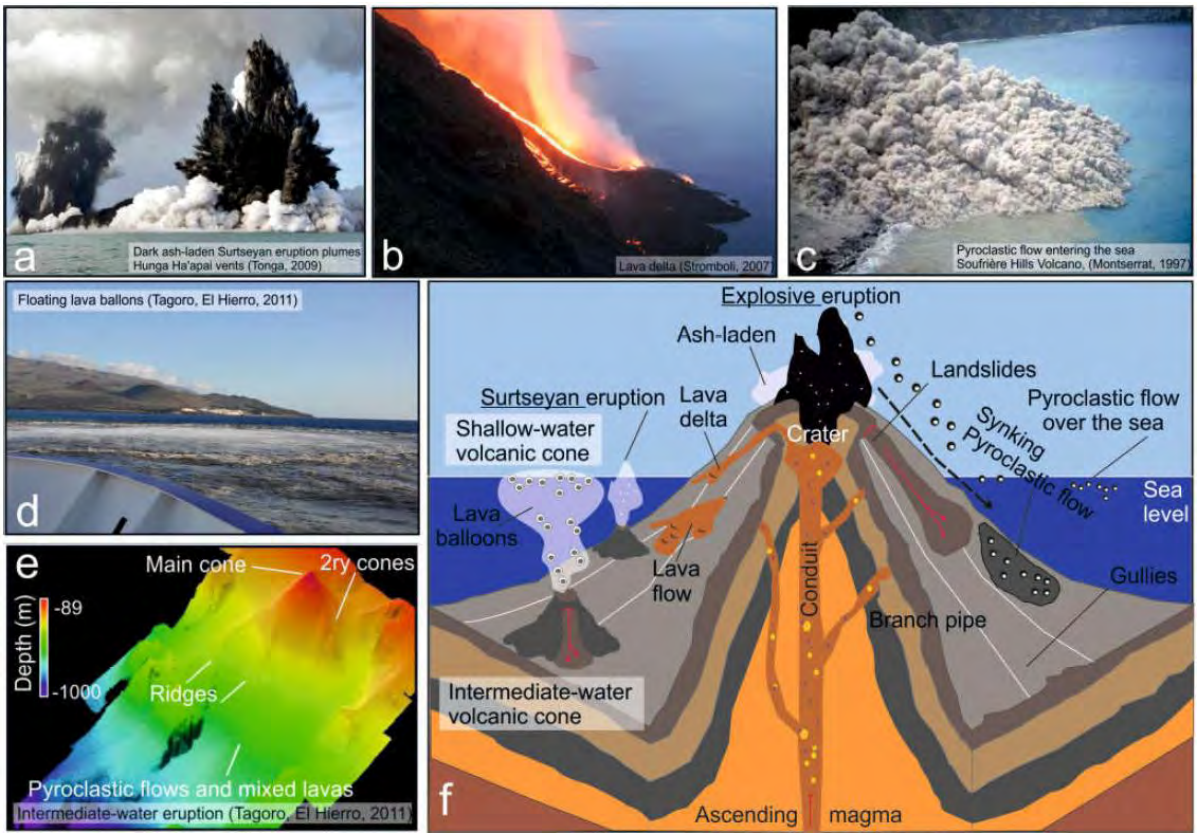

Figure 1-4. Main types of eruptions examples. Subaerial eruptions: (**a**) Sinking pyroclastic flows in Montserrat island and (**b**) emplacement of the 2007 lavadelta at Stromboli. Shallow water eruptions: **(c)** Surtseyan eruption plumes from Hunga Ha'apai vents (Tonga) in 2009. Intermediate-water eruptions: (**d**) floating volcaniclastic materials and gas emissions during the Tagoro volcanic eruption offshore El Hierro in 2011. Deep eruptions: (**e**) 3D bathymetric map of the Tagoro volcano showing the main morphological characteristics. (**f**) 3D simplified sketch of the main types of eruptions affecting insular volcanoes (Ercilla et al., 2021).

There are several examples of *extraterrestrial bolide-associated craters*, most of which have been identified on land (Fig. 1-5). In general, these structures are identified by a depression with concentric fractures and a mound in the centre of the impact. Some examples of ground-based impacts are: Berringer crater in Arizona (Masaitis, 2006; Osinski et al., 2015) or Vredefort crater in South Africa (Carporzen et al., 2005; Galdeano et al., 2008), among others. Those identified in marine environments are scarce, although several cases have been reported: the Chicxulub submarine crater in Yucatán (Gulick et al., 2013; Canales-García et al., 2018), submarine Silverpit crater in the North Sea (Stewart and Allen, 2005), Chesapeake Bay Crater in Virginia (USA) (Collins and Wünnrmann, 2005), and Mjolnir Crater in the Barents Sea (Dypvik et al., 1996).

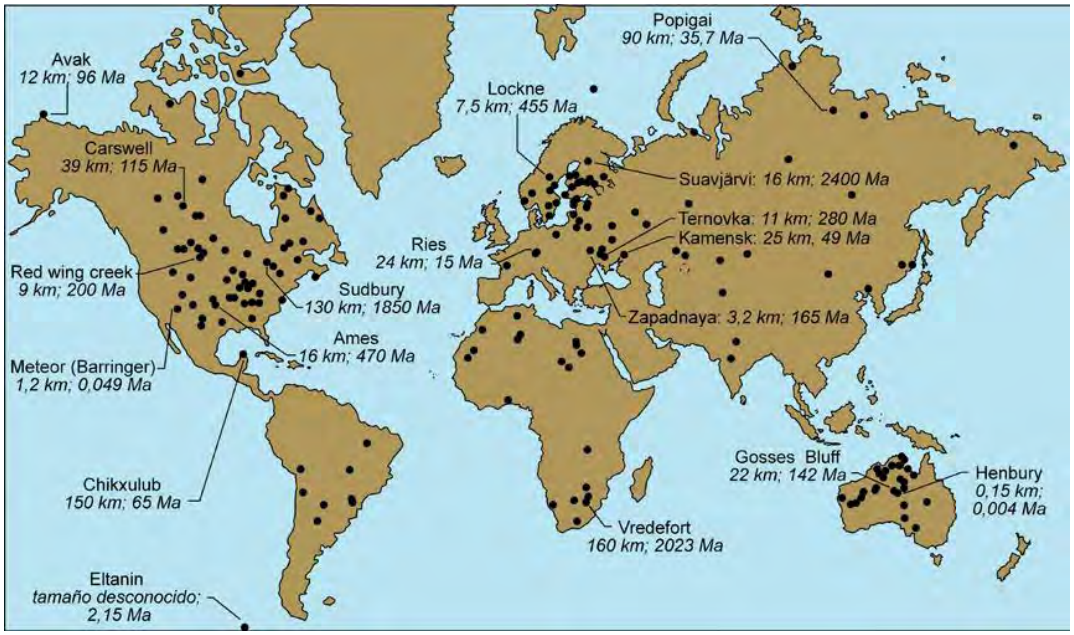

Figure 1-5 Impact structures according to the Earth Impact Database. The diameter of the crater (in kilometres) and its age of formation (in millions of years) are given. The largest on Earth are Vredefort (160 km) and Chicxulub (150 km) and the oldest are Suavjärvi (2400 Ma) and Vredefort (2023 Ma) (Ormö and Oms, 2013).

1.2 Hypothesis, aims and Ph.D. Thesis structure

1.2.1 Hypothesis

The working hypothesis of this doctoral thesis proposes that convulsive geological events have occurred in the Alborán Sea favoured by its tectonic framework of interaction between the Eurasian-African plate boundary geodynamic activity. The convulsive consequences can be identified, both from the sedimentary record and through mathematical modelling. The two convulsive events proposed are: i) the potential tsunamis triggered by active faults and ii) the megaflooding of the Mediterranean by Atlantic waters, associated with the end of the Messinian Salinity Crisis (MSC).

In relation to tsunamigenic events, the Alborán Basin is also considered to be an excellent setting for their study, given that its recent active tectonics reveals active faults frequently triggering earthquakes. In this case, the dense seismic grid with different degrees of resolution will allow us to assess the tsunamigenic potential of the seismic

active faults, based on numerical modelling, in order to establish the tsunami wave progration, its controlling factors, and its impact on coastal areas. This study will contribute to the knowledge of the geological risks of the Alborán Sea of great importance for the planning of strategies to mitigate their impact on society.

In the case of the Messinian Flood (i), this is thought to have occurred through the Strait of Gibraltar, but its occurrence is based on indirect proofs from other areas of the Mediterranean. The Alborán Sea is considered to be the best area to identify that flood, to decode how it occurred, and to analyse the regional impact, given its connection to the Atlantic Sea trough the oceanographic gateway of the Strait of Gibraltar. In addition, today's availability of a dense seismic grid is a key factor that guarantees its detailed analysis. This factor, combined with numerical models, will foster a better understanding of the behaviour and consequences of the Messinian Flood. The determination of the existence of a large flood will shed light on the debate as to whether the Mediterranean became disconnected from the Atlantic Ocean during the Messinian Salinity Crisis (MSC).

1.2.2 Aims

This working hypothesis is broken down into the following specific objectives:

1- Characterisation of the main tectonic structures formed in the framework of Eurasian and African tectonic plate interactions, in order to typify and catalogue seismic active faults.

2- Assessment of the tsunamigenic potentially of the active strike-slip Averrores fault by modelling seafloor deformation, propagation of the tsunami and its impact (i.e., flooding) on the coastal areas. Analysis of the formation of recent structures and the associated geological risks in one of the most seismologically active areas of the Alborán Sea.

3- Identification and geomorphosedimentary characterisation of structures (discontinuities, erosive surfaces, deposits) related to the convulsive event of the megaflood at the end of the Messinian Salinity Crisis, i.e. the Atlantic Zanclean flooding.

4-Numerical Modelling of the Atlantic Zanclean flooding using algorithms that link the erosion produced by water on rocks with hydrodynamic equations.

5- Integration of results from 3 and to 4 with other recent stratigraphic evidence to test the megaflood on other Messinian Salinity Crisis models.

6- Comparison of the two convulsive events and their implications in other similar geological contexts. Terminological and conceptual analysis of the appropriateness of the term catastrophic in relation to a convulsive event.

1.2.3 Ph.D. Thesis structure

In the following, the structure of this thesis is briefly described in order to facilitate the understanding of the text and the pursuit of the topics of this research. The configuration of this thesis is presented as a set of four publications from the Science Citation Index that qualify for the thesis by article format according to the rules of the University of Granada. In order to give more coherence and entity to the thesis and to achieve the objectives, an additional chapter with other three publications has been included. The thesis is divided into four main parts.

- **Part I** consists of chapters 1, 2 and 3.

  Chapter 1 is comprised of an introduction about convulsive events, where the main types and known examples are presented. Also, the hypothesis of this work and the objectives of the thesis are presented.

  In *Chapter 2*, the general regional background of the study area is established, although due to the nature of the thesis by articles, more specific background information appears in each of them.

  Finally, *Chapter 3* presents the data used in this Thesis and the general methodology, and in each chapter a specific methodology will be included, for the same reason as in the background.

- **Part II** is made up of chapters 4, 5 and 6, which correspond to three published articles, two as first author and one as third author. These chapters deal with the

characterisation of the tectonic activity of the central Alborán area in order to select a main active fault to study a tsunamigenic convulsive event.

In *Chapter 4*, the geodynamic setting of the central Alborán area is analysed and the main tectonic structures are identified and characterised. Finally, a model of tectonic indentation characterising this area is presented.

Chapter 5 studies several seismic shocks related the formation of a new fault zone, the Incrisis fault zone, about 10 km west at the southern end of the Al Idrisi fault, thus complementing the tectonic indentation model of Chapter 4. It also characterises the sedimentary instability zones associated with seismotectonic activity and the associated geological hazards.

Chapter 6 mathematically models the potential tsunami associated with the Averroes fault, identified and characterised in Chapter 4, and its impact on coastal zones.

- **Part III** consists of chapters 7 and 8 where the convulsive event of the Zanclean megaflood that ended the Messinian Salinity Crisis is geologically analysed and mathematically modelled. Chapter 7 is made up of additional works to the thesis format by articles, but which are related to, and complement, the study of the megaflood. Chapter 8 is part of the articles of the citation Index that are presented, in order to be eligible for the presentation of the Thesis in article format.

Chapter 7 analyses the geological evidence related to the megaflood (subchapter 7.1), the mathematical modelling and characterisation of the event (subchapter 7.2), and the integration of the mathematical model with the geological evidence (7.3).

Chapter 8 discusses the Zanclean megaflood in the context of the main hypotheses on the MSC and provides new evidence of the megaflood both in the Alborán Sea and in other areas of the Mediterranean (Sicily threshold).

- Finally, **Part IV** discusses and compares both convulsive events and their consequences in the Alborán Sea, and presents the main conclusions of this Thesis.

Chapter 2

2. REGIONAL SETTING

The Alborán Sea is located in the southwesternmost part of the Mediterranean Sea (Fig. 2-1). It is an east-west basin 150 km wide, 350 km long, and with an areal extension of 54,000 km^2. It is a semi-enclosed basin with a maximum depth of 2294 m, bounded to the north and south, respectively, by the Betic and Rif mountains, to the west by the Strait of Gibraltar, and to the east by the Algero-Balear Basin.

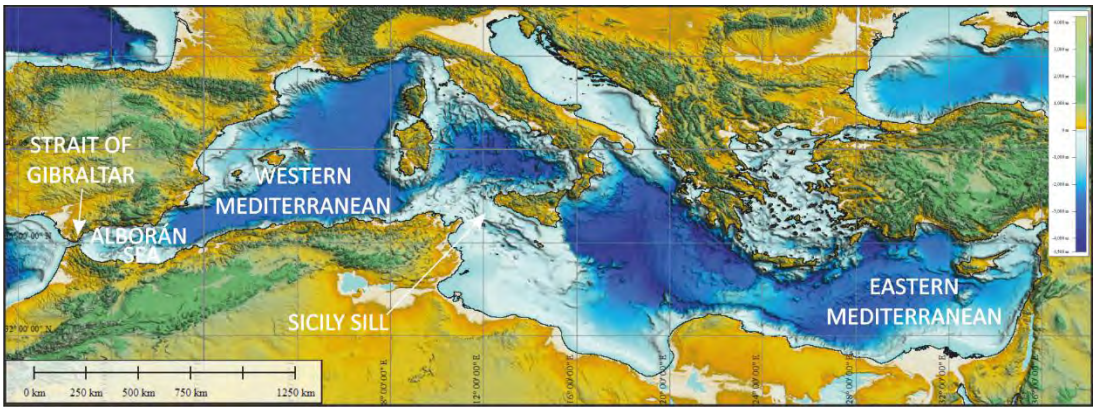

Figure 2-1. Mediterranean bathymetric map displaying the eastern and western basins and the location of the Alborán Sea in the westernmost end (Bathymetry from GEBCO).

2.1. Geodynamic setting

The tectonic evolution of the Alboran basin is characterized by two main tectonic events (Comas et al., 1992; Watts et al., 1993; Chalouan et al., 1997; Comas et al., 1999; Mauffret et al., 2007) in a general context of N-S to NW-SE Africa-Eurasia plate convergence. The first tectonic phase coincides with a synsedimentary extensional deformation, from the Oligocene to the late Tortonian, during a westward displacement of the Alborán domain with respect to the present position (Fig. 2-2). Initially, this extension was approximately NNE-SSW and changed to approximately E-W in the Burdigalian (Bourgois et al., 1992; Mauffret et al., 1992; Crespo-Blanc, 1995; Jolivet et al., 2006). The second phase started in the late Tortonian under an NNW-SSE

convergence (Weijermars et al., 1985; Vissers et al., 1995) and represents a period of tectonic inversion characterized by large strike-slip faults (Martínez-García et al., 2011, 2013) (Figs. 2-3 and 2-4).

During the Langhian-Messinian period, calc-alkaline to shoshonitic volcanism occurred and formed several volcanic edifices, mainly north of the Alborán Ridge and the eastern part of the Alborán Basin (Duggen et al., 2004). The Western Alborán Basin (WAB) has an active polyphase mud diapirism that initiated during the middle Miocene and is still active today, as it is evidenced by several mud volcanoes rooted in mud diapirs and related faults cutting the seafloor (Pérez-Belzuz et al., 1997; Sautkin et al., 2003; Soto et al., 2010; Somoza et al., 2012).

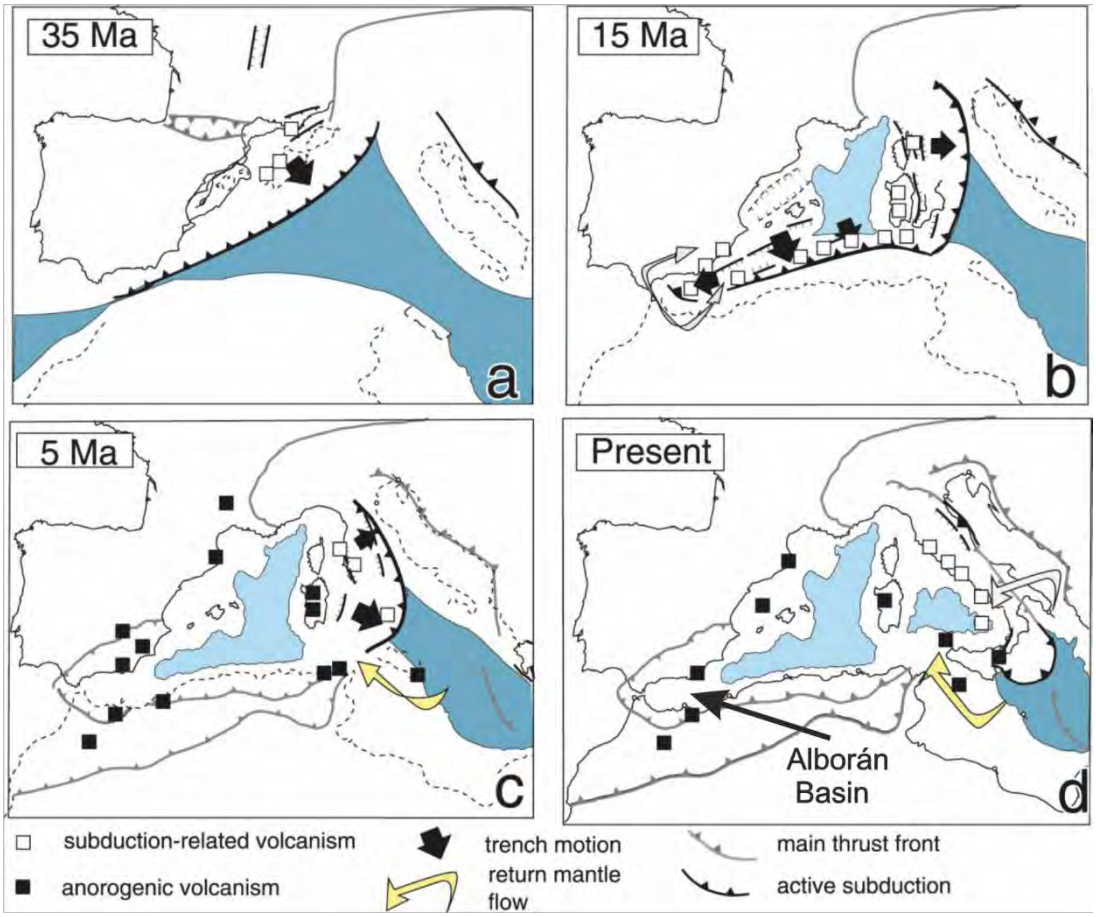

Figure 2-2. Reconstruction of the evolution of the western Mediterranean (Faccenna et al., 2004) from the Oligocene to the present (Do Couto, 2014).

Currently the Alborán Basin is a tectonically and seismically active zone that accommodates the NW-SE oblique convergence between the Eurasian and African plates at a rate of 4.5 mm/year (De Mets et al., 2015). The westward displacement of the Alborán Domain between the two main plates has determined the development of the Gibraltar Arc (Betic and Riff mountain ranges) that surrounds the Alborán Sea (Fig. 2-3). Fold and fault activity accommodate plate boundary deformation, while discontinuous fault slips release elastic deformation and produce seismicity (Figs. 2-4, 2-5 and 2-6).

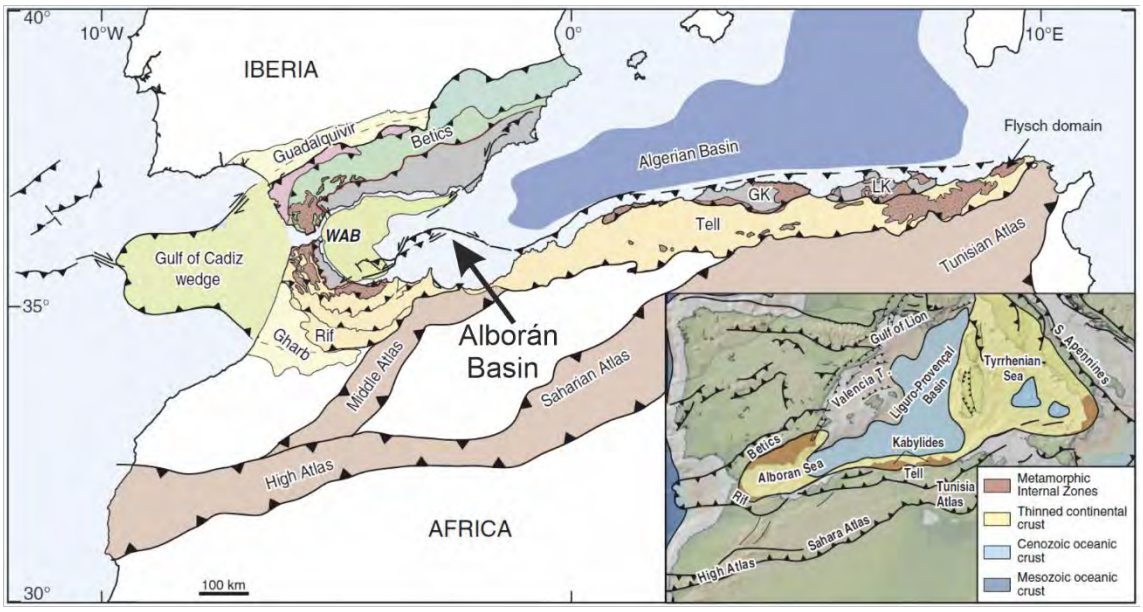

Figure 2-3. Structural maps of the western Mediterranean Sea showing the main tectonic units. GK: Greater Kabylide; LK: Lesser Kabylide. The inset map shows the location of the Apennines, Tellian, Rif and Betic fold and thrust belts in the western Mediterranean (Do Couto et al., 2016).

The origin and present-day setting of the Alborán Sea is controversial due to the geological complexity of the region. Several tectonic models have been proposed for the region involving delamination (e.g., Seber et al., 1996; Lis Mancilla et al., 2013), or subduction with or without rollback (e.g., Pedrera et al., 2011; Ruiz-Constán et al., 2011; Gutscher et al., 2012; González-Castillo et al., 2015; Spakman et al., 2018). Although the controversy remains alive, the most accepted models suggest that the main tectonic structure driving the deformation is a subduction zone starting in the western part of the Gibraltar Arc and subducting eastwards beneath the Alborán Sea (Fig. 2-5) (Gutscher

et al., 2002; Perouse et al., 2010; Ruiz-Constán et al., 2011). This active subduction is evidenced by the NE-SW to NNE-SSW arcuate band of intermediate seismicity in the western Alborán Sea (Figs. 2-5 and 2-6) (Buforn et al., 2017). The presence of a roll-back subduction zone determines that the western region of the Alborán Sea is a low-deformation subsidence zone, where a large depocenter has developed. In contrast, the central and eastern regions show marked tectonic deformation that produced its complex physiography (Martínez-García et al., 2011) (Fig. 2-4).

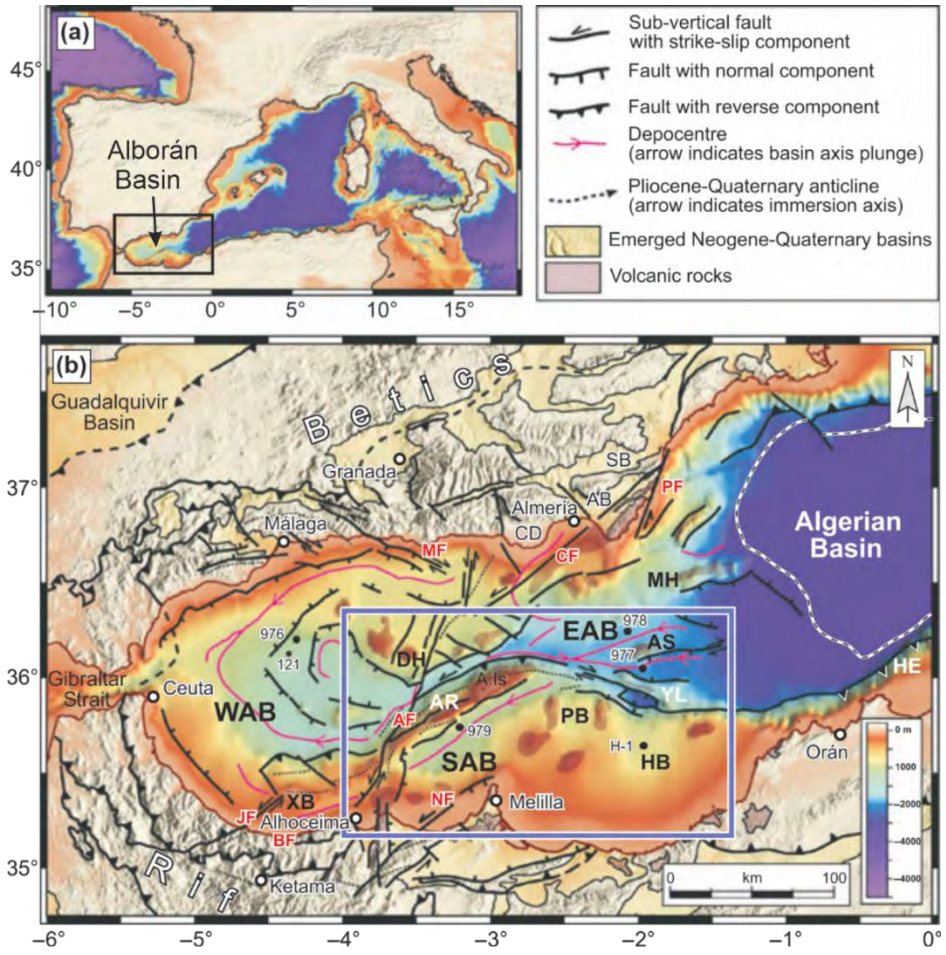

Figure 2-4. Tectonic map of the Gibraltar Arc system with the main faults of the Alborán Basin. Legend: The black dots are the ODP sites (976 to 979), the DSDP 121 site and the Habibas-1 well (H-1). Abbreviations: A. Is, Alborán Island; AB, Almería-Nıíjar Basin; AF, Al-Idrisi Fault; AR, Alborán Ridge; AS, Al-Mansour Seamount; BF, North Bokkoya Fault; CD, Campo de Dalías; CF, Carboneras Fault; DH, Djibouti High; EAB, East Alborán Basin; HB, Habibas Basin; HE, Habibas Escarpment; JF, Jebha Fault; MF, Maro-Nerja Fault; MH, Maimonides High; NF, Nekor Fault; PB, Pytheas Basin; PF, Palomares Fault; SAB, South Alborán Basin; SB, Sorbas Basin; XB, Xauen Bank; YL, Yusuf Lineament and WAB, Western Alborán Basin (Martínez-García et al., 2013).

The NW-SE shortening is accommodated by compressional tectonics that determines the presence of two main sets of faults with orientations N25ºE and N130ºE (Martínez-García et al., 2011) (Fig. 2-4). These faults are highly seismically active and determine the NNE-SSW seismicity band that crosses the Alborán Sea from Campo de Dalías to Al-Hoceima (Fig. 2-6). The Al Idrisi fault and new faults developing to the west, constitute the most active seismogenic faults at present (Galindo-Zaldívar et al., 2018). The Yusuf dextral fault constitutes the main NW-ESE conjugate fault that delimits its northern boundary. NNW-SSE normal faults located along the northern boundary of the Alborán Sea, such as the Balanegra Fault (Galindo-Zaldívar et al, 2015) also play an important role in accommodating ENE-WSW extension related to both compressional tectonics and roll-back.

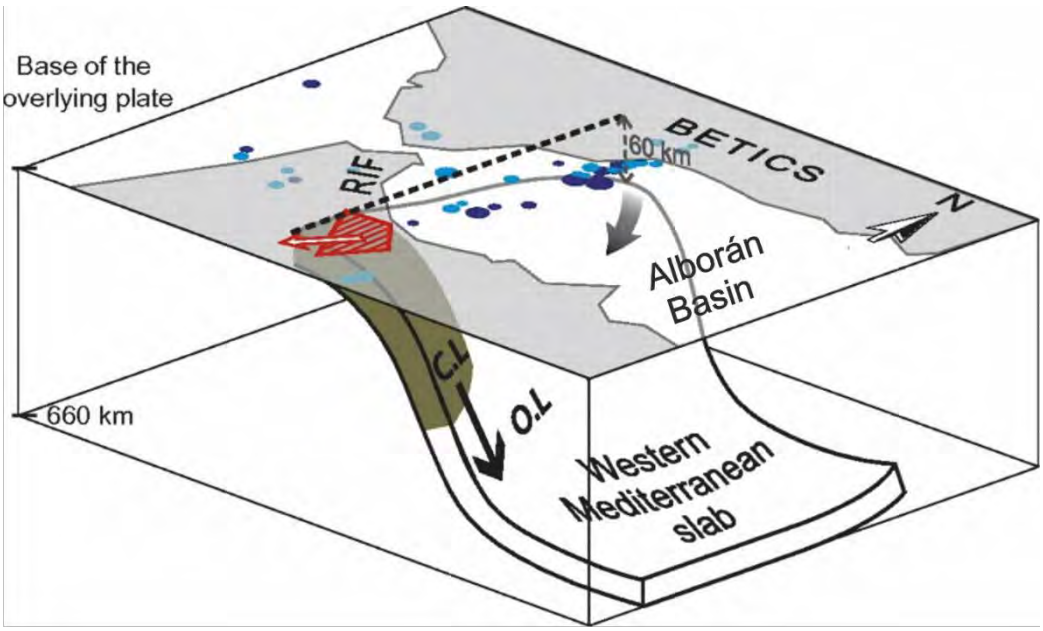

Figure 2-5. 3D Scheme of the lithospheric structures beneath the Alborán domain. Legend: C.L. continental crust and O.L. oceanic lithosphere (Perouse et al., 2010).

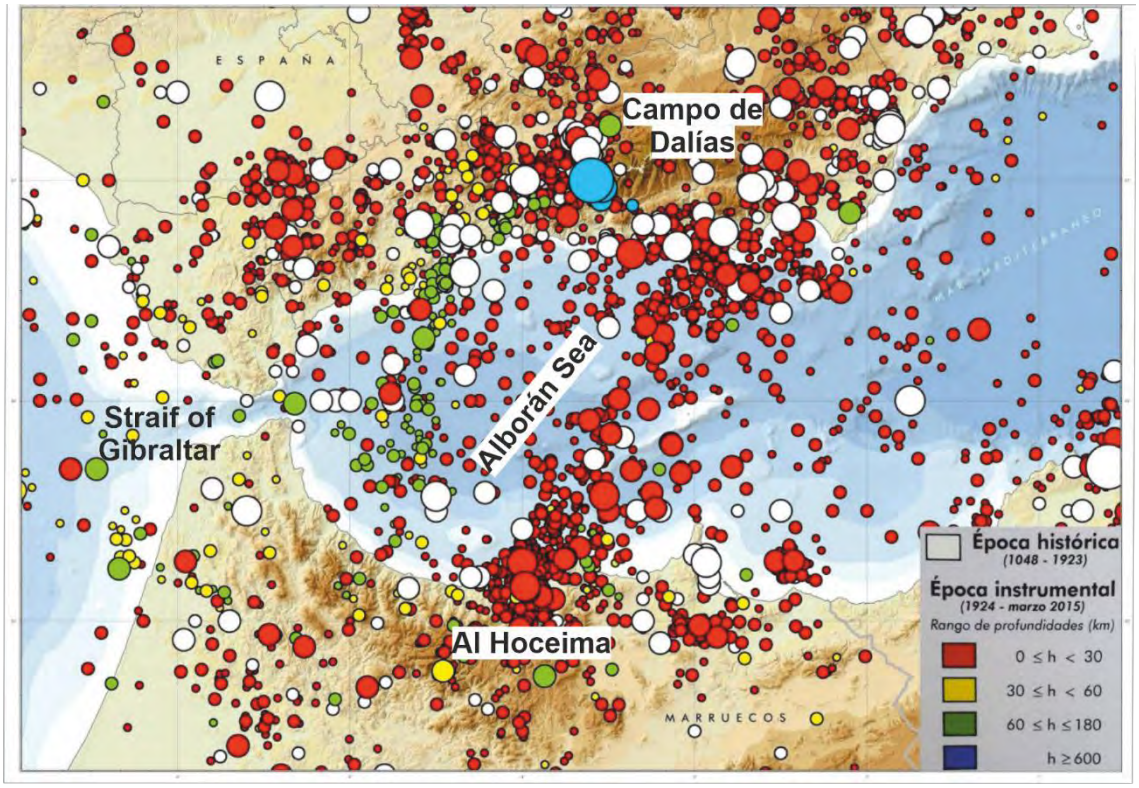

Figure 2-6. Historical and instrumental seismicity of the Alborán Sea-Strait of Gibraltar area (Source: IGN).

2.2. General seismic stratigraphy

The Alborán Sea is made up of three sub-basins: the western (WAB), the southern (SAB) and the eastern Alborán basins (EAB) (Fig. 2-4). The age of the sedimentary fill ranges from Miocene to Quaternary, with the WAB having the greatest thickness of up to 10 km (Do Couto et al., 2016). Eight seismic units have been defined from the Andalucía-G1 and El Jebha commercial boreholes in combination with the seismic record (Do Couto et al., 2016) (Figs. 2-7 and 2-8).

In the following, the seismic units that characterised the Alborán Basin are described according to Do Couto et al. (2016) where the units described by Comas et al., (1992), Comas et al., (1999) and Jurado and Comas (1992) are reviewed.

Seismic unit SU1 has been interpreted as turbidític deposits and carbonate levels of Late Oligocene-Early Miocene age, reaching a thickness of up to 3 km.

Seismic Unit SU2 has been interpreted as coarse-grained siliciclastic deposits and carbonate levels of Late Aquitanian-Burdigalian age with a maximum thickness of 300 m.

Seismic unit SU3 is composed of a shaly level developed on top of a basal level of marine conglomerates with an approximated thickness of 700 m, whose age comprises the Early to Middle Miocene. This unit, and probably SU2, are the source of the mud diapirism of the WAB.

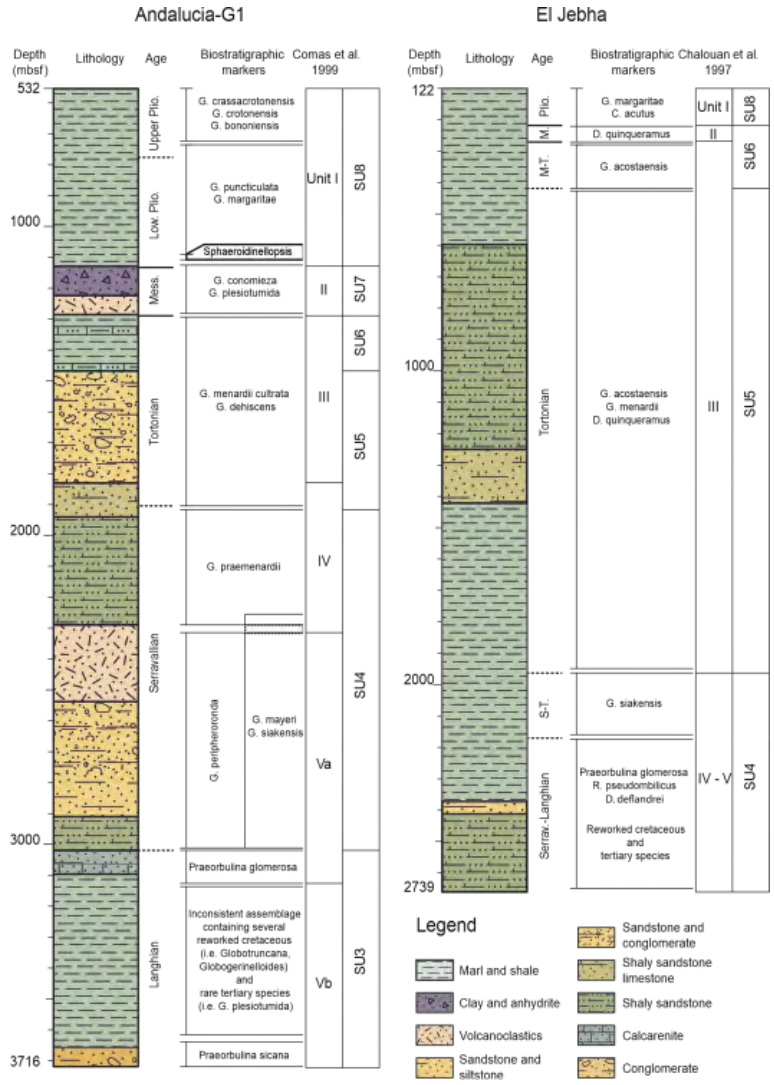

Figure 2-7. Commercial boreholes Andalucía-G1 (Spanish margin) and El jebha (Moroccan margin) showing the sedimentary sequences of the Western Alboran Basin and their lithology (Do Couto et al., 2016).

Seismic unit SU4, approximately 1000 m thick, is composed mainly of sandstones, conglomerates, shaly sandstones and clayey layers dated from the Serravallian. In the middle of this unit there are 240 m of volcanoclastic materials.

Seismic unit SU5 is composed of materials similar to US4 and is approximately 450 m thick. It is characterised by fine- to coarse-grained sandstones together with shaly sandstones, marls and shales dated Tortonian.

Seismic unit SU6 comprises sandstones interbedded with marls and clays from the Upper Tortonian to Lower Messinian. These layers have been interpreted as turbidític deposits interbedded within hemipelagic sediments. The basal discontinuity of this unit marks the tectonic inversion that affected the entire Alborán Basin.

Seismic unit SU7 is characterised by volcanoclastic series consisting of interbedded clays and basaltic layers beneath marine sandstones interbedded with finely laminated beds and shallow carbonates with some intervals of gypsum and fine anhydrite. The upper chaotic facies have been interpreted as mass transport deposits related to the lowering of sea level during the Messinian Salinity Crisis in the Mediterranean Sea.

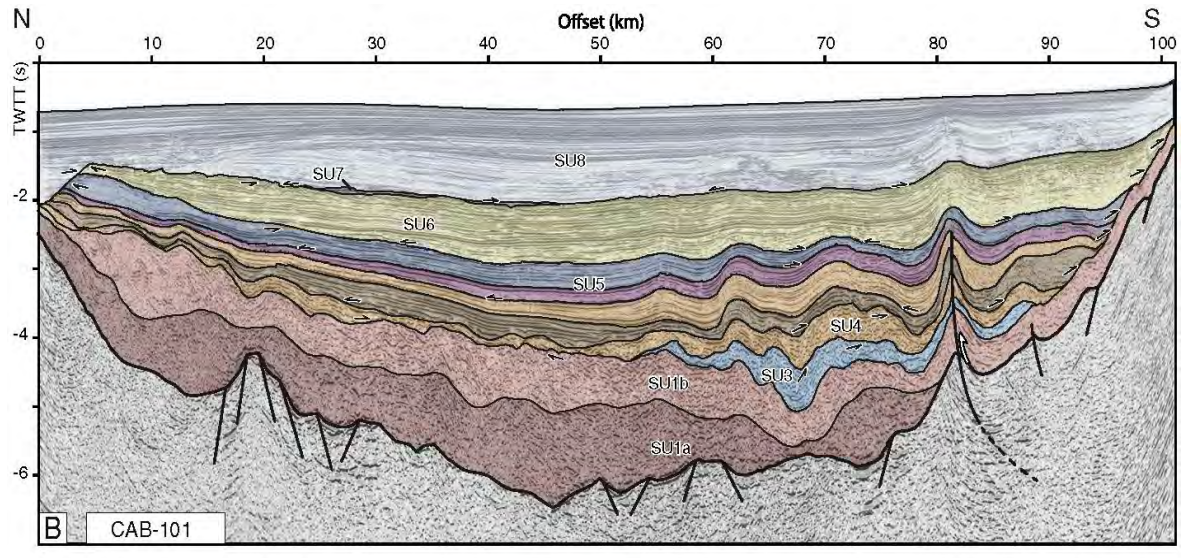

Figure 2-8. Multi-channel seismic profile illustrating the seismic units (SU1 to SU8) defined in the Western Alborán Basin (Do Couto et al., 2016).

Seismic unit SU8 consists of pelagic to hemipelagic marls and clays, interlayered with sandy turbidites dated from the Pliocene to the Quaternary. The stratigraphy of these sequences has been refined by Juan et al. (2016; 2020), allowing the updating and renaming of the stratigraphic boundaries and the establishment of a new Pliocene and Quaternary seismic stratigraphy for the Alborán Sea, after the relocation of the base of the Quaternary from 1.8 to 2.6 Ma. The boundaries of the stratigraphic division are as follows: the Messinian (5.96 to 5.33 Ma), the intra-lower Pliocene (P0 at ca. 4.5 Ma), the top of the Zanclean (P1 at ca. 3.3 Ma), the base of the Quaternary (BQD at ca. 2.6 Ma), the top of the Gelasian (Q0 at ca. 1.8 Ma), the intra-lower Quaternary (Q1 at ca. 1.12 Ma), and the top of the Calabrian (Q2 at ca. 0.7 Ma). These Pliocene and Quaternary units are mostly made up of contourites that contribute to the outbuilding of the margins and infilling of the basins. Contourites are laterally interrupted by several turbidite systems on the Iberian margin (Juan et al., 2016; 2020). The base of the Plio-Quaternary sequences is a striking erosional surface that results from the Messinian Salinity Crisis.

2.3. Messinian Salinity Crisis

In the late Miocene (5.96-5.33 Ma) what is known as the Messinian Salinity Crisis (MSC) (Selli, 1954) took place, causing the progressive isolation of the Mediterranean Sea from the rest of the oceans (Hsü et al., 1972) and the accumulation of up to 3 km of saline deposits representing 4% of the salt dissolved in the present-day oceans (Haq et al., 2020) (Fig. 2-9). Sea level is estimated to have dropped by 1500 m (Clauzon, 1982; Bache et al., 2011) causing widespread erosion of the continental margins of the Mediterranean Basin and deepening of canyons and associated river systems (Ryan, 1978; Clauzon, 1982). The MSC was an ecological crisis induced by a combination of geodynamic and climatic factors (Roveri et al., 2014). From a geodynamic point of view, the progressive restriction of the Mediterranean is associated with the westward displacement of the Gibraltar Arc to its present location, which caused the closure of the Mediterranean basin with respect to the Atlantic Ocean (Figs. 2-2 and 2-10).

The MSC developed in three main stages (CIESM, 2008), each characterised by different palaeoenvironmental conditions. During the first stage, evaporites in the form

of gypsum precipitated in shallow sub-basins. During the second stage, the MSC acme occurred and was characterized by evaporite precipitation, mainly salt, shifted to deeper depocenters. The third stage was characterised by large-scale environmental fluctuations in a Mediterranean transformed into a brackish water lake.

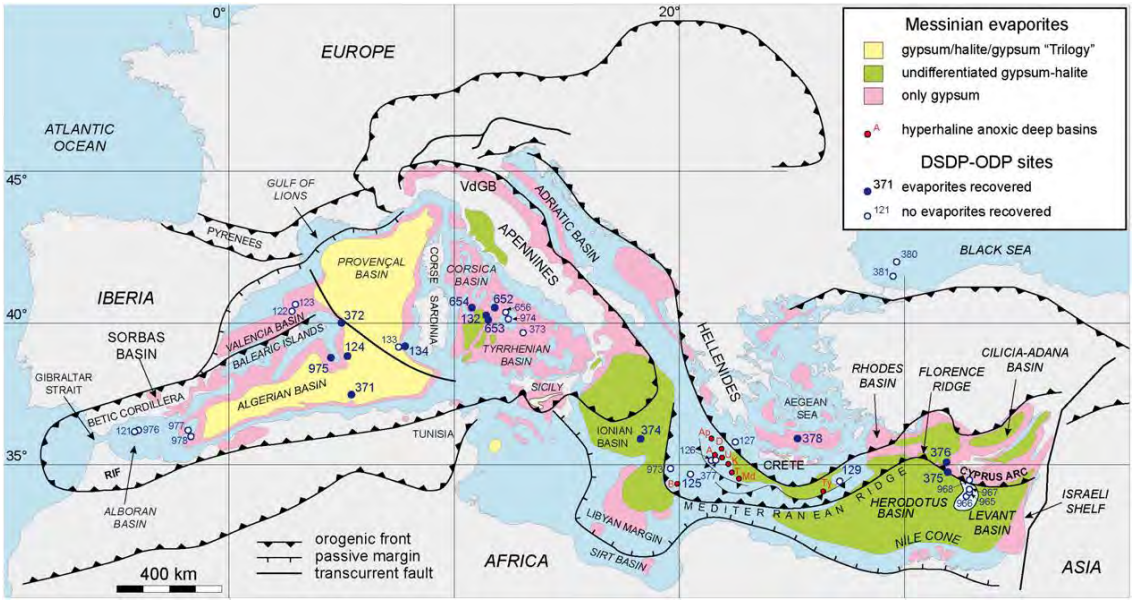

Figure 2-9. Distribution of Messinian evaporites and location of the DSDP-ODP boreholes which recovered Messinian deposits. The location of the main hyperhaline anoxic deep basins on top of the Mediterranean Ridge is also shown: Ap, Aphrodite; A, Atlante; B, Bannock; D, Discovery; K, Kryos; M, Medee; T, Thetis; Ty, Tyro; U, Urania (Roveri et al., 2014).

Different nomenclatures have been proposed for the onshore and offshore MSC units with varying chronostratigraphic correlations, although there is now some consensus, summarised in Figure 2-11. The onshore units, from base to top, are: Lower Gypsum (LG); Primary Lower Gypsum (PLG); halite (H); resedimented Lower Gypsum (RLG); Upper Gypsum (UG) and LagoMare (LM). The equivalent of the different units described onshore are summarised in three offshore units (Figs. 2-11 and 2-12), Lower Unit (LU), Mobile Unit (MU), Upper Unit (UU) and a Complex Unit (CU) that temporally encompasses the previous three, although it is not always present (Lofi, 2018).

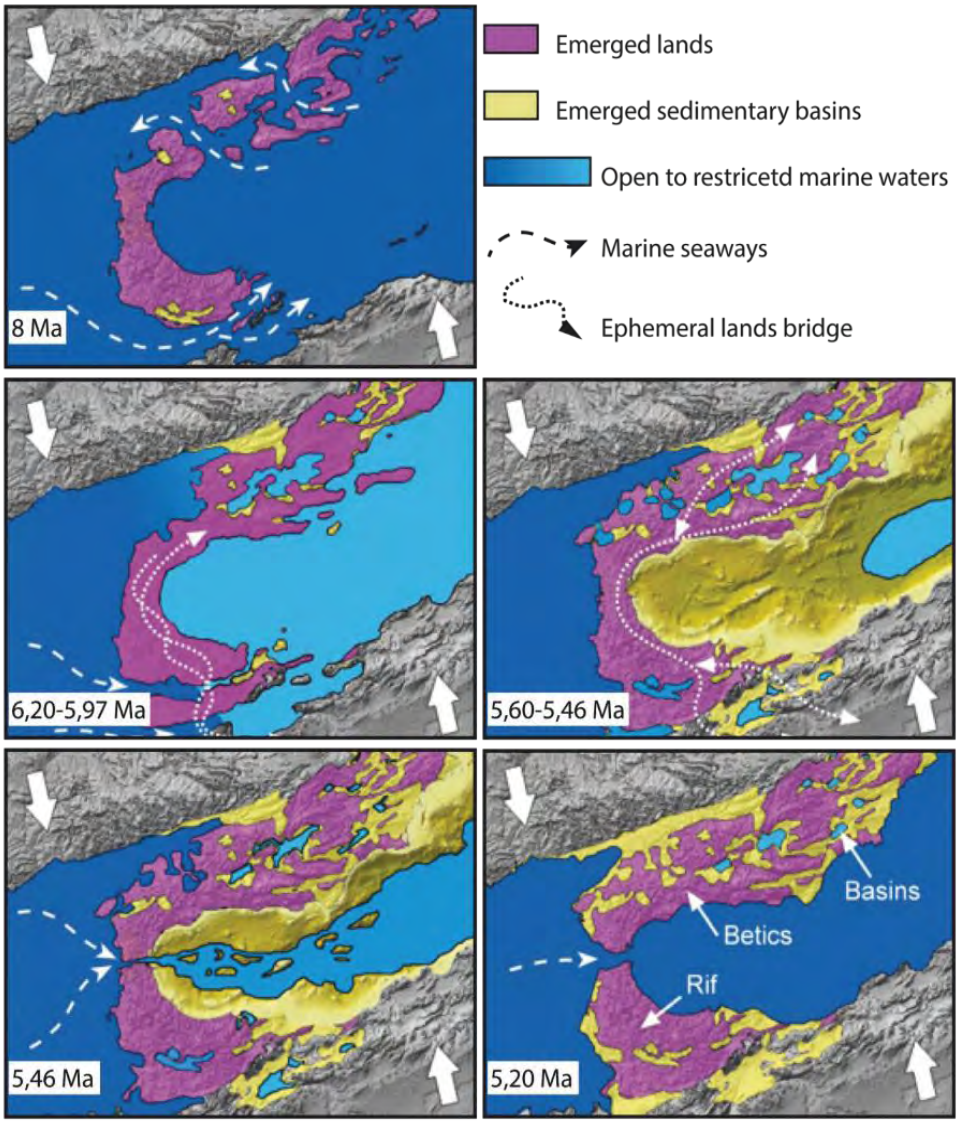

Figure 2-10. Palaeogeographic reconstruction of the Alborán Sea from the Late Tortonian to the Pliocene illustrating the progressive disconnection from the Mediterranean Sea. Ages according to Bache et al., 2011 (Do Couto, 2014).

The end of the MSC occurred at the Messinian/Zanclean transition when the isolated (or restricted) Mediterranean Sea was reconnected to the Atlantic Ocean through the Strait of Gibraltar (Hsü et al., 1973), presumably by a catastrophic flood (Blanc, 2002) produced by a combination of tectonic and river-erosion processes. Evidence of this rapid palaeoceanographic change to open marine conditions in the sedimentary record is seen in the form of abrupt lithological and palaeontological changes (Hsü et al., 1973).

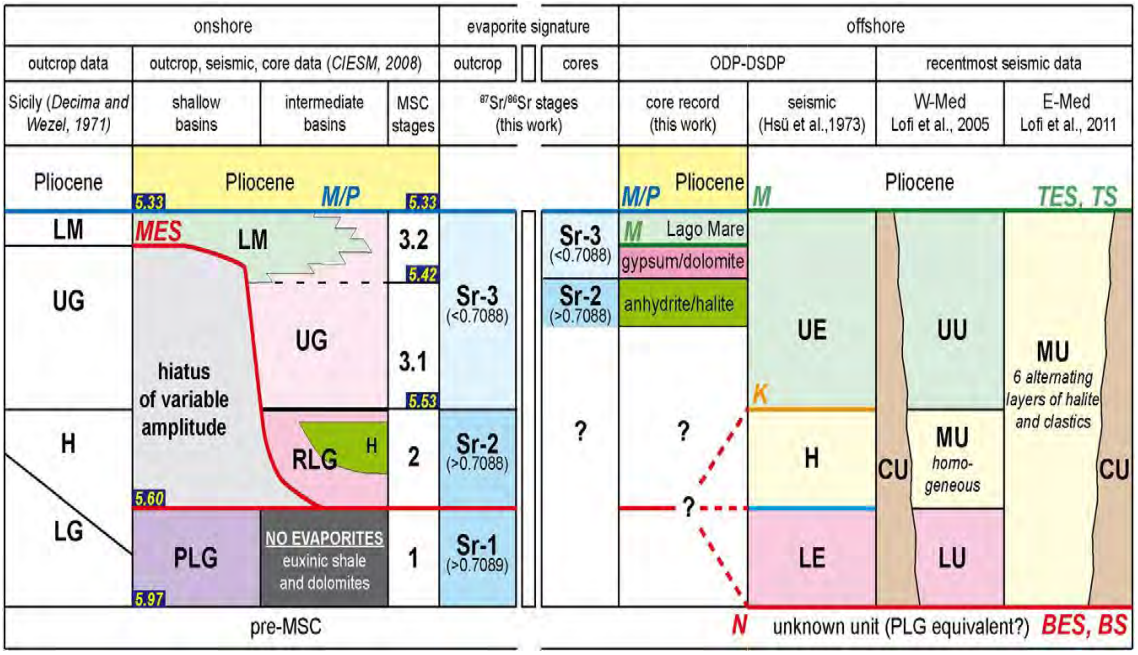

Figure 2-11. Synthesis of nomenclature assigned in the literature to onshore and offshore Messinian stratigraphic units. Onshore units: LG, Lower Gypsum; PLG, Primary Lower Gypsum; H, halite; RLG, Resedimented Lower Gypsum; UG, Upper Gypsum; LM, LagoMare; MES, Messinian erosional surface. M/P, Miocene–Pliocene Boundary. MSC stages: 1, 2, 3.1, 3.2. Strontium isotope stages: Sr-1, Sr-2, Sr-3. Offshore units: LE, Lower Evaporites=LU, Lower Unit; H, Messinian Salt= MU, Mobile Unit; UE, Upper Evaporites= UU, Upper unit; CU, Complex Unit. Offshore surfaces: MES, marginal erosional surface; horizon N=BES, basal erosional surface/BS, basal surface, base ofMessinian evaporites; horizonM=TES, Top erosional surface/TS, Top Surface: top of Messinian evaporites (Roveri et al., 2014).

Some new recent studies have questioned the classical desiccated basin model based on several reasons. The thickness of salt identified in deep basins requires 7-8 complete dewatering cycles of the Mediterranean (Haq et al., 2020), which implies the need for a permanent seawater connection. Some authors propose through modelling that halite precipitation does not require disconnection from the Atlantic, and propose a situation of Atlantic water inflow into a basin with blocked Mediterranean water outflow (MOW) (Roveri et al., 2014; Krijgsman et al., 2018).

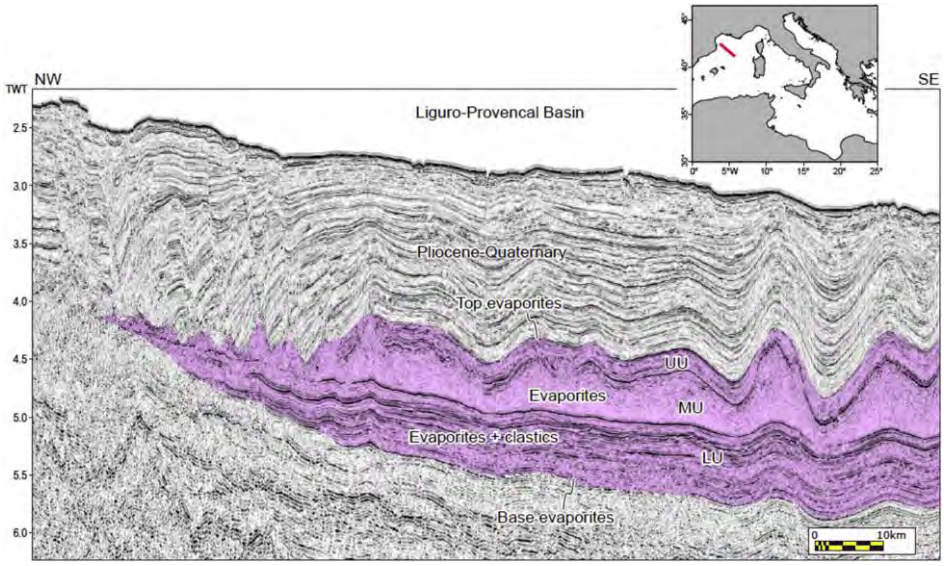

Figure 2-12. Seismic profile showing the offshore messinian units in the Liguro-Provençal Basin (Haq et al., 2020).

Another reason is related to the $^{87}Sr/^{86}Sr$ isotope ratio which is an indicator of palaeosalinity. Measures of this ratio in the MSC deposits point to the fact that the variation in Sr isotope ratio during the MSC does not require complete isolation from the Mediterranean (Flecker et al., 2002; Roveri et al., 2014) (Fig. 2-13).

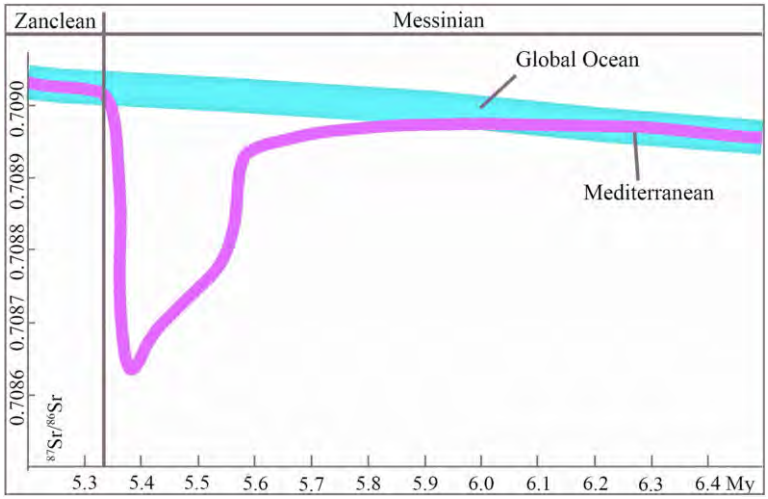

Figure 2-13. Strontium isotopic variations during the Messinian (Mascle and Mascle, 2019).

Currently, two competing hypotheses are put forward to explain the formation of the MSC (Fig. 2-14): a deep desiccated basin hypothesis with a 1500 m sea level lowering that ended with a megaflood (Hsü et al., 1973) and a deep non-desiccated basin hypothesis with dense stratified brines under a "normal" sea level (Roveri et al.,

2014). The non-desiccated basin hypothesis postulates that the convulsive event of the Zanclean megaflood did not exist, because there was a permanent Atlantic-Mediterranean connection during the MSC that is located in the Strait of Gibraltar.

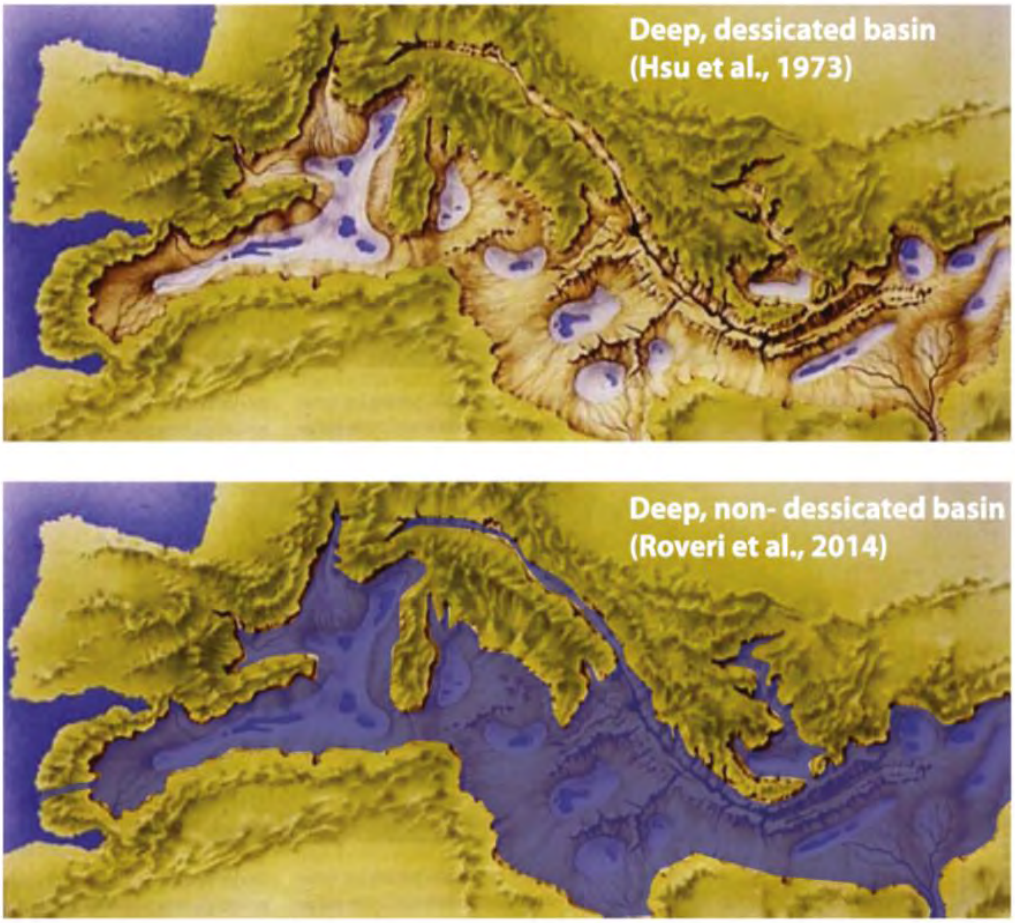

Figure 2-14. Palaeogeographic reconstruction illustrating the two main models of the Messinian Salinity Crisis (Krijgsman et al., 2018).

Recently, a new hypothesis has been postulated (Mascle and Mascle, 2019) that brings together the different evidence on the MSC into a new mixed model of the two previous hypotheses. This model proposes that the first two phases of the MSC (5.96-5.55 Ma), the Lower Unit (LU) and halite (MU) precipitation, occurred at sea level equivalent to that of the Atlantic, in agreement with strontium levels (Fig. 2-13). Only during the Upper Unit (UU), between 5.55 and 5.33 Ma, did sea level drop by 1500 m and erosion occurred at the margins of the entire Mediterranean basin. Finally, the Zanclean megaflood re-established the connection with the Atlantic Ocean.

Chapter 3

3. DATASET AND METHODS

This chapter specifies the origin and type of data used in this Ph. D. thesis, as well as general methodologies and concepts. The articles in chapters 4-8 detail the specific methodologies used in each investigation. This Ph. D. study has been based on the analysis of seismic profiles with different resolutions, multibeam bathymetry and commercial and scientific boreholes.

3.1 Oceanographic campaigns

The geophysical seismic profiles come from 45 oceanographic surveys conducted in the Alborán Sea, from the 1970s to 2018 (Table 3-1 and Fig. 3-1). These data are available online in the ICM-CSIC seismic database (http://gma.icm.csic.es/sites/default/files/geowebs/OLsurveys/index.htm). Part of the oceanographic campaigns come from the geophysical exploration of the hydrocarbon industry and the rest from academic scientific research. The older data, both multi-and single-channel profiles, were obtained in analogue (paper) format, while the most recent campaigns were obtained in digital format (SGY).

Ultra-high-resolution parametric profiler data from the Kronsberg TOPAS and Atlas Parastore Parasound echosounders (Table 3-2 and Fig. 3-2), from 10 scientific campaigns, have also been used (Table 3-2 and Fig. 3-2). Most of the parametric profiles were acquired simultaneously with the multibeam bathymetry data.

82AD-AG-ABA (1982)	(MC) Vaporchoc		He 91-3 (1991)	(MC) Airgun
AG (1972)	(MC) Vaporchoc		IZD (1982)	(MC) Airgun
ALB (1981)	(MC) Airgun		Marlboro (2011)	(MC) Airgun, Sparker
ALM (1978)	(MC) Airgun		Marsibal (2006-2010)	(SC-MC) Airgun
AM (1974)	(MC) Airgun		MC-75 (1975)	(MC) Airgun
AS (1977)	(MC) Airgun		MO-75 (1975)	(MC) Vaporchoc
BRPM (1975)	(MC) Airgun		Montera (2012)	(SC) Airgun
CAB00 (2000)	(MC) Airgun		Perpignan Univ. Ceuta (N/A)	(MC) Airgun
CAB01 (2001)	(MC) Airgun		Perpignan Univ. Alhoceima (1981)	(MC) Airgun
CD 64 (1991)	(SC) Airgun		RAY (1972)	(SC) Airgun
Contouriber (2010)	(SC) Airgun		S-83 (1983)	(MC) Airgun
Conrad C2911 (1988)	(MC) Airgun		Sagas (2008-2010)	(MC) Airgun
DBS (N/A)	(MC) Airgun		Saras (2012)	(MC) Airgun
EA (N/A)	(MC) Airgun		SH-73 (1973)	(MC) Airgun
EAS (1974)	(MC) Airgun		TALB (2000)	(MC) Airgun
Fauces (2017-2018)	(MC) Sparker		TSH (1984)	(MC) Airgun
Gasalb (N/A)	(MC) Airgun		TTR (N/A)	(SC) Airgun
Gardline-86 (1986)	(SC) Airgun		TTR-9 (N/A)	(SC) Airgun
GBT (N/A)	(MC) Airgun		TTR-12 (2002)	(SC) Airgun
GC-83-2 (1983)	(SC) Sparker		TTR-14 (N/A)	(SC) Airgun
GC-89-1 (1989)	(SC) Airgun		TTR-17 (N/A)	(SC) Airgun
GC-90-1 (1990)	(SC) Airgun, Boomer		Tyro (1991)	(SC) Airgun
GC-90-2 (1990)	(SC) Airgun			

Table 3-1. List of seismic campaigns used in this Ph. D. Thesis. Legend: Single-channel (SC), multi-channel (MC), no data (N/A).

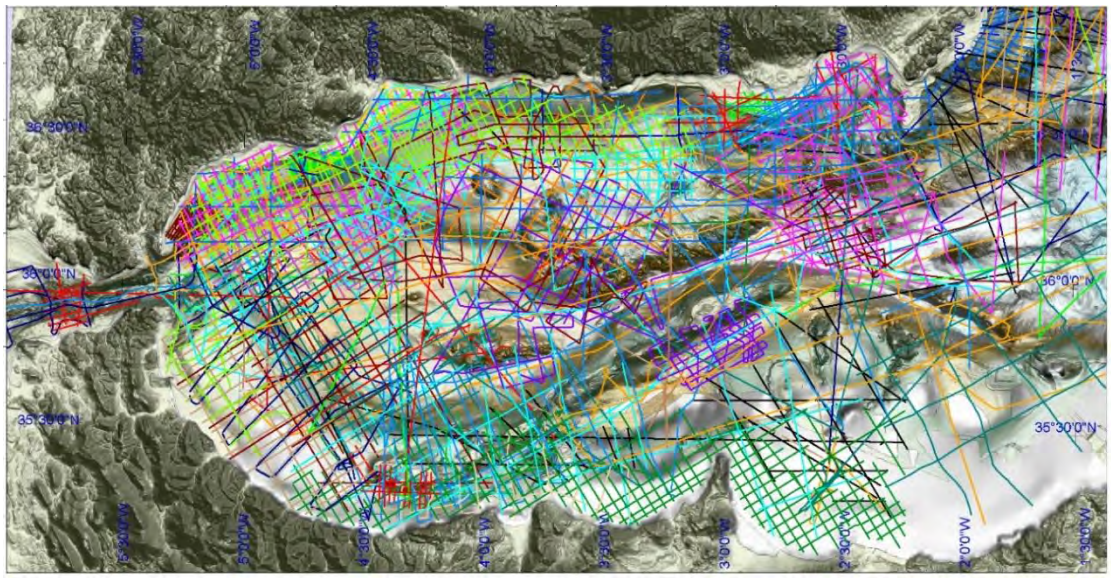

Figure 3-1. Location map of the de multi-channel, single-channel and Sparker seismic lines used in this study.

Contouriber (2010)	PARASOUND
ESPACE (2001-2002-2003)	TOPAS
Fauces (2017-2018)	PARASOUND/TOPAS
Incrisis (2016)	TOPAS
Marsibal (2006-2010)	TOPAS
Ministerio Pesca-IEO (2002-2003-2004)	TOPAS
Montera (2012)	PARASOUND
Sagas (2008-2010)	PARASOUND
Saras (2012)	TOPAS
TOPOMED (2011)	PARASOUND

Table 3-2. List of parametric profiling campaigns used in this Ph. D. Thesis (TOPAS and Atlas Parasound).

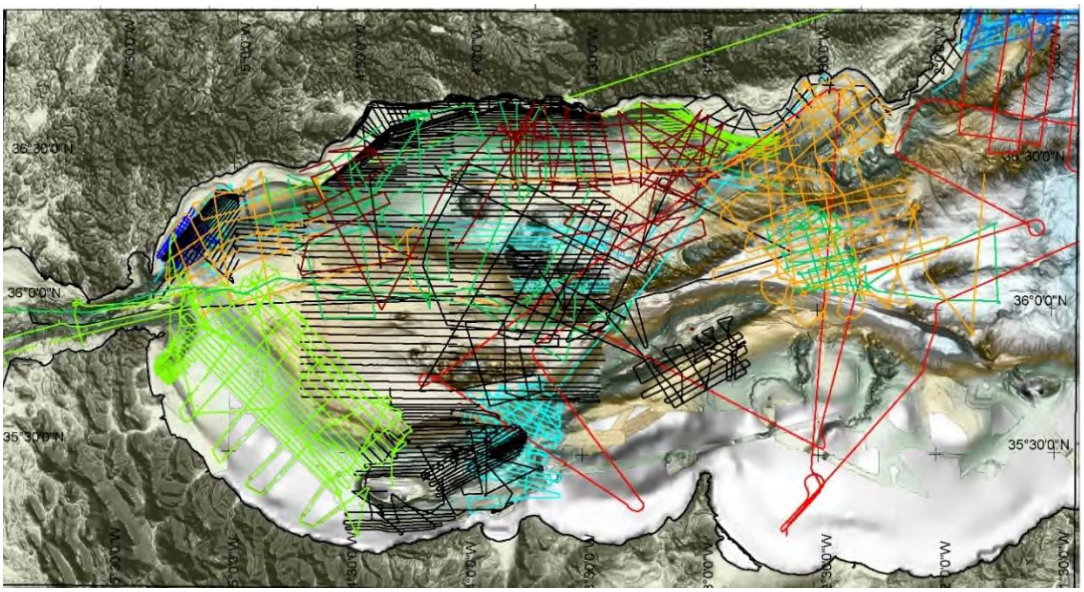

Figure 3-2. Map of the location of the TOPAS and Parasound parametric profiler lines used in this study.

The boreholes used for the chronostratigraphic correlation come mainly from several scientific campaigns of DSDP (site 121), ODP (976, 977, 978 and 979), and to a lesser extent from commercial boreholes (Andalucía G-1 and A1, Alborán A-1, El Jebha and Habibas) (Fig. 3-3).

Figure 3-3. Map of the Alborán Sea with the location of commercial (Andalucía G-1 and A1, Alborán A-1, El Jebha and Habibas) and scientific (DSDP-121, ODP-976, 977, 978, 979 and MD-952043) boreholes.

The multibeam bathymetric database comprises a compilation of several oceanographic campaigns: bathymetric data acquired by the Spanish Institute of Oceanography (IEO) for the Spanish Fisheries Office, ALBA (1992), MARSIBAL (2006), SAGAS (2008 and 2010), CONTOURIBER (2010), MONTERA (2012), SARAS (2012), INCRISIS (2016) and FAUCES (2017-2018). These data were acquired with Simrad EM12 and Atlas HYDROSWEEP DS multibeam sounders. Areas with data gaps were filled with regional bathymetry data from the GEBCO Digital Atlas, and surfaced areas with ETOPO data. The integrated bathymetric grid for the entire Alborán Sea (Fig. 3-4) has a 40x40 m grid with a variable resolution. Bathymetry editing and map creation has been performed using Goldensoftware's SURFER and Globalmapper programs.

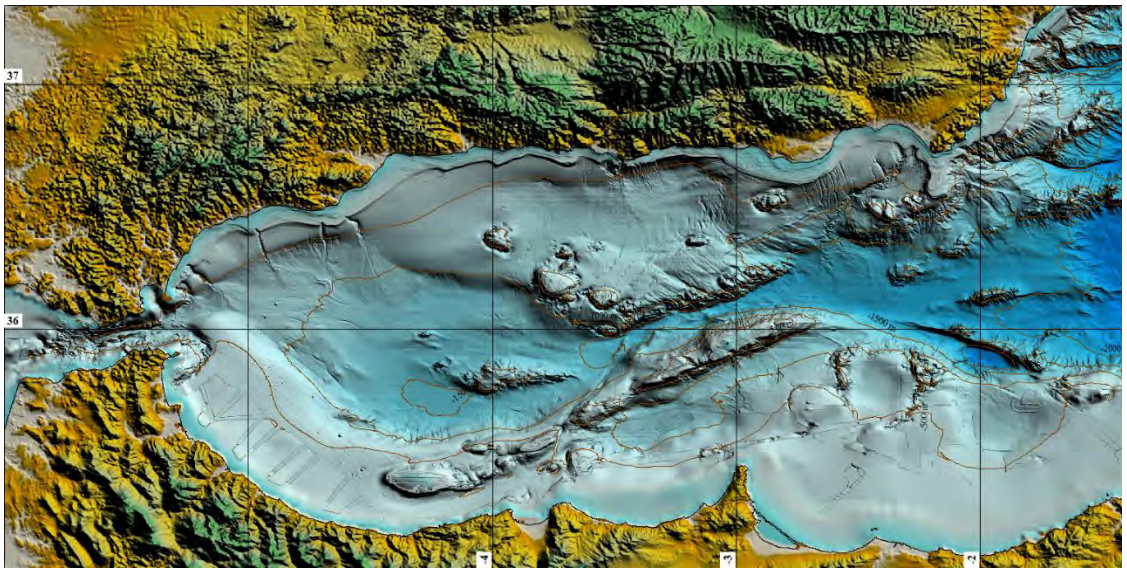

Figure 3-4. Topographic and bathymetric map of the Alborán Sea and surroundings made by integrating several campaigns.

3.1.1 Seismic data

The development of this Ph. D. Thesis has been based on the interpretation of more than 66,000 km of reflection seismic profiles with different degrees of resolution (from high to low) and of different types, airgun and sparker of multi-and single-channel. These data were collected in several commercial and scientific oceanographic campaigns from the 1970s to the present. The oldest originals were in analogue format (paper profiles) and were transformed into the standard SEG-Y (Society of Exploration

Geophysicists) digital format. In addition, about 47,000 km in ultra-high-resolution parametric profiles (TOPAS and Atlas Parasound) were recorded.

3.1.2 Seismic systems

Seismic acquisition equipment, in general, consists of three main elements: the energy source, the receiving system, and the acquisition and recording system. The resolution and penetration of the seismic recording is a function of the source energy and the frequency of the resulting waveform. Systems operating at high frequencies and relatively lower energy will result in low penetration and high-resolution recordings, while systems operating at low frequencies and high energy will result in higher penetration and lower resolution.

3.1.2.1 Parametric echosounders

Ultra-high-resolution parametric systems are characterised by the transmission of two close primary pulses that give rise to a low-frequency secondary wave. The TOPAS system uses primary frequencies close to 16 and 20 kHz and the Atlas Parasound system uses frequencies between 18 and 39 kHz, giving rise to frequencies ranging from 0.5 to 6 kHz. These systems make it possible to study surface sediments (approximately the upper 100 m) with high resolution and with a signal that generates little reverberation or hyperbole.

The TOPAS sediment profiler consists of a directional multiple transducer with several independent transducers for transmission and reception of the acoustic pulse (Fig. 3-5). The width of the acoustic pulse, depending on the emitted frequency, ranges between 4 and 6 degrees, resulting in better penetration and resolution (approximately 150 m). In order to correct for ship motion (attitude) and waves during acquisition, the TOPAS system is electronically stabilised by the acquisition software itself, which receives the information from the ship's attitude sensors.

Figure 3-5. Image showing TOPAS hull mounted transducer (Source: Krongsberg).

The Atlas Parasound sediment profiler is characterised by a single transducer mounted on the hull of the vessel that emits a narrow Chirp-type acoustic pulse. In parallel, the emitted signals are connected to auxiliary position, sound velocity and attitude sensors which are electronically corrected to improve the quality of the recording. The theoretical penetration of this system is approximately 200 m, although this may vary depending on the depth and nature of the sediments sounded.

3.1.2.2 High- and low-resolution seismic systems

Two systems have been used for recording high- and low-resolution seismic profiles: airgun and sparker. *The airgun system* is characterised by a source of one or more pneumatic compressed air chambers which are towed behind the vessel by several buoys at a depth of approximately 5 m. The capacity of the guns varies according to the depth and resolution targeted (Fig. 3-6). In the campaigns carried out by the PhD student, volumes between (140 and 620 c.i.) have been used. The sudden release of compressed air from the airguns generates a bubble that implodes and produces an

acoustic pulse that penetrates the sediment layers producing a series of reflections. These are recorded by a streamer with several hydrophones located at approximately 1.5 m depth. The firing rate varies according to the targets of each campaign, but it is generally calculated at multiple distance intervals. In the older single-channel profiles, the shooting cadence was time-based. The recorded raw data were further processed, and different filters (50-180 Hz) and corrections such as spherical divergence for signal energy loss or lateral stacking were applied to reinforce coherence between traces, among others.

Figure 3-6. Airgun seismic array with 8 guns.

The sparker system allows high to medium resolution recordings to be obtained using a high voltage source composed of several electrodes (Fig. 3-7). The energy generated varies according to the depth and resolution (500-2000 J). The synchronised electrical discharge generates a bubble that implodes and gives rise to an acoustic pulse that penetrates the seabed sediments and is reflected back to a single-channel streamer towed behind the ship. Depending on the nature of the subsurface, the penetration of

the acoustic signal can reach several hundred metres below the seabed with metric resolution. These data require only basic processing consisting of bandpass filtering (low cut-off at 200 Hz, high cut-off at 4000 Hz), to attenuate noise, and wave filtering.

Figure 3-7. Image showing an example of sparker system with several electrodes.

Multi-channel seismic profile acquisition is generally characterised by a low frequency source (although it is also used with high frequencies) which can be of different types: airgun, a bubble is generated by compressed air; sparker, in this case the bubble is generated by an electrical discharge; vaporchoc, the bubble is generated by steam, although this system is currently in disuse. Multi-channel acquisition is characterised by the streamer, which consists of several active sections (channels) of hydrophones. The length of the streamer is usually longer than the single-channel and will depend on the geological target of the survey; in general, the deeper the target, the longer the streamer it can be, up to several kilometres. The number of hydrophones per channel, the number of channels and the distance between channels can vary from one multi-channel configuration to another, resulting in variable penetration and resolution.

The most typical configuration for multi-channel seismic acquisition is called common midpoint mode (CMP) Fig. 3-8). The CMP is defined as the point midway between the source and receiver that is shared by several source-receiver pairs. This is achieved by recording the reflected signal from the same shot at many receivers (shot gather), and then moving the source position by a multiple of the distance between the receivers. The CMPs are placed at half the distance between receivers.

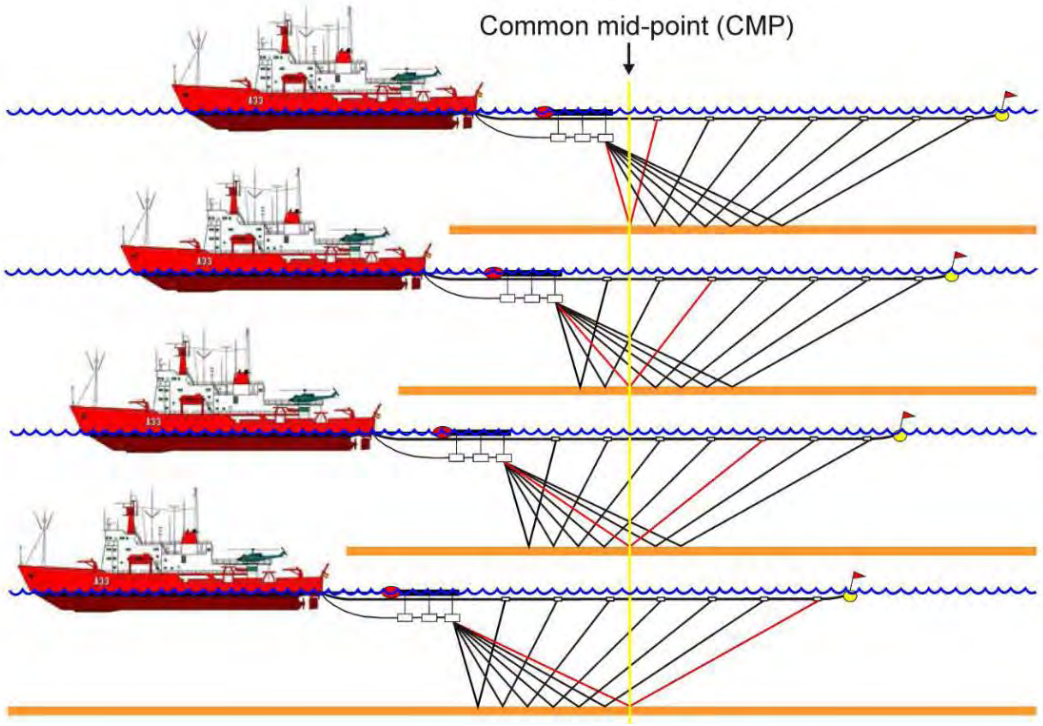

Figure 3-8. Scheme showing the common mid-point technique, considering four shots of the airgun array and seven active sections (channels) in the streamer, while the vessel is displacing to the left.

In the case of ideally flat horizons, the acoustic energy pulse will be reflected at a Common Depth Point (CDP) for each interface that will be located below the CMP. However, when sediment layers show a certain dip angle, not all traces are reflected at the same midpoint location, and no CDP will be shared by multiple source-receiver pairs. As a result, this seismic system requires significant processing work to reconstruct the geometry of the sediment layers: Dip Displacement Processing (DMO), Normal Move Out (NMO), migration, deconvolution, etc. The multi-channel profiles used in this thesis

have not been processed by the PhD student, in some cases. They were obtained already processed and, in most cases, they were obtained in analogue format (paper rolls).

3.1.3 Multibeam bathymetric echosounders

The development of this Ph. D. Thesis has also been based on the interpretation of multibeam bathymetric data obtained with echosounders that are based on the synchronised emission of several acoustic pulses arranged in a fan pattern and directed towards the seabed (Fig. 3-9). The echosounder transducers used in the different campaigns were arranged on the hull of the ship, measuring the bidirectional travel time required for each of the acoustic pulses to travel from the echosounder to the seabed and return, after reflecting off the seabed, to the ship's transducer. The arrival time of the pulses depends on the sound speed of the water, which in turn depends on the water temperature and salinity, so several water velocity profiles were acquired throughout the campaigns using XBT sounders to transform the arrival time to metres.

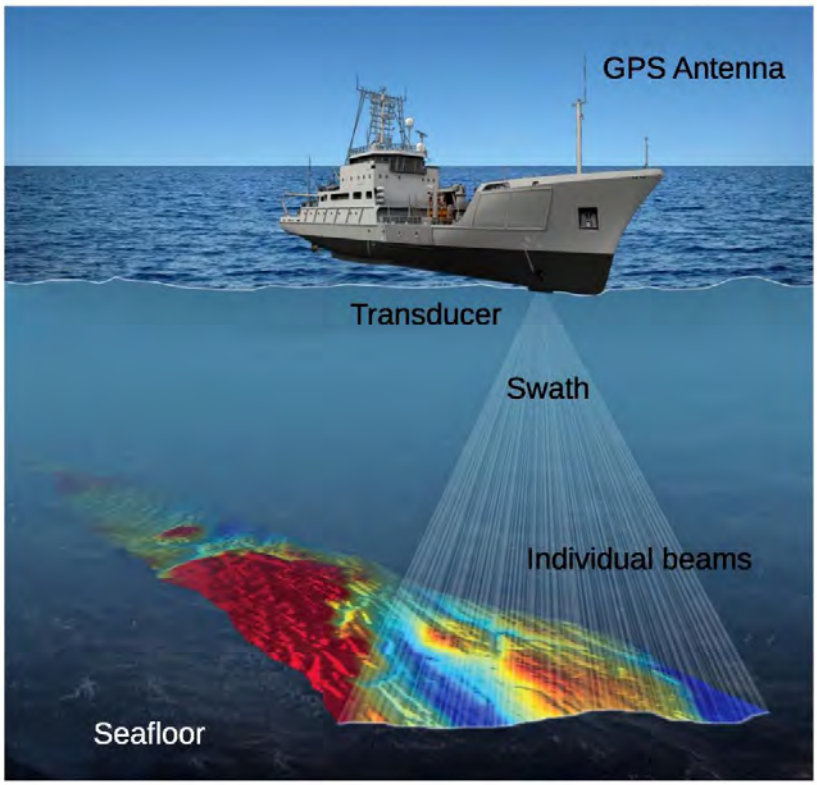

Figure 3-9. Schematic diagram of the operation of a multibeam echosounder (Maleika et al., 2018).

3.2 Lab work

The lab work mostly involved the seismic processing of seismic records on paper or film, the stratigraphic, sedimentary and tectonic analysis of all the seismic profiles, as well as the multibeam processing and its geomorphological analysis.

3.2.1 Image2Sgy

The IMAGE2SEGY (http://gma.icm.csic.es/node/67) software transforms raster images of seismic records on paper, or film, to geo-referenced Seg-Y files, that are compatible with "IHS Kingdom", "Promax", "SeiSee" and other industry standard software for seismic interpretation. This free software developed in the Institute of Marine Sciences of Barcelona (ICM-CSIOC) allows the user to scan old seismic paper records, or downloaded images from Geological Surveys GIS servers, and compile them in a georeferenced seismic project (Fig. 3-10).

This software corrects offsets in the seismic records due to changes in time delays and even distortions produced during the scanning of long rolls of paper. The data needed to transform to SEGY is the seismic line navigation file and an image. Next, a text file is created that relates the pixels of the image with known points of the seismic profile, such as the vertical scale in time, the position of the shotpoints or the delays. Through the MATLAB software, the image of the seismic profile and the previously created text file are integrated into a SEGY file.

3.2.2 IHS Kingdom Project

In order to work in a georeferenced and three-dimensional environment, seismic profiles, bathymetry and borehole data have been integrated into a project in the IHS Kingdom software. This allows interaction between different types of data and makes geological interpretation in a digital environment more effective and accurate. The correlation of the boreholes (in meters) with the seismic profiles (in time) has been done from the sonic log obtained during drilling (Fig. 3-11), thus the main limits identified in

the boreholes have been transferred to the seismic profiles allowing to establish the chronostratigraphy of the Alborán Sea.

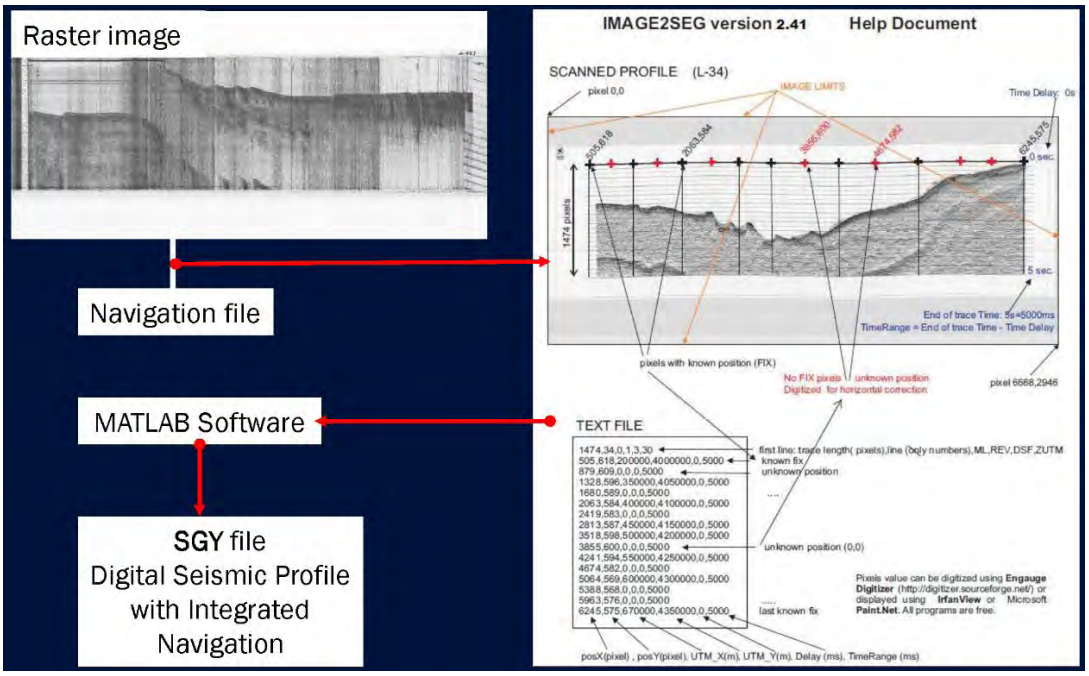

Figure 3-10. Summary diagram of the transforming process of seismic profiles from paper to digital format SGY.

3.2.3 Multibeam processing

The acquired multibeam data require further processing with specific software (e.g. NEPTUNE, CARIS) to apply other calibrations and corrections, such as tide, wave height and vessel motion (Roll, Heave, Pitch and Yaw). To correctly position the soundings, the multibeam echo sounders are also connected to the on-board GPS positioning system, recording data such as heading, speed and attitude. Modern systems operate with an acoustic frequency of 13kHz and a power of 12 kW, and emit up to 141 equi-angular and equidistant acoustic beams, reaching a maximum angle of 120°. The acoustic footprint depends on seabed depth and beam angle, but is typically approximately 3.5 times the seabed depth.

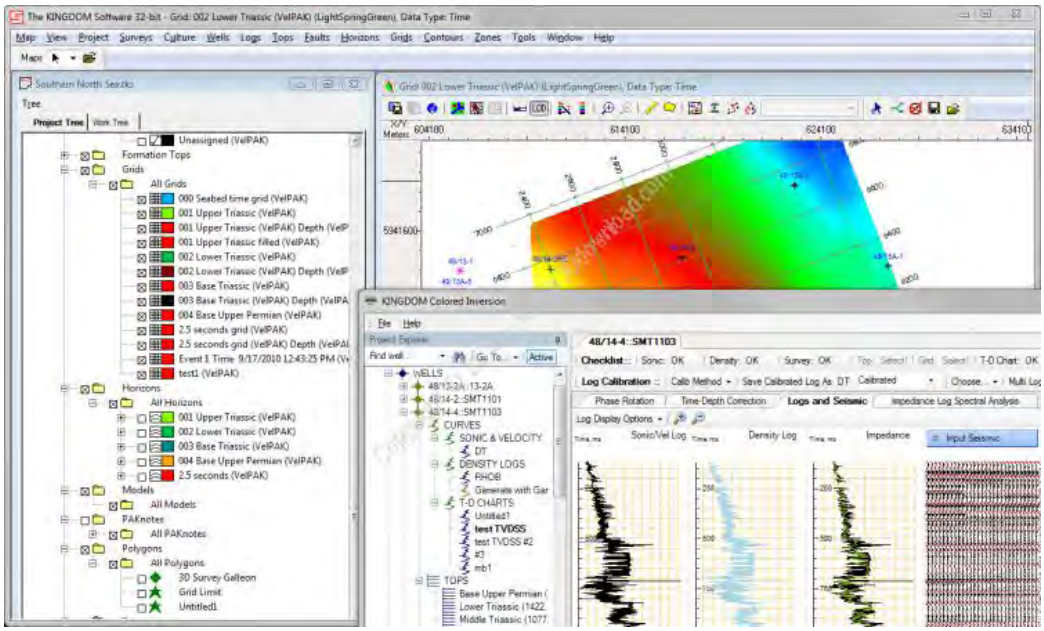

Figure 3-11. IHS-Kingdom software screenshot showing well log edition.

3.3 Seismic stratigraphy analysis

Data obtained from seismic profiles provide a reflection image of the subsurface generated by the acoustic waves. Seismic stratigraphy techniques help us in the stratigraphic interpretation of seismic reflectors. The geological concepts of stratigraphy can be applied to seismic data and therefore seismic stratigraphy can be used as a tool for the interpretation of subsurface geology.

The basic concept of seismic stratigraphy is that individual reflectors can be considered timelines, i.e. they represent a very short time interval of similar sedimentation conditions. This assumption means that the seismic reflector may have a different depositional environment and therefore has information from several lithofacies units. The analysis and interpretation of seismic profiles has been based on the principle that any variation in acoustic impedance results in the formation of a reflection. Acoustic impedance variations occur in relation to surfaces separating media with different density and/or compressional wave velocity. Surfaces separating media with different acoustic impedance correspond to stratification surfaces or geological discontinuities (Anderson and Hampton, 1974; Bouye, 1983).

The main criteria used in the recognition of reflectors in seismic stratigraphy are four: amplitude, continuity, frequency and type of signal (Leenhardt, 1972; Vail et aI., 1977). The first criterion deals with the maximum amplitude of the reflected wave whose value is showed in the seismic record by a more or less dark signal. Continuity is based on the power of visual integration of successive reflections from the same reflector. The frequency is linked to the vertical spacing between two successive positive phases. Signal type defines the characteristic appearance of a reflector by relating the three criteria above.

Unconformities are erosional and/or non-depositional surfaces. They indicate temporal gaps in the geological record. Unconformities can generate reflections because they separate strata of different lithologies and therefore different physical properties. Often, there may be an angular contact between the layers of two units through an unconformity. This angular relationship indicates tectonic deformation prior to deposition of the younger sediments. Erosion truncates the underlying strata. If the layers of both units are parallel, it is difficult to recognise the unconformity from seismic. In this case, other techniques such as biostratigraphy or isotopic analysis may be useful.

Different types of reflector termination relationships are recognised in unconformities (Fig. 3-12). *Erosional truncation*: older sediments are eroded. The underlying sediments may be deformed. This may indicate a hiatus in time before other overlying strata were deposited. *Toplap*: if erosion affects a progradational geometry. The underlying unit should show tilted layering by deposition. *Concordance*: where the interface and the overlying or underlying strata are deformed in the same way. *Onlap*: where younger sediments are progressively overlain. *Downlap*: where foresets of younger strata abut the unconformity. The inclination of the foresets indicates the direction of sedimentary input.

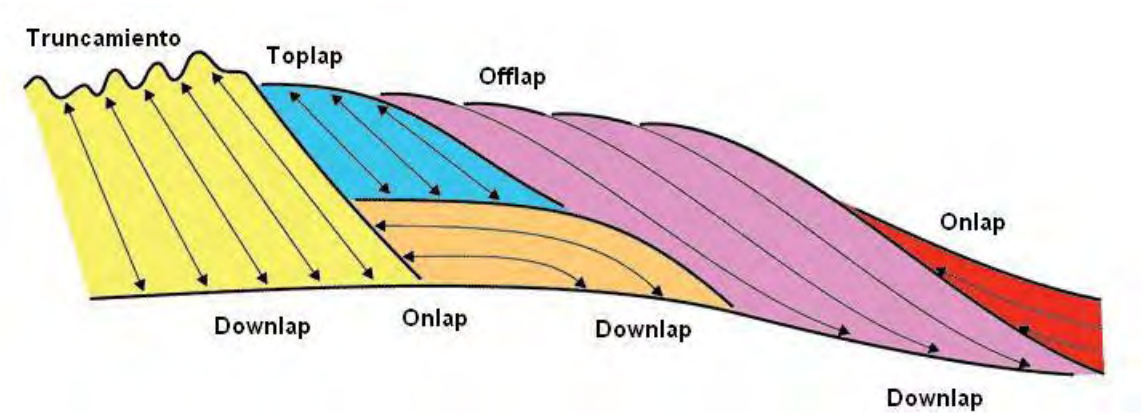

Figure 3-12. Types of seismic reflection terminations (Cataneanu, 2002).

Seismic facies (Fig. 3-13) are the seismic equivalent of the lithofacies. They are three-dimensional units with a specific geometry made up of a relatively homogeneous group of internal reflections associated with the same sedimentary environment. A seismic facies is determined by the parameters that allow the definition of reflectors (amplitude, continuity and frequency), and from the study of the arrangement of the reflections in space (Mitchum and Vail, 1977).

Seismic sequence is a term introduced by Vail et al. (1977) as an equivalent to the term depositional sequence (Mitchum et al., 1977) in seismic stratigraphy. A seismic sequence is defined as a set of genetically related spatially and temporally continuous reflectors, bounded at base and top by discontinuities, or by their correlative continuities developed during consecutive sea-level changes (Vail et al., 1977).

A seismic unit corresponds to a set of genetically related reflectors bounded by discontinuities and their relative continuities. The establishment of seismic sequences and units is based on the study of a series of fundamental aspects recognisable through the study of seismic stratigraphy that allow their individualisation within a stratigraphic series. These are: boundaries, seismic facies, seismic bodies and geometry. These aspects are used both in the establishment of seismic sequences and seismic units (Mitchum et al., 1977, Brown and Fischer, 1980; Alonso et al., 1989). Boundaries are one of the most important criteria in the establishment of seismic sequences and units. Boundaries can have different configurations. For instance, the lower boundary can behave as a concordant surface, or be characterised by onlap or downlap seismic

reflector terminations. The upper boundary of a seismic sequence may consist of a concordant surface, an erosional surface, or correspond to a toplap termination (Mitchum et al., 1977).

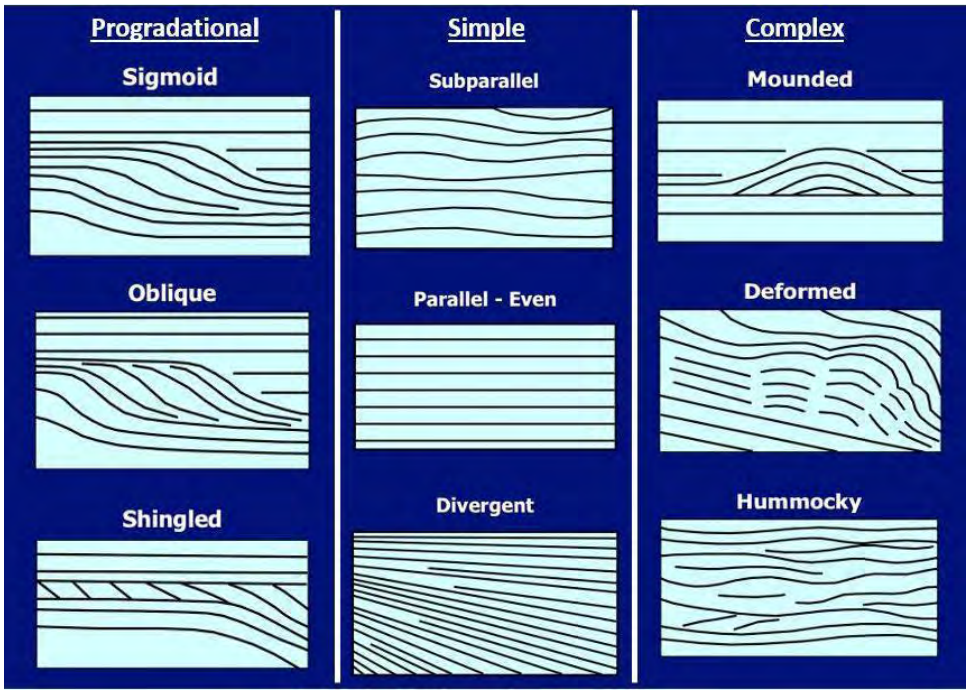

Figure 3-13. Example of different seismic facies types (https://wiki.seg.org/wiki/Seismic_Facies_Classification).

Seismic facies are defined by taking into consideration the geometry of the seismic reflector array, in addition to the characteristics of the seismic reflectors and their configuration (acoustic facies), (Mitchum et al.,1977, Brown and Fischer, 1980). When seismic facies contain sufficient information to relate them to a sedimentary environment or subenvironment, it is possible to establish interpretative seismic facies that allow the definition of sedimentary facies.

PART II

TECTONIC STRUCTURES TRIGGERING CONVULSIVE HAZARDOUS EVENTS

Chapter 4. Tectonic indentation in the central Alborán Sea (Westernmost Mediterranean)

Chapter 5. Imaging the Growth of Recent Faults: The Case of 2016–2017 Seismic Sequence Sea Bottom Deformation in the Alborán Sea (Western Mediterranean)

Chapter 6. Tsunami generation potential of a strike-slip fault tip in the westernmost Mediterranean

Part II of this Ph.D. Thesis deals with the study of convulsive events associated with the tectonic activity of the Alborán Sea and the geological hazards derived from them. Chapters 4, 5 and 6, which make up Part II, analyze the recent seismic and tectonic activity and the potential of some structures to generate tsunamis.

Chapter 4 deals with the tectonic dynamics of the central area of the Alborán basin and analyzes the characteristics of the main faults, framing them in the geodynamic context of the collision between the African and Eurasian plates. Finally, a geological model of tectonic indentation that reflects the dynamics of the central Alborán basin during the Plio-Quaternary is established.

Chapter 5 discusses the recent seismic activity and tectonics in the southern margin of the central Alborán basin area near Al hoceima (Morocco). The seismic activity of one of the most active faults in the area, the Al Idrisi fault and the three seismic shocks that occurred between 1993 and 2017 are discussed in detail. Likewise, the sedimentary instability processes associated with the seismic activity were mapped. Finally, by analyzing the 2016-2017 seismic crisis in relation to the existing onshore/offshore faults, a model of recent fault growth in the Al Hoceima area is proposed.

In Chapter 6, the Averroes fault, defined and characterized in Chapter 4, is studied in depth to determine its tsunamigenic capacity. The mathematical model of tsunami propagation makes it possible to determine the convulsive nature of this event and to determine the areas potentially affected and to what extent.

Chapter 4

Tectonic indentation in the central Alborán Sea (Westernmost Mediterranean)

Ferran Estrada,[1] Jesús Galindo-Zaldívar,[2,3] Juan Tomás Vázquez,[4] Gemma Ercilla,[1] Elia D'Acremont,[5] Belén Alonso[1] and Christian Gorini[5]

[1]Institut de Ciències del Mar, ICM-CSIC, Barcelona 08003, Spain;

[2]Instituto Andaluz de Ciencias de la Tierra, CSIC- UGR, Granada 18071, Spain;

[3]Dpto. de Geodinámica, Universidad de Granada, Granada 18071, Spain;

[4] Instituto Español de Oceanografía, C.O. Málaga, Fuengirola 29640, Spain;

[5] Sorbonne Universités, UPMC Université Paris 06, UMR 7193, ISTeP, F-75005, Paris, France

Published on: Terra Nova, 2018.

Volume 30, pages 24-33

DOI: 10.1111/ter.12304

Impact Factor (JCR): 2.464 (2018), Q2 Geosciences, multidisciplinary. 74/231

ABSTRACT

The Alborán Sea constitutes a Neogene-Quaternary basin of the Betic-Rif Cordillera, deformed since Late Miocene during the collision between the Eurasian and African plates in the westernmost Mediterranean. NNE-SSW sinistral and WNW-ESE dextral conjugate fault sets forming a 75º angle surround a rigid basement spur of the African plate, and are the origin of most of the shallow seismicity of the central Alborán Sea. Northward, the faults decrease their transcurrent slip, becoming normal close to the tip point, while NNW-SSE normal and sparse ENE-WSW reverse to transcurrent faults are developed. The uplifting of the Alborán Ridge ENE-WSW antiform above a detachment level was favoured by the crustal layered structure. In spite of the recent anticlockwise rotation of the Eurasian-African convergence trend in the westernmost Mediterranean, these recent deformations that are consistent with indenter tectonics characterized by N164ºE trend of maximum compression, entailed the highest seismic hazard of the Alborán Sea.

4.1 Introduction

The style of deformation during plate convergence related to build-up mountain belts is a consequence on the rheological behaviour of convergent lithospheres (Pysklywec et al., 2002; Willett et al., 2003; Moore et al., 2005). Similar buoyancy of continental crusts in collisional orogens, in addition to the rigid rheological behaviour of colliding tectonic elements, favours indenter tectonics (Cobbold and Davy, 1988; Davy and Cobbold, 1988) related to escape tectonics (Jacobs and Thomas, 2004). Analogue modelling suggests conjugate sets of transcurrent faults occur when confinement decreases (Tapponier et al., 1982; Davy and Cobbold, 1988). At any rate, conjugate fault sets generally form at a higher angle during indenter tectonics than the classical Anderson model (~60 º; Anderson, 1942), and moreover end suddenly, far away from the deformation front (Tapponier et al., 1982). Many studies have focussed on the Himalayas as the most relevant example of evolved collision in which the presence of rigid crustal blocks led to great heterogeneities in the indenter-tectonic deformation pattern (Molnar and Tapponier, 1975; Coward et al., 1986). The initial stages of collisional processes are poorly known, being mainly analysed in emerged orogenic belts like the Caucasus (Philip et al., 1989) and New Zealand (Pysklywec et al., 2002).

The Alborán Sea (southwestermost Mediterranean) constitutes a natural example of initial stage of continental collision between the Eurasian and African plates (Carminati et al., 2012). It is a main Neogene basin surrounded by the Betic-Rif Cordillera that made up the Arc of Gibraltar (Fig. 4-1) (Comas et al., 1992). Since the Early Oligocene, the Alborán basin shifted westward till the present-day position. During the Early Miocene continental crustal thinning occurred (Vissers et al., 1995), followed by a compressive period since the Late Tortonian and relief uplift that determined the present-day morphology (Sanz de Galdeano and Alfaro, 2004). Several tectonic models for the recent evolution of the area support the subduction activity (Morales et al., 1999; Doglioni et al., 1997, 1999; Gutscher et al., 2002; Ruiz-Constán et al., 2011) and possible roll-back processes (Zeck, 1999; González-Castillo et al., 2015, do Couto et al., 2016) or delamination (Docherty and Banda, 1995; Seber et al., 1996; de Lis Mancilla et al., 2013). All the models hold that the internal zones of the Betic-Rif Cordillera move westward above the Africa-Eurasia plate boundary (Koulali et al., 2011; Palano et al., 2015).

Rheological lithospheric heterogeneities led recent and active deformations with a heterogeneous distribution, thereby favouring indenter and escape tectonics (Chalouan et al., 2006; Chabli et al., 2014). A 30º anticlockwise rotation of Eurasian-African plate convergence trend at 3.16 Ma (Calais et al., 2003) determines at present a N141ºE trend of convergence at a rate of 4.93 mm/yr in the western Mediterranean (GEODVEL models, Argus et al., 2010), supported by GPS data (Fadil et al., 2006; Nocquet, 2012). The region is affected by widespread seismicity (Buforn et al., 1995) taking place in an E-W broad deformation band —over 300 km wide— related to the plate boundary. Diverse proposals regarding the precise location are based on areas with intense seismicity (Fadil et al., 2006), most signaling the importance of the NE-SW Al Idrissi fault zone, in the southern Alborán Sea.

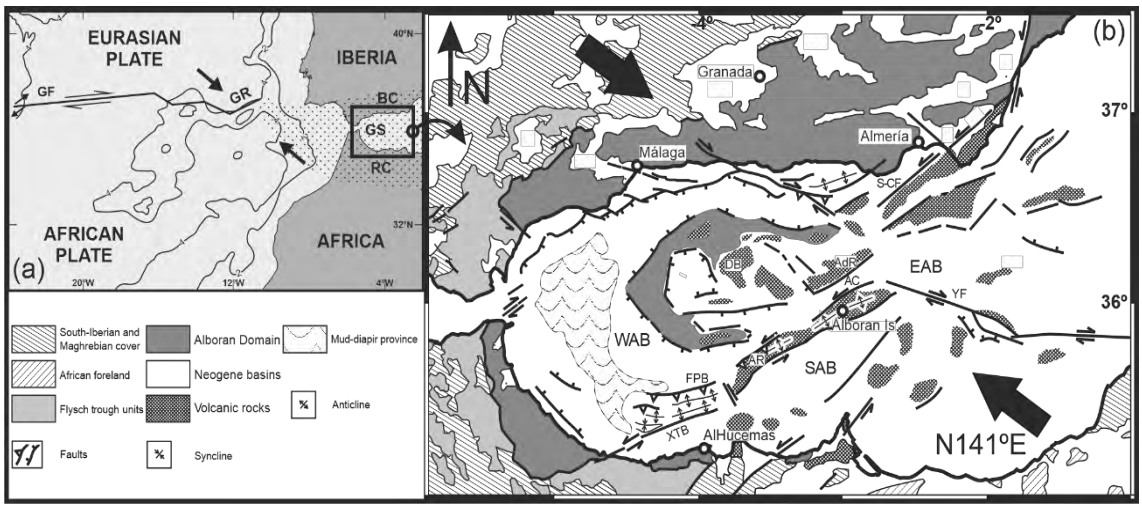

Figure 4-1. Regional setting of the Alborán Sea in the frame of the Eurasian African plate boundary and the westernmost Mediterranean. (a) Plate boundaries in the Azores-Gibraltar area (modified from Galindo-Zaldivar et al. 2003). Dots indicate areas of distributed deformation. BC, Betic Cordillera. GF, Gloria Fault. GR, Gorringe Ridge. GS, Gibraltar Strait. RC, Rif Cordillera. Contour lines in km. (b) Geological sketch of the main structural features and basins of the Alborán Sea (modified from Comas et al. 1999). AR, Alborán Ridge. AC, Alborán Channel. AdR, Adra Ridge. DB, Djibouti Bank. EAB, East Alborán Basin. FPB, Francesc Pagès Bank. SAB, South Alborán Basin. S-CF, Serrata-Carboneras Fault. WAB, Western Alborán Basin. XTB, Xauen-Tofiño Bank. YF, Yusuf Fault. Black arrows indicate present-day direction of shortening.

The Alborán Sea is floored by a thin asymmetric continental crust above an anomalous mantle (Bonini, 1973). Crust reaches about 15 km northward, near the boundary with the Betic Cordillera, and increases southward, to the African margin (up

to 24 km) (Suriñach and Vegas, 1993; Soto et al., 2008; Petit et al., 2015). The crustal structure is formed by a metamorphic basement composed by alpine (Aparicio et al., 1991; Platt et al., 1996) and variscan tectonic units that are thrusted in Betics (Galindo-Zaldívar et al., 1997). The Neogene cover includes sedimentary rocks deposited since the Early Miocene along with basic and intermediate volcanic edifices of Tortonian age (Duggen et al., 2004).

Large magnetic anomaly dipoles are related to ENE-WSW elongated basic rock bodies (Galindo-Zaldívar et al., 1998), the largest one roughly constituting the basement of the Alborán Channel (Fig. 4-2). This active tectonic region is deformed by faults (e.g., Serrata-Carboneras, Yusuf, and Al Idrissi faults) and folds (e.g., Alborán Ridge) (Ammar et al., 2007; Martínez-García et al., 2010) (Fig. 4-1) that determine the main bathymetrical features (Ballesteros et al., 2008; Lafosse et al., 2016). These structures extend northward to the Campo de Dalias, being deformed by ENE-WSW oriented folds developed progressively since the Tortonian (Fig. 4-1); a system of conjugated hybrid and tensional fractures supports ENE-WSW extension and orthogonal NNW-SSE compression (Marín-Lechado et al., 2005; Pedrera et al., 2015). Southwards, deformation extends towards the Rif through the region of Al Hoceima, affected by normal and strike-slip faults (Galindo-Zaldívar et al., 2009, 2015; d'Acremont et al., 2014; Lafosse et al., 2016).

The collisional tectonic setting is highly relevant in the eastern (Robertson, 1988) and western Mediterranean (Ruiz-Constán et al., 2011; Carminati et al., 2012; Roure et al., 2012; Estrada et al., 2014), being the Alborán Sea the best region to analyse the main tectonic features developed in the initial stages, and not yet studied in detail. The aim of this contribution is to analyse the recent and active tectonic deformation of the central Alborán Sea in the framework of recent relative plate motions. Mapping and study of the faults and folds, plus their distribution and relationship with the main crustal structures, will allow us to propose a new model by indenter tectonics for the frica-Eurasia convergence in the Alborán Sea, during an initial stage of continental collision.

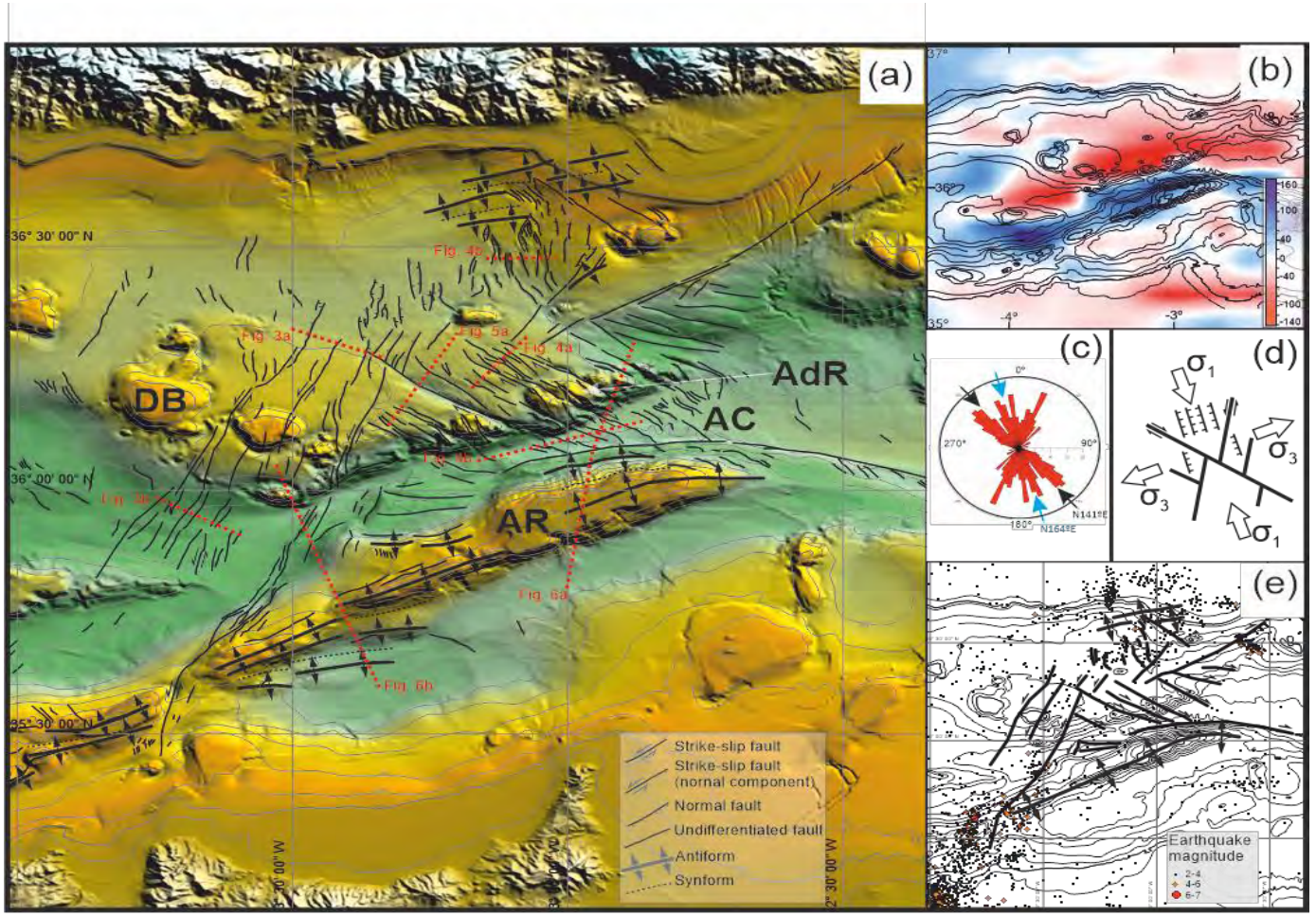

Figure 4-2. Main tectonic features of the central Alborán Basin (a) Detailed tectonic map. AC, Alborán Channel. AdR, Adra Ridge. ALF, Al-Idrisi Fault. AR, Alborán Ridge. CD, El campo de Dalías. DB, Djibouti Bank. FPB, Francesc Pagès Bank. S-CF, Serrata-Carboneras Fault. YF, Yusuf Fault. WAB, Western Alborán Basin. EAB, Eastern Alborán Basin. SAB, Southern Alborán Basin (b) Magnetic anomaly map (nT) and bathymetric contours. Note the dipole bounding the northern side of the Alborán Ridge. (c) Fault set orientation. Blue arrow indicates paleo-plate convergence and black present-day convergence. (d) General structural sketch. (e) Main tectonic structures map and seismicity location since 2000.

4.2 Main tectonic structures

Multibeam bathymetry (Ercilla et al., 2016) masked by the GEBCO bathymetry in areas poorly covered, and multi- and single-channel seismic profiles with different degrees of resolution reveal that both faults and folds deform the Central Alborán Sea since the Miocene (Figs. 4-2 to 4-6). Regional seismicity and morphological features suggest that most of these structures are active (Fig. 4-2a, e).

Faults are distributed in two main well-defined N25ºE sinistral and N130ºE dextral conjugate sets that form an angle of 75º (Fig. 4-2a, c). The strike-slip character is inferred by the roughly vertical fault dip (Figs. 4-3 to 4-5), the displacement of morphological features mainly in the Alborán Channel boundaries (Fig. 4-2a), and earthquake focal mechanisms resembling those of the nearby Al Idrissi fault zone (Martínez-García et al., 2013; d'Acremont et al., 2014). Faults with a normal component and intermediate N130ºE to N170ºE strikes are also recognized, dipping northeastward and southwestward, and mostly affecting recent sediments or even reaching the surface (Figs. 4-3 and 4-4). ENE-WSW faults constitute main structures in the Serrata-Carboneras fault (Gracia et al., 2006) and Alborán Ridge; however, they are scarcely represented in the central fault system (Fig. 4-2a).

The distribution of the fault sets reflects two main fault zones surrounding the South Alborán basement rigid spur attached to the African margin (Fig. 4-2a). The NNE-SSW sinistral fault zone, including the Al-Idrissi fault, reaches lengths of up to 38 km. Meanwhile, the eastern boundary is constituted by the NW-SE dextral set, with the Yusuf Fault zone (120 km length) and other faults reaching 40 km in length.

The Alborán Ridge mainly corresponds to an ENE-WSW elongated southwards vergent antiform (Fig. 4-6) over 120 km long that crosses the northern part of the basement spur and divides the Alborán Sea into the Eastern and Western Alborán basins; it is affected by the Al Idrissi fault, causing a short sinistral displacement with respect to the Frances Pages Bank (Fig. 4-2a). In the Alborán Channel and Northern Alborán Sea, these two sets exhibit cross-cut relationships supporting their simultaneous development, and geometry roughly symmetrical in the central part (Fig. 4-2a). The NW-SE Averroes Fault (Figs. 4-2a and 4-5) is considered representative of the

behaviour of most of these structures. Its strike-slip component, well-marked by the displacement of the northern slopes of the Alborán Channel, decreases northward until becoming normal towards the tip line. Found to the north is a N130º to N170º set of short-length normal faults with both eastward and westward dips; it affects the coast near El Campo de Dalías (Fig. 4-2a), where the presence of ENE-WSW folds with progressive activity since the Late Miocene is also evidenced by seismic profiles and field observations (Pedrera et al., 2015). Finally, the trace of the Serrata-Carboneras Fault is further evidenced by the bathymetry (Fig. 4-2a), although no recent activity can be demonstrated.

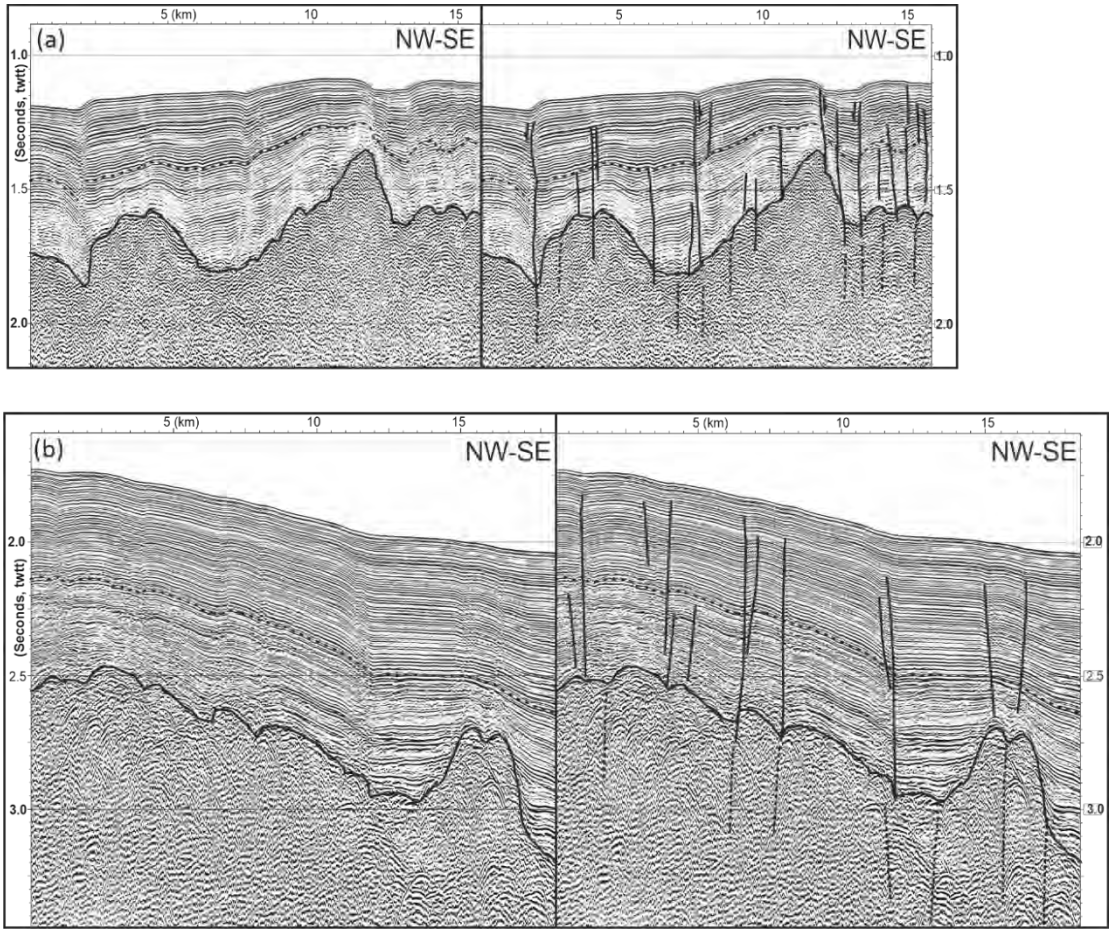

Figure 4-3. Seismic profiles showing NNE-SSW subvertical strike-slip faults of the central Alborán Basin. (a) Strike-slip faults with normal component located in the volcanic edifice of Djibou Bank. (b) Same faults as in figure (a) at the westernmost end of the Alborán Channel. Legend: black line represents the base of Pliocene, and dashed line the base of Quaternary. Scale: vertical in seconds (two-way travel time) and horizontal scale in kilometers. Location in Fig. 4-2

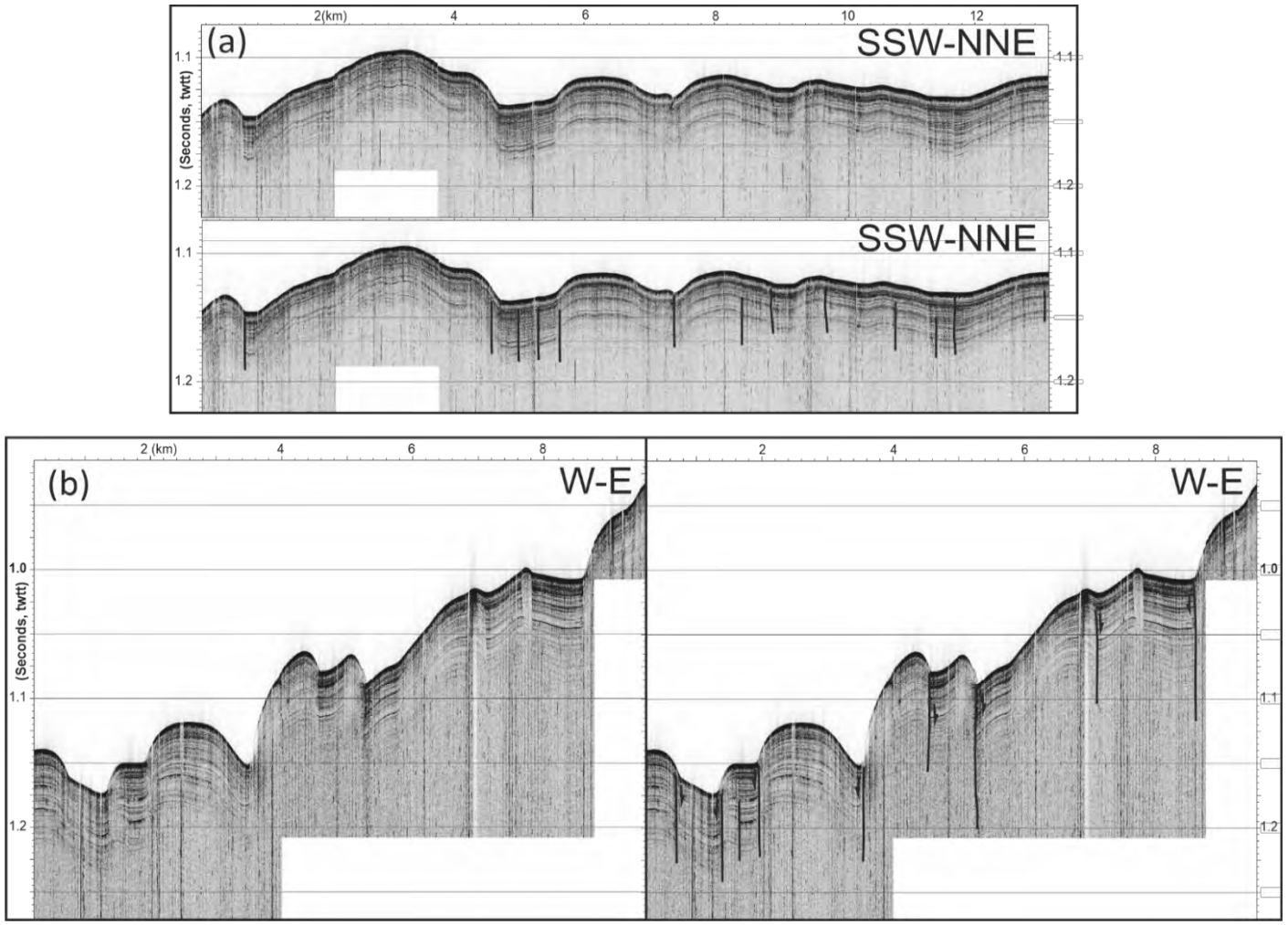

Figure 4-4. Parametric TOPAS profiles showing conjugated subvertical faults affecting the seafloor of the central Alborán Basin (penetration about 60m). (a) Strike-slip faults north of Adra Ridge. (b) Normal faults at the northern end of the conjugated fault system. Scale: vertical in seconds (two-way travel time) and horizontal in kilometers. Location in Fig. 4-2.

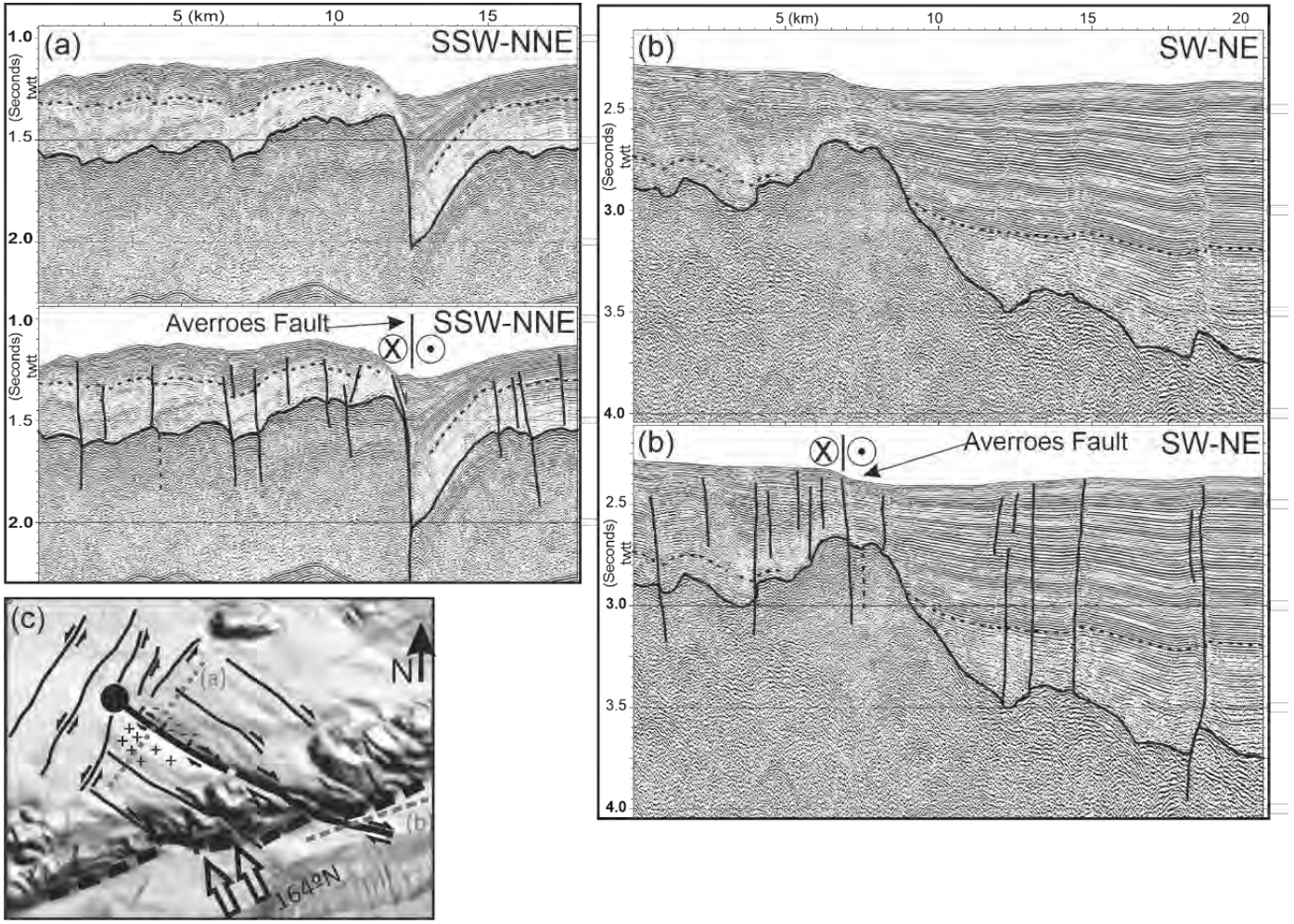

Figure 4-5. Seismic profiles showing the Averroes strike-slip fault in the central zone of the Alborán Basin. (a) Its northern end is characterized by a remarkable normal component, while the southern reach (b) displays a right lateral component. (c) Tectonic sketch of the Averroes fault and profile location (note the 164ºN paleostress vector); positive and negative signs respectively represent uplifted and sunken areas. Black line represents the base of Pliocene, and dashed line the base of Quaternary. Vertical scale in seconds (two-way travel time) and horizontal in kilometers. Location in Fig. 4-2.

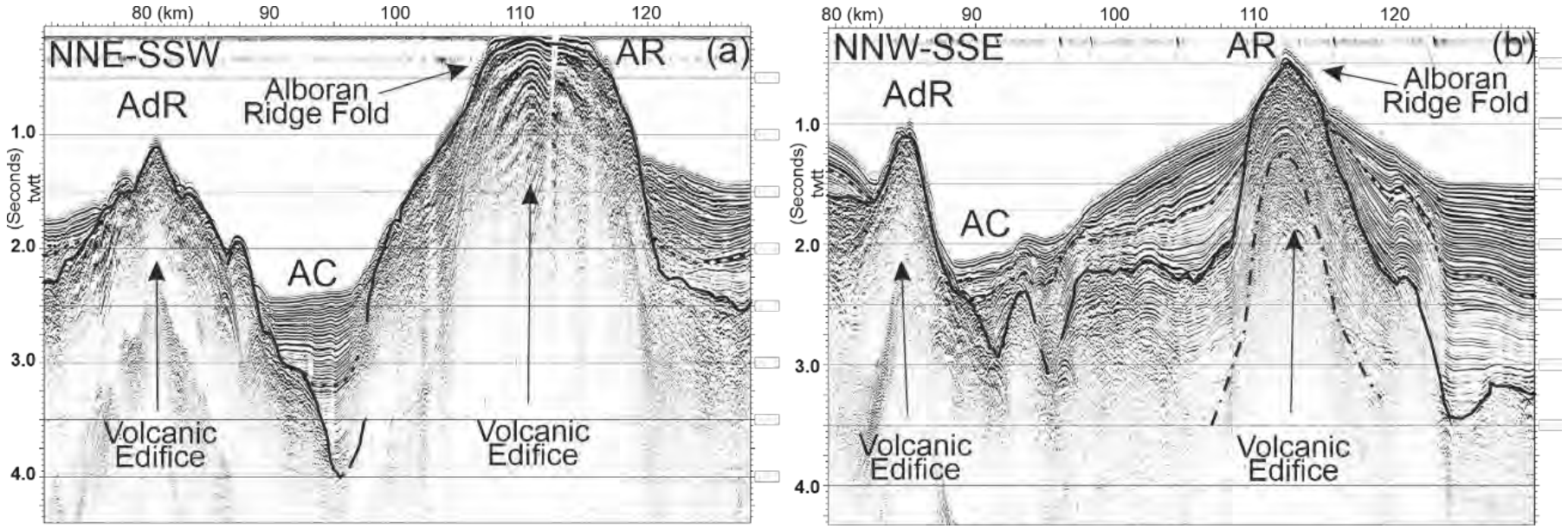

Figure 4-6. Seismic profiles showing the geological structure across the central zone of the Alborán Basin. The Alborán Ridge antiform deforms Miocene deposits and tilts the Plio-Quaternary cover. (a) Eastern Alborán Ridge. (b) Western Alborán Ridge. AR, Alborán Ridge; AC, Alborán Channel; AdR, Adra Ridge. Black line represents the base of Pliocene, and dashed line the base of Quaternary. Vertical scale in seconds (two-way travel time) and horizontal scale in kilometers. Location in Fig. 4-2.

4.3 Discussion and conclusions

Deformation related to the Eurasian-African plate boundary has a heterogeneous distribution in the westernmost Mediterranean. It is concentrated in the central and northern Alborán Sea, floored by easily deformable thin continental crust. The presence of ENE-WSW rigid elongated basic rocks of the Alborán Channel (Fig. 4-2b) and the rigid and resistant to deformation South Alborán basement spur attached to African margin, constitute inherited lithospheric heterogeneities that favours its heterogeneous behaviour (Fig. 4-7). The higher rigidity and resistance to deformation of the South Alborán basement spur versus a less rigid and deformable North Alborán basement is supported by the distribution of recent tectonic deformation and seismicity. The deformation propagated from basement spur towards the northern Alborán Sea, where most of the faults in the sector of thinned continental crust are located. The two sets of conjugate wrench faults, the WNW-ESE dextral fault zone including Yusuf Fault and the NNE-SSW sinistral Al Idrissi fault zone (Figs. 4-2a, c, d, and 4-7), are distributed roughly symmetrically, into two fault zones that reflect the northward basement African margin spur boundaries. A scenario of indenter tectonics is supported by: i) the simultaneous development of the two sets determined from cross-cut relationships (Fig. 4-2a); ii) the northward decrease of the fault slip becoming in some cases normal before the tip point (like the Averroes Fault, Fig. 4-5); and iii) the presence of short irregular NNW-SSE normal faults in the northern Alborán Sea (Fig. 4-2a). The fault system pattern evokes laterally unlocked boundary experiments, developing conjugate faults where the slip decreases, far from the indenter (Tapponier et al., 1982; Davy and Cobbold, 1988). This setting suggests that both the East and West Alborán basins could be free boundaries (Fig. 4-2a), involving fault architecture different from the classical asymmetrical models of Himalaya collision unlocked by one side (Tapponier et al., 1982). Moreover, the 75º conjugate fault angle (Fig. 4-2c, d) exceeds the typical 60º of Anderson (1942) described in the context of indenter tectonics (Tapponier et al., 1982; Davy and Cobbold, 1988).

The presence of the ENE-WSW Alborán Ridge, an isolated antiform affecting the frontal part of the African margin including the basement spur, was likely favoured by the development of detachments at relatively shallow levels that formed during the

collision of a mechanically layered crust (Fig. 4-7). The detachments would have separated the folded sedimentary and volcanic cover from a metamorphic basement. Basement shortening may be accommodated by deep ductile distributed deformation (Fig. 4-7b) or by local thrusting developing pop-up structure (Fig. 4-7c), but there is no evidence of the presence of local subduction. The NE region, near Campo de Dalías, is also deformed by folds suggesting the presence of similar detachment structures (Pedrera et al., 2015). Yet in the Alborán Channel and northern Alborán Sea, the thin crust is intruded by igneous edifices, favouring the development of conjugate strike-slip faults. These sectors evidence how the different behaviour of the continental crust is determined by the intracrustal and basement-sedimentary cover anisotropies. The indenter tectonics is then responsible of the heterogeneous relief in the central Alborán Sea during the closure of the oceanic gateway developing a main barrier separating eastern and western Alborán Sea.

Paleostress determination in view of conjugate fault sets and folds, as the large Alborán Ridge antiform, indicates a N165ºE compressional trend and orthogonal extension (Figs. 4-2 and 4-7) in contrast with the present day N141ºE trend predicted by Geodvel model based on GPS data (Argus et al., 2010). This study reveals that the recent tectonic structures of the central Alborán Sea were formed in an initial stress field, and continue to be active at present despite a recent 30º anticlockwise rotation of the stress axes (Calais et al., 2003).

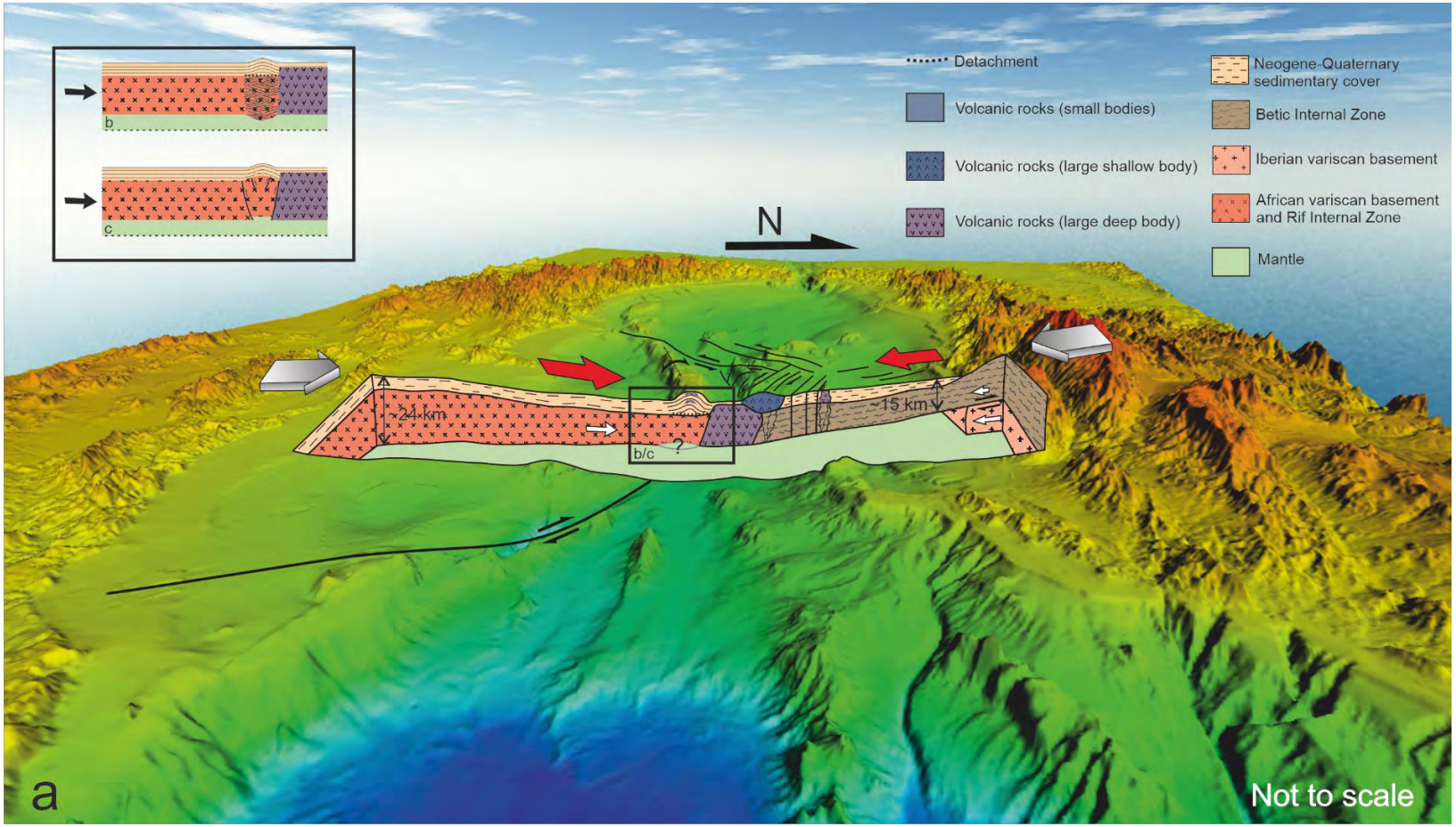

Figure 4-7. Sketch of indenter tectonic deformation of the central Alborán Sea. The model takes into account previous models based on deep crustal structures (Galindo-Zaldívar et al., 1998; Soto et al., 2008) as well as the detailed information available on recent tectonics of the Alborán Sea (e.g. Comas et al., 1992; Maldonado et al., 1992; Ballesteros et al., 2008; Maestro et al., 2008; Martínez- García et al., 2013; d'Acremont et al., 2014; Vázquez et al., 2015; Estrada et al., 2015; Lafosse et al., 2016; Do Couto et al., 2016), integrating the results into a new database of Alborán Sea geophysical data. a) westward oblique view of main structures of Central Alborán Sea (not to scale). Two models of crustal shortening are proposed to explain the Alborán Ridge antiform: b) detach level resulting from crustal thickening by means of deep ductile deformation and c) crustal pop-up through reverse faults.

In summary, the Central Alborán Sea —located in the westernmost Mediterranean between the Western Alborán and the Algerian basins— is a region undergoing the initial stages of continental collision between Eurasian and African crusts of similar buoyancy, deformed by laterally unlocked indentation tectonics. Our tectonic model reveals for the first time the role played by indentation tectonics in the Eurasian-African plate collisional context. This model increases our understanding of recent geodynamic evolution of the Alborán Sea, consequence of the inherited heterogeneities of the African margin that include a rigid spur pushing a frontal rigid basement basic rock body, finally indented in the easily deformable thinned continental crust in the northern Alborán Sea. The indenter structures would therefore be the main deformations accommodating Eurasian-African plate motion in the central Alborán Sea. Al-Idrisi and Yusuf fault zones and the Alborán Ridge antiform constitute the northern boundary between the African Plate and the deformation zone related to the plate boundary, entailing the highest seismic hazard of the region. This tectonic model may have important implications because it can be considered for other Mediterranean regions as well as improve the knowledge of the initial stages of continental collision in other geographic areas, past and present.

4.4 Acknowledgements

Prof. M. Corsini and an anonymous reviewer have improved this contribution. Financed by the projects FAUCES (CTM2015-65461-C2-1-R), DAMAGE (AEI/FEDER CGL2016-80687-R) and RNM 148 projects. We thank to IHS for the Kingdom Suite software educational license.

4.5 References

Ammar, A., Mauffret, A., Gorini, C. and Jabour, H., (2007). The tectonic structure of the Alborán Margin of Morocco. *Revista de la Sociedad Geológica de España*, 20, 247-271.

Anderson, E. M., (1942). The Dynamics of Faulting 1st ed., 206, Olivier and Boyd, Edinburgh, 1942.

Aparicio, A., Mitjavila, J. M., Araña, V. and Villa, M., (1991). La edad del volcanismo de las islas Columbrete Grande y Alborán (Mediterraneo occidental). *Bol. Geol. Miner.*, 102–104, 74–82.

Argus, D.F., Gordon, R. G., Heflin, M.B., Ma, C., Eanes, R. J., Willis, P., Peltier, W. R., and Owen, S. E., (2010). The angular velocities of the plates and the velocity of the Earth's centre from space geodesy. *Geophys*. J. Anderson Int., 18, 1-48.

Ballesteros, M., Rivera, J., Munoz, A., Munoz-Martin, A., Acosta, J., Carbó, A. and Uchupi, E., (2008). Alborán Basin, southern Spain--Part II: Neogene tectonic implications for the orogenic float model. *Marine and Petroleum Geology*, 25, 75–101.

Bonini, W. E., Loomis, T. P. and Robertson, J. D., (1973). Gravity anomalies, ultramafic intrusions, and the tectonics of the region around the Strait of Gibraltar. *JGR*, 78, 1372–1382.

Bonini, M., (2007). Deformation patterns and structural vergence in brittle–ductile thrust wedges: an additional analogue modelling perspective. *Journal of Structural Geology*, 29, 141-158.

Buforn, E., Sanz de Galdeano, C., and Udías, A., (1995). Seismotectonics of the Ibero-Maghrebian region. *Tectonophysics*, 248, 247-261.

Calais, E., De Mets, C. and Nocquet, J.M., (2003). Evidence for a post-3.16-Ma change in Nubia–Eurasia–North America plate motions?. *Earth and Planetary Science Letters*, 216, 81–92.

Carminati, E., Lustrino, M., and Doglioni, C., (2012). Geodynamic evolution of the central and western Mediterranean: Tectonics vs. igneous petrology constraints. *Tectonophysics*, 579, 173-192.

Chabli, A., Chalouan, A., Akil, M., Galindo-Zaldívar, J., Ruano, P., Sanz de Galdeano, C., López-Garrido, A. C., Marín-Lechado, C. and Pedrera, A., (2014). Plio-Quaternary paleostresses in the Atlantic passive margin of the Moroccan Meseta: Influence of the Central Rif escape tectonics related to Eurasian-African plate convergence. *Journal of Geodynamics*, 77, 123-134.

Chalouan, A., Galindo-Zaldívar, J., Akil, V., Marín, C., Chabli, A., Ruano, P., Bargach, K., Sanz de Galdeano, C., Benmakhlouf, M., Ahmamou, M. and Gourari, L., (2006). Tectonic wedge escape in the southwestern front of the Rif Cordillera (Morocco). *Geological Society, London, Special Publications 2006*, 262, 101-118.

Cobbold, P. R., and Davy, P. H., (1988). Indentation tectonics in nature and experiment. 2. *Central Asia, Bull. Geol. Inst. Univ. Uppsala*, 14, 143-162.

Comas, M. C., García-Dueñas, V., and Jurado, M. J., (1992). Neogene tectonic evolution of the Alborán Sea from MCS data. *Geo-Marine Letters*, 12, 157-164.

Comas, M.C., Platt, J.P., Soto, J.I. and Watts, A.B. (1999). The Origin and Tectonic History of the Albora´n Basin: insights from Leg 161 Results. In: Proc. ODP, Sci. Results (Ed. by R. Zahn, M.C. Comas and A. Klaus), Ocean Drilling Program, College Station, TX., 161, 555–580.

Coward, M. P., Rex, D. C., Khan, M. A., Windley, B. F., Broughton, R. D., Luff, I. W., Petterson, M. G. and Pudsey, C. J. (1986). Collision tectonics in the NW Himalayas. *Geological Society, London, Special Publications*, 19, 203-219.

d'Acremont, E., Gutscher, M. A., Rabaute, A., de Lépinay, B. M., Lafosse, M., Poort, J., Ammar, A., Tahayt A., Le Roy, P., Smit, J., do Couto, D., Cancouët; R., Prunier, C., Ercilla, G. and Gorini, C. (2014). High-resolution imagery of active faulting offshore Al Hoceima, Northern Morocco. *Tectonophysics*, 632, 160-166.

Davy, P., and Cobbold, P. R. (1988). Indentation tectonics in nature and experiment. 1. Experiments scaled for gravity. *Bull. Geol. Inst. Univ. Uppsala*, 14, 129-141.

de Lis Mancilla, F., Stich, D., Berrocoso, M., Martín, R., Morales, J., Fernandez-Ros, A., Páez, R. and Pérez-Peña, A. (2013). Delamination in the Betic Range: Deep structure, seismicity, and GPS motion. *Geology*, 41, 307-310.

Docherty, C., and Banda, E. (1995). Evidence for the eastward migration of the Alborán Sea based on regional subsidence analysis: a case for basin formation by delamination of the subcrustal lithosphere?. *Tectonics*, 14, 804-818.

Do Couto, D., Gorini, C., Jolivet, L., Lebret, N., Augier, R., Gumiaux, C., d'Acremont, E., Ammar, A., Jabour, H. and Auxietre, J. L. (2016). Tectonic and stratigraphic evolution of the Western Alborán Sea Basin in the last 25 Myrs. *Tectonophysics*, 677–678, 280–311.

Doglioni, C., Gueguen, E., Sabat, F. and Fernandez, M., (1997). The western Mediterranean extensional basins and the Alpine orogen. *Terra Nova*, 9, 109–112.

Doglioni, C., Gueguen, E., Harabaglia, P. and Mongelli, F., (1999). On the origin of W-directed subduction zones and applications to the western Mediterranean. *Geol. Soc. Spec. Publ.*, 156, 541–561.

Duggen, S., Hoernle, K., van den Bogaard, P. and Harris, C. (2004). Magmatic evolution of the Alborán region: The role of subduction in forming the western Mediterranean and causing the Messinian Salinity Crisis. *Earth and Planetary Science Letters*, 218, 91–108.

Ercilla, G., Juan, C., Hernández-Molina, F.J., Bruno, M., Estrada, F., Alonso, B., Casas, D., Farran, M., Llave, E., García, M., Vázquez, J.T., D'Acremont, E., Gorini, C., Palomino, D., Valencia, J., El Moumni, B., Ammar, A. (2016). Significance of bottom currents in deep-sea morphodynamics: An example from the Alborán Sea. *Marine Geology*, 378, 157-170.

Estrada F., Vázquez J.T., Ercilla G., Alonso B., d'Acremont E., Gorini C., Gómez M., Fernández-Puga M.C., Ammar A., El Moumni B. (2014). Inversión tectónica reciente de la zona central de Alborán. In "Una aproximación multidisciplinar al estudio de las fallas activas, los terremotos y el riesgo sísmico", (J. A. Álvarez-Gómez and F. Martín González, eds.). *Segunda reunión ibérica sobre fallas activas y paleosismología*, Lorca, España, 93-96.

Fadil, A., Vernant, P., McClusky, S., Reilinger, R., Gomez, F., Ben Sari, D., Mourabit, T., Feigl, K. and Barazangi, M. (2006). Active tectonics of the western Mediterranean: geodetic evidence for rollback of a delaminated subcontinental lithospheric slab beneath the Rif Mountains, Morocco. *Geology*, 34, p. 529.

Galindo-Zaldivar, J., Jabaloy, A., Gonzalez-Lodeiro, F. and Aldaya, F. (1997). Crustal structure of the central sector of the Betic Cordillera (SE Spain). *Tectonics*, 16, 18-37.

Galindo-Zaldivar, J., Gonzalez-Lodeiro, F., Jabaloy, A., Maldonado, A., and Schreider, A. A., (1998). Models of magnetic and Bouguer gravity anomalies for the deep structure of the central Alborán Sea basin. *Geo-Marine Letters*, 18, 10-18.

Galindo-Zaldívar, J., Maldonado, A. and Schreider, A. A., (2003). Gorringe Ridge gravity and magnetic anomalies are compatible with thrusting at a crustal scale. *Geophysical Journal International*, 153, 586-594.

Galindo-Zaldívar, J., Chalouan, A., Azzouz, O., Sanz De Galdeano, C., Anahnah, F., Ameza, L., Ruano, P., Pedrera, A., Ruiz-Constán, A., Marín-Lechado, C., Benmakhlouf, M., López-Garrido, A. C., Ahmamou, M., Saji, R., Roldán-García, F. J., Akil, M. and Chabli, A., (2009). Are the seismological and geological observations of the Al Hoceima (Morocco, Rif) 2004 earthquake (M= 6.3) contradictory?. *Tectonophysics*, 475, 59-67.

Galindo-Zaldívar, J., Azzouz, O., Chalouan, A., Pedrera, A., Ruano, P., Ruiz-Constán, A., Sanz de Galdeano, C., Marín-Lechado, C., López-Garrido, A. C., Anahnah, F. and Benmakhlouf, M., (2015). Extensional tectonics, graben development and fault terminations in the eastern Rif (Bokoya–Ras Afraou area). *Tectonophysics*, 663, 140-149.

Gonzalez-Castillo, L., Galindo-Zaldivar, J., de Lacy, M. C., Borque, M. J., Martinez-Moreno, F. J., García-Armenteros, J. A., and Gil, A. J. (2015). Active rollback in the Gibraltar Arc: Evidences from CGPS data in the western Betic Cordillera. *Tectonophysics*, 663, 310-321.

Gràcia, E., Pallàs, R., Soto, J.I., Comas, M., Moreno, X., Massana, E., Santanach, P., Díez, S., García, M. and Dañobeitia, J. (2006). Active faulting offshore SE Spain (Alborán Sea): implications for earthquake hazard assessment in the Southern Iberian Margin. *Earth Planet. Sci. Lett*., 241, 734–749.

Gutscher, M. A., Malod, J., Rehault, J. P., Contrucci, I., Klingelhoefer, F., Mendes-Victor, L., and Spakman, W. (2002). Evidence for active subduction beneath Gibraltar. *Geology*, 30, 1071-1074.

Huiqi, L., McClay, K. R., and Powell, D. (1992). Physical models of thrust wedges. In *Thrust tectonics* (pp. 71-81). Springer Netherlands.

Jacobs, J. and Thomas, R. J. (2004). Himalayan-type indenter-escape tectonics model for the southern part of the late Neoproterozoic–early Paleozoic East African– Antarctic orogeny. *Geology*, 32, 721–724.

Koulali, A., Ouazar, D., Tahayt, A., King, R. W., Vernant, P., Reilinger, R. E., McClusky, S., Mourabit, T., Davila, J. M. and Amraoui, N. (2011). New GPS constraints on active deformation along the Africa–Iberia plate boundary. *Earth and Planetary Science Letters*, 308, 211–217.

Lafosse, M., d'Acremont E., Rabaute A., Mercier de Lépinay B., Tahayt A., Ammar A., Gorini C. (2016). Imagery of recent offshore tectonic Quaternary structures of the Nekor basin (Morocco): evidence of an offshore/ onshore transtensive basin. *Tectonophysics*, 632, 160-166.

Maestro-González, A., Bárcenas, P, Vázquez, J. T. and Díaz-del-Río V. (2008). The role of basement inheritance faults in the recent fracture system of the inner shelf around Alborán Island, Western Mediterranean. *Geo-Marine Letters*, 28, 53–64.

Maldonado, A., Campillo, A. C., Mauffret, A., Alonso, B., Woodside, J. M. and Campos, J. (1992). Alborán Sea Late Cenozoic tectonic and stratigraphic evolution. *Geo-Marine Letters*, 12, 179-186.

Marín-Lechado, C., Galindo-Zaldívar, J., Rodríguez-Fernández, L. R., Serrano, I. and Pedrera, A. (2005). Active faults, seismicity and stresses in an internal boundary of a tectonic arc (Campo de Dalías and Níjar, southeastern Betic Cordilleras, Spain). *Tectonophysics*, 396, 81–96.

Martínez-García, P., Soto, J. I. and Comas, M. (2010). Structural analysis and recent tectonics in the central Alborán Sea. *Trabajos de Geología, Universidad de Oviedo*, 30, 44-48.

Martınez-Garcia, P., Comas, M., Soto, J. I., Lonergan, L. and Watts, A. B. (2013). Strike-slip tectonics and basin inversion in the Western Mediterranean: the Post-Messinian evolution of the Alborán Sea. *Basin Research*, 25, 1–27.

Molnar, P., and Tapponnier, P. (1975). Cenozoic tectonics of Asia: effects of a continental collision. *Science*, 189, 419-426.

Moore, V. M., Vendeville, B. C., and Wiltschko, D. V. (2005). Effects of buoyancy and mechanical layering on collisional deformation of continental lithosphere: Results from physical modeling. *Tectonophysics*, *403*, 193-222.

Morales, J., Serrano, I., Jabaloy, A., Galindo-Zaldivar, J., Zhao, D., Torcal, F., Vidal, F. and Gonzalez-Lodeiro, F. (1999). Active continental subduction beneath the Betic Cordillera and the Alborán Sea. *Geology*, *27*, 735-738.

Nocquet, J. M. (2012). Present-day kinematics of the Mediterranean: A comprehensive overview of GPS results. *Tectonophysics*, 579, 220–242.

Palano, M., González, P. J. and Fernández, J., (2015). The Diffuse Plate boundary of Nubia and Iberia in the Western Mediterranean: Crustal deformation evidence for viscous coupling and fragmented lithosphere. *Earth and Planetary Science Letters*, 430, 439–447.

Pedrera, A., Marín-Lechado, C., Galindo-Zaldívar, J. and Lobo, F. J. (2015). Smooth folds favoring gypsum precipitation in the Messinian Poniente marginal basin (Western Mediterranean). *Tectonophysics*, 663, 48–61.

Petit, C., Le Pourhiet, L., Scalabrino, B., Corsini, M., Bonnin, M., and Romagny, A. (2015). Crustal structure and gravity anomalies beneath the Rif, northern Morocco: implications for the current tectonics of the Alborán region. *Geophys. J. Int*, 202, 640-652.

Philip, H., Cisternas, A., Gvishiani, A., and Gorshkov, A. (1989). The Caucasus: an actual example of the initial stages of continental collision. *Tectonophysics*, 161, 1-21.

Platt, J. P., Soto, J. I., and Comas, M. C. (1996). Decompression and high-temperature–low-pressure metamorphism in the exhumed floor of an extensional basin, Alborán Sea, western Mediterranean. *Geology*, 24, 447-450.

Pysklywec, R. N., Beaumont, C., and Fullsack, P. (2002). Lithospheric deformation during the early stages of continental collision: Numerical experiments and comparison with South Island, New Zealand. *Journal of Geophysical Research: Solid Earth*, *107* (B7).

Robertson, A. H. (1998). Tectonic significance of the Eratosthenes Seamount: a continental fragment in the process of collision with a subduction zone in the eastern Mediterranean (Ocean Drilling Program Leg 160). *Tectonophysics*, 298, 63-82.

Roure, F., Casero, P. and Addoum, B. (2012). Alpine inversion of the North African margin and delamination of its continental lithosphere. *Tectonics*, 31 (3).

Ruiz-Constán, A., Galindo-Zaldívar, J., Pedrera, A., Celerier, B., and Marín-Lechado, C. (2011). Stress distribution at the transition from subduction to continental collision (northwestern and central Betic Cordillera). *Geochemistry, Geophysics, Geosystems*, 12.

Sanz de Galdeano, C. S., and Alfaro, P. (2004). Tectonic significance of the present relief of the Betic Cordillera. *Geomorphology*, 63, 175-190.

Seber, D., Barazangi, M., Ibenbrahim, A., and Demnati, A., (1996). Geophysical evidence for lithospheric delamination beneath the Alborán Sea and Rif–Betic mountains. *Nature*, 379, 785-790.

Soto, J. I., Fernández-Ibáñez, F., Fernández, M., and García-Casco, A. (2008). Thermal structure of the crust in the Gibraltar Arc: Influence on active tectonics in the western Mediterranean. Geochem. Geophys. Geosyst., 9 (10).

Suriñach, E., and Vegas, R. (1993). Estructura general de la corteza en una transversal del Mar de Alborán a partir de datos de sísmica de refracción-reflexión de gran ángulo. Interpretación geodinámica. *Geogaceta*, 14, 126-128.

Tapponier, P., Peltzer, A., Le Dain, Y., and Armijo, R. (1982). Propagating extrusion tectonics in Asia: new insights from simple experiments with plasticine. *Geology*, 10, 611-616.

M. Torne, M. Fernandez, M. C. Comas and J. I. Soto (2000). Lithospheric Structure Beneath the Alborán Basin: Results from 3D Gravity Modeling and Tectonic Relevance. *Journal of Geophysical Research*, 105, 3209-3228.

Vazquez, J.T., Alonso, B., Fernandez-Puga, M.C., Gomez-Ballesteros, M., Iglesias, J., Palomino, D., Roque, C., Ercilla, G., Diaz-Del-Rio, V. (2015). Seamounts along the Iberian continental margins. *Boletin Geologico y Minero*, 126, 483-514.

Vissers, R. L. M., Platt, J. P., and Wal, D. (1995). Late orogenic extension of the Betic Cordillera and the Alborán Domain: a lithospheric view. *Tectonics*, 14, 786-803.

Willett, S., Beaumont, C., and Fullsack, P. (1993). Mechanical model for the tectonics of doubly vergent compressional orogens. *Geology*, 21, 371-374.

Zeck, H. P. (1999). Alpine plate kinematics in the western Mediterranean: a westward-directed subduction regime followed by slab roll-back and slab detachment. *Geological Society, London, Special Publications*, 156, 109-120.

Chapter 5

Imaging the Growth of Recent Faults: The Case of 2016–2017 Seismic Sequence Sea Bottom Deformation in the Alborán Sea (Western Mediterranean)

J. Galindo-Zaldivar[1,2], G. Ercilla[3] , F. Estrada[3] , M. Catalán[4], E. d'Acremont[5], O. Azzouz[6], D. Casas[7], M. Chourak[6], J. T. Vazquez[8], A. Chalouan[9], C. Sanz de Galdeano[1], M. Benmakhlouf[10], C. Gorini[5], B. Alonso[3], D. Palomino[8], J. A. Rengel[11], and A. J. Gil[12,13]

[1]Instituto Andaluz de Ciencias de la Tierra, CSIC-UGR, Granada, Spain.
[2]Departamento de Geodinámica, Universidad de Granada, Granada, Spain.
[3]Institut de Ciències del Mar, GMC, ICM-CSIC, Barcelona, Spain.
[4]Real Instituto y Observatorio de la Armada, San Fernando, Spain.
[5]Sorbonne Universités, UPMC Université Paris 06 UMR 7193, ISTeP, Paris, France.
[6]Université Mohammed Premier, Oujda, Morocco.
[7]Instituto Geológico y Minero de España, Madrid, Spain.
[8]Instituto Español de Oceanografía, Fuengirola, Spain.
[9]Faculté des Sciences, Université Mohammed V-Agdal, Rabat, Morocco,
[10]Faculté des Sciences, Université Abdelmalek Essaadi, Tetouan, Morocco.
[11]Instituto Hidrográfico de la Marina IHM, Cádiz, Spain.
[12]Departamento Ingenieria Cartográfica, Geodesia y Fotogrametría, Universidad de Jaén, Jaén, Spain.
[13]CEACTierra, Universidad de Jaén, Jaén, Spain.

Key Points:

• The 2016–2017 seismic sequence is related to the wide NNE-SSW sinistral fault zone located in the central part of the Alborán Sea.
• Epicentral sea bottom deformations include mass transport deposits and recent faults.
• Seismicity and sea bottom deformations are located west of the main Al Idrisi Fault, supporting the westward widening of the fault zone.

Published on: Tectonics, 2018.

Volume 37, pages 2513-2530

DOI: 10.1029/2017TC004941.

Impact Factor (JCR): 3.975 (2018), Q1 Geochemistry & Geophysics. 14/84

ABSTRACT

The Eurasian-African NW-SE oblique plate convergence produces shortening and orthogonal extension in the Alborán Sea Basin (westernmost Mediterranean), located between the Betic and Rif Cordilleras. A NNE-SSW broadband of deformation and seismicity affects the Alborán central part. After the 1993–1994 and 2004 seismic series, an earthquake sequence struck mainly its southern sector in 2016–2017 (main event Mw = 6.3, 25 January 2016). The near-surface deformation is investigated using seismic profiles, multibeam bathymetry, gravity and seismicity data. Epicenters can be grouped into two main alignments. The northern WSW-ENE alignment has reverse earthquake focal mechanisms, and in its epicentral region recent mass transport deposits occur. The southern alignment consists of a NNE-SSW vertical sinistral deformation zone, with early epicenters of higher-magnitude earthquakes located along a narrow band 5 to 10-km offset westward of the Al Idrisi Fault. Here near-surface deformation includes active NW-SE vertical and normal faults, unmapped until now. Later, epicenters spread eastward, reaching the Al Idrisi Fault, characterized by discontinuous active NNE-SSW vertical fractures. Seismicity and tectonic structures suggest a westward propagation of deformation and the growth at depth of incipient faults, comprising a NNE-SSW sinistral fault zone in depth that is connected upward with NW-SE vertical and normal faults. This recent fault zone is segmented and responsible for the seismicity in 1993–1994 in the coastal area, in 2004 onshore, and in 2016–2017 offshore. Insights for seismic hazard assessment point to the growth of recent faults that could produce potentially higher magnitude earthquakes than the already formed faults.

5.1 Introduction

Continuous plate motion has led to the activity of tectonic structures developed along plate boundaries, including faults with related seismicity. Seismic or creep behavior of a fault is constrained by the rheology of the deformed rocks (Sibson, 1977). Brittle deformation is generally accommodated by previous fractures because the low cohesion with respect to the undeformed host rock causes them to be more easily reactivated (Anderson, 1951; Bott, 1959). When deformation propagates, the growth of fault zones is produced by stress concentrations at the boundaries of previous fault surfaces (Scholz, 2002), and the larger the fault, the higher the magnitude of the related earthquakes (Wells and Coppersmith, 1994). The activity of a fault requires the shear stress on its surface to exceed the values of cohesion and friction (Hajiabdolmajid et al., 2002). On a fault surface, the cohesion is low and needs lower shear stresses than on the new developing fault segments at the edge of the previous fault (Hajiabdolmajid et al., 2002). Thus, the propagation of a fault in unfractured resistant rocks can imply a high accumulation of elastic energy that may generate earthquakes of magnitudes higher than those triggered by a reactivation of previous fractures.

The Eurasian-African plate boundary in the Alborán Sea (westernmost Mediterranean) offers a unique research opportunity in a natural example that can provide insights as to the propagation of fault zones (Cowie and Scholz, 1992; Fig. 5-1). The Alborán Basin is a Neogene-Quaternary extensional basin located within the Betic (Spain)-Rif (Morocco) alpine cordilleras, connected by the Gibraltar Arc (Andrieux et al., 1971). The major Trans-Alborán Shear zone (Frasca et al., 2015; Larouzière et al., 1988) accommodated the westward displacement of the Betic-Rif orogen during the development of the Gibraltar Arc.

The Alborán Basin is floored by a thin continental crust made up of the alpine Internal Zone metamorphic complexes, with a Variscan basement located in the southeastern area (Ammar et al., 2007) resting above an anomalous mantle (Comas et al., 1992; Hatzfeld, 1976). The sedimentary infill consists of unconformable Miocene to Quaternary deposits (Comas et al., 1992; Juan et al., 2016).

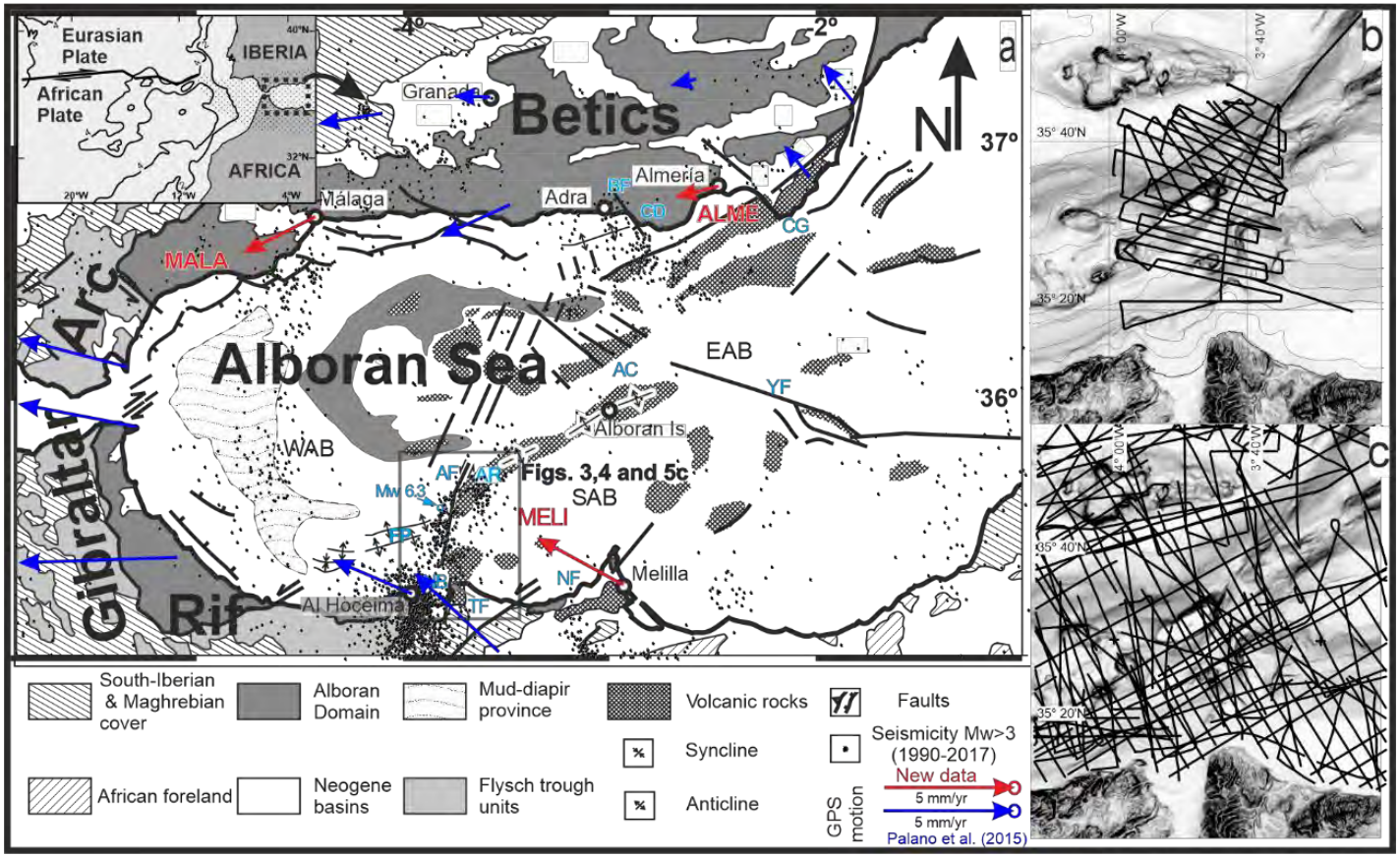

Figure 5-1. Geological setting including regional faults and seismicity. (a) Plate boundaries in the Azores-Gibraltar area (modified from Galindo-Zaldívar et al., 2003) and geological sketch of the main structural features and basins of the Alborán Sea (modified from Comas et al., 1999). Displacement of GPS stations around the Alborán Sea with respect to stable Eurasia are indicated (red arrows). The dotted area within the inset indicates the deformation area. (b) Tracklines of multibeam, very high resolution seismics (TOPAS) and gravity surveyed simultaneously during the INCRISIS cruise. (c) Tracklines of single-channel and multi-channel seismics (airguns) from the ICM database (http://gma.icm.csic.es/sites/default/files/geowebs/OLsurveys/index.htm). Legend: AF, Al Idrisi Fault; AR, Alborán Ridge; AC, Alborán Channel; BF, Balanegra Fault; CD, Campo de Dalías; CG, Cabo de Gata; EAB, East Alborán Basin; FP, Francesc Pagès seamount; NB, Nekor Basin; NF, Nekor Fault; SAB, South Alborán Basin; TF, Trougout Fault; WAB, Western Alborán Basin; YF, Yusuf Fault.

This sedimentary record is mostly deformed by two conjugated sets of dextral WNW-ESE and sinistral NE-SW faults and folded by ENE-WSW oriented folds (Estrada et al., 2018; Martínez-García et al., 2017), the Alborán Ridge and Francesc Pagès seamount, pertaining to the main antiforms (Bourgois et al., 1992). The growth of faults and folds takes place in the framework of recent NNW-SSE shortening and regional Eurasian-African plate convergence (de Mets et al., 2015). The Eurasian-African plate boundary shows N-S to NW-SE convergence at present (Fadil et al., 2006; Koulali et al., 2011; Palano et al., 2015), at a rate of 4.93 mm/yr (Argus et al., 2010). Regional present-day ENE-WSW extensional stress is coeval with orthogonal compression, and main stress axes are inclined (de Vicente et al., 2008; Stich et al., 2010).

The Betic-Rif Cordillera and Alborán Sea are affected by a 300-km broad and heterogeneous seismicity band related to the Eurasian-African plate boundary (Buforn et al., 1988). Seismicity generally occurs at shallow crustal levels (Buforn et al., 1995). Intermediate seismicity (40 to 120-km deep) is mainly located along a N-S elongated band in the western Alborán Basin that becomes NE-SW northward (Buforn et al., 2017; López-Casado et al., 2001; Medina and Cherkaoui, 2017; Morales et al., 1999). Deep seismicity (600 to 640-km deep) is scarce but also occurs beneath the central Betic Cordilleras (Buforn et al., 1991, 2011). The area has heterogeneous local stresses probably due to fault interaction (Stich et al., 2010).

Several geodynamic models have been proposed for the region, including delamination (e.g., Lis Mancilla et al., 2013; Seber et al., 1996) or subduction with or without rollback (e.g., González-Castillo et al., 2015; Gutscher et al., 2012; Pedrera et al., 2011; Ruiz-Constán et al., 2011; Spakman et al., 2018), yet discussion remains alive. Moreover, in the central and eastern Alborán Sea, the recent fault system mainly composed by two conjugate WNW-ESE dextral and NNE-SSW sinistral fault sets evidences the activity of continental indentation tectonics (Estrada et al., 2018). Within this structural framework, a present-day zone of deformation with high seismic activity crossing the Alborán Sea—from Al Hoceima in the Rif to Adra and Cabo de Gata in the Betics (Fig. 5-1) oblique to the previous Trans-Alborán Shear zone (Larouzière et al., 1988) has been proposed to be a main plate boundary (Fadil et al., 2006; Grevemeyer et al., 2015). However, relationships with the main tectonic structures observed in the

seafloor have not yet been analyzed in detail. The few available studies (Martínez-García et al., 2013, 2017, and references herein; Estrada et al., 2018) suggest that the NNE-SSW sinistral Al Idrisi Fault is the main structure with recent and present-day activity in the southern Alborán Sea (Fig. 5-1). This fault is connected onshore with the Trougout Fault in the Al Hoceima region (Morocco margin), which bounds the Nekor Basin (d'Acremont et al., 2014; Lafosse et al., 2017), and its propagation toward the Rif is discussed by Galindo-Zaldívar et al. (2009, 2015) and Poujol et al. (2014). The Al Hoceima region is deformed mainly by faults that determine a succession of horsts and grabens, probably developed above crustal detachments (Galindo-Zaldívar et al., 2009, 2015). In the northern Alborán Sea, the fault zone extends onshore toward the Campo de Dalías area, connecting with the Balanegra Fault in the boundary of the Betic Cordillera and Alborán Sea (Marín-Lechado et al., 2010).

The 25 January 2016 marked the onset of a seismic sequence in the central southern Alborán Sea (www.ign.es), with a main shock of Mw = 6.3 (Figs. 5-1 and 5-2) and whose activity continues up to 2017. The área affected extends from the Francesc Pagès seamount and westernmost Alborán Ridge to the Nekor Basin. The main earthquake was felt in several coastal cities of northern Morocco and southern Spain, causing economic losses in both countries (http://www.ign.es/resources/noticias/Terremoto_Alborán.pdf). The earthquakes of this seismic sequence have been analyzed in detail by the IGN (www.ign.es), Buforn et al. (2017), Medina and Cherkaoui (2017), and Kariche et al. (2018). They consider different velocity models for epicenter locations, suggesting that activity occurred in the area nearby Al Idrisi Fault, yet they do not compare their results with the more accurate position of this fault obtained by marine geophysical research (Estrada et al., 2018; Lafosse et al., 2017; Martínez-García et al., 2013, 2017). The comparison of seismological and marine geophysical researches clearly shows that the epicenters of the earliest stage of the sequence are located to the west of the Al Idrisi Fault.

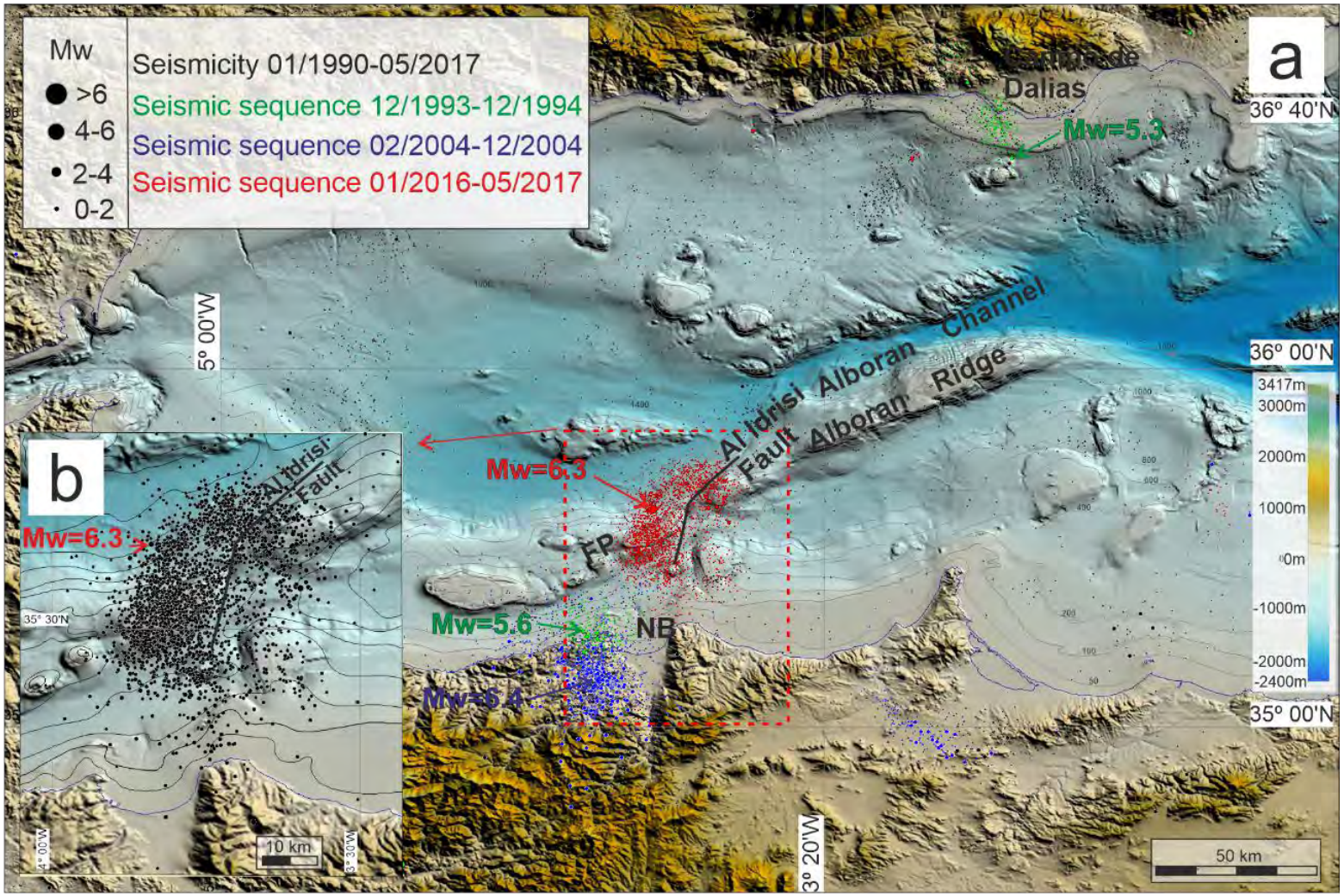

Figure 5-2. Seismicity distribution during the 2016–2017 seismic sequence and other recent seismicity (including 1993–1994 and 2004 series; (2004 seismic sequence from Van der Woerd et al., 2014; other seismicity from www.ign.es database). (a) Epicenters considering a standard velocity model. (b) Relocated epicenters for the highest-magnitude earthquakes of the 2016–2017 seismic sequence according to El Moudnib et al. (2015). Legend: FP, Francesc Pagès seamount; NB, Nekor Basin.

This paper offers a multidisciplinary analysis of the recent and active near-surface tectonic deformations related to the 2016–2017 seismic sequence within the greater context of the 1993–1994 and 2004 sequences in the central Alborán Sea. Our contribution provides insights into the propagation of recent fault zones and how they are linked to seafloor deformations in addition to their relationships with the former Al Idrisi Fault.

5.2 Methodology and Data

The combination of different geodetic and geophysical data made it possible to map the area affected by the 2016–2017 seismic sequence, from the deep structure to near-surface morphology and the overall geodynamic setting.

5.2.1 Regional GPS Data

Permanent GPS stations surrounding the central Alborán Sea served as the reference for present-day deformation in the region. MALA and ALME stations (respectively by Malaga and Almeria) along the Betic Cordillera coast, and MELI (by Melilla) on the African coast, time series were obtained from the EUREF permanent Network. Data were considered up to June 2017, and these stations were in operation: ALME since 2001, MALA since 2005, and MELI since 2012. Global Navigation Satellite System (GNSS) data were processed by means of Bernese Software to determine the displacement vectors.

5.2.2. Seismicity Data

The seismicity database of the Spanish National Geographic Institute (IGN) (www.ign.es) registered the 2016–2017 seismic sequence and the two previous main seismic series, in 1993–1994 and 2004. The 2004 seismic sequence was carefully relocated by Van der Woerd et al. (2014). As the precise location of seismicity is sensitive to velocity models and to the distance of the seismic stations (Michelini and Lomax,

2004), literature (Buforn et al., 2017; Kariche et al., 2018; Medina and Cherkaoui, 2017) shows a noncoincident location for the 2016–2017 seismic sequence' epicenters. The 1993–1994 and 2016–2017 seismic sequences' epicenter and hypocenter locations were calculated through a standard procedure considering the first arrivals of P and S waves and a standard velocity model (Carreño-Herrero and Valero-Zornoza, 2011). A careful relocation of the main events was provided by Buforn et al. (2017) and the IGN (IGN, 2016; www.ign.es) in light of the standard and recent velocity model (El Moudnib et al., 2015). Earthquake focal mechanisms were also obtained from the IGN database (www.ign.es), established from first arrival P wave polarity. The presentday stress tensor was determined from seismicity using the method by Michael (1984), improved by Vavrycuk (2014).

5.2.3. Marine Geophysics

The area affected by the 2016–2017 seismic series was surveyed during the INCRISIS cruise on board the R/V Hesperides in May 2016. A dense grid of 31 survey lines, with a total length of about 900 km, was designed taking into account the regional water depths and the general orientation of the morphological and structural features (Fig. 5-1b). Data positioning was determined via a Global Positioning System (GPS). The studied area was covered by a multibeam SIMRAD EM120 echosounder (frequency 12 kHz) that enabled us to record high-resolution bathymetry. Vertical resolution was approximately 0.025% of water depth. CARIS Hips software was used for multibeam data processing. This bathymetry was integrated with previous data sets in the area (http://gma.icm.csic.es/sites/default/files/geowebs/OLsurveys/index.htm) and gridded at 25 m. Simultaneously with multibeam bathymetry, very high-resolution seismic profiles were acquired with the SIMRAD TOPAS PS18 system (frequencies of 18 kHz to 1 to 6 kHz). In addition to this information, multi-channel and single-channel seismic records from the Instituto de Ciencias del Mar-CSIC database (http://gma.icm.csic.es/sites/default/files/geowebs/OLsurveys/index.htm) were considered (Fig. 5-1c). All seismic profiles were integrated into a Kingdom Suite project (IHS Kingdom) for their correlation and interpretation. Likewise, gravity data were obtained during the INCRISIS cruise using a Lockheed Martin BMG3 marine

gravimeterwith a precision of 0.7 mGal. Gravity Free air and Complete Bouguer anomalies were determined considering a standard density of 2.67 g/cm3. To extend the gravity anomalies to the shoreline, we used the global free air data set from Sandwell et al. (2014). Directional filters (horizontal gravity gradient) were applied in order to analyze the main tectonic structures.

5.3 Results

The area affected by the 2016–2017 seismic sequence is located in the southern sector of the Alborán Sea central part (from 125 to 1,450-m water depth), from the Nekor Basin to the vicinity of Alborán Ridge and Francesc Pagès seamount (Figs. 5-1 and 2). The northern steep side of the Alborán Ridge gives way abruptly to the Alborán Channel, whereas that of the Francesc Pagès seamount evolves to flat-lying seafloor of the deep basin through a terraced-shaped sector that parallels the seamount.

5.3.1 Present-Day Alborán Sea Shortening from GPS Data and Plate Deformation

Deformation within the Alborán Sea is driven in part by the NW-SE regional convergence of the Eurasian and African plates (de Mets et al., 2015). The west to west-southwestward motion of the Betic-Rif Alborán block (Koulali et al., 2011; Palano et al., 2015) may also be the result of ongoing slab rollback toward the west (González-Castillo et al., 2015; Gutscher et al., 2012; Pedrera et al., 2011; Ruiz-Constán et al., 2011; Spakman et al., 2018), which would explain the E-W to ENE-WSW extensional focal mechanisms observed in the West Alborán Sea (Stich et al., 2010). At present, the GEODVEL plate model (Argus et al., 2010) indicates a N141°E trend of convergence at a rate of 4.93 mm/yr in this region, supported by regional GPS data (Fadil et al., 2006). This regional deformation produces an NNW-SSE shortening, which, in the central part of the Alborán Sea, may be constrained by the MALA and ALME stations in Spain and by MELI station in Morocco (Fig. 5-1). The higher rates of MALA station with respect to ALME evidence ENE-WSW extension in the Betic Cordillera (Galindo-Zaldivar, Gil, et al., 2015). The southern displacement of ALME and MALA stations relative to the European Plate contrasts with the northern displacement of MELI, supporting present-day

shortening in the central Alborán Sea. The most intensely seismic area in 2016–2017 is located in between MALA and MELI stations, with a relative NNW-SSE (N173°E) shortening of 3.3 mm/yr.

5.3.2 Recentmost Seismic Sequence

A seismic zone of intense activity affects the central Alborán Sea, from the Campo de Dalias region in the north to the Al Hoceima region in the south (Figs. 5-1 and 2), it being most intense at the southern end (Grevemeyer et al., 2015). The most recent seismic sequences were in 1993–1994, 2004, and 2016–2017 (Fig. 5-2). The 1993–1994 seismic sequence affected the coastal region nearby Al Hoceima, with a main earthquake of Mw = 5.6 (26 May 1994), after an earlier earthquake in the Campo de Dalías area, of Mw = 5.3 (23 December 1993). In 2004, another seismic sequence with a devastating earthquake event of Mw = 6.4 (24 February) occurred onshore in the Al Hoceima region causing nearly 600 deaths and with aftershocks reaching the Alborán Sea (Van der Woerd et al., 2014). Earthquake focal mechanisms were very similar in all cases, pointing mainly to sinistral strike-slip along the NNE-SSW oriented deformation zone (El Alami et al., 1998; Stich et al., 2006, 2010), although also possible is the activity of WNW-ESE dextral faults in the 2004 sequence that affect Al Hoceima onshore areas (Akoglu et al., 2006; Van der Woerd et al., 2014).

The 2016–2017 seismic sequence (Figs. 5-2 and 5-3) was initiated by a moderate earthquake (21 January 2016, Mw = 5.1) followed closely by a stronger event (25 January, Mw = 6.3) and by a long seismic series of decreasing activity during 2016–2017 (Buforn et al., 2017; Kariche et al., 2018; Medina and Cherkaoui, 2017). The relatively long distances from hypocenters to seismic stations, generally greater than 50 km and in some cases reaching more than 80 km, decrease the quality of earthquake locations. Buforn et al. (2017) recognize average horizontal errors of 5 km and vertical errors of 10 km, comprised between 2 to 10 km horizontally and 3 to 17 km vertically. The location of 2016–2017 seismic activity established by the IGN standard terrain velocity model (Carreño-Herrero and Valero-Zornoza, 2011; Figs. 5-2a and 5-3) or El Moudnib et al. (2015) velocity model (Fig. 5-2b) shows a deformation band with two alignments, the

main one, oriented NNE-SSW, changing sharply to an ENE-WSW trend. Considering the IGN standard terrain velocity model (Carreño-Herrero and Valero-Zornoza, 2011; Figs. 5-2a and 5-3), the NNE-SSW alignment is about 40 km in length and 10–20-km wide and includes shallow earthquakes (<35-km depth) that affect the crust and upper mantle. It is parallel and significantly displaced westward (up to 10 km) with respect to the Al Idrisi Fault (Fig. 5-2). The ENE-WSW alignment, about 20-km long and 10–15-km wide, is located along the northern side of the westernmost Alborán Ridge and the Francesc Pagès seamount and is also characterized by a shallow seismicity (<35 km). During month 1 (January 2016), the seismicity clearly defines the two alignments with widths of less than 10–20 km, the main southern one being displaced 5 to 10 km westward with respect to the trace of the main Al Idrisi Fault (Figs. 5-2 and 5-3a). During month 2 (February 2016), seismic activity decreases and both alignments become wider (10–20 km; Fig. 5-3b). Then, from month 3 (March 2016) to present, seismicity gradually decreased and affected a broader area, more than 15–25-km wide (Fig. 5-3c), in between the one clearly defined in month 1, and bounded eastward by the main trace of Al Idrisi Fault. Buforn et al. (2017) relocate the earthquakes considering El Moudnib et al. (2015) velocity model and also obtain the same pattern formed by two alignments, the NNE-SSW with a westward offset with respect to the Al Idrisi Fault sea bottom location.

The earthquake focal mechanisms of the two seismicity alignments show different behaviors (Fig. 5-3d). The main NNE-SSW alignment is characterized by sinistral earthquake focal mechanisms related to NNE-SSW subvertical faults, roughly parallel to the elongation of the alignment. There is also heterogeneity of earthquake focal mechanisms with inclined P and T axes and normal faults, supporting ENE-WSW extension toward the southern deformation zone. In contrast, the ENE-WSW alignment is characterized by highly homogeneous reverse earthquake focal mechanisms associated with ENE-WSW faults. Present-day stress (Fig. 5-3) supports low NNW (N320°E to N332°E) inclined compression and orthogonal horizontal extension in both segments linked to prolate stress ellipsoids. Inclination is higher (47°) in the main alignment and its axial ratio is closer to triaxial stress.

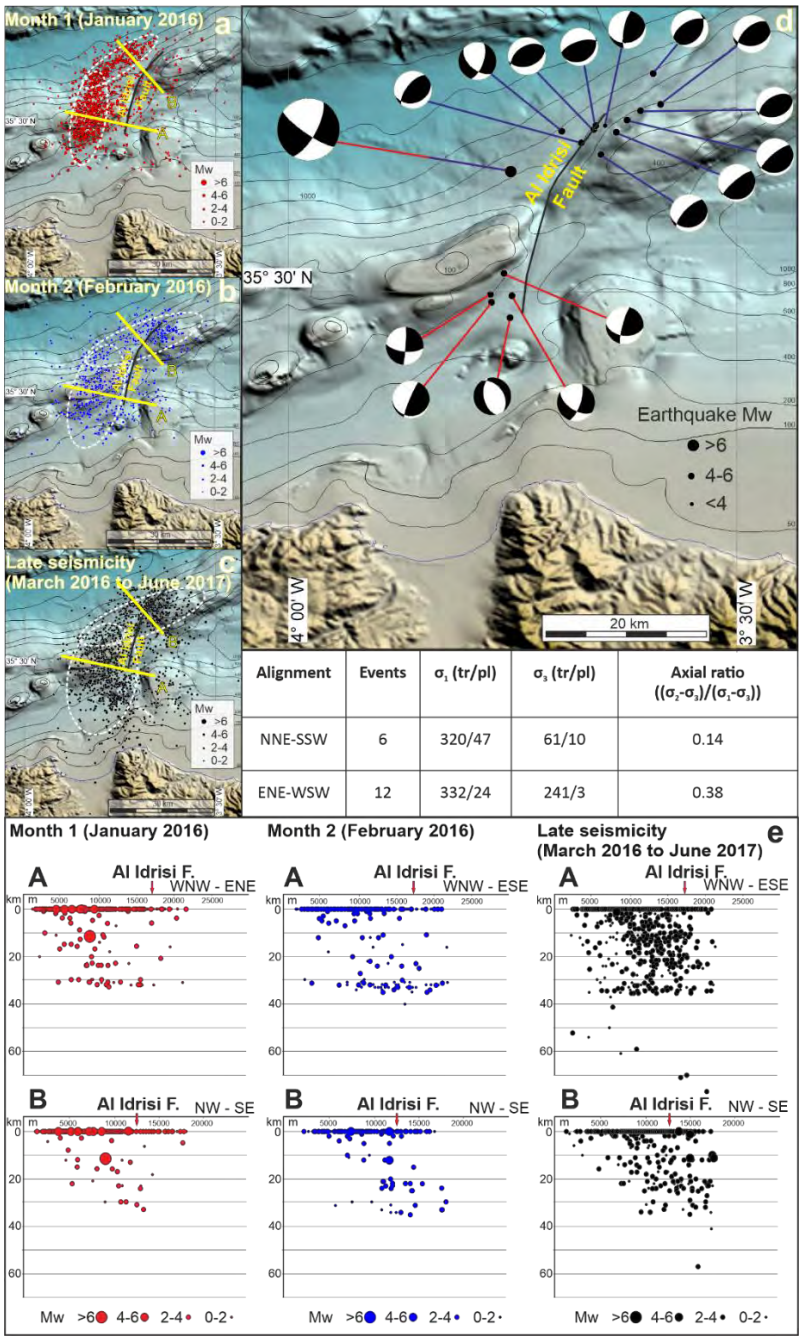

Alignment	Events	σ_1 (tr/pl)	σ_3 (tr/pl)	Axial ratio $((\sigma_2-\sigma_3)/(\sigma_1-\sigma_3))$
NNE-SSW	6	320/47	61/10	0.14
ENE-WSW	12	332/24	241/3	0.38

Figure 5-3. Seismicity during the 2016–2017 seismic sequence. (a) Epicenters month 1 (January 2016). (b) Epicenters month 2 (February 2016). (c) Late epicenters (March 2016 to June 2017). (d) Earthquake focal mechanisms from 2016 to 2017 seismic crisis (data from IGN, www.ign.es). NNE-SSW alignment in red, ENE-WSW alignment in blue. The main earthquake, located at the edge of the two alignments, is shared by the two groups. Present-day stress is determined in the two main sectors of 2016–2017 Alborán Sea seismic crisis area (by the methods of Michael, 1984; improved by Vavrycuk, 2014). (e) Cross sections of seismic activity orthogonal to the main alignments.

5.3.3 Deep Structure from Gravity Data

Bouguer complete gravity anomalies decrease in the Alborán Sea, from 110 to 30 mGal, in a smooth transition from the east to the west up to 4.5°W (Casas and Carbó, 1990). As the amplitude decreases, it narrows to the west, so that the greatest values are located in the central part.

The Bouguer complete anomaly map of the 2016–2017 seismic sequence area and its surroundings shows values between 100 and 10 mGal. Despite some isolated highs, the values decrease progressively from north in the central Alborán to south in the Moroccan margin. Bouguer anomaly highs in the central Alborán (northern part of Fig. 5-4a) support the presence of a local thinning of the continental crust (Galindo-Zaldivar et al., 1998). The shaded relief of the complete Bouguer anomaly map with illumination from the east (Fig. 5-4b) is sensitive to N-S trends and tracks the extension of alignments coming out of Nekor Basin, at least as far as the Alborán Ridge. One alignment (labeled “B” in Fig. 5-4b) nearly parallels the Al Idrisi Fault, though displaced westward. The plots of the 2016–2017 epicenters of earthquakes having magnitude over 3.9, once relocated, show that the southern sector lies over the alignment located in the middle.

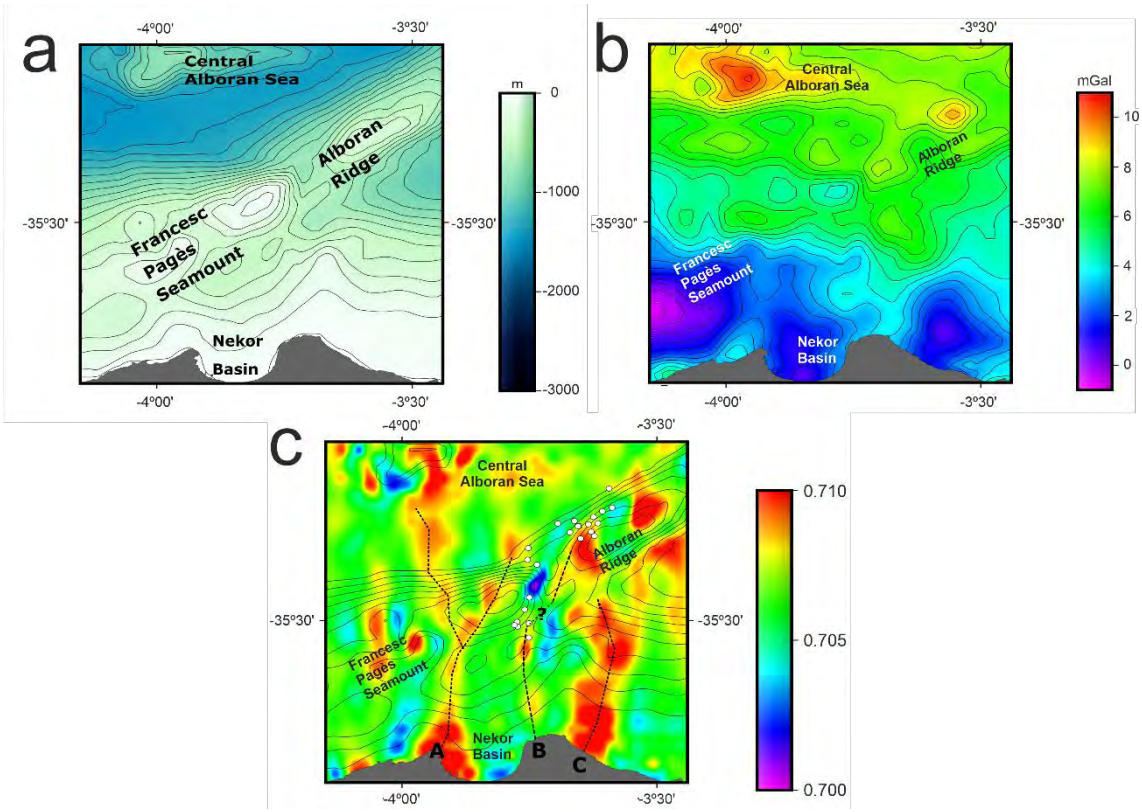

Figure 5-4. Gravity anomaly maps and main tectonic features. (a) Bathymetry map, contour lines every 100 m. (b) Complete Bouguer gravity anomaly map at 2-km resolution. Contour lines every 5 mGal. (c) A shaded relief map (illuminated from the east) of the complete Bouguer gravity anomaly. Black dashed lines denote offshore N-S alignments (labeled as A, B, and C); white dots mark earthquakes with magnitude >3.9; thin contour lines represent bathymetry.

5.3.4 Recent and Active Near-Surface Tectonic and Sedimentary Deformations

The morpho-bathymetric and seismic analysis of the near-surface sediments affected by the 2016–2017 seismic sequence provides evidence of recent and active faults, as well as folds and mass transport deposits (MTDs; Figs. 5-5 to 5-9). MTDs are located on the northern side of the Francesc Pagès seamount and Alborán Ridge, along the ENE-WSW active seismicity alignment and the main earthquake (Figs. 5-5 and 5-6). Based on the thickness of remobilized sediment, small-scale MTDs (a few ms thick) and large-scale MTDs (tens of ms thick) were identified.

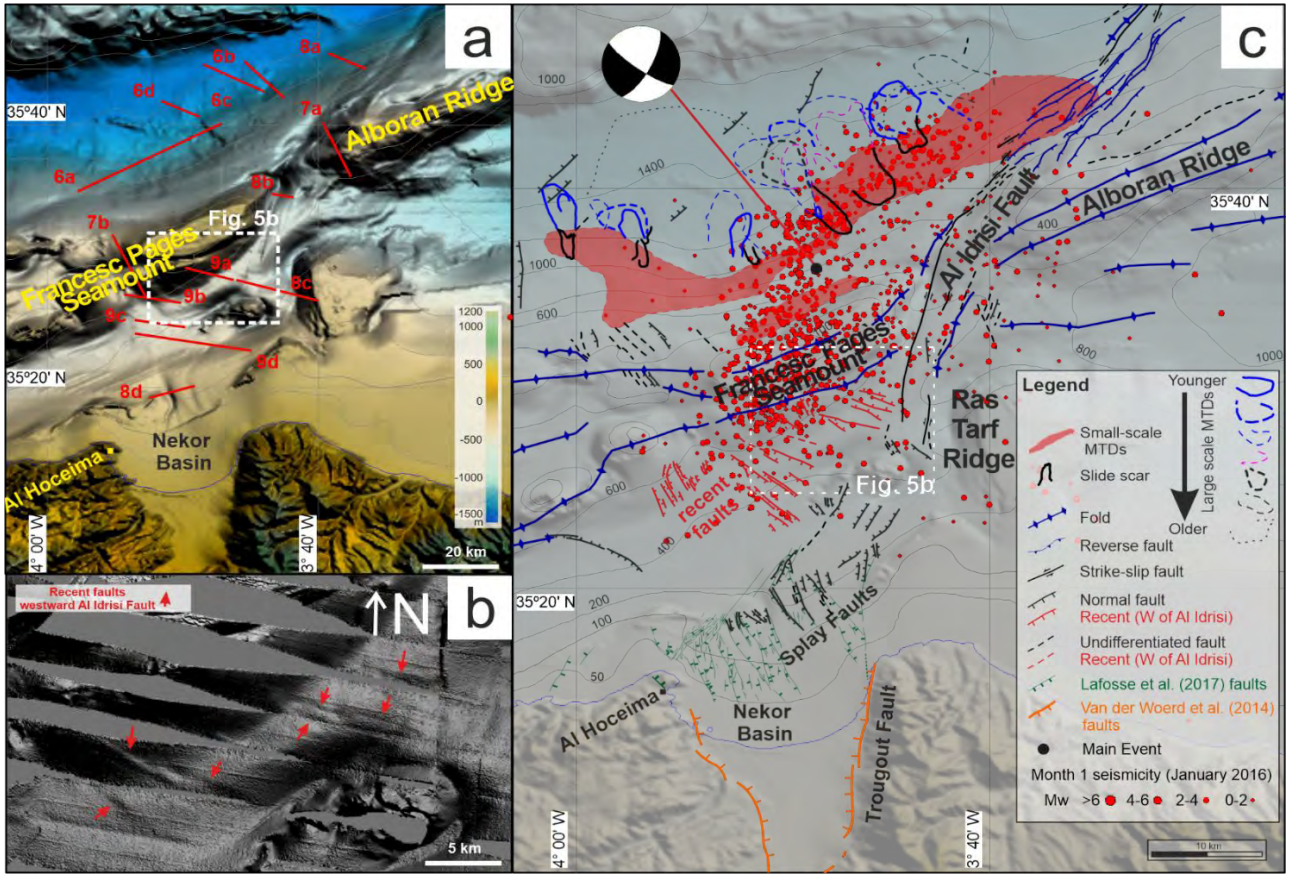

Figure 5-5. Recent sea bottom deformation affecting the 2016–2017 Alborán Sea seismic active area: MTDs, faults, and folds INCRISIS bathymetry integrated withprevious datasets in the (http://gma.icm.csic.es/sites/default/files/geowebs/OLsurveys/index.htm). Data are gridded at a resolution of 25 m. (b) Deta view of recent fault scarps mapped during the INCRISIS multibeam bathymetry. The gray plain areas were not covered by multibeam echosounder. (c) Geomorphological and tectonic map. The INCRISIS TOPAS seismic profiles were also integrated the multi-channel and single-channel seismic records from the Instituto de Ciencias del Mar-CSIC datal (http://gma.icm.csic.es/sites/default/files/geowebs/OLsurveys/index.htm). The 2016 seismicity is from www.ign.es database.

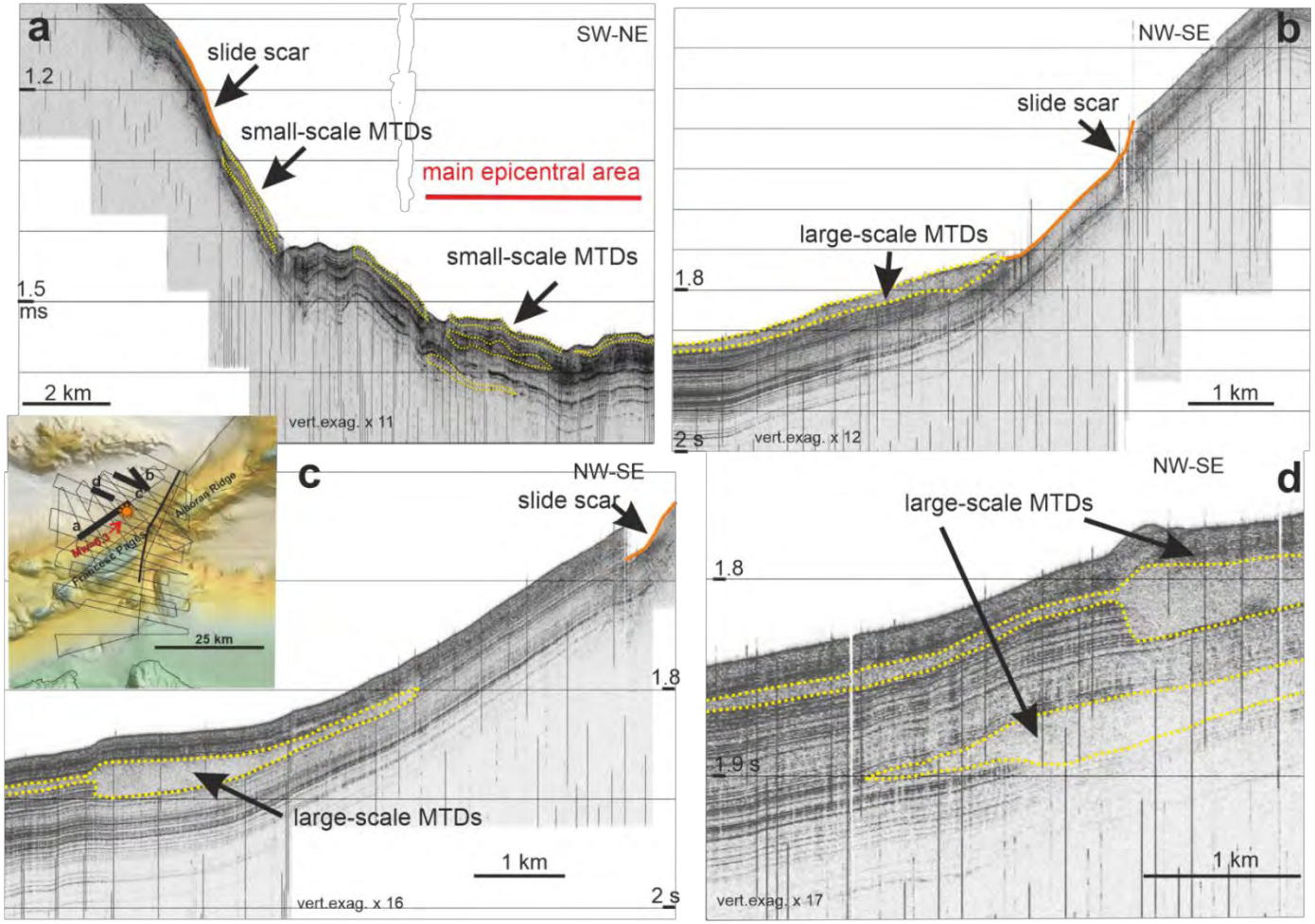

Figure 5-6. Segments of TOPAS seismic records displaying the small- and large-scale MTDs mapped in the ENE-WSW seismicity alignment. Thin vertical discontinuouslines, noise.

The small-scale MTDs occur mostly on the relatively steep slopes (~ < 5°) of the northern side of both seamounts, from >250 to 1,000-m water depth. They appear as vertically stacked subtabular units (a few tens of milliseconds) of unconsolidated deposits and lenticular and irregular bodies of semitransparent, contorted, and discontinuous stratified facies, separated by relatively high reflectivity surfaces with local hyperbolic echoes. The strata pattern suggests the recurrent nature of gravity drive transport. These facies conform an irregular seafloor surface with gentle undulations (metric in scale). The large-scale MTDs mainly occur seaward with respect to the previous ones and extend down to the deep basin (as much as 1,450-m water depth). They are related to slide scars, most of them removing the small-scale MTDs. The slide scars display an amphitheater shape (up to 1-km wide, 40-m relief) recognizable at seafloor, where they extend along a fringe at the foot of the Francesc Pagès seamount. Most of these MTDs are detached from the slide scars and are acoustically defined by lenticular bodies (up to 55-ms thick) internally characterized by semitransparent and discontinuous stratified facies and having a distinctive irregular seafloor surface recognized bathymetrically. Their acoustic character indicates disintegration of the removed mass, just after the initiation of mass flow-type movement. Seismic records also provide evidence of buried largescale MTDs that interrupt and erode the surrounding basinal undeformed stratified facies, suggesting the episodic nature of such slope sedimentary instabilities, at least in recent geological times. Their stratigraphic position points to a simultaneous occurrence of some MTDs (Fig. 5-6).

With respect to the folds, the Alborán Ridge and Francesc Pagès seamount constitute the main antiformal structures deforming the region (Figs. 5-5 and 5-7). The ENE-WSW folds affect Miocene age deposits (Martínez-García et al., 2013). The fold geometry is irregular, with variable wavelengths (kilometer in scale) and vergences (NNW or SSE). In addition, smaller-scale folds (hundreds of meters in scale) are identified in relation to the Al Idrisi Fault (Fig. 5-8), with axes oriented parallel to it.

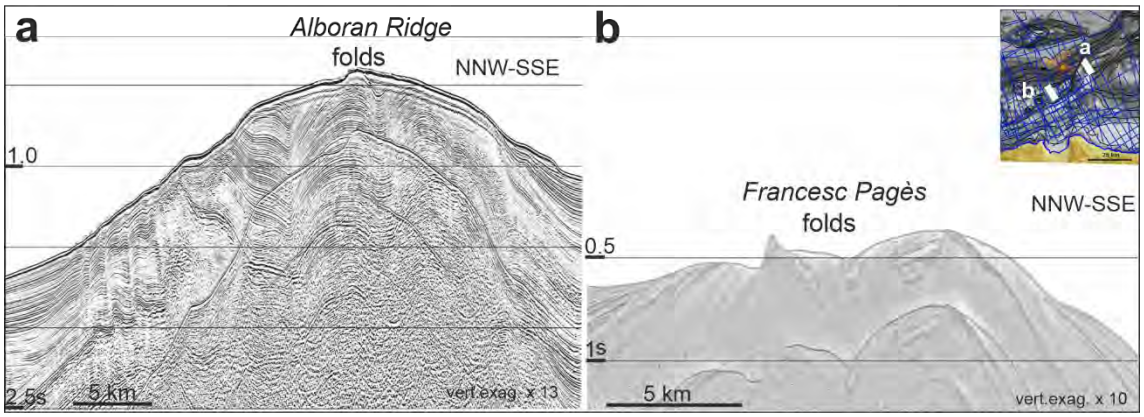

Fig. 5-7. Segments of multi-channel seismic records displaying the (a) Alborán Ridge and (b) Francesc Pagès seamount folds.

The main fracture of morphological and seismic expression, deforming the most recent sediments, is the sinistral Al Idrisi Fault zone (Martínez-García et al., 2011, 2013, 2017; Figs. 5-5 and 5-8). This fault has a 50-km-long northern segment with N35°E trend. It develops a recent fault scarp of about 20 to 30 ms (15 to 23 m) at the northwestern edge of the Alborán Ridge that constitutes the upthrown block (Figs. 5-5 and 5-8). In the hanging wall, small-scale MTDs are recognized. The near-surface sediments in this sector are affected by folds. Al Idrisi Fault changes its direction suddenly to N15°E in the area between the Francesc Pagès seamount and the westernmost end of the Alborán Ridge. Here it is characterized by a sharp elongated depression covered by undeformed recent sediments. The main N15°E southern segment is about 20-km long and extends discontinuously southward, toward the Nekor Basin in relay with the Trougout Fault, forming splay faults (Lafosse et al., 2017). The southern end of Al Idrisi Fault trace is located at a deformation zone with smaller faults reaching the sea bottom (Fig. 5-5). Previous research of earthquake focal mechanisms (Grevemeyer et al., 2015; Martínez-García et al., 2011, 2013, 2017) suggests a sinistral slip on the Al Idrissi Fault NNE-SSW vertical fault plane, further confirmed by the short displacement, roughly 5 km, of the antiformal axis of Alborán Ridge with respect to the Francesc Pagès seamount (Martínez-García et al., 2011, 2013, 2017).

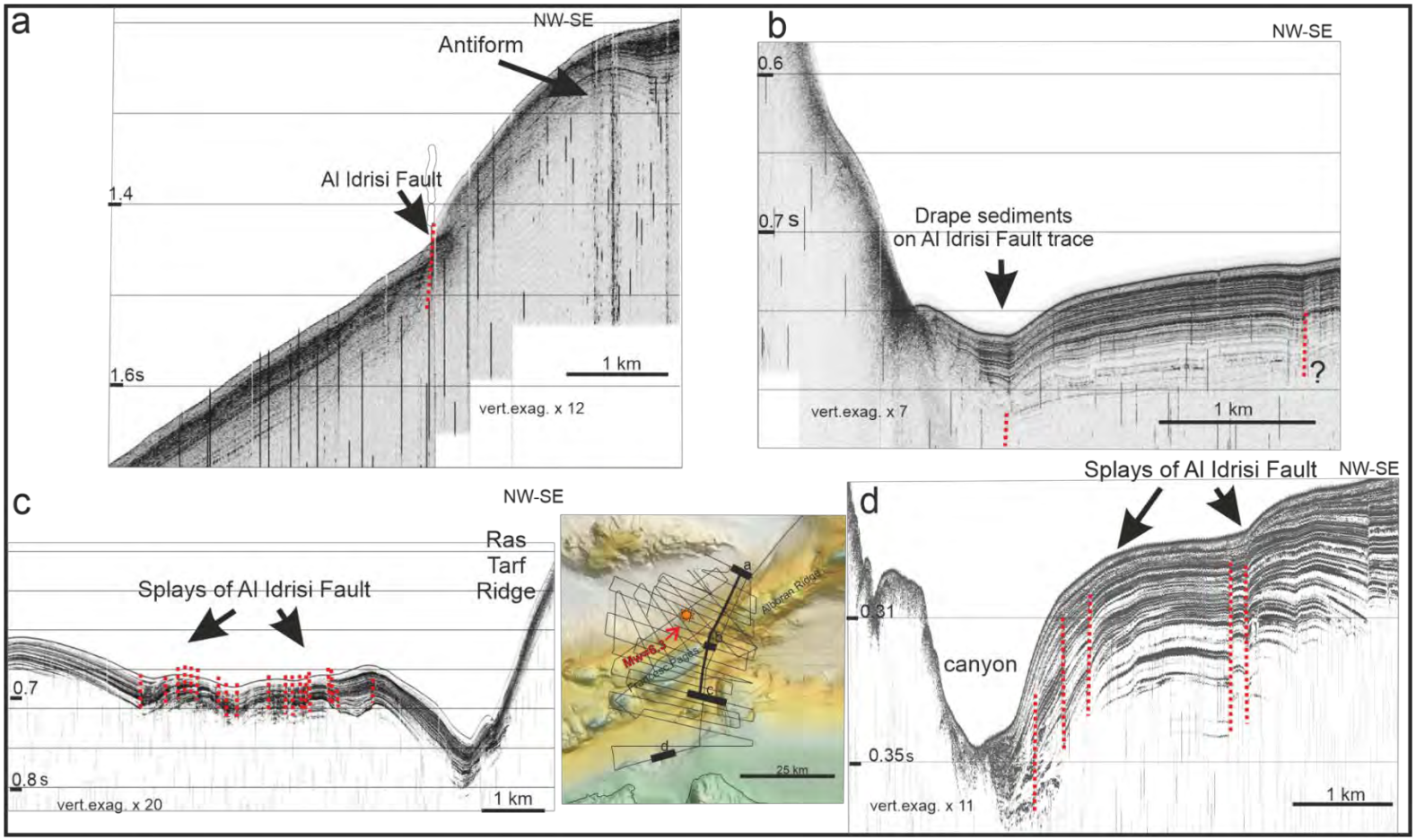

Figure 5-8. Segments of TOPAS seismic records displaying the Al Idrisi Fault deformation along its trace. The fault generally affects recent sediments, although undeformed sediments cover the central part of the fault trace. Thin vertical discontinuous lines, noise.

Our new geomorphological and tectonic map evidences, for the first time, a recent fault zone to the north of the Nekor Basin affected by the 2016–2017 seismic sequence (Figs. 5-5 and 5-9). It is located approximately 5 to 10 km westward of the Al Idrisi Fault, south of Francesc Pagès seamount. Its bathymetric expression (a few meters of relief) correlates with the epicentral area. The faults have NW-SE orientation, with high northeastward or southwestward dips. The very high resolution seismic images of this recent fault zone suggest that they are grouped in conjugate faults with a normal component affecting the most recent sediments, some of them reaching up to the seafloor (Fig. 5-9).

5.4 Discussion

This multidisciplinary focus on the 2016–2017 seismic sequence in the Alborán Sea—in the wake of previous sequences in 1993–1994 and 2004, and the former Al Idrisi Fault—sheds light on the seafloor deformation and relevant implications in terms of geological hazard. The results help to constrain the processes that occur during migration and propagation of active tectonic brittle deformations.

5.4.1 Constraining Active Tectonics: Seismicity and Seafloor Deformations

Epicenters related to wrench faults are expected to be located along the fault zone trace. Vertical nodal planes of earthquake focal mechanisms from the main 2016 earthquake and most of the events in the southern Alborán Sea undoubtedly evidence the vertical dip of the seismic active faults (Fig. 5-3), in agreement with the seismological results of Buforn et al. (2017). Anyway, aftershock sequences can affect a wide zone (e.g., >10-km wide with respect to the main fault during the Landers 1992 seismic sequence; Hauksson et al., 1993) favored by the structural complexity and preexisting structures.

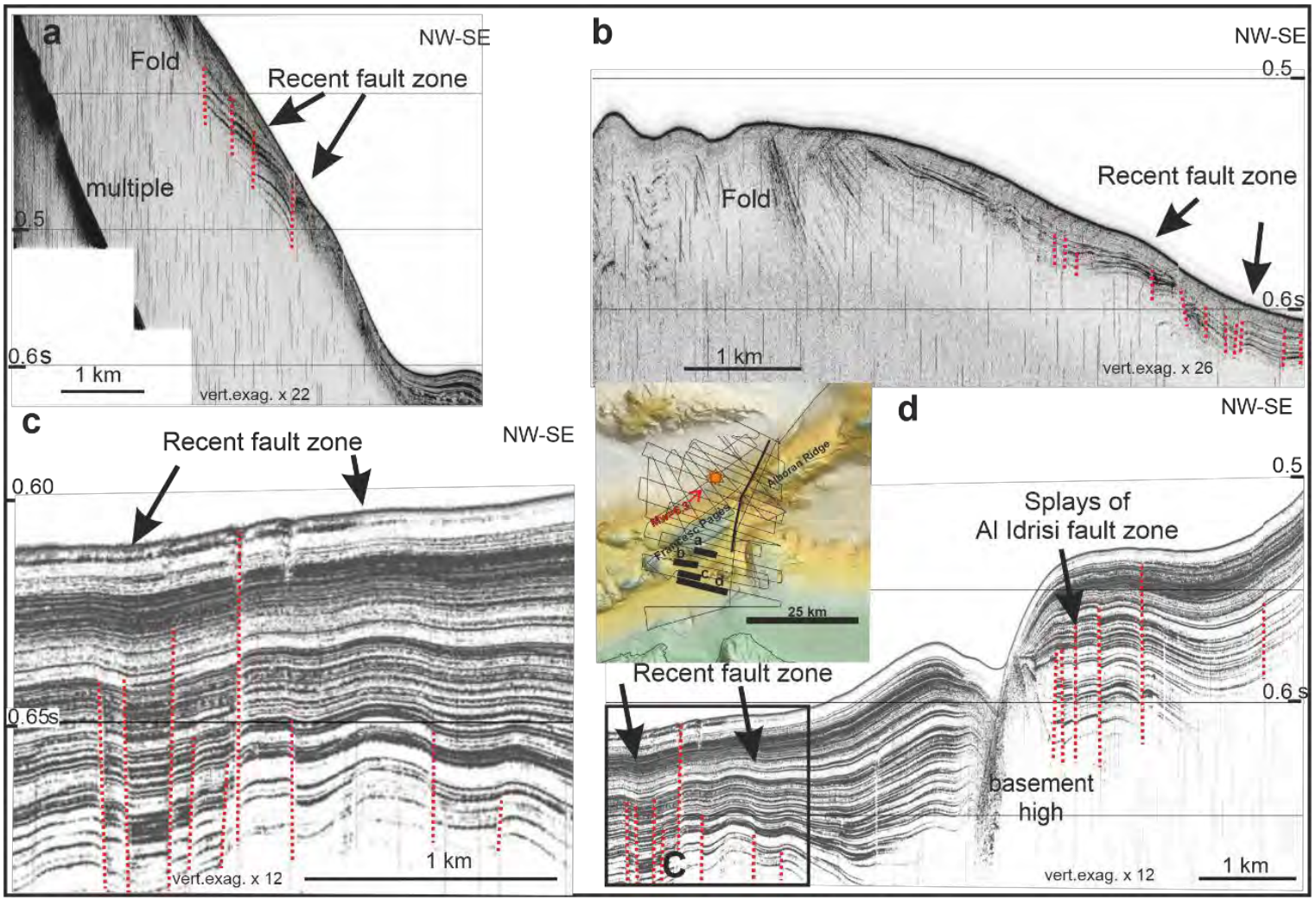

Figure 5-9. Segments of TOPAS seismic records displaying the recent fault zone identified in this study. This zone is located 5 to 10 km westward of the Al Idrisi Fault (d). Thin vertical discontinuous lines, noise.

Despite that Buforn et al. (2017) establish horizontal and vertical errors for the 2016–2017 seismic sequence location, and Buforn et al. (2017) and Medina and Cherkaoui (2017) relate the seismicity with the Al Idrisi Fault, the careful analyses of epicenter locations for most of the NNE-SSW seismicity alignment (IGN, www.ign.es; Buforn et al., 2017; Kariche et al., 2018; Medina and Cherkaoui, 2017) point to that they are displaced westward with respect to the seafloor trace of the Al Idrisi Fault determined by marine geophysical data (Estrada et al., 2018; Martínez-García et al., 2013, 2017; Figs. 5-2, 5-3, and 5-5). This displacement of the earthquakes is higher when the standard velocity model (Carreño-Herrero and Valero-Zornoza, 2011) is considered (IGN, www.ign.es; Kariche et al., 2018; Medina and Cherkaoui, 2017): roughly 10 km for the first stage earthquakes (Figs. 2a and 3a), as opposed to the roughly 5 km (Buforn et al., 2017) with the model by El Moudnib et al. (2015; Fig. 2b). Although the mislocation of earthquakes by the poorly constrained velocity models and far seismic stations may produce a westward shift of the seismicity with respect to the Al Idrisi Fault, all the available seismological studies (IGN, www.ign.es; Buforn et al., 2017; Kariche et al., 2018; Medina and Cherkaoui, 2017) support the offset to the west of the seismicity and fault activity with respect to the former Al Idrisi Fault that roughly constitutes the eastern boundary of the fault zone. Our findings based on the marine geophysical data set demonstrate the development of recent faults west of the former Al Idrisi Fault related to the westward propagation of the deformation (Figs. 5-2, 5-3, and 5-8 to 5-10).

The early earthquakes of the 2016–2017 series are clearly grouped in the two relatively narrow (~10–20-km wide) NNE-SSW and ENE-WSW alignments, starting with the highest magnitude event (Mw = 6.3, 25 January) where they join (Fig. 5-3a). The depth of seismicity is not well constrained because of the variability of crustal velocities and the few and far onshore stations; still, they correspond to crustal levels (<35-km depth), in agreement with Buforn et al. (2017), Medina and Cherkaoui (2017), and Kariche et al. (2018). New seismic faults started to develop at shallow crustal levels (roughly 5 to 10-km depth), as generally occurs in continental crust (Meissner and Strehlau, 1982). If an elliptical fault surface shape is considered (Watterson, 1986), the recent fault should extend in depth northward and southward into the seismogenic crustal layer. When deformation propagates upward, the triggering fault is expected to

reach the seafloor in the NNE-SSW epicenters alignment, due to the high dip of fault plane solutions in most of the earthquake focal mechanisms. According to empirical fault scaling relationships (Wells and Coppersmith, 1994), the main seismic event would be related to a surface rupture between 15 and 20 km and might deform the area. In the 2016–2017 seismic series, a recent fault zone (10–20-km wide) reaching up to the seafloor was recognized in the main NNE-SSW seismicity alignment, south of Francesc Pagès seamount. This recent zone comprises NW-SE oriented conjugated normal faults coeval with the recent sedimentation, reaching different near-surface stratigraphic levels, probably rotating and connecting in depth with the major recent NNE-SSW vertical sinistral fault (Fig. 5-10). These shallow faults accommodate the NE-SW extension compatible with the activity of the main wrench fault and are in agreement with crustal thinning in the Nekor Basin confirmed by Bouguer gravity anomalies (Fig. 5-4); they would be in line with the recent normal faults described by Lafosse et al. (2017) that demonstrate that the Nekor Basin is floored by a set of splay faults with normal slip component related to the southern prolongation of Al Idrisi Fault.

During later earthquakes, the 2016–2017 seismic series deformation extended to a broad 10–20-km-wide fault zone in the NNE-SSW alignment, bounded westward by the recent faults and eastward by the Al Idrisi Fault and the Alborán Ridge. Al Idrisi Fault, in contrast, only deforms discontinuously near-surface sediments along the fault trace by recent or active faults and folds, suggesting the recentmost activity of some segments. Although the discontinuous evidences of activity may be the consequence of a seismic character of Al Idrisi Fault, with segments accumulating elastic deformation before the seismic rupture, alternatively, they could indicate that the activity of those segments has been replaced by that of other recent faults offset to the west.

In the ENE-WSW alignment, the morphostructural pattern and deformation behavior are different. The presence of MTDs (Figs. 5-5 and 5-6) and reverse earthquake focal mechanisms (Fig. 5-3d), and the absence of clear reverse faults affecting the near-surface, would suggest the presence of blind reverse faults at the core of the Alborán Ridge antiform (Fig. 5-10; Martínez-García et al., 2013).

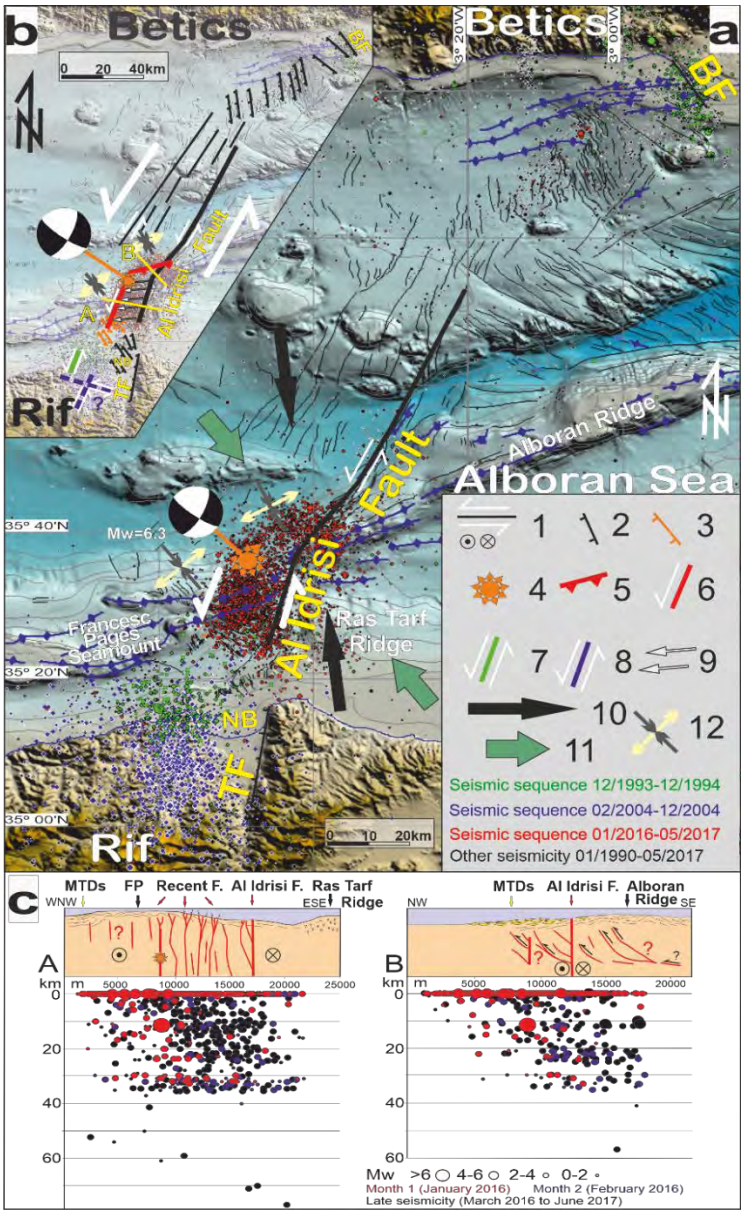

Figure 5-10. Sketch illustrating the westward propagation of recent tectonic and seismic activity in the main NNE-SSW deformation zone crossing the Alborán Sea. (a) Seismicity, main active structures, stress and shortening. The 2004 seismic sequence from Van der Woerd et al. (2014); other seismicity from www.ign.es database. (b) Sketch of main tectonic structures and westward migration of deformation from main Al Idrisi Fault trace. (c) Interpretative cross sections and seismicity orthogonal to the main earthquake alignments: 1, sinistral fault (map and cross section); 2, normal fault; 3, recent normal fault; 4, epicenter of main event (Mw = 6.3, 25 January 2016); 5, active blind thrust; 6, active NNE-SSW sinistral deep vertical crustal fault segment bounding westwards the NNE-SSW 2016–2017 seismicity alignment; 7, active NNE-SSW vertical sinistral crustal fault segment related to the 1993–1994 seismic crisis; 8, active NNE-SSW vertical sinistral crustal fault segment related to the 2004 seismic crisis; 9, offset to the west of recent deformation and seismicity in respect to Al Idrisi Fault; 10, estimated convergence trend from GPS data; 11, regional plate convergence trend; 12, present-day trends of compression and extension determined from earthquake focal mechanisms. FP, Francesc Pagès seamount. MTD, mass transport deposits.

Earthquakes may be assumed to be the main mechanism triggering the MTDs, deforming the near-surface sediment of the ENE-WSW alignment (Figs. 5-5 and 5-6; Casas et al., 2011). The initiation of slope failure is due to cyclic loading applied on the sediment and a decreasing shear strength through the development of pore overpressure. Other factors, such as tectonic deformations resulting in seabed, may also contribute to increasing shear stress on the slope or a decreasing sediment strength due to shearing, dilatancy, and possible sediment creep (Locat and Lee, 2002).

5.4.2 Geodynamic Implications and Seismic Hazard

The former NE-SW sinistral Trans Alborán Shear Zone (Larouzière et al., 1988) constituted a main tectonic structure during the Miocene, later becoming inactive and overprinted by the recent NNE-SSW deformation zone (Stich et al., 2006, 2010) between Campo de Dalías (Balanegra Fault) and the Al Hoceima region (Trougout Fault), including the Al Idrisi Fault (Fig. 5-10). This evolution reveals a progressive offset to the west and rotation of the central Alborán Sea active deformation zone. The recent shear zone has incipient low deformation. Al Idrisi Fault, which constitutes the longest fault in this deformation zone, has short strike-slip, however. It is expressed by low interaction at the edge where the Al Idrisi Fault orientation trace changes and also by the short displacement between the Alborán Ridge and Francesc Pagès seamount antiform axes (Fig. 5-10).

At present, seismological and GPS studies hold the active seismic zone in the central Alborán Sea to be a main weak zone related to the Eurasian-African plate boundary (Buforn et al., 2017; Fadil et al., 2006; Grevemeyer et al., 2015; Medina and Cherkaoui, 2017; Palano et al., 2015). The fact that seismicity occurred near the African coastline in 1994, with maximum magnitude ofMw = 5.6 (26 May), and later propagated toward the continent in 2004 with a main event ofMw = 6.4 on 24 February (e.g., Akoglu et al., 2006; Van der Woerd et al., 2014, and references therein) would indicate that the 2016–2017 seismicity (main eventMw = 6.3) is most likely located within the same regional deformation band (Figs. 5-2 and 5-10), at its northern edge. Accordingly, the recent fault zone exhibits a segmented behavior with the progressive reactivation of 15–20-km length stretches demonstrated by the recent seismic series (1993–1994, 2004,

and 2016–2017; Buforn et al., 2017; Kariche et al., 2018; Medina and Cherkaoui, 2017). In the Rif, seismic faults have rupture in depth but with no clear surface expression (Galindo-Zaldívar et al., 2009; Galindo-Zaldívar, Azzouz, et al., 2015; Van der Woerd et al., 2014). Akoglu et al. (2006) and Van der Woerd et al. (2014) show that seismicity onshore Al Hoceima region has been produced by the activity of NNE-SSW but probably also WNW-ESE conjugated faults in NNW-SSE compression and ENE-WSW orthogonal extensional stresses.

Northward, toward the Betic Cordillera, the deformation zone is connected with the Campo de Dalías and its seismicity during the 1993–1994 series (Marín-Lechado et al., 2005; Fig. 5-10).

The present-day stresses determined from regional seismicity studies (de Vicente et al., 2008; Stich et al., 2010) agree with the data obtained in the context of the 2016–2017 seismic sequence (Figs. 5-3 and 5-10). The NW-SE compression is prolate to triaxial and inclined toward N319°E in the NNE-SSW seismicity alignment, while N332°E in the ENE-WSW alignment, with related orthogonal extension. Thus, compression is rotated in the two alignments and is compatible with sinistral fault kinematics (Fig. 5-10). Whereas at the Earth's surface, main stresses should be horizontal or vertical due to an absence of shear stress (Anderson, 1951; Bott, 1959), the inclination of main compression toward the NW at crustal depths suggests activity of northwestward thrusting to some extent. Moreover, this setting could be a consequence of the presence of a low-deformed resistant domain attached to the African plate, here corresponding to the external Rif units on the Variscan basement (Estrada et al., 2018; Galindo-Zaldívar, Azzouz, et al., 2015; Pedrera et al., 2011).

There is furthermore some disagreement between the maximum horizontal compression (between N139°E and N152°E) and maximum local shortening (N173°E; Fig. 5-10), estimated by the MALA and MELI GPS stations across the seismic active area. It may be that fault activity is not due to a simple strike-slip fault driven by a far-field stress in the sense of Anderson (1951) but could accommodate crustal block displacement. The NE-SW extension that occurs toward the fault tips, at the northern edge of Campo de Dalías normal faults (Galindo-Zaldívar et al., 2013; Marín-Lechado et al., 2005), is transferred toward the southern edge, where normal faults splay at the Nekor Basin (Fig.

5-10; Galindo-Zaldívar et al., 2009; Lafosse et al., 2017), and crustal thinning is confirmed by gravity results (Fig. 5-4a).

The epicenters of three seismic series are located west of the main faults recognized at surface, both in the Alborán Sea (Al Idrisi Fault) and in the northern Rif (Trougout Fault; Figs. 5-2 and 5-10; Galindo-Zaldívar et al., 2009; Galindo-Zaldívar, Azzouz, et al., 2015; d'Acremont et al., 2014). Hence, the development of the seismic active fault zone west of the well-exposed Al Idrisi and Trougout faults might be attributed to the growth of recent faults owing to westward migration (Vitale et al., 2015) of the deformation during development of the Gibraltar Arc.

The westward migration of the Gibraltar Arc is well constrained by geological (Crespo-Blanc et al., 2016) and GPS data (Fadil et al., 2006; Koulali et al., 2011; Palano et al., 2015). However, the driving mechanism remains a matter of debate, with geodynamic models considering delamination (e.g., Lis Mancilla et al., 2013; Seber et al., 1996) and subduction (e.g., González-Castillo et al., 2015; Gutscher et al., 2012; Pedrera et al., 2011; Ruiz-Constán et al., 2011; Spakman et al., 2018), while rollback is a suitable mechanism for Gibraltar Arc westward displacement and Alborán Sea development. The growth of this seismic NNE-SSW fault zone occurs in the area of weakest and most attenuated continental crust, corresponding to the central Alborán Sea, bounded by the thick continental crust of the Betic and Rif Cordilleras. In this regional setting, the Eurasian-African convergence developed indentation tectonics (Estrada et al., 2018) accommodated by the Al Idrisi fault zone, which now extends to westward areas.

The development of active fault zones has vast implications for seismic hazard. The reactivation of an existing fracture calls for shear stress on the surface to attain the value of the friction and cohesion (Bott, 1959). Immediately previous to the formation of new fractures, shear stress would have to be above the values of friction in addition to cohesion—considerably higher (Anderson, 1951; Hajiabdolmajid et al., 2002). Given the same background setting, the development of a recent fault zone would allow for the accumulation of higher elastic deformation at the fault edges than along a well-developed previous fracture. These factors determine that the propagation of a recent fault, as occurs in the southern Alborán Sea, can produce earthquakes of higher magnitudes than preexisting faults. The highest-magnitude earthquakes of 2004

(d'Acremont et al., 2014; Galindo-Zaldívar et al., 2009) and 2016–2017 occurred in areas of recently developed fault segments with scarce evidence of deformation at the surface (Fig. 5-10). Such faults tend to be particularly active in their initial stage of development, entailing high seismic hazard, and are moreover difficult to detect because of the low amount of accumulated deformation due to their recent age.

5.5 Conclusions

The Alborán Sea 2016–2017 seismic sequence constitutes a unique opportunity to analyze the development of recent faults in conjunction with seismic hazard. This sequence occurred in the southern part of an active deformation zone crossing the central Alborán Sea and had a main event (Mw = 6.3, 25 January 2016) located along the corner between the NNE-SSW and ENE-WSW deformation alignments, which are 10–20-km wide. The 40-km-long NNE-SSW alignment is located in the Nekor Basin and Francesc Pagès seamount, west of the sea bottom Al Idrisi Fault trace, and the ENE-WSW one is along the northern side of Alborán Ridge and Francesc Pagès seamount. Data recorded during the INCRISIS cruise reveal that the ENE-WSW alignment is mainly characterized by recurrent MTDs that could be linked to earthquake and tectonic activity owing to uplift of the Alborán Ridge and Francesc Pagés antiforms. The NNE-SSW seismicity alignment is related to deep vertical sinistral faults, demonstrated by earthquake focal mechanisms, offset 5 to 10 km westward from the former Al Idrisi Fault. The major NNE-SSW deep sinistral fault zone responsible for the 2016–2017 main events would have activated fault segments up to 15 to 20 km in length for single events. The INCRISIS cruise reveals evidence for recent near-surface ruptures in NW-SE normal faults. These recent faults are related to the western boundary of the deformation zone, bounded eastward by the Al Idrisi Fault; although it is the main fault with seafloor expression, it has segments without recent activity. The present-day stress from earthquake focal mechanisms of 2016–2017 constrains a maximum prolate to triaxial compression inclined toward N319°E in the NNE-SSW alignment, and N332°E in the ENE-WSW alignment, with related orthogonal extension. Stresses are oblique to the N173°E shortening determined by GPS data that support sinistral slip behavior, with some extent of northwestward thrusting.

These data reveal a westward migration and offset of active deformation with respect to the already developed Al Idrisi Fault (Fig. 5-10) that may be linked to the westward development of the Gibraltar Arc. Moreover, the NNE-SSW deformation zone is segmented and was progressively reactivated near the African coast in the 1993–1994 seismic sequence, the southern onshore part being affected in 2004 and probably activating NNE-SSW sinistral and WNW-ESE dextral faults, with deformation later propagating offshore toward the northeast in 2016–2017. The present-day NW-SE Eurasian-African plate convergence in the westernmost Mediterranean and the inherited heterogeneous rigid basement structures determine the location of deformation areas. At present, a main NNE-SSW sinistral deformation fault zone, including the Al Idrisi Fault and recent developed faults offset to the west, connects the NW-SE extensional faults of the Campo de Dalias's northern edge (Betic Cordillera) with the southern edge's normal splay faults located at the Nekor Basin in the Rif (Fig. 5-10). This setting also contributes to the local crustal thinning of Nekor Basin supported by gravity data.

Geological hazard in the central Alborán Sea is closely related to the seismicity that constitutes a main triggering mechanism of MTDs and is moreover responsible for coseismic seafloor displacements. The development of recent faults that condition the westward widening of the fault zone compared with the already developed faults would imply the activity of the largest segments and the greatest accumulation of elastic energy, producing high-magnitude earthquakes that increase seismic hazard. In any case, low accumulated deformation and recent activity are predominant features making it possible to recognize such faults and therefore deserving further analysis through a multidisciplinary approach.

5.6 Acknowledgments

We acknowledge the comments of Prof. N. Niemi, Prof. J. Bruce H. Shyu, Prof. MA. Gutscher, and three anonymous reviewers, which served to improve the quality of this paper. We also thank A. Mandarieta for his help with the figures. The geological data referenced in this paper are available in the text, the seismicity data are available on the

IGN website at http://www.ign.es/web/ign/portal/sis-catalogo-terremotos, and the marine geophysical data are available on the ICM-CSIC website at http://gma.icm.csic.es/sites/default/files/geowebs/OLsurveys/index.htm. This study was supported by the Spanish projects: INCRISIS, DAMAGE (CGL2016-80687-R AEI/FEDER) and FAUCES (CTM2015-65461-C2-1-R), RNM 148 - Junta de Andalucía, and Marlboro cruises. French program Actions Marges, the EUROFLEETS program-SARAS cruise (FP7/2007-2013; 228344). The participation of D. Palomino and J. T. Vazquez was funded by the IEO project RIGEL.

5.7 References

Akoglu, A. M., Cakir, Z., Meghraoui, M., Belabbes, S., El Alami, S. O., Ergintav, S., and Akyüz, H. S. (2006). The 1994–2004 Al Hoceima (Morocco) earthquake sequence: Conjugate fault ruptures deduced from InSAR. Earth and Planetary Science Letters, 252(3-4), 467–480. https://doi.org/10.1016/j.epsl.2006.10.010.

Ammar, A., Mauffret, A., Gorini, C., and Jabour, H. (2007). The tectonic structure of the Alborán Margin of Morocco. Revista de la Sociedad Geológica de España, 20, 247–271.

Anderson, E. M. (1951). The dynamics of faulting and dyke formation with applications to Britain. New York: Hafner Pub. Co. Andrieux, J., Fontbote, J. M., and Mattauer, M. (1971). Sur un modèle explicatif de l'Arc de Gibraltar. Earth and Planetary Science Letters, 12(2), 191–198. https://doi.org/10.1016/0012-821X(71)90077-X.

Argus, D. F., Gordon, R. G., Heflin, M. B., Ma, C., Eanes, R. J., Willis, P., et al. (2010). The angular velocities of the plates and the velocity of Earth's centre from space geodesy. Geophysical Journal International, 180(3), 913–960. https://doi.org/10.1111/j.1365-246X.2009.04463.x.

Bott, M. H. P. (1959). The mechanics of oblique slip faulting. Geological Magazine, 96(2), 109–117. https://doi.org/10.1017/S0016756800059987.

Bourgois, J., Mauffret, A., Ammar, A., and Demnati, A. (1992). Multi-channel seismic data imaging of inversion tectonics of the Alborán Ridge (western Mediterranean Sea). Geo-Marine Letters, 12(2-3), 117–122. https://doi.org/10.1007/BF02084921.

Buforn, E., Pro, C., Cesca, S., Udias, A., and del Fresno, C. (2011). The 2010 Granada, Spain, deep earthquake. Bulletin of the Seismological Society of America, 101(5), 2418–2430. https://doi.org/10.1785/0120110022.

Buforn, E., Pro, C., Sanz de Galdeano, C., Cantavella, J. V., Cesca, S., Caldeira, B., et al. (2017). The 2016 south Alborán earthquake (Mw = 6.4): A reactivation of the Ibero-Maghrebian region? Tectonophysics, 712-713, 704–715. https://doi.org/10.1016/j.tecto.2017.06.033.

Buforn, E., Sanz de Galdeano, C., and Udías, A. (1995). Seismotectonics of the Ibero-Maghrebian region. Tectonophysics, 248(3-4), 247–261. https://doi.org/10.1016/0040-1951(94)00276-F.

Buforn, E., Udias, A., and Colombas, M. (1988). Seismicity, source mechanisms and tectonics of the Azores-Gibraltar plate boundary. Tectonophysics, 152(1–2), 89–118.

Buforn, E., Udias, A., and Madariaga, R. (1991). Intermediate and deep earthquakes in Spain. In A. Udías and E. Buforn (Eds.), Source Mechanism and Seismotectonics (pp. 375–393). Basel: Springer, Birkhäuser. https://doi.org/10.1007/978-3-0348-8654-3_2.

Carreño-Herrero, E., and Valero-Zornoza, J. F. (2011). Sismicidad de la Península Ibérica en el periodo instrumental: 1985-2011. Enseñanza de las Ciencias de la Tierra, 19, 289–295.

Casas, A., and Carbó, A. (1990). Deep structure of the Betic Cordillera derived from the interpretation of a complete Bouguer anomaly map. Journal of Geodynamics Series, 12(2-4), 137–147. https://doi.org/10.1016/0264-3707(90)90003-D.

Casas, D., Ercilla, G., Yenes, M., Estrada, F., Alonso, B., García, M., and Somoza, L. (2011). The Baraza Slide: Model and dynamics. Marine Geophysical Researches, 32(1-2), 245–256. https://doi.org/10.1007/s11001-011-9132-2.

Comas, M., García-Dueñas, V., and Jurado, M. (1992). Neogene tectonic evolution of the Alborán Sea from MCS data. Geo-Marine Letters, 12(2-3), 157–164. https://doi.org/10.1007/BF02084927.

Comas, M. C., Platt, J. P., Soto, J. I., and Watts, A. B. (1999). The origin and tectonic history of the Alborán Basin: Insights from Leg 161 results. In R. Zahn, M. C. Comas and A. Klaus (Eds.), Proceedings of the ocean drilling program scientific results (Vol. 161, pp. 555–580). College Station, TX: Ocean Drilling Program.

Cowie, P. A., and Scholz, C. H. (1992). Growth of faults by accumulation of seismic slip. Journal of Geophysical Research, 97(B7), 11,085–11,095. https://doi.org/10.1029/92JB00586.

Crespo-Blanc, A., Comas, M., and Balanyá, J. C. (2016). Clues for a Tortonian reconstruction of the Gibraltar Arc: Structural pattern, deformation diachronism and block rotations. Tectonophysics, 683, 308–324. https://doi.org/10.1016/j.tecto.2016.05.045.

d'Acremont, E., Gutscher, M. A., Rabaute, A., Mercier de Lépinay, B., Lafosse, M., Poort, J., et al. (2014). High-resolution imagery of active faulting offshore Al Hoceima, Northern Morocco. Tectonophysics, 632, 160–166. https://doi.org/10.1016/j.tecto.2014.06.008.

El Alami, S. O., Tadili, B. A., Cherkaoui, T. E., Medina, F., Ramdani, M., Brahim, L. A., and Harnafi, M. (1998). The Al Hoceima earthquake of May 26, 1994 and its aftershocks: A seismotectonic study. Annales de Geophysique, 41, 519–537.

El Moudnib, L., Villaseñor, A., Harnafi, M., Gallart, J., Pazos, A., Serrano, I., et al. (2015). Crustal structure of the Betic–Rif system, western Mediterranean, from local earthquake tomography. Tectonophysics, 643, 94–105. https://doi.org/10.1016/j.tecto.2014.12.015.

Estrada, F., Galindo-Zaldívar, J., Vázquez, J. T., Ercilla, G., D'Acremont, E., Alonso, B., and Gorini, C. (2018). Tectonic indentation in the central Alborán Sea (westernmost Mediterranean). Terra Nova, 30(1), 24–33. https://doi.org/10.1111/ter.12304.

Fadil, A., Vernant, P., McClusky, S., Reilinger, R., Gomez, F., Sari, D. B., et al. (2006). Active tectonics of the western Mediterranean: Geodetic evidence for rollback of a delaminated subcontinental lithospheric slab beneath the Rif Mountains, Morocco. Geology, 34(7), 529–532. https://doi.org/10.1130/G22291.1.

Frasca, G., Gueydan, F., and Brun, J. P. (2015). Structural record of Lower Miocene westward motion of the Alborán Domain in the western Betics, Spain. Tectonophysics, 657, 1–20. https://doi.org/10.1016/j.tecto.2015.05.017.

Galindo-Zaldívar, J., Azzouz, O., Chalouan, A., Pedrera, A., Ruano, P., Ruiz-Constán, A., et al. (2015). Extensional tectonics, graben development and fault terminations in the eastern Rif (Bokoya–Ras Afraou area). Tectonophysics, 663, 140–149. https://doi.org/10.1016/j.tecto.2015.08.029.

Galindo-Zaldívar, J., Borque, M. J., Pedrera, A., Marín-Lechado, C., Gil, A. J., and López-Garrido, A. C. (2013). Deformation behaviour of the lowrate active Balanegra Fault Zone from high-precision levelling (Betic Cordillera, SE Spain). Journal of Geodynamics, 71, 43–51.

Galindo-Zaldívar, J., Chalouan, A., Azzouz, O., Sanz de Galdeano, C., Anahnah, F., Ameza, L., et al. (2009). Are the seismological and geological observations of the Al Hoceima (Morocco, Rif) 2004 earthquake (M = 6.3) contradictory? Tectonophysics, 475(1), 59–67. https://doi.org/10.1016/j.tecto.2008.11.018.

Galindo-Zaldívar, J., Gil, A. J., Borque, M. J., González-Lodeiro, F., Jabaloy, A., Marin-Lechado, C., et al. (2003). Active faulting in the internal zones of the central Betic Cordilleras (SE, Spain). Journal of Geodynamics, 36(1), 239–250.

Galindo-Zaldivar, J., Gil, A. J., Sanz de Galdeano, C., Lacy, M. C., García-Armenteros, J. A., Ruano, P., et al. (2015). Active shallow extension in central and eastern Betic Cordillera from CGPS data. Tectonophysics, 663, 290–301. https://doi.org/10.1016/j.tecto.2015.08.035.

Galindo-Zaldivar, J., González-Lodeiro, F., Jabaloy, A., Maldonado, A., and Schreider, A. (1998). Models of magnetic and Bouguer gravity anomalies for the deep structure of the central Alborán Sea basin. Geo-Marine Letters, 18(1), 10–18. https://doi.org/10.1007/s003670050046.

González-Castillo, L., Galindo-Zaldivar, J., de Lacy, M., Borque, M., Martinez-Moreno, F., García-Armenteros, J., and Gil, A. (2015). Active rollback in the Gibraltar Arc: Evidences from CGPS data in the western Betic Cordillera. Tectonophysics, 663, 310–321. https://doi.org/10.1016/j.tecto.2015.03.010.

Grevemeyer, I., Gràcia, E., Villaseñor, A., Leuchters, W., and Watts, A. B. (2015). Seismicity and active tectonics in the Alborán Sea, western Mediterranean: Constraints from an offshore-onshore seismological network and swath bathymetry data. Journal of Geophysical Research: Solid Earth, 120, 8348–8365. https://doi.org/10.1002/2015JB012073.

Gutscher, M. A., Dominguez, S., Westbrook, G. K., Le Roy, P., Rosas, F., Duarte, J. C., et al. (2012). The Gibraltar subduction: A decade of new geophysical data. Tectonophysics, 574–575, 72–91. https://doi.org/10.1016/j.tecto.2012.08.038.

Hajiabdolmajid, V., Kaiser, P. K., and Martin, C. D. (2002). Modelling brittle failure of rock. International Journal of Rock Mechanics and Mining Sciences, 39(6), 731–741. https://doi.org/10.1016/S1365-1609(02)00051-5.

Hatzfeld, D. (1976). Deep-structure of Alborán Sea. Comptes Rendus Hebdomadaires des Séances de l'Académie des Sciences, D283, 1021–1024.

Hauksson, E., Jones, L. M., Hutton, K., and Eberhart-Phillips, D. (1993). The 1992 Landers earthquake sequence: Seismological observations. Journal of Geophysical Research: Solid Earth, 98(B11), 19,835–19,858. https://doi.org/10.1029/93JB02384

IGN (2016). Informe de la actividad sísmica en el Mar de Alborán 2016. (http://www.ign.es/resources/noticias/Terremoto_Alborán.pdf). Instituto Geográfico Nacional – Red Sísmica Nacional, 1–14.

Juan, C., Ercilla, G., Hernández-Molina, J. F., Estrada, F., Alonso, B., Casas, D., et al. (2016). Seismic evidence of current-controlled sedimentation in the Alborán Sea during the Pliocene and Quaternary: Palaeoceanographic implications. Marine Geology, 378, 292–311. https://doi.org/10.1016/j.margeo.2016.01.006.

Kariche, J., Meghraoui, M., Timoulali, Y., Cetin, E., and Toussaint, R. (2018). The Al Hoceima earthquake sequence of 1994, 2004 and 2016: Stress transfer and poroelasticity in the Rif and Alborán Sea region. Geophysical Journal International, 212(1), 42–53.

Koulali, A., Ouazar, D., Tahayt, A., King, R. W., Vernant, P., Reilinger, R. E., et al. (2011). New GPS constraints on active deformation along the Africa–Iberia plate boundary. Earth and Planetary Science Letters, 308(1-2), 211–217. https://doi.org/10.1016/j.epsl.2011.05.048.

Lafosse, M., d'Acremont, E., Rabaute, A., Mercier de Lépinay, B., Tahayt, A., Ammar, A., and Gorini, C. (2017). Evidence of Quaternary transtensional tectonics in the Nekor basin (NE Morocco). Basin Research, 29(4), 470–489. https://doi.org/10.1111/bre.12185.

Larouzière, F., Bolze, J., Bordet, P., Hernandez, J., Montenat, C., and Ott d'Estevou, P. (1988). The Betic segment of the lithospheric Trans-Alborán shear zone during the Late Miocene. Tectonophysics, 152(1-2), 41–52. https://doi.org/10.1016/0040-1951(88)90028-5.

Lis Mancilla, F. D., Stich, D., Berrocoso, M., Martín, R., Morales, J., Fernandez-Ros, A., et al. (2013). Delamination in the Betic Range: Deep structure, seismicity, and GPS motion. Geology, 41(3), 307–310. Locat, J., and Lee, H. J. (2002). Submarine landslides: Advances and challenges. Canadian Geotechnical Journal, 39(1), 193–212. https://doi.org/10.1139/t01-089.

López-Casado, C., Sanz de Galdeano, C., Palacios, S. M., and Romero, J. H. (2001). The structure of the Alborán Sea: An interpretation from seismological and geological data. Tectonophysics, 338(2), 79–95. https://doi.org/10.1016/S0040-1951(01)00059-2.

Marín-Lechado, C., Galindo-Zaldívar, J., Gil, A. J., Borque, M. J., De Lacy, M. C., Pedrera, A., et al. (2010). Levelling profiles and a GPS network to monitor the active folding and faulting deformation in the Campo de Dalias (Betic Cordillera, southeastern Spain). Sensors, 10(4), 3504–3518. https://doi.org/10.3390/s100403504.

Marín-Lechado, C., Galindo-Zaldívar, J., Rodríguez-Fernández, L. R., Serrano, I., and Pedrera, A. (2005). Active faults, seismicity and stresses in an internal boundary of a tectonic arc (Campo de Dalías and Níjar, southeastern Betic Cordilleras, Spain). Tectonophysics, 396(1-2), 81–96. https://doi.org/10.1016/j.tecto.2004.11.001.

Martínez-García, P., Comas, M., Lonergan, L., and Watts, A. B. (2017). From extension to shortening: Tectonic inversion distributed in time and space in the Alborán Sea, western Mediterranean. Tectonics, 36, 2777–2805. https://doi.org/10.1002/2017TC004489.

Martínez-García, P., Comas, M., Soto, J. I., Lonergan, L., and Watts, A. (2013). Strike-slip tectonics and basin inversion in the western Mediterranean: The post-Messinian evolution of the Alborán Sea. Basin Research, 25(4), 361–387. https://doi.org/10.1111/bre.12005.

Martínez-García, P., Soto, J. I., and Comas, M. (2011). Recent structures in the Alborán Ridge and Yusuf fault zones based on swath bathymetry and sub-bottom profiling: Evidence of active tectonics. Geo-Marine Letters, 31(1), 19–36. https://doi.org/10.1007/s00367-010-0212-0.

Medina, F., and Cherkaoui, T. E. (2017). The south-western Alborán earthquake sequence of January-March 2016 and its associated coulombstress changes. Open Journal of Earthquake Research, 6(1), 35–54. https://doi.org/10.4236/ojer.2017.61002.

Meissner, R., and Strehlau, J. (1982). Limits of stresses in continental crusts and their relation to the depth-frequency distribution of shallow earthquakes. Tectonics, 1(1), 73–89. https://doi.org/10.1029/TC001i001p00073.

De Mets, C., Laffaldano, G., and Merkouriev, S. (2015). High-resolution Neogene and Quaternary estimates of Nubia-Eurasia-North America plate motion. Geophysical Journal International, 203(1), 416–427. https://doi.org/10.1093/gji/ggv277.

Michael, A. J. (1984). Determination of stress from slip data: Faults and folds. Journal of Geophysical Research: Solid Earth, 89(B13), 11,517–11,526. https://doi.org/10.1029/JB089iB13p11517.

Michelini, A., and Lomax, A. (2004). The effect of velocity structure errors on double-difference earthquake location. Geophysical Research Letters, 31, L09602. https://doi.org/10.1029/2004GL019682.

Morales, J., Serrano, I., Jabaloy, A., Galindo-Zaldivar, J., Zhao, D., Torcal, F., and González-Lodeiro, F. (1999). Active continental subduction beneath the Betic Cordillera and the Alborán Sea. Geology, 27(8), 735–738. https://doi.org/10.1130/0091-7613(1999)027<0735: ACSBTB>2.3.CO;2.

Palano, M., González, P. J., and Fernández, J. (2015). The diffuse plate boundary of Nubia and Iberia in the western Mediterranean: Crustal deformation evidence for viscous

coupling and fragmented lithosphere. Earth and Planetary Science Letters, 430, 439–447. https://doi.org/10.1016/j.epsl.2015.08.040.

Pedrera, A., Ruiz-Constán, A., Galindo-Zaldívar, J., Chalouan, A., Sanz de Galdeano, C., Marín-Lechado, C., et al. (2011). Is there an active subduction beneath the Gibraltar orogenic arc? Constraints from Pliocene to present-day stress field. Journal of Geodynamics, 52(2), 83–96. https://doi.org/10.1016/j.jog.2010.12.003.

Poujol, A., Ritz, J. F., Tahayt, A., Vernant, P., Condomines, M., Blard, P. H., et al. (2014). Active tectonics of the Northern Rif (Morocco) fromgeomorphic and geochronological data. Journal of Geodynamics, 77, 70–88. https://doi.org/10.1016/j.jog.2014.01.004.

Ruiz-Constán, A., Galindo-Zaldívar, J., Pedrera, A., Celerier, B., and Marín-Lechado, C. (2011). Stress distribution at the transition from subduction to continental collision (northwestern and central Betic Cordillera). Geochemistry, Geophysics, Geosystems, 12, Q12002. https://doi.org/10.1029/2011GC003824.

Sandwell, D. T., Müller, R. D., Smith, W. H., Garcia, E., and Francis, R. (2014). New global marine gravity model from CryoSat-2 and Jason-1 reveals buried tectonic structure. Science, 346(6205), 65–67. https://doi.org/10.1126/science.1258213.

Scholz, C. H. (2002). The mechanics of earthquakes and faulting. Cambridge, UK: Cambridge University Press. https://doi.org/10.1017/CBO9780511818516.

Seber, D., Barazangi, M., Ibenbrahim, A., and Demnati, A. (1996). Geophysical evidence for lithospheric delamination beneath the Alborán Sea and Rif–Betic mountains. Nature, 379(6568), 785–790.

Sibson, R. (1977). Fault rocks and fault mechanisms. Journal of the Geological Society, 133(3), 191–213. https://doi.org/10.1144/gsjgs.133.3.0191.

Spakman, W., Chertova, M. V., van den Berg, A., and van Hinsbergen, D. J. J. (2018). Puzzling features of western Mediterranean tectonics explained by slab dragging. Nature Geoscience, 11(3), 211–216. https://doi.org/10.1038/s41561-018-0066-z.

Stich, D., Martín, R., and Morales, J. (2010). Moment tensor inversion for Iberia–Maghreb earthquakes 2005–2008. Tectonophysics, 483(3-4), 390–398. https://doi.org/10.1016/j.tecto.2009.11.006.

Stich, D., Serpelloni, E., de Lis Mancilla, F., and Morales, J. (2006). Kinematics of the Iberia–Maghreb plate contact from seismic moment tensors and GPS observations. Tectonophysics, 426(3-4), 295–317. https://doi.org/10.1016/j.tecto.2006.08.004.

Van der Woerd, J., Dorbath, C., Ousadou, F., Dorbath, L., Delouis, B., Jacques, E., et al. (2014). The Al HoceimaMw 6.4 earthquake of 24 February 2004 and its aftershocks sequence. Journal of Geodynamics, 77, 89–109. https://doi.org/10.1016/j.jog.2013.12.004.

Vavrycuk, V. (2014). Iterative joint inversion for stress and fault orientations from focal mechanisms. Geophysical Journal International, 199(1), 69–77. https://doi.org/10.1093/gji/ggu224.

De Vicente, G., Cloetingh, S., Muñoz-Martín, A., Olaiz, A., Stich, D., Vegas, R., et al. (2008). Inversion of moment tensor focal mechanisms for active stresses around the microcontinent Iberia: Tectonic implications. Tectonics, 27, TC1009. https://doi.org/10.1029/2006TC002093.

Vitale, S., Zaghloul, M. N., El Ouaragli, B., Tramparulo, F. D. A., and Ciarcia, S. (2015). Polyphase deformation of the Dorsale Calcaire complex and the Maghrebian Flysch Basin units in the Jebha area (Central Rif, Morocco): New insights into the Miocene tectonic evolution of the Central Rif belt. Journal of Geodynamics, 90, 14–31. https://doi.org/10.1016/j.jog.2015.07.002.

Watterson, J. (1986). Fault dimensions, displacements and growth. Pure and Applied Geophysics, 124(1-2), 365–373. https://doi.org/10.1007/BF00875732.

Wells, D. L., and Coppersmith, K. J. (1994). New empirical relationships among magnitude, rupture length, rupture width, rupture area, and surface displacement. Bulletin of the Seismological Society of America, 84, 974–1002.

Chapter 6

Tsunami generation potential of a strike-slip fault tip in the westernmost Mediterranean

*F. Estrada[1], J. M. González-Vida[2], J. A. Peláez[3], J. Galindo-Zaldívar[4, 5], S. Ortega[2], J. Macías[6], J. T. Vázquez[7], G. Ercilla[1]

[1]Institut de Ciències del Mar, CSIC. 08003, Barcelona, Spain

[2]Departamento de Matemática Aplicada, Escuela Politécnica Superior, Universidad de Málaga, 29071, Málaga, Spain,

[3]Universidad de Jaén, Dpt. Of Physics, 23071, Jaén, Spain,

[4]Departamento de Geodinámica, Universidad de Granada, 18071, Granada, Spain,

[5] Instituto Andaluz de Ciencias de la Tierra (CSIC-UGR), Granada, Spain.

[6]Departamento de Análisis Matemático, Facultad de Ciencias, Universidad de Málaga, Campus de Teatinos s/n, 29080 Málaga, Spain,

[7]Instituto Español de Oceanografía, Centro Oceanográfico de Málaga, Puerto Pesquero s/n, 29640 Fuengirola, Spain,

Published on: Scientific Reports, 2021.

Volume 11 (1), 16253

DOI: 10.1038/s41598-021-95729-6

Impact Factor (JCR): 4.380 (2020), Q1 en Multidisciplinary. 19/128

ABSTRACT

Tsunamis are triggered by sudden seafloor displacements, and usually originate from seismic activity at faults. Nevertheless, strike-slip faults are usually disregarded as major triggers, as they are thought to be capable of generating only moderate seafloor deformation; accordingly, the tsunamigenic potential of the vertical throw at the tips of strike-slip faults is not thought to be significant. We found the active dextral NW-SE Averroes Fault in the central Alborán Sea (westernmost Mediterranean) has a historical vertical throw of up to 5.4 m at its northwestern tip corresponding to an earthquake of Mw 7.0. We modelled the tsunamigenic potential of this seafloor deformation by Tsunami-HySEA software using the Coulomb 3.3 code. Waves propagating on two main branches reach highly populated sectors of the Iberian coast with maximum arrival heights of 6 m within 21 and 35 min, which is too quick for current early-warning systems to operate successfully. These findings suggest that the tsunamigenic potential of strike-slip faults is more important than previously thought, and should be taken into account for the re-evaluation of tsunami early-warning systems.

6.1 Introduction

Tsunamis, catastrophic natural hazards that pose a significant threat to major infrastructure and many densely populated coastal regions, are generated by the rapid deformation of the seafloor due to fault or landslide activity (Okal and Synolakis, 2003; Borrero et al., 2004; Gerardi et al., 2008; Geist and Lynett, 1974). Seismic strike-slip faults do not significantly displace the seafloor in flat-lying and smooth areas, and are therefore not generally considered as potential triggers of tsunamis (Yamashita and Sato, 1974; Bletery et al., 2015; Elbanna et al., 2021). Yet, tsunamis triggered by strike-slip faults have been reported worldwide as a result of either vertical seafloor displacements in over-steepened areas (e.g., the 1994 Mindoro earthquake, Tanioka and Satake, 1996) and on restraining and releasing bends (the 1906 San Francisco earthquake, Geist and Lou Zoback, 1999; Lorito et al., 2008 and events in other areas of southern California, Borrero et al., 2004), or seismogenic submarine landslides (the 2010 Haiti earthquake, Hornbach et al., 2010). The triggers of other historical strike-slip earthquake-related tsunamis, such as the 1999 Izmit tsunami (Altinok et al., 2001) and the 2012 and 2016 tsunamis in the Indian Ocean, (Heidarzadeh and Satake, 2017), remain unknown. To date, despite the noteworthy vertical offsets at the tips of strike-slip faults, these faults have not been considered a main tsunamigenic source.

The strike-slip Averroes Fault is located in the Alborán Sea (westernmost Mediterranean Sea), which has been a tectonically active basin since the late Miocene (Comas et al., 1999) (Fig. 6-1). The Alborán Sea is deformed by strike-slip faults under laterally unlocked tectonic indentation driven by Eurasian-African plate convergence (Estrada et al., 2018) at a rate of 4.5 mm/yr (De Mets et al., 2015) (Fig. 6-1) The Alborán Sea, whose Iberian coast annually receives the highest number of tourists from all of Europe, has been historically afflicted by tsunamis (Espinar, 1994; Becker-Heidmann et al., 2007; IGN, 2009). Historical records show the simultaneous occurrence of tsunamis striking the Adra and Malaga coasts at 365 CE (Espinar, 1994). However, little is known about the tsunamigenic potential of the faults in this basin.

To resolve this problem, we identified the NW-SE dextral Averroes Fault as the structure in the fault system with the strongest evidence of recent and active seafloor offset at its northern termination (Figs. 6-1b, c and 6-2). Subsequent modelling the

tsunamigenic potential of this structure reveals the potential for tsunami generation triggered by vertical offset at the tip of a strike-slip fault, providing knowledge crucial for reviewing potential tsunami hazards related to strike-slip faults worldwide.

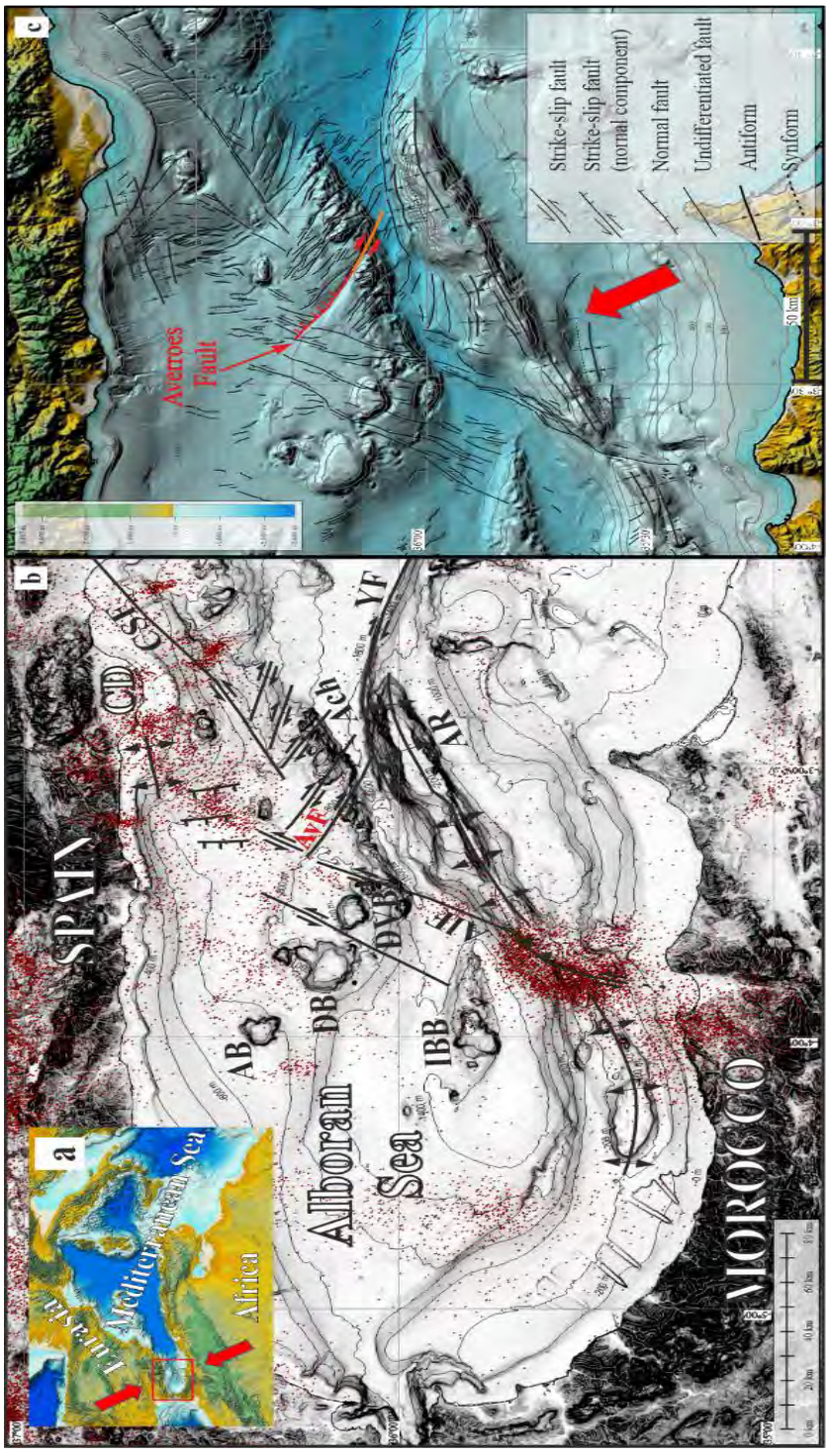

Figure 6-1. The Averroes Fault in the tectonic framework of the Alborán Sea. a) Location of the study area; b) Multibeam bathymetric map displaying the main NNE-SSW shear zone seismicity (red dots) and main tectonic features and seamounts; c) detailed tectonic map of the central Alborán Sea highlighting the presence of the Averroes Fault northern segment in red and southern segment in orange. Modified from Estrada et al. (2018)[15]. Legend: ACh, Alborán Channel; AR, Alborán Ridge; AB, Algarrobo Bank; DB, Djibouti Bank; DVB, Djibouti Ville Bank; IBB, Ibn Batouta Bank; CD, Campo de Dalias; YF, Yusuf Fault; AIF, Al Idrisi Fault; AvF, Averroes Fault; and CSF, Carboneras-Serrata Fault. Red arrow indicates direction of tectonic indentation. (Figures generated using Globalmapper v.19, https://www.bluemarblegeo.com, and mounted with CorelDRAW v. X7, https://www.corel.com).

6.2 Results

6.2.1 The strike-slip Averroes Fault

The Averroes Fault is a component of the NW-SE conjugate dextral strike-slip fault set of the main NNE-SSW shear zone crossing the Alborán Sea (Estrada et al., 2018) (Fig. 6-1b). The Averroes Fault, which is predominantly affected by shallow earthquakes at present (up to 15 km deep, Grevemeyer et al., 2015), has a steeply dipping main fault surface with a length of 38 km (Figs. 6-1b, c and 6-2) that splits upward into two faults surfaces, the eastern one being currently deforming the seafloor (Fig. 6-2a).

The main Averroes Fault comprises two main segments: the southern segment (16 km long) horizontally displaces the seafloor surface by 4.1 km with dextral kinematics, while its northern segment (22 km long) has a maximum vertical offset of 470 m at its tip (Fig. 6-2a), with a northeastern downthrown block that creates a half-graben-like feature (Figs. 6-1c and 6-2). Tectonic activity initiated along the Averroes Fault during the late early Pliocene (Perea et al., 2018; Estrada et al., 1997; Pérez-Belzuz, 1999; Martínez-García et al., 2013), giving it an age of 4.57 Ma (Martínez-García et al., 2017; Perea et al., 2018). Considering the age of the fault and the vertical offset along its northern segment, we calculate an average vertical slip rate of 0.1 mm/yr.

Activity of the Averroes Fault is driven by the tectonic inversion of the central Alborán basin (Estrada et al., 2018). This activity has a co-seismic character evidenced in our ultra-high-resolution parametric seismic profiles by interbedded sedimentary wedges (up to 4.5 to 5.4 m thick) vertically stacked which represent mass-wasting events coming from the upthrown block (Fig. 6-2b). We have established a chronostratigraphic control of activity spanning the last 124,000 yr (Fig. 6-2b). From young to old, four events can be seen, with fault throws of 3.7 (seafloor), 5.4, 5.4 and 4.5 m (unloaded successive fault offsets), and with ages of recent, 20,590 yr, 63,350 yr and 124,060 yr, respectively (Fig. 6-2b and Suppl. Fig. 6-S1). We therefore propose an approximate average recurrence period of approximately 31,000 yr.

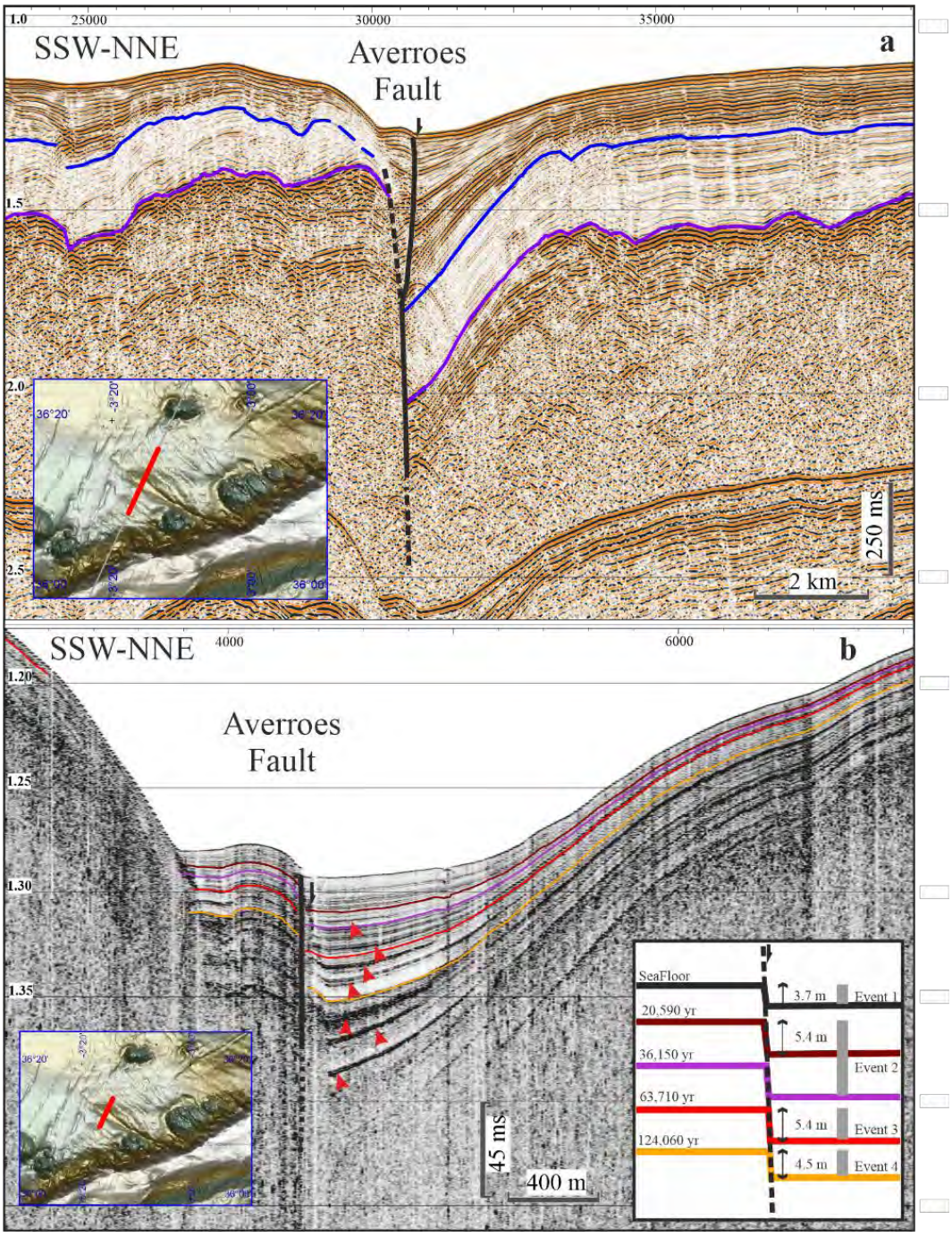

Figure 6-2. Seismic profiles illustrating the Averroes Fault. a) Airgun seismic profile showing the deep structure. Legend: purple line corresponds with top of Miocene and blue line with base of Quaternary. Horizontal and vertical scale respectively in metres and seconds, two-way travel time (twtt). Vertical exaggeration x8.7; b) Parametric TOPAS profile (ultra-high-resolution) illustrating the upper reach (75 m) of the Averroes Fault. Inlet shows chronostratigraphic boundaries and fault events over the last 124,060 years. Red arrows indicate co-seismic wedges. Horizontal scale in metres and vertical scale in seconds (twtt). Vertical exaggeration x12.4. (Figures generated using IHS Kingdom v. 2017, https://ihsmarkit.com, and mounted with CorelDRAW v. X7, https://www.corel.com).

6.2.2 Seafloor deformation and tsunamigenic potential

Next, we modelled the tsunamigenic potential of the vertical seafloor offsets related to the fault tip of the NW segment of the Averroes strike-slip Fault. Although seafloor deformation may also occur by horizontal displacement of slope areas in the southern segment, it would be reasonable to assume that horizontal displacement away from the tip might not lead to significant vertical offset.

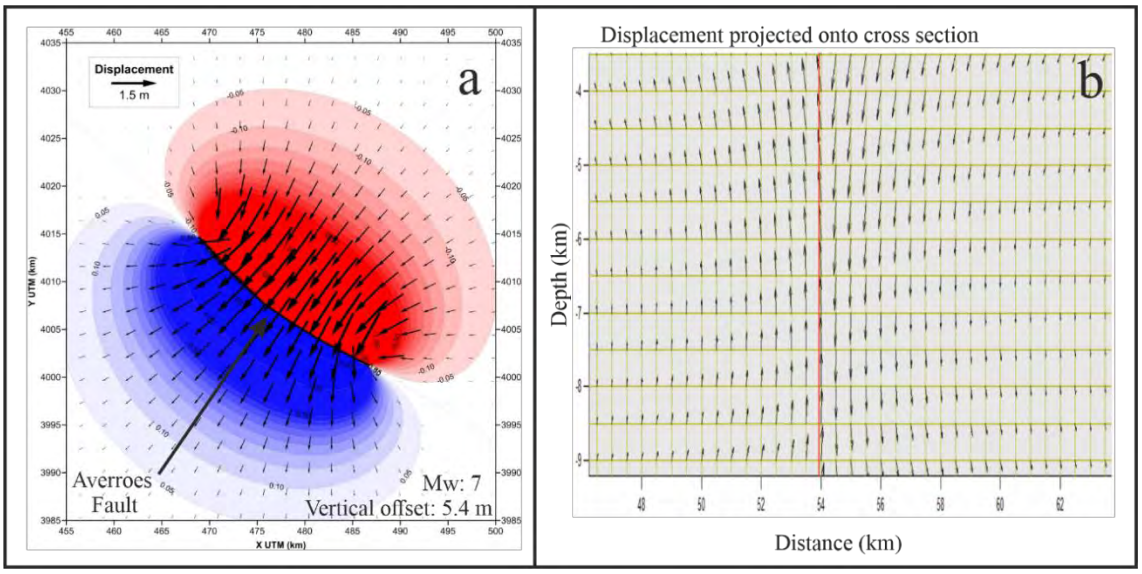

Figure 6-3. Seafloor deformation. Computed deformation pattern of the crust affected by the Averroes Fault for a vertical offset of 5.4 m and an associated magnitude of Mw 7. a) Seafloor plan view: red indicates downthrow and blue indicates uplift; b) Vertical section: red line represents the Averroes Fault trace. (Figures generated with Coulomb, v. 3.3, USGS, https://www.usgs.gov/software/coulomb-3 and Surfer, v. 12.0.626, Golden Software, https://www.goldensoftware.com and mounted with CorelDRAW v. X7, https://www.corel.com).

We employed Okada's approach (Okada, 1985; Okada, 1992) to calculate deformation, by determining a displacement on the fault plane of the SW (uplifted) block equal to one-half of the net slip; i.e., the displacement of the SW block was equivalent in magnitude to the displacement of the NE (downthrown) block. We modelled a rapid co-seismic displacement of the seafloor considering a vertical fault with a length of 22 km extending to a depth of 10 km and a uniform net slip of 5.4 m (with the NE block downthrown). This net slip corresponds to the historical maximum throw, and was determined for two of the four events mentioned above. Our model

suggests a corresponding seismic moment equal to 3.88×10^{26} dyn/cm and an earthquake magnitude of Mw 7. Both the vertical and the horizontal computed deformations are depicted in Fig. 6-3, which demonstrates that deformation lobes affect both fault blocks with vertical displacements of 0.1 m even at distances (perpendicular to the fault plane) of 17 km for the simulated Mw 7.0 event (Fig. 6-3). The maximum horizontal displacements perpendicular to the fault plane are on the order of 1.7 m.

Next, we modelled the tsunami generation that might occur as a result of a vertical throw of 5.4 m on the northern segment of the Averroes Fault, using the non-linear hydrostatic shallow-water model Tsunami-HySEA applied to a high-resolution ambient grid (~50 m). Despite the hydrostatic nature of the numerical model used, it have been shown (Macías et al., 2017) that the hydrostatic version of the Tsunami-HySEA model is capable of accurately assess tsunami hazard as runup estimations agreed with lab data and essentially coincide with non-dispersive simulation results. We identified a heterogeneous tsunami propagation pattern, comprising two branches orthogonal to the fault trace; the main branch directed to the NE and the minor one directed to the SW (Fig. 6-4a and Suppl. Video 6-S1). The NE branch has a straight path, and reaches land in the area of Campo de Dalías (Fig. 6-4a, Fig. 6-S2 and Suppl. Videos 6-S2 and 6-S3); a positive wave with maximum height (6 m) and shortest arrival time (21 min) occurs near the village of Balerma (Figs. 6-4a, c and Suppl. Video 6-S2). In contrast, the SW branch initially corresponds to deep waters, and the propagating tsunami impinges against three elongated seamounts acting as morphological barriers, namely, the relatively long ENE-WSW Alborán Ridge, the E-W Ibn Batouta and three seamounts aligned NW-SE (Algarrobo, Djibouti and Djibouti Ville banks) (Figs. 6-1a, 6-4a and Suppl. Video 1). This impingement modifies the tsunami propagation path, forcing it to split into three subbranches directed to the NW and approximately to the W and S. The former reaches the Málaga coast with a wave height of up to 2 m and an arrival time of up to 35 min (Fig. 6-4a, Fig. 6-S2 and Suppl. Video 6-S4), whereas the latter reaches landfall along the Moroccan coast, in locations such as Ras Tarf cape (wave height 1 m; arrival time 21 min), Punta Negri (wave height 1 m; arrival time 20 min) and the new Nador Harbour (Port Nador West Med) (wave height 1 m; arrival time 27 min) (Fig. 6-4a, Fig. 6-S2 and Suppl. Video 6-S1).

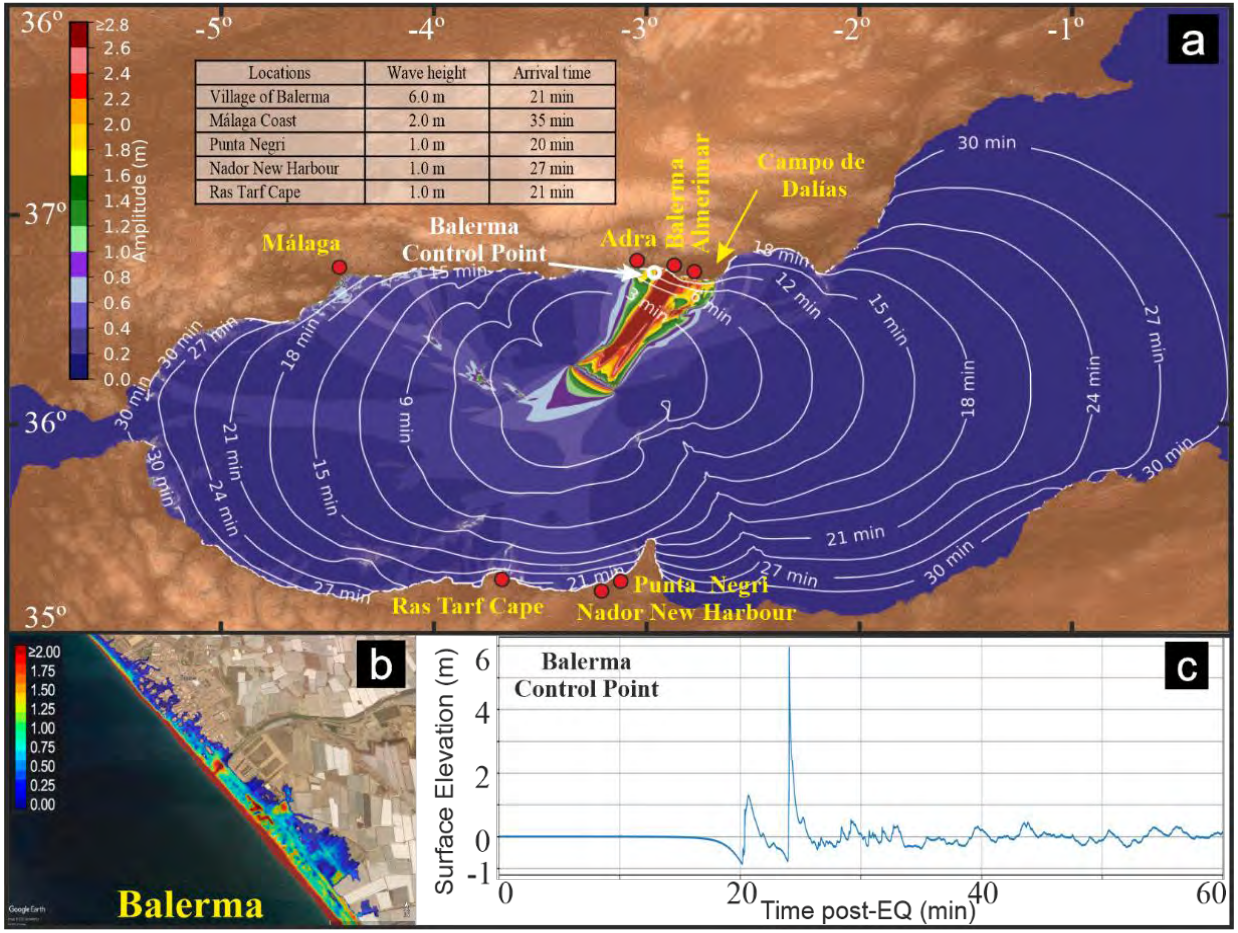

Figure 6-4. Modelled tsunami for the Averroes Fault. a) Tsunami propagation considering a vertical offset of 5.4 m and an associated magnitude of Mw 7. Colour scale represents wave heights in metres and contours represent first arrival times in minutes. The highest wave heights and their arrival times impacting coastal localities are shown in the inset table. b) Balerma tsunami water-level inundation. Colour scale in meters. c) Tsunami wave height at Balerma control point based on seasurface time series simulated by Tsunamni-HySEA. (Figures generated using Python, v. 3.7.3, https://www.python.org, and Matplotlib v. 3.4.2, https://matplotlib.org and mounted with CorelDRAW v. X7, https://www.corel.com).

6.3 Discussion

After an earthquake strikes, it is crucial for early-warning systems to issue a rapid assessment while minimizing false alerts, based on the event magnitude, focal mechanism and potential tsunamigenic trigger.

The Averroes Fault in the Alborán Sea (Fig. 6-1a and b) with offsets that can reach 5.4 m (Fig. 6-2), suggesting earthquake magnitudes up to Mw 7, provides a fundamental opportunity to analyze this tsunamigenic mechanism, namely, the vertical offset of the seafloor concentrated at the northern fault tip.

Our modelling of tsunami propagation related to seafloor deformation along the Averroes Fault (Fig. 6-4 and Suppl. Video 6S-1) provides a means to assess the potential tsunamigenic hazard of strike-slip fault tips. As already mentioned, despite the limitation in the tsunami model used, not able to reproduce the dispersive characteristics of the generated waves, it has been shown (Macías et al., 2017) that regarding hazard assessment, the model used provides accurate estimations for runup as main indicator of the hazard. The propagation of tsunami is controlled by fault kinematics (Yamashita and Sato, 1974) and we found that the vertical throw at the tip of the Averroes Fault determines the onset of positive and negative waves. The vertical deformation lobe of the NE downthrown block triggers an initial negative wave followed by a striking positive wave raising up to 6 m above the usual water level at Balerma coast (Fig. 6-4 and Suppl. Video 6-S2). Contrasting, the vertical deformation of the SW uplifted block forms an initial positive wave with a remarkable negative wave dropping up to 1.5 m in Malaga and 1.5 m in Moroccan coasts, and wave trains with significant withdrawal in both areas (Fig. 6-S2).

The propagation of tsunami is also controlled by the interplay between fault orientation and seafloor morphology (Yamashita and Sato, 1974; Bletery et al., 2015), and we found that the NW-SE-oriented Averroes Fault focuses waves mainly towards the NE and, to a lesser extent, the SW. The NE branch is predicted to cross an area of smooth bathymetry, enabling linear propagation towards the Campo de Dalías coast, which is characterized by tourist beaches and dominated inland by greenhouse agriculture (Fig. 6-4 and Suppl. Video 6-S1); likewise, the coastal proximity of the villages

of Balerma, Almerimar and Adra, and the short propagation time increase their vulnerability to tsunamis (Fig. 6-4, Fig. 6-S2 and Suppl. Videos 6-S2 and 6-S3). The NW subbranch focuses the highest waves towards the Malaga coast, which exhibits a moderate tsunami hazard that may affect infrastructures and beaches (Fig. 6-4, Fig. 6-S2 and Suppl. Videos 6-S1 and 6-S4). Moreover, the coastline in this region becomes densely populated in summer, with large stretches of beach that can be fully occupied. Meanwhile, the S subbranch influences the Moroccan coast, but to a lesser extent (Fig. 6-4, Fig. 6-S2 and Suppl. Video 6-S1).

Our findings demonstrate the need to reevaluate tsunamigenic hazards related to strike-slip fault tips. Such faults are found predominantly in marine areas related to transform plate boundaries, such as the northern San Andreas Fault (Goldfinger et al., 2007) and the northeastern Caribbean plate (Mann et al., 1995), as well as small seas, such as the Marmara Sea (Hébert et al., 2005). Likewise, vertical offsets at fault tips may be found along strike-slip faults related to segmented subduction zones, such as the Nazca plate below the Ecuador-Colombia segment of the South American plate margin (Collot et al., 2004). All the mentioned examples, are similar enough to the Averroes Fault and might also pose a significant threat to the local population.

Here, we demonstrate that following a seismic event, vertical offset at the NW tip of the Averroes Fault has the potential to generate destructive tsunamis in the westernmost Mediterranean, with rapid arrival times at densely populated coastlines (21 min) that are too short for existing early-warning systems to operate properly. Moreover, this study highlights the need for coastal communities worldwide to review the tsunamigenic potential of strike-slip faults through vertical offsets near their tips as a new tsunamigenic mechanism that may be of great importance along transform and segmented convergent plate boundaries characterized by submarine strike-slip faults. These findings justify the necessity of considering the tsunamigenic hazard potential of strike-slip faults to improve the accuracy of tsunami early-warning systems in geodynamic contexts of tectonic indentation, transform plate boundaries and subduction zones.

6.4 Methods

6.4.1 Marine geophysics

The geologic history and structure of the Averroes Fault were studied by means of seismic profiles and swath bathymetric data. The seismic profiles come from the following 17 cruises: AS, CONOCO Cab-01, R/V Robert D. Conrad cruise, DBS, EAS, Fauces, Fauces-1bis, GC-83-2, GC-90-1, GC-90-2, He-91-3, RRS Charles Darwin cruise, Marsibal, Montera, RAY, SAGAS, (http://gma.icm.csic.es/sites/default/files/geowebs/OLsurveys/index.htm). The cruises were independent to this study, except 4 of them (Montera, GC-90-1, SAGAS, Fauces-1) where the surveys of the Averroes Fault was included in the cruise objectives and provided new and relevant information; these 4 cruises were led by scientists of the Continental Margins Group from the Institute of Marine Science, ICM-CSIC, and were conducted onboard the Spanish research vessels García del CID, Hespérides; Sarmiento de Gamboa and Angeles Alvariño. The seismic profiles have different resolutions (high and ultrahigh) and utilize different techniques: multi-channel seismic (MCS), single-channel and parametric. Multi-channel seismic profiles were downloaded from the Spanish Hydrocarbon Technical Archive (https://geoportal.minetur.gob.es/ATHv2/welcome.do) and they are commercial data from oil companies. These profiles have a vertical standard resolution of tens of meters with a penetration of up to 10 seconds. The single-channel profiles were obtained with airgun systems (140 to 530 c.i.), have an average vertical resolution of < 15 m of few meters time with a penetration of up to <3s seconds. The parametric seismic profiles were acquired with the TOPAS (TOpographic Parametric Echosounder) whose vertical resolution is about <30±40 cm within the upper 150 ms of the sediment column. The seismic lines were integrated into a IHS Kingdom project for their correlation and interpretation.

The swath bathymetric data were recorded with a SIMRAD EM120 multibeam echosounder with a frequency of 12 kHz. Multibeam bathymetry datasets independent to this study were also compiled and integrated for the present study. These bathymetries were obtained from the MARSIBAL and Fauces 1bis projects and the Fishing General Secretary (Spanish Government). The data are available at a repository

(http://gma.icm.csic.es/sites/default/files/geowebs/OLsurveys/index.htm). The Global Mapper software, a versatile GIS application from Blue Marble Geographics, was selected for integrating all those bathymetries in order to generate a gridded bathymetric map at 50 m. The vertical resolution was approximately 0.025% of the water depth. The mapping of the Averroes Fault trace and its analysis on the multibeam map was also done with drawing and measurement tools in Global Mapper and IHS Kingdom project.

For plotting the epicentre locations at the seafloor of the Alborán Sea, the seismicity database of the Spanish National Geographic Institute (IGN) (www.ign.es) was used. The epicentre datasets were plotted on the multibeam bathymetric map using visualization tools from the Global Mapper.

6.4.2 Chronostratigraphy

The available scientific well information for the study area (ODP Site 977) was integrated into the IHS Kingdom project with seismic lines for their chronostratigraphy correlation and interpretation. A precise chronology of the seismic stratigraphic boundaries was developed through an age calibration based primarily on data from that Site (Fig. 6-S1). In order to confirm the chronology, the chronostratigraphic boundaries were also correlated with those in commercial and scientific wells for across the entire Alborán Basin (Juan et al., 2016). The velocity-to-depth (ms to m) conversion was performed using the speed of sound (1500 m/s) for the parametric profiles (Fig. 6-S1) and a weighted average velocity (1779 m/s) from ODP Site 976 (Soto et al., 2012) for the multi- and single-channel profiles.

6.4.3 The Averroes Fault rate of tectonic activity

The average vertical slip rate (0.1 mm/yr) results from divide the vertical offset (470 m) by the age of the oldest materials affected by the Averroes Fault (4.57 myr). In the same way, the averaged period of fault recurrence (31,000 yr) has been calculated dividing the oldest known age (124,060 yr) by the number of fault events (4).

6.4.4 Seafloor deformation

The crustal deformation at the seafloor generated by a given earthquake along the Averroes Fault was computed using the Coulomb 3.3 code (Lin and Stein, 2004; Toda et al., 2005), in which calculations were performed using an established approach (Okada, 1985; Okada 1992) assuming an elastic half-space with uniform elastic properties. The fault was modelled using different vertical planes to better fit the curved geometry of the fault trace. All of these planes extended from the surface of the seafloor to a depth of 10 km, where the majority of hypocentres near the Averroes Fault are located. Typical values of 0.25 for Poisson's ratio and 8×10^{25} bar for Young's modulus were applied.

6.4.5 Tsunami model

Tsunami-Hyperbolic Systems and Efficient Algorithms (Tsunami-HySEA) (De la Asunción et al., 2013; Castro et al., 2015) is a finite-volume numerical hydrostatic model that solves the 2D non-linear shallow water equations in spherical coordinates. It has been developed by the EDANYA group of the University of Malaga specifically for simulations of seismically induced tsunamis. This model, based on a graphic processing unit (GPU) architecture, is robust, reliable and accurate. The combination of this kind of numerical model with an efficient GPU results in a faster than real-time (FTRT) numerical model capable of simulating the generation, propagation and inundation of a tsunami in a region covered by a grid with several million cells in only a few minutes. This model has been extensively validated under the standard benchmarks proposed by the National Tsunami Hazards Mitigation Program (NTHMP) of the U.S.A. (Macías et al., 2017; Lynett et al., 2017) and has been extensively tested in several scenarios and compared with other well-established tsunami models (Macías et al., 2016; Molinari et al., 2016).

Tsunami-HySEA has been implemented using CUDA and MPI in order to take advantage of the massive parallel architecture of multi-GPU clusters, so that the computing time required could be dramatically reduced with respect to the use of a single CPU core or even a multi-core processor and, at the same time, numerical

resolution could be increased still computing extremely fast. The Tsunami-HySEA model includes many features such as various options for the initial condition (as the computation of the initial seafloor deformation using Okada (1992) model or support for rectangular or triangular faults among others), it implements two-way nested meshes, direct output of time series from a list of points of interest, etc (González-Vida et al., 2021). A 2D domain decomposition is performed, and load balancing techniques are also used considering the wet and dry zones and the nested meshes, so that the computational load of all the MPI processes is as similar as possible. The entire numerical computation is carried out in multi-GPUs, using double numerical precision, including the nested meshes processing. Multiple CUDA kernels have been implemented, and CUDA streams are used to compute in parallel different meshes in a same level of the grid hierarchy. Furthermore, the MPI communications can overlap with kernel computations and memory transfers between CPU and GPU memory in order to increase the efficiency of the solver. By means of this very efficient implementation, the model is able to simulate 8 hours of real time tsunami in the Mediterranean Sea (in a mesh with 10 million volumes and a resolution of 30 arc-sec) in 257 seconds using two NVIDIA Tesla P100, or even in 284 seconds with one NVIDIA Tesla V100.

Bathymetric DEM data has been extracted from the 15 arc-sec resolucion global GEBCO database. Topographic data has been extracted from the MDT05 DEM with 5 m resolution provided by the IGN (National Geographic Institute from Spain). The topobathymetric ambient grid covers the Alborán Sea from 5.0ºW to 1.8353ºW and 35.0598ºN to 36.8499ºN (Fig. 6-4) with a resolution of 1.611 arc-sec (~50 m). The ambient grid 314 contains 28.284 million cells. Six high-resolution nested grids with a resolution of 0.201 arc-sec 315 (~6 m) and 52.522 million cells, has been defined along the Spanish coasts where the impact of 316 the tsunami is more important (Fig. 6-S3). Mean sea level is used as initial condition as tides are negligible in this area of the Mediterranean. Friction Manning coefficient is set to 0.02 and CFL stability number is set to 0.5.

6.5 Acknowledgements

This study was supported by the Spanish projects DAMAGE (CGL2016-80687-R AEI/FEDER), FAUCES (CTM2015-65461-C2-1-R), RNM148 and AGORA P18-RT-3275 Junta de Andalucía. The authors appreciate the IHS-Kingdom educational license. Research partially funded by the Programa Operativo FEDER Andalucía 2014-2020, call made by the University of Jaén 2018. The ICM-CSIC authors acknowledge Severo Ochoa funding from the Spanish government through the "Severo Ochoa Centre of Excellence" accreditation (CEX2019-000928-S).

6.6 Author contributions

F.E., J.G. and G.E conceived the idea for the study and wrote the paper with methodological contributions from J.G.V. in the tsunami mathematical model and J.P. in the seafloor deformation and tsunami potential. The geodynamic framework and fault characterization was done by F.E., J.G. and J.V., while the chronostratigraphic correlation with ODP sites was carry out by F.E. and G.E.. All these authors designed and performed the specific oceanographic cruises to study the Averroes Fault and its geologic context. F.E. also processed and compiled the seismic profiles and well data, integrating them into a IHS Kingdom project. J.P. calculated the seafloor deformation and tsunami potential model. The propagation tsunami model was done by J.G.V., J.M. and S.O. as well as associated figures and videos. All authors provided guidance on the analyses and commented on the manuscript.

6.7 Supplementary material

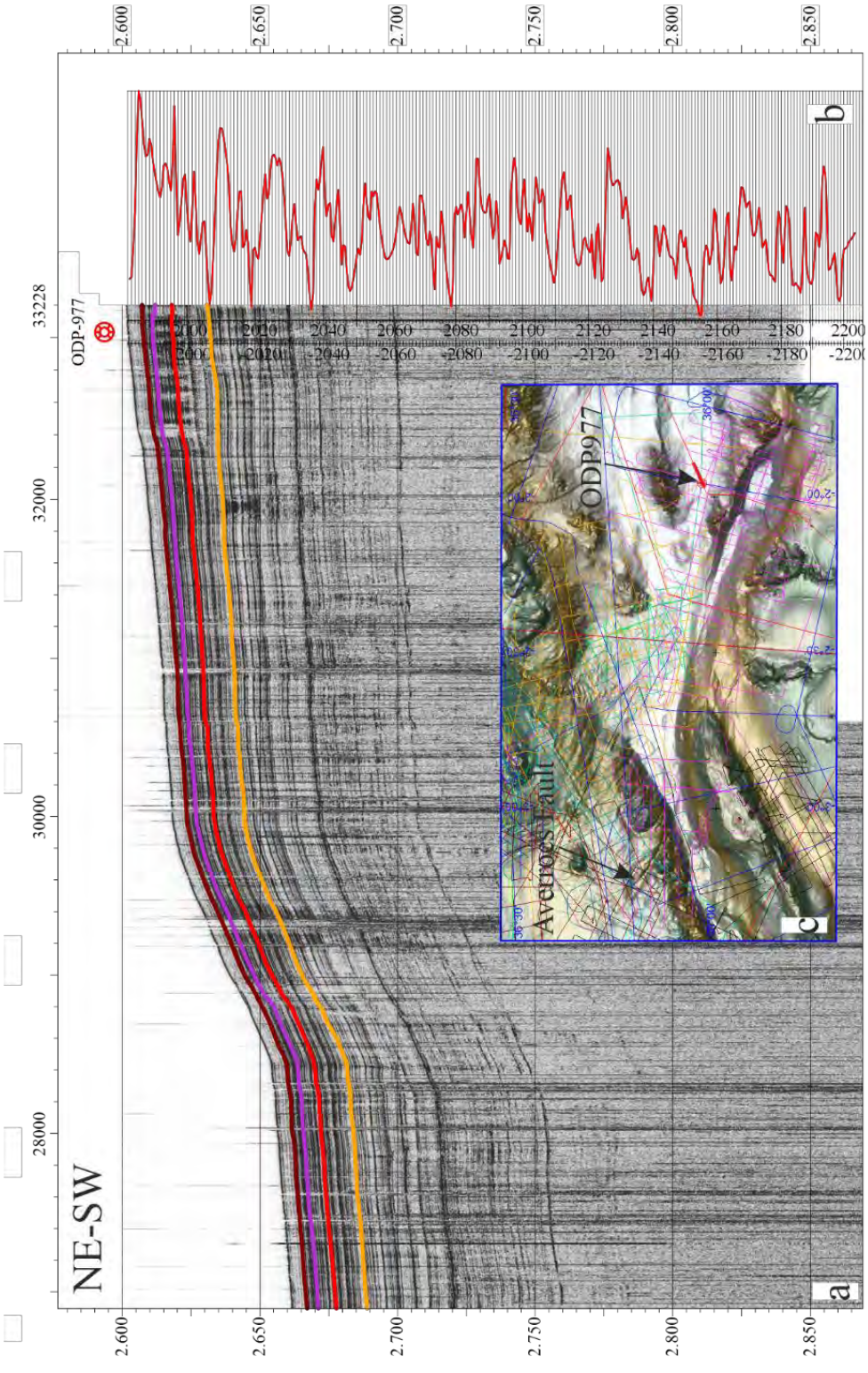

Supplementary Figure 6-S1: Chronostratigraphy correlation. Correlation between the TOPAS parametric seismic profile (ultra-high-resolution) (a) and oxygen-18 isotope curve; (b) stablished by Martrat et al. (2004) at ODP Site 977 well through a dense net of parametric seismic profiles. Seismic profile and well locations in c; there, also the seismic profiles (coloured lines) crossing the Averroes Fault that have been used for the strike-slip characterization can been seen. Horizontal and vertical scales respectively in meters and seconds (two-way travel time). (Figures generated using IHS Kingdom v. 2017, https://ihsmarkit.com, and mounted with CorelDRAW v. X7, https://www.corel.com).

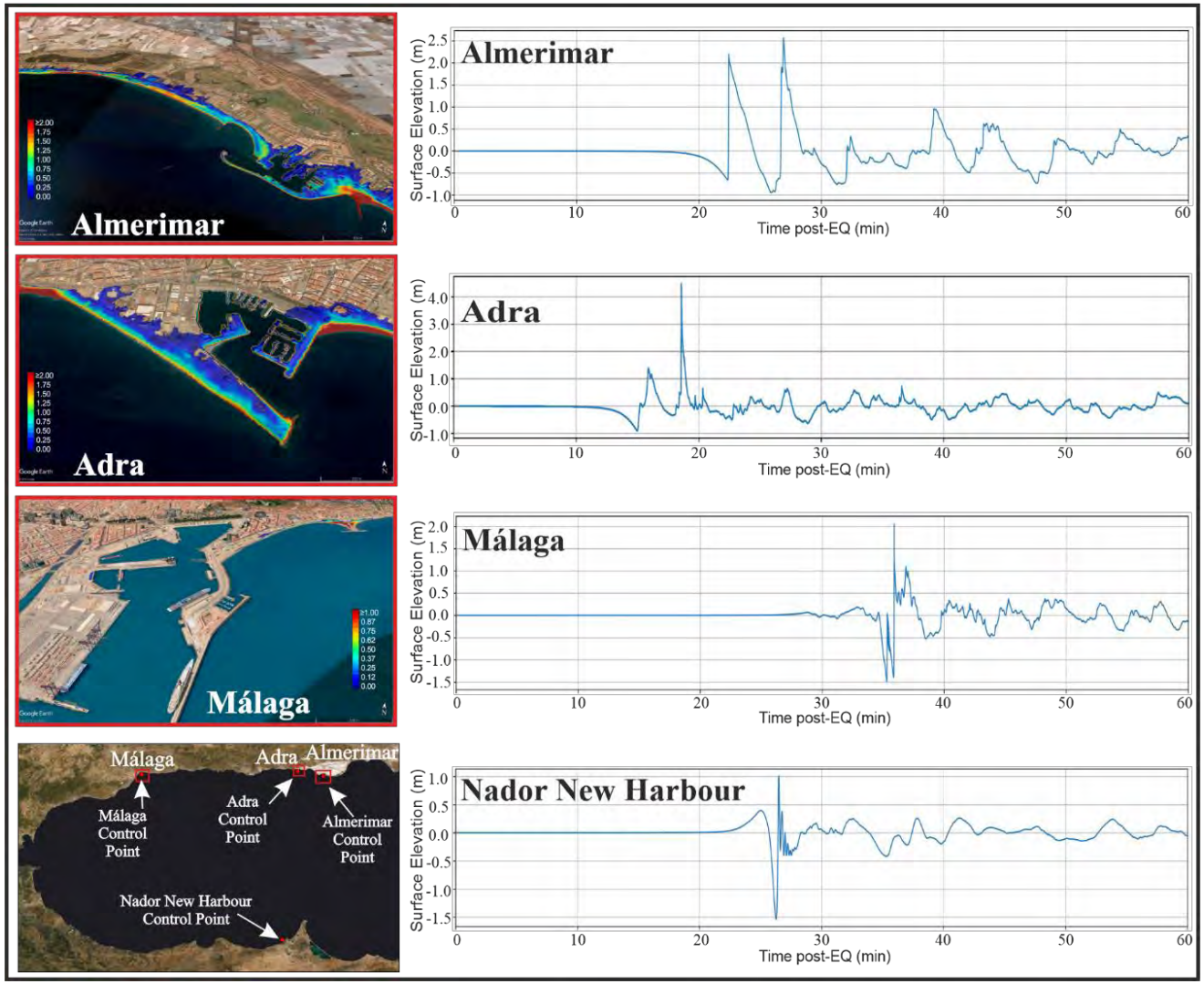

Supplementary Figure 6-S2: Tsunami impact. Satellite images from Google Earth (red squares) showing superimposed the tsunami water-level inundations of the Almerimar, Adra and Málaga zones; colour scale in metres. Plots represent tsunami wave height at control points based on seasurface time series simulated by Tsunami-HySEA stations (red dots). (Figures generated using Python, v. 3.7.3, https://www.python.org, and Matplotlib v. 3.4.2, https://matplotlib.org and mounted with CorelDRAW v. X7, https://www.corel.com).

Submesh	Size (number of volumes)	Longitude	Latitude
1	5968 x 1048 = 6254464	[-4.52107, -4.18754]	[36.6659, 36.7241]
2	5984 x 3128 = 18717952	[-4.52129, -4.18763]	[36.496, 36.6702]
3	3216 x 1880 = 6046080	[-4.69997, -4.52086]	[36.4949, 36.5994]
4	5984 x 1672 = 10005248	[-3.18805, -2.85362]	[36.6663, 36.7595]
5	6000 x 1672 = 10032000	[-2.85502, -2.51969]	[36.6663, 36.7595]
6	1024 x 1432 = 1466368	[-2.9629, -2.90696]	[35.2541, 35.3325]

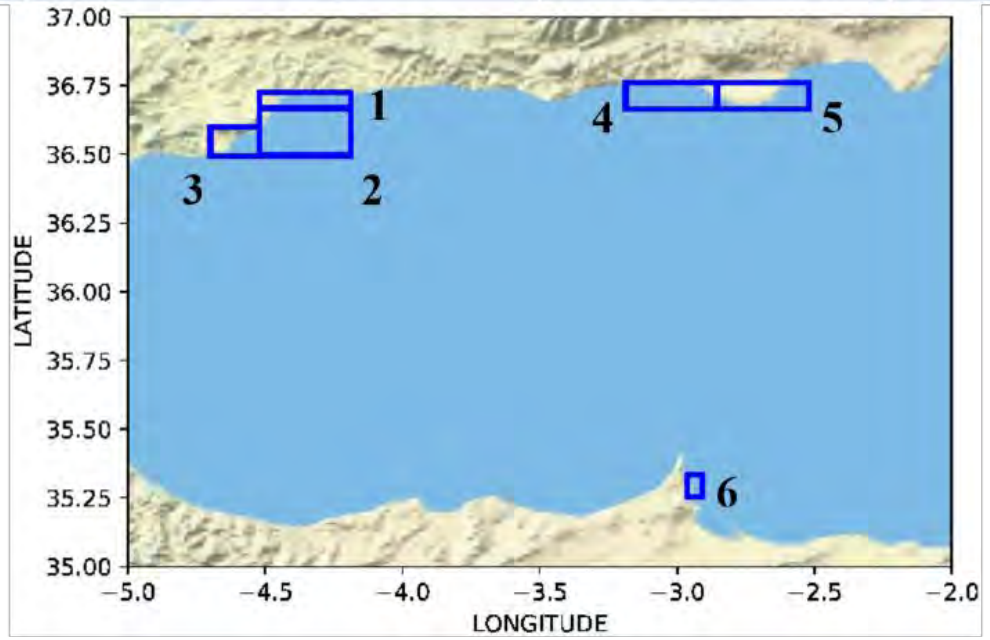

Supplementary Figure 6-S3: Nested meshes. Table showing the size and location of the 6 nested meshes. The figure below displays their situation in the Alborán Sea. (Figure generated using Python, v. 3.7.3, https://www.python.org, and Matplotlib v. 3.4.2, https://matplotlib.org and mounted with CorelDRAW v. X7, https://www.corel.com).

Supplementary Video 6-S1: tsunami propagation video of the Alborán Sea. Video length 31 seconds for 47 minutes of tsunami propagation.

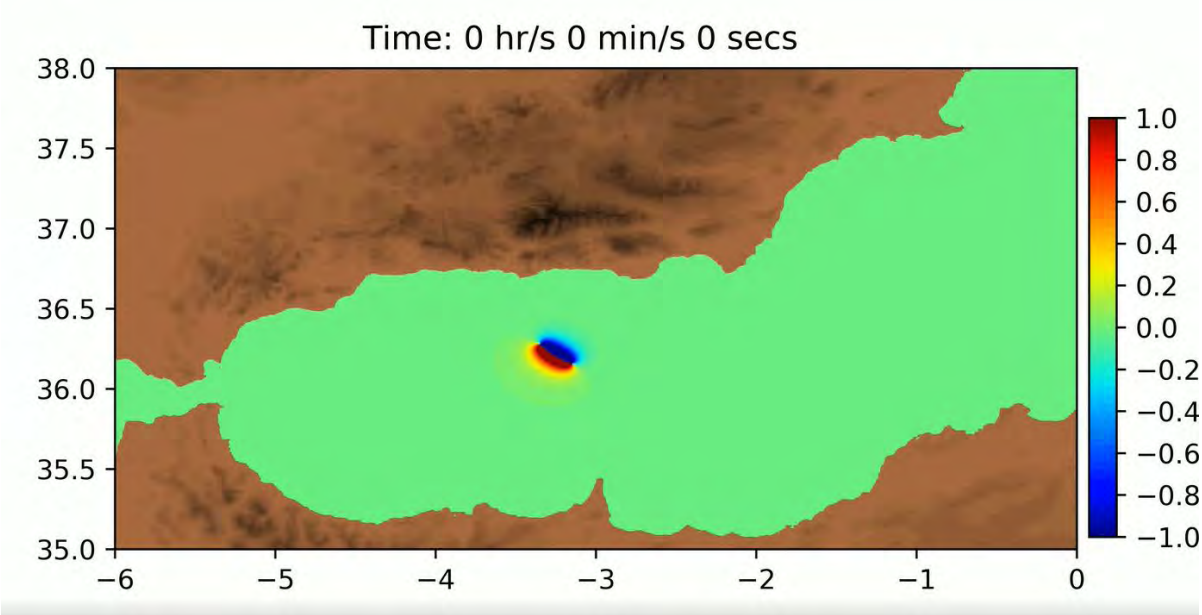

Supplementary Video 6-S2: tsunami propagation video of the Balerma zone Video length 1 minute for 1 hour of tsunami propagation.

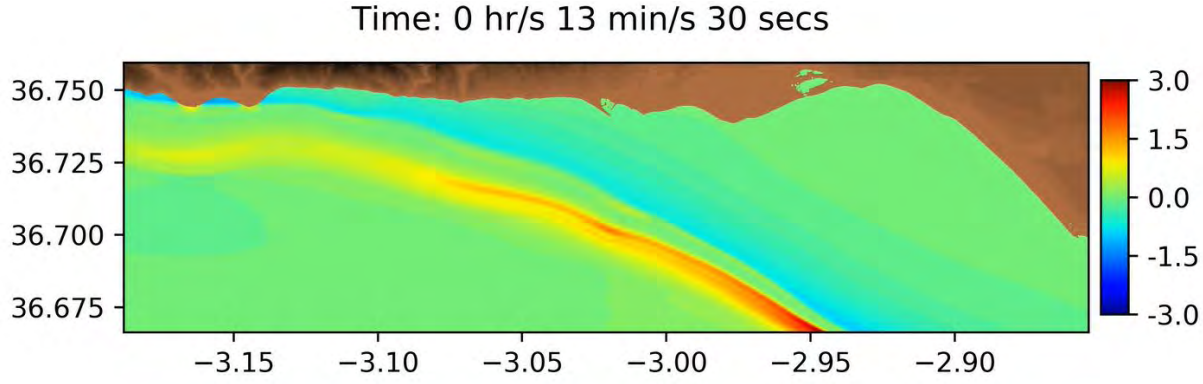

Supplementary Video 6-S3: tsunami propagation video of the Almerimar zone. Video length 1 minute for 1 hour of tsunami propagation.

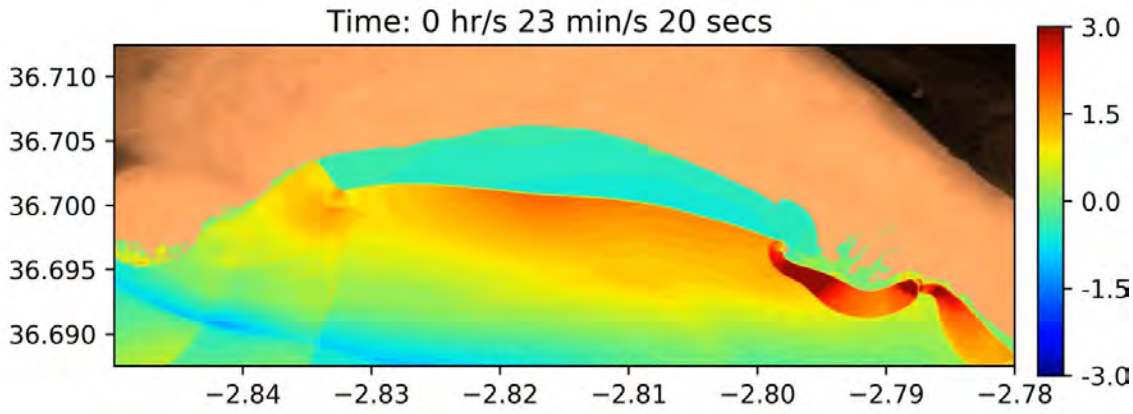

Supplementary Video 6-S4: tsunami propagation video of the Málaga zone. Video length 50 seconds for 1 hour of tsunami propagation.

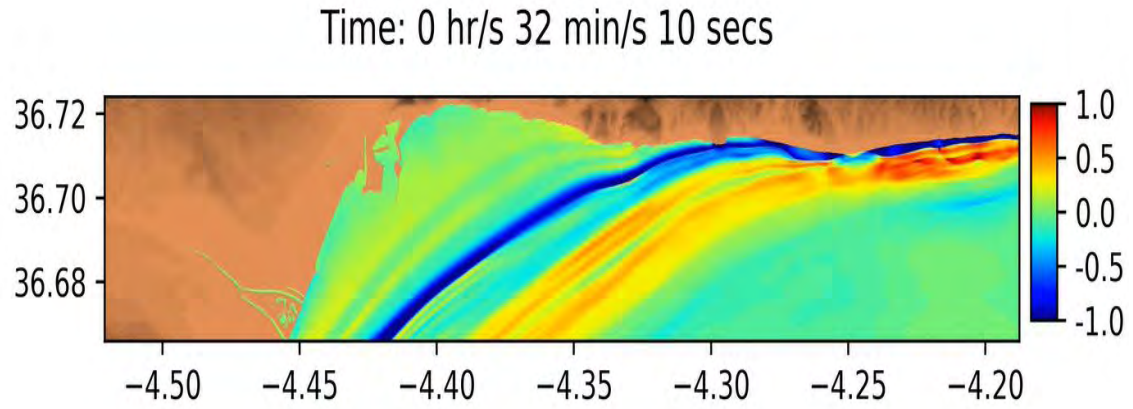

6.8 References

Altinok, Y., Ersoy, S., Yalciner, A. C., Alpar, B. and Kuran, U. Historical tsunamis in the Sea of Marmara. In International Tsunami Symposium ITS Proceedings, Session 4, Number 4-2, 527-534 (2001).

Becker-Heidmann, P., Reicherter, K. and Silva, P. G. 14 C-Dated Charcoal and Sediment Drilling Cores as First Evidence of Holocene Tsunamis at the Southern Spanish Coast. Radiocarbon, 49 (2), 827-835. https://doi.org/10.1017/S0033822200042703 (2007).

Bletery, Q., Sladen, A., Delouis, B. and Mattéo, L. Quantification of tsunami bathymetry effect on finite fault slip inversion. Pure Appl. Geophys. 172 (12), 3655-3670. https://doi.org/10.1007/s00024-015-1113-y (2015).

Borrero, J. C., Legg, M. R., and Synolakis, C. E. Tsunami sources in the southern California bight. Geophys. Res. Lett. 31, 13. https://doi.org/10.1029/2004GL020078 (2004).

Castro, M.J., González-Vida, J.M., Macías, J., Ortega, S. and de la Asunción, M. Tsunami-HySEA: A GPU-based model for Tsunami Early Warning Systems. Proceedings of the XXIV Congress on Differential Equations and Applications. XIV Congress on Applied Mathematics, 1-6 (2015).

Collot, J. Y., Marcaillou, B., Sage, F., Michaud, F., Agudelo, W., Charvis, P. ... and Spence, G. Are rupture zone limits of great subduction earthquakes controlled by upper plate structures? Evidence from multi-channel seismic reflection data acquired across the northern Ecuador–southwest Colombia margin. J. Geophys. Res.: Solid Earth, 109 (B11). https://doi.org/10.1029/2004JB003060 (2004).

Comas, M. C., Platt, J. P., Soto, J. I. and Watts, A. B. The origin and tectonic history of the Alborán Basin: Insights from Leg 161 results. In Proceedings of the Ocean Drilling Program Scientific Results (eds Zahn, R., Comas, M. C. and Klaus, A.) 161, 555–580 (Ocean Drilling Program, 1999).

De la Asunción, M., Castro, M.J., Fernández-Nieto, E. D., Mantas, J.M., Ortega-Acosta S. and González-Vida, J. M. Efficient GPU implementation of a two waves TVD-WAF method for the two-dimensional one layer shallow water system on structured meshes", Computers and Fluids 80, 441-452. https://doi.org/10.1016/j.compfluid.2012.01.012 (2013).

De Mets, C., Iaffaldano, G. and Merkouriev, S. High-resolution Neogene and Quaternary estimates of Nubia–Eurasia–North America plate motion. Geophys. J. Int. 203, 416–427. https://doi.org/10.1093/gji/ggv277 (2015).

Elbanna, A., Abdelmeguid, M., Ma, X., Amlani, F., Bhat, H. S., Synolakis, C., and Rosakis, A. J. Anatomy of strike-slip fault tsunami genesis. PNAS, 118 (19). https://doi.org/10.1073/pnas.2025632118 (2021).

Espinar, M. Los estudios de sismicidad histórica en Andalucía: los terremotos históricos de la provincia de Almería. In Instituto de Estudios Almerienses (eds. Posadas A. M. and Vidal F.). El Estudio de los Terremotos en Almería, 115-180. ISBN 84-8108-047-0 (1994).

Estrada, F., Ercilla, G. and Alonso, B. Pliocene-Quaternary tectonic-sedimentary evolution of the NE Alborán Sea (SW Mediterranean Sea). Tectonophysics, 282, 1-4, 423-442. https://doi.org/10.1016/S0040-1951(97)00227-8 (1997).

Estrada, F., Galindo-Zaldívar, J., Vázquez, J. T., Ercilla, G., D'Acremont, E., Alonso, B. and Gorini, C. Tectonic indentation in the central Alborán Sea (westernmost Mediterranean). Terra Nova, 30 (1), 24–33. https://doi.org/10.1111/ter.12304 (2018).

Geist, E. L. and Lou Zoback, M. Analysis of the tsunami generated by the Mw 7.8 1906 San Francisco earthquake. Geology 27 (1), 15-18. https://doi.org/10.1130/0091-7613(1999)027<0015:AOTTGB>2.3.CO;2 (1999).

Geist, E. L. and Lynett, P. J. Source processes for the probabilistic assessment of tsunami hazards. Oceanography 27, 2, 86-93. https://www.jstor.org/stable/24862158 (2014).

Gerardi, F., Barbano, M. S., De Martini, P. M. and Pantosti, D. Discrimination of tsunami sources (earthquake versus landslide) on the basis of historical data in eastern Sicily and southern Calabria. Bull. Seismol. Soc. Am. 98 (6), 2795-2805. https://doi.org/10.1785/0120070192 (2008).

Goldfinger, C., Morey, A. E., Nelson, C. H., Gutiérrez-Pastor, J., Johnson, J. E., Karabanov, E. ... and Party, S. S. Rupture lengths and temporal history of significant earthquakes on the offshore and north coast segments of the Northern San Andreas Fault based on turbidite stratigraphy. Earth Planet. Sci. Lett., 254 (1-2), 9-27. https://doi.org/10.1016/j.epsl.2006.11.017 (2007).

González-Vida J.M., Castro M.J., Macías J., de la Asunción M., Ortega S., Parés C. Tsunami-HySEA: A Numerical Model Developed for Tsunami Early Warning Systems (TEWS). In: Progress in Industrial Mathematics: Success Stories. SEMA SIMAI Springer Series, v. 5. Springer, Cham (eds. Cruz M., Parés C., Quintela P.). https://doi.org/10.1007/978-3-030-61844-5_12 (2021).

Grevemeyer, I., Gràcia, E., Villaseñor, A., Leuchters, W. and Watts, A. B. Seismicity and active tectonics in the Alborán Sea, Western Mediterranean: Constraints from an offshore-onshore seismological network and swath bathymetry data. J. Geophys. Res.: Solid Earth, 120 (12), 8348-8365. https://doi.org/10.1002/2015JB012073 (2015).

Heidarzadeh, M. and Satake, K. (2017). Possible Dual Earthquake–Landslide Source of the 13 November 2016 Kaikoura, New Zealand Tsunami. Pure Appl. Geophys. 174 (10), 3737-3749. https://doi.org/10.1007/s00024-017-1637-4 (2017).

Hébert, H., Schindele, F., Altinok, Y., Alpar, B. and Gazioglu, C. Tsunami hazard in the Marmara Sea (Turkey): a numerical approach to discuss active faulting and impact on the Istanbul coastal areas. Mar. Geol., 215 (1-2), 23-43. https://doi.org/10.1016/j.margeo.2004.11.006 (2005).

Hornbach, M. J., Braudy, N., Briggs, R. W., Cormier, M. H., Davis, M. B., Diebold, J. B. et al. High tsunami frequency as a result of combined strike-slip faulting and coastal landslides. Nat. Geosci. 3 (11), 783-788. https://doi.org/10.1038/NGEO975 (2010).

IGN: Catálogo de Tsunamis en las Costas Españolas, www.ign.es (Instituto Geográfico Nacional, 2009).

Juan, C., Ercilla, G., Hernández-Molina, J. F., Estrada, F., Alonso, B., Casas, D. et al. Seismic evidence of current-controlled sedimentation in the Alborán Sea during the Pliocene and Quaternary: Palaeoceanographic implications. Mar. Geol., 378, 292–311. https://doi.org/ 10.1016/j.margeo.2016.01.006 (2016).

Lin, J., and Stein, R.S. Stress triggering in thrust and subduction earthquakes, and stress interaction between the southern San Andreas and nearby thrust and strike-slip faults. J. Geophys. Res.: Solid Earth 109, B02303. https://doi.org/10.1029/2003JB002607 (2004).

Lorito, S., Piatanesi, A. and Lomax, A. Rupture process of the 18 April 1906 California earthquake from near-field tsunami waveform inversion. Bull. Seismol. Soc. Am. 98 (2), 832-845. https://doi.org/10.1785/0120060412 (2008).

Lynett, P.J., Gately, K., Wilson R., Montoya, L., Arcas, D., Aytore, B. et al. Inter-model analysis of tsunami-induced coastal currents. Ocean Modelling, 114, 14-32. https://doi.org/10.1016/j.ocemod.2017.04.003 (2017).

Macías, J., Mercado, A., González-Vida, J.M., Ortega, S. and Castro, M.J. Comparison and numerical performance of Tsunami-HySEA and MOST models for LANTEX 2013 scenario. Impact assessment on Puerto Rico coasts. Comparison and computational performance of Tsunami-HySEA and MOST models for LANTEX 2013 scenario: Impact assessment on Puerto Rico coasts. In Global Tsunami Science: Past and Future, Volume I (eds. Geist E.L., Fritz H.M., Rabinovich A.B. and Tanioka Y.) 3973-3997. Birkhäuser, Cham. ISBN 978-3-319-55479-2 (2016).

Macías, J., Castro, M.J., Ortega, S., Escalante, C. and González-Vida, J.M. Performance benchmarking of Tsunami-HySEA model for NTHMP's inundation mapping activities. Pure Appl. Geophys, 174 (8), 3147-3183. https://doi.org/10.1007/s00024-017-1583-1 (2017).

Mann, P., Taylor, F. W., Edwards, R. L. and Ku, T. L. Actively evolving microplate formation by oblique collision and sideways motion along strike-slip faults: An example from the northeastern Caribbean plate margin. Tectonophysics, 246 (1-3), 1-69. https://doi.org/10.1016/0040-1951(94)00268-E (1995).

Martínez-García, P., Comas, M., Soto, J. I., Lonergan, L. and Watts, A. B. Strike-slip tectonics and basin inversion in the Western Mediterranean: the Post-Messinian evolution of the Alborán Sea. Basin Res. 25 (4), 361-387. https://doi.org/10.1111/bre.12005 (2013).

Martínez-García, P., Comas, M., Lonergan, L. and Watts, A. B. From extension to shortening: tectonic inversion distributed in time and space in the Alborán Sea, Western Mediterranean. Tectonics, 36 (12), 2777-2805. https://doi.org/10.1002/2017TC004489 (2017).

Martrat, B., Grimalt, J. O., Lopez-Martínez, C., Cacho, I., Sierro, F. J., Flores J.A. et al. Abrupt temperature changes in the Western Mediterranean over the past 250,000 years. Science, 306 (5702), 1762-1765. https://doi.org/10.1126/science.1101706 (2004).

Molinari, I., Tonini, R., Piatanessi, A., Lorito, S., Romano, F., Melini, D. et al. Fast evaluation of tsunami scenarios: uncertainty assessment for a Mediterranean Sea database. Nat. Hazards Earth Syst. Sci. 16, 2593-2602. https://doi.org/10.5194/nhess-16-2593-2016 (2016).

Okada, Y. Surface deformation due to shear and tensile faults in a half-space. Bull. Seismol Soc. Am. 75, 1135-1154 (1985).

Okada, Y. Internal deformation due to shear and tensile faults in a half-space. Bull. Seismol Soc. Am. 82, 1018-1040 (1992).

Okal, E. A. and Synolakis, C. E. A theoretical comparison of tsunamis from dislocations and landslides. Pure Appl. Geophys. 160 (10-11), 2177-2188. https://doi.org/10.1007/s00024-003-2425-x (2003).

Perea, H., Gràcia, E., Martínez-Loriente, S., Bartolome, R., de la Peña, L. G., de Mol, B. et al. Kinematic analysis of secondary faults within a distributed shear-zone reveals fault linkage and increased seismic hazard. Mar. Geol. 399, 23-33. https://doi.org/10.1016/j.margeo.2018.02.002 (2018).

Pérez-Belzuz, F. Geología del Margen y Cuenca del Mar de Alborán Durante el Plio-Cuaternario: Sedimentación y Tectónica. PhD Thesis, University of Barcelona (1999).

Soto, J. I., Fernández-Ibáñez, F. and Talukder, A. R. Recent shale tectonics and basin evolution of the NW Alborán Sea. The Leading Edge, 31 (7), 768-775 (2012).

Tanioka, Y. and Satake, K. Tsunami generation by horizontal displacement of ocean bottom. Geophys. Res. Lett. 23 (8), 861-864. https://doi.org/10.1029/96GL00736 (1996).

Toda, S., Stein, R.S., Richards-Dinger, K. and Bozkurt, S. Forecasting the evolution of seismicity in southern California: animations built on earthquake stress transfer. J. Geophys. Res.: Solid Earth, 110, B05S16. https://doi.org/10.1029/2004JB003415 (2005).

Yamashita, T., and Sato, R. Generation of tsunami by a fault model. J. Phys. Earth 22 (4), 415-440. https://doi.org/10.4294/jpe1952.22.415 (1974).

PART III

THE SEDIMENTARY CONVULSIVE EVENT OF THE ATLANTIC ZANCLEAN FLOODING

Part III of this Ph. D. Thesis deals with the study of the convulsive event of the Zanclean megaflood that put an end to the Messinian Salinity Crisis. Chapters 7 and 8, which make up Part III, analyse the geological evidence of the megaflood, model it mathematically, compare it with other areas of the Mediterranean Sea and discuss its implications for the Messinian Salinity Crisis model.

In Chapter 7, the megaflood geological evidences are analysed by means of seismic profiles, chronostratigraphic correlation and multibeam bathymetry data. The geomorphological elements associated with this event are mapped and the isochore of the top Messinian surface of the Alborán Basin is reconstructed. Then, by integrating the mapped elements a geological model of the Zanclean megaflood is presented. Finally, the opening of the Strait of Gibraltar and its impact on the Alborán Sea is mathematically modelled and the geomorphological results are integrated with the mathematical modelling.

Chapter 8 studies the regional impact and consequences of the megaflood convulsive event by comparing the threshold of the Strait of Gibraltar with that of the Strait of Sicily. Likewise, the implications of the megaflood on the Messinian Salinity Crisis model are discussed in relation to whether or not there was a disconnection between the Mediterranean and the Atlantic Ocean.

Chapter 7

7. Zanclean Megaflood geologic evidences and mathematical modelling

7.1 Geologic evidences

7.2 Megaflood modelling

7.3 Integration of the mathematical model with the geomorphological evidences

7.1 Geologic evidences

Impact of pulsed Atlantic water inflow into the Alboran Basin at the time of the Zanclean flooding

Ferran Estrada and Gemma Ercilla and Christian Gorini and Belén Alonso and Juan Tomás Vázquez and Daniel García-Castellanos and Carmen Juan and Andrés Maldonado and Abdellah Ammar and Mohammed Elabbassi

F. Estrada (*), G. Ercilla, B. Alonso, C. Juan: Instituto de Ciencias del Mar, CSIC, Passeig Marítim de la Barceloneta 37-49, 08003 Barcelona, Spain e-mail: festrada@icm.csic.es

C. Gorini: Université Pierre et Marie Curie, ISTEP, Paris 6, France

J. T. Vázquez: Instituto Español de Oceanografía, Puerto Pesquero s/n, 29640 Fuengirola, Spain

D. García-Castellanos: Instituto de Ciencias de la Tierra Jaume Almera, CSIC, Solé i Sabaría s/n, Barcelona, Spain

A. Maldonado: Instituto Andaluz de Geología Mediterránea, CSIC, Universidad de Granada, 18002 Granada, Spain

A. Ammar, M. Elabbassi: Université Mohammed V,

Published on: Geo-Mar Lett, 2011.

Volume 31, pages 361-376

DOI: 10.1007/s00367-011-0249-8

Impact Factor (JCR): 1.472 (2011), Q2 en Geosciences, multidisciplinary. 75/170

ABSTRACT

The study of more than 500 single-and multi-channel seismic records enabled the generation of a detailed palaeo-bathymetric map of the Messinian surface over most of the Alborán Basin, Western Mediterranean. This regional surface is characterized by several erosional features (channels, terraces and canyons) and topographic highs (structural, volcanic and diapiric in origin). The most prominent feature is the incised Zanclean Channel crossing the entire basin, its entrenchment having been associated with the opening of the Strait of Gibraltar and subsequent inflow of Atlantic waters. The incision depth of the channel is variable, suggesting local variations in the erosive capacity of the Atlantic inflow, conditioned mainly by the regional basin topography and the local presence of topographic highs. Adjacent to this channel along the Spanish and Moroccan margins, and near the Strait of Gibraltar, several submarine terraces developed at different depths suggest a pulsed flooding of the Alborán Basin. There could have been two major inflow phases of Atlantic water, one shortly before and another during the Zanclean flooding, the latter accompanied by periods of relative sea-level stillstands that enabled terrace development. Alternatively, these features were all generated during the main flooding evident and subsequent pulsed infilling of the basin.

7.1.1 Introduction

The Alborán Sea is located in the westernmost part of the Mediterranean Sea, close to the Strait of Gibraltar (Fig. 7.1-1). This oceanographic setting makes this a pivatol region for the study of events at the time of the Strait of Gibraltar opening at 5.33 Ma, thereby ending the Messinian Salinity Crisis (MSC; Krijgsman et al. 1999). The MSC was associated with the partial or near-total desiccation of the Mediterranean Basin from 5.96 to 5.33 Ma. This period is widely documented by seismic data that reveal the existence of the high-amplitude M (Messinian) reflector in the deep basin (Ryan et al. 1973). This reflector was created by the deposition of a salt layer, although several interpretations have been proposed for the depositional processes involved (Hsü et al., 1973; Clauzon, 1978; Maillard et al. 2006; CIESM, 2008; Bache et al. 2009). The MSC is also documented by an extensive erosion surface along the basin margins, the Messinian Erosion Surface (Hsü et al. 1973; Clauzon 1978; Montadert et al. 1978; CIESM 2008; Bache et al. 2009). In terms of this salt layer and erosion surface, the M reflector forms the base of the Pliocene sequence.

The MSC ended at 5.33 Ma when the Mediterranean– Atlantic connection was re-established through the Strait of Gibraltar in the course of a catastrophic event known as the Zanclean flooding (Krijgsman et al. 1999; Blanc 2002; García-Castellanos et al. 2009). This event formed a deep erosional channel in the strait, its trajectory having been mapped up to the westernmost sector of the Western Alborán Basin (Campillo et al. 1992; Blanc 2002; García-Castellanos et al. 2009; Estrada et al. 2010). This channel is incised into Miocene deposits and filled by Pliocene– Quaternary sediments, and merges laterally with the basinwide Messinian Erosion Surface. Several authors have modelled the flooding event mathematically but little is known about how it affected the Messinian floor in the Alborán Basin. Seeing that the region faced the new marine gateway, it must have experienced the greatest impact of the catastrophic inflow (Mulder and Parry 1977; Weijermars 1988; Campillo et al. 1992; Bache et al. 2009; Estrada et al. 2010). Indeed, deposits related to the MSC are expected to be rare in the Alborán Basin, due to both the erosional character of the Messinian surface and the lack of evaporite deposition in this region (Montadert et al. 1978; Rouchy and Caruso 2006; Bache et al. 2009).

The present study reports novel findings on the morpho-logical imprints of Atlantic water inflow into the Alborán Basin at the time of the Zanclean flooding event. It interprets the morphological features characterizing the MSC surface in terms of their morpho-seismic expression within the context of the regional physiographic and structural setting.

7.1.2 Geological and oceanographic setting

The Alborán Basin is the westernmost basin of the Mediterranean Sea (Fig. 7.1-1). It is 150 km wide and 350 km long, and is bounded by the Gibraltar Arc with the Spanish Betic mountains in the north and the Moroccan Rif mountains in the south. This extensional basin developed during the Neogene in the course of lithospheric convergence between the African and Eurasian tectonic plates (Dewey et al. 1989). It is considered to have been formed during the Early Miocene by means of lithospheric thinning that occurred on a former Late Cretaceous–Palaeogene (?) collisional orogen (Balanyá and García-Dueñas 1987; Platt and Vissers 1989; García-Dueñas et al. 1992; Watts et al. 1993; Comas et al. 1999). The basement of the Alborán Basin is composed mainly of metamorphic and volcanic rocks of the Alborán Domain, which currently outcrops on land in the Spanish and Moroccan peripheries (Betics and Riffean internal zones; Fig. 7.1-1). The regional lithospheric thinning was concomitant with compression, crustal thickening and westward shifting of the Gibraltar Arc (Comas et al. 1999).

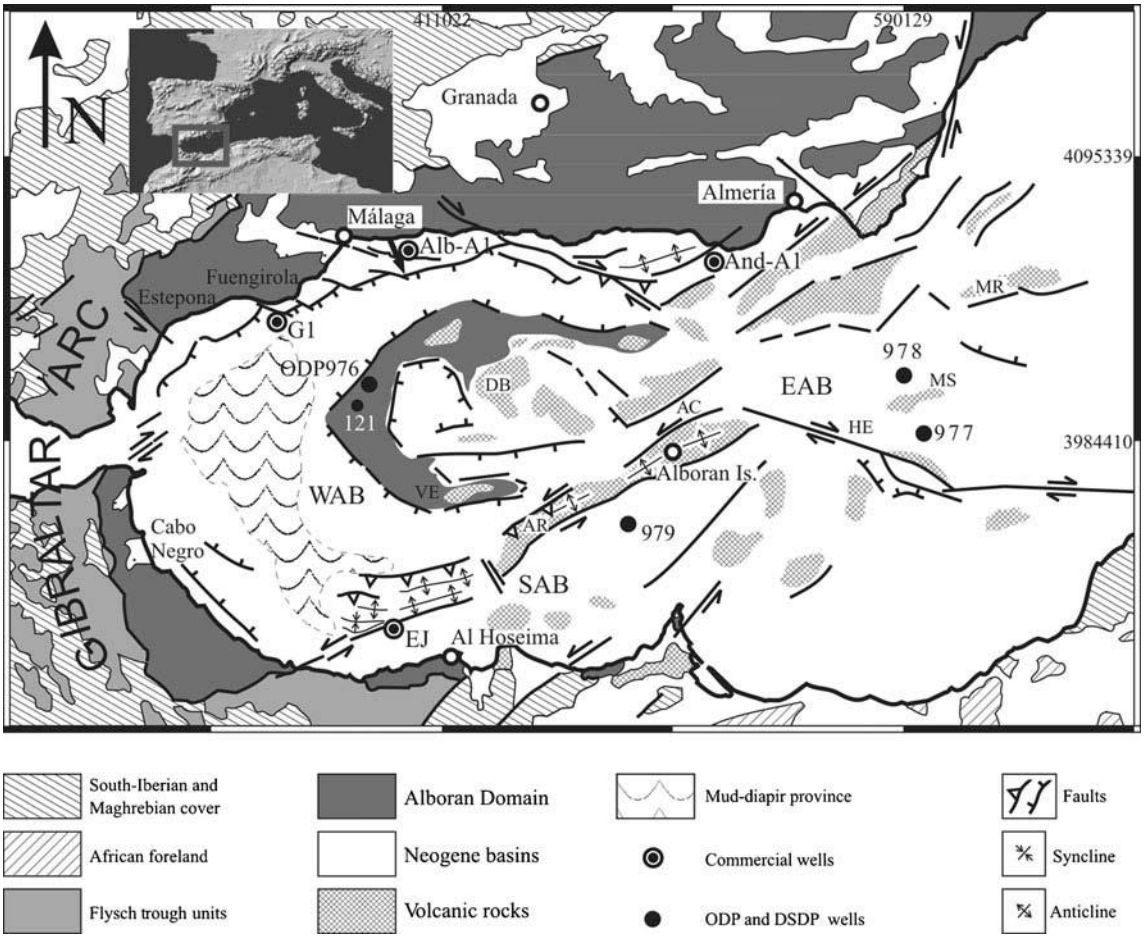

Figure 7.1-1 Locality map of the study area, and geological sketch of the main structural features and sub-basins of the Alborán Sea (modified from Comas et al. 1999). AC Alborán Channel, AR Alborán Ridge, DB Djibouti Bank, EAB East Alborán Basin, HE Habibas Escarpment, MR Maimonides Ridge, MS Al-Mansour Seamount, SAB South Alborán Basin, VE Vizconde de Eza High, WAB Western Alborán Basin. Commercial wells: EJ, G1, Alb-A1, And-A1. ODP and DSDP wells: 121, 976, 977, 978, 979.

The Alborán Basin can be subdivided into three major morpho-structural sub-basins, the Western Alborán Basin (WAB), East Alborán Basin (EAB) and South Alborán Basin, delimited by the Alborán Ridge, a major structural high that divides the region obliquely (Maldonado et al. 1992; Fig. 7.1-1). Topographic highs along the margins and in the sub-basins vary in nature, being composed of volcanic rocks, basement blocks and mud diapirs. The present-day configuration of the Alborán Basin has resulted from the superimposition of consecutive stages of rifting during the Miocene (22-8/9 Ma) and a subsequent Late Miocene (8/ 9 Ma to present) compressive reorganization (Bourgois et al. 1992; Maldonado et al. 1992; Mauffret et al. 1992; Watts et al. 1993; Comas et al. 1999). Backstripping analysis indicates two main stages of tectonic subsidence during the Early and Middle Miocene and a generalized uplifting from the Late Miocene

onwards (Cloetingh et al. 1992; Docherty and Banda 1995). There is active mud diapirism in the WAB (Fig. 7.1-1) where the sedimentary cover reaches a thickness of more than 8 km, contrasting with the EAB and the South Alborán Basin where it barely reaches 3 km (Soto et al. 1996; Pérez-Belzuz et al. 1997).

The filling of the Alborán Basin is composed of Early Miocene to Quaternary marine deposits. Six seismic units bounded by regional unconformities have been identified: I to VI, from young to older (Comas et al. 1992). Unit VI is composed of olistostromes containing metamorphic clasts from the Alborán Domain, flysch deposits, and undercompacted muds related to mud diapirism in the WAB. Unit V is Langhian-Serravallian in age and composed of two subunits, whereas unit IV is Upper Serravallian-Tortonian in age and composed of clays and silty clays with sandy interbeds and some marly intervals (Jurado and Comas 1992). Unit III is Tortonian in age and composed mostly of clays and silty clays with interbedded sandstones. Unit II is of Messinian age and characterized by marine siliciclastic sediments and shallow limestones that occasionally contain gypsum and anhydrite. The top of unit II is marked by a discontinuity that corresponds to the M reflector and can be traced over the whole Mediterranean Basin (Ryan et al. 1973). Unit I is defined by Plio-Quaternary deposits with different depositional patterns controlled by the interplay of glacio-eustatic changes, tectonism and marine water circulation (Ercilla et al. 1992; Hernández-Molina et al. 1994; Ercilla and Alonso 1996; Chiocci et al. 1997; Lobo et al. 2008).

Existing knowledge of the general present-day circulation indicates that, after entering the Alborán Sea through the Strait of Gibraltar, the surficial Atlantic water (down to 150–200 m water depth) describes two anticyclonic gyres, one in the WAB and another in the EAB (Parrilla et al. 1986; Millot 1999; Vargas-Yañez et al. 2002). Mediterranean waters comprise two distinct water masses that converge on the Strait of Gibraltar: the Levantine Intermediate Water, which extends down to 600 m water depth, and the Western Mediterranean Deep Water (below 600 m water depth) restricted largely to the Moroccan margin. Nelson (1990) suggested that this circulation pattern developed after the opening of the strait, although it was interrupted by an estuarine-type exchange of water masses during the early Quaternary (Huang and Stanley 1972).

7.1.3 Materials and methods

The dataset comprises a large number (>500) of industrial multi-channel seismic profiles downloaded from the SIGEOF and ICM-CSIC databases (http://www.igme.es/internet/sistemas_infor/BASESINTERNET/sigeof.htm and http://www.icm.csic.es/geo/gma/SurveyMaps/ respectively), and academic multi-and single-channel seismic profiles obtained during several scientific cruises (1975–2010) (Fig. 7.1-2). The analogue records were digitized and transformed to the standard SEGY format by means of the free software IMAGE2SEGY (http://www.icm.csic.es/gma/ca/content/image2segy-0; Farran 2008).

All seismic profiles were integrated in a Kingdom Suite project. The profile grid covers practically the whole Alborán Sea, except for the continental shelves and some sectors of the Moroccan continental slope. To establish the chronostratigraphic framework, the seismic data were correlated with several commercial (Andalucia G-1, Alborán A-1 and Andalucia A-1) and scientific (DSDP-121, ODP-976-977-978-979) well records, as well as with previous stratigraphic studies (e.g. Jurado and Comas 1992; Campillo et al. 1992; Tandon et al. 1998; Pérez-Belzuz 1999; Comas et al. 1999; Vázquez 2001; Martínez del Olmo and Comas 2008).

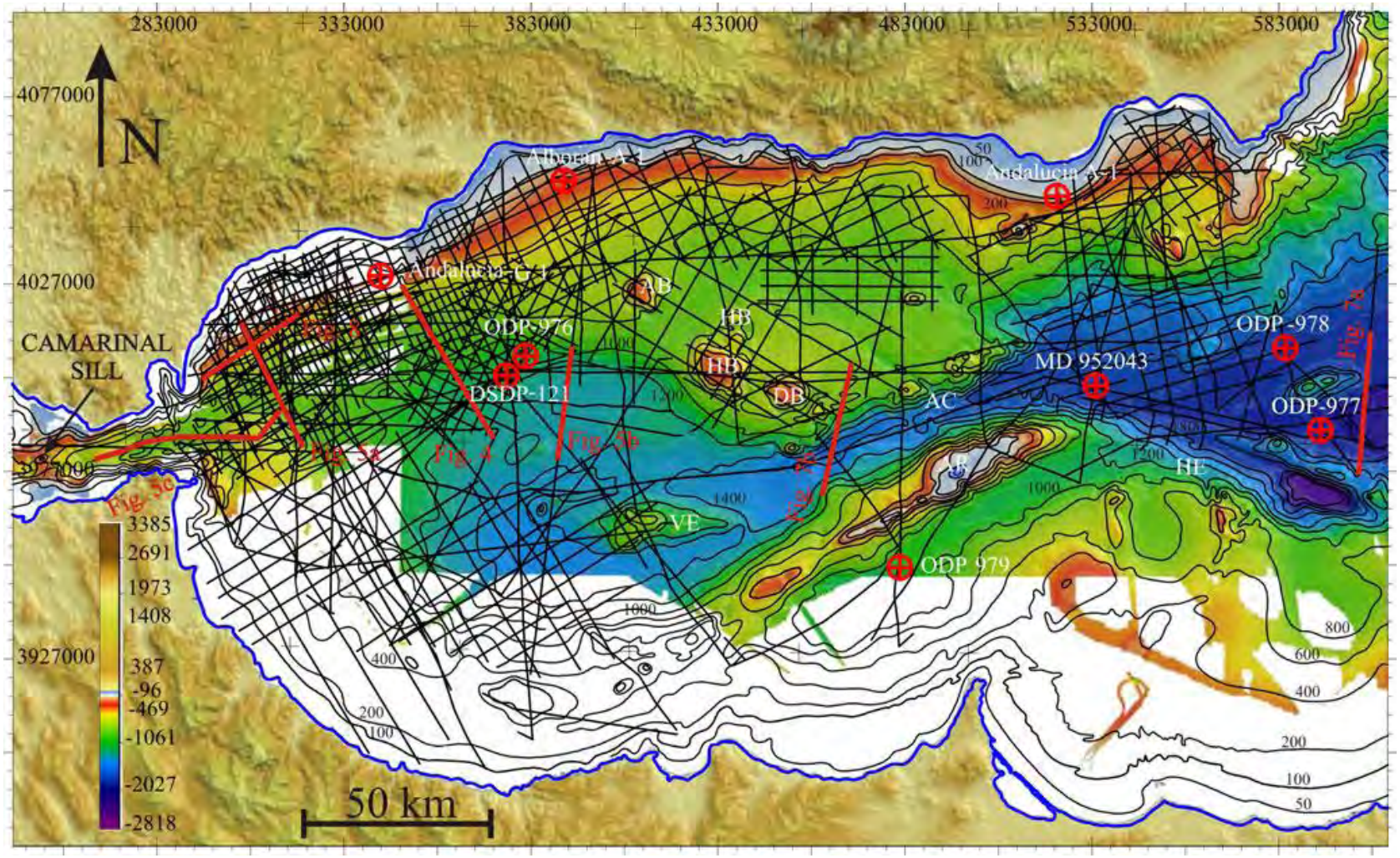

Figure 7.1-2. Multibeam bathymetric map of the Alborán Sea, showing the seismic database and commercial and scientific wells integrated in a Kingdom Suite project. AB Algarrobo Bank, AC Alborán Channel, AR Alborán Ridge, DB Djibouti Bank, HB Herradura Bank, HE Habibas Escarpment, VE Vizconde de Eza High, red lines locations of seismic profiles reported in this study.

7.1.4 Chronostratigraphic boundary marking the end of the Messinian Salinity Crisis

The surface defined by the M reflector in the Alborán Basin, hereafter called the Messinian surface, displays a strong erosional character of variable magnitude (up to 860 ms TWTT, two-way travel time) that truncates upper Miocene deposits and morphological highs (basement, diapirs and volcanoes; Figs. 7.1-3 and 7.1-4). It mainly involves tilted Tortonian (750–1,250 ms depth) or older deposits, as found in the tectonically active areas close to the Strait of Gibraltar (Fig. 7.1-5a).

The incision into Miocene deposits is of variable depth, high values having been recorded in tilted Miocene deposits on the upper slope (tens to hundreds of ms), and between the Strait of Gibraltar and the 976ODP well (about 500 ms) on the lower slope (Figs. 7.1-4 and 7.1-5a). Relatively high values occur also in the deep parts of the WAB (up to 860 ms), which contrasts with other basins of the Mediterranean Sea where the erosion is essentially restricted to the slopes of the basin margins (Gargani, 2004; Lofi et al. 2005; Bache et al. 2009; Gargani et al. 2010).

The Messinian surface has an irregular pattern along the Spanish margin (Figs. 7.1-4, 7.1-5a, b), but a smoother pattern along the Moroccan margin. Locally, these patterns are modified by the existence of mud diapirs or structural highs.

The few identified deposits related to the MSC are characterized by thin chaotic wedges (less than 100 ms), except along the Spanish slope margin between Estepona and Malaga where they are better preserved (up to 200 ms; Fig. 7.1-4). These deposits have been correlated with the Andalucia G-1 commercial well (Martínez del Olmo and Comas 2008) and are composed of clay with anhydrite, salt and pyrite. The material may have been supplied from the erosion of peripheral marginal evaporites during the drawdown in the course of the MSC, as has been the case in other areas of the Mediterranean Basin (Maillard et al. 2006; Bache et al. 2009).

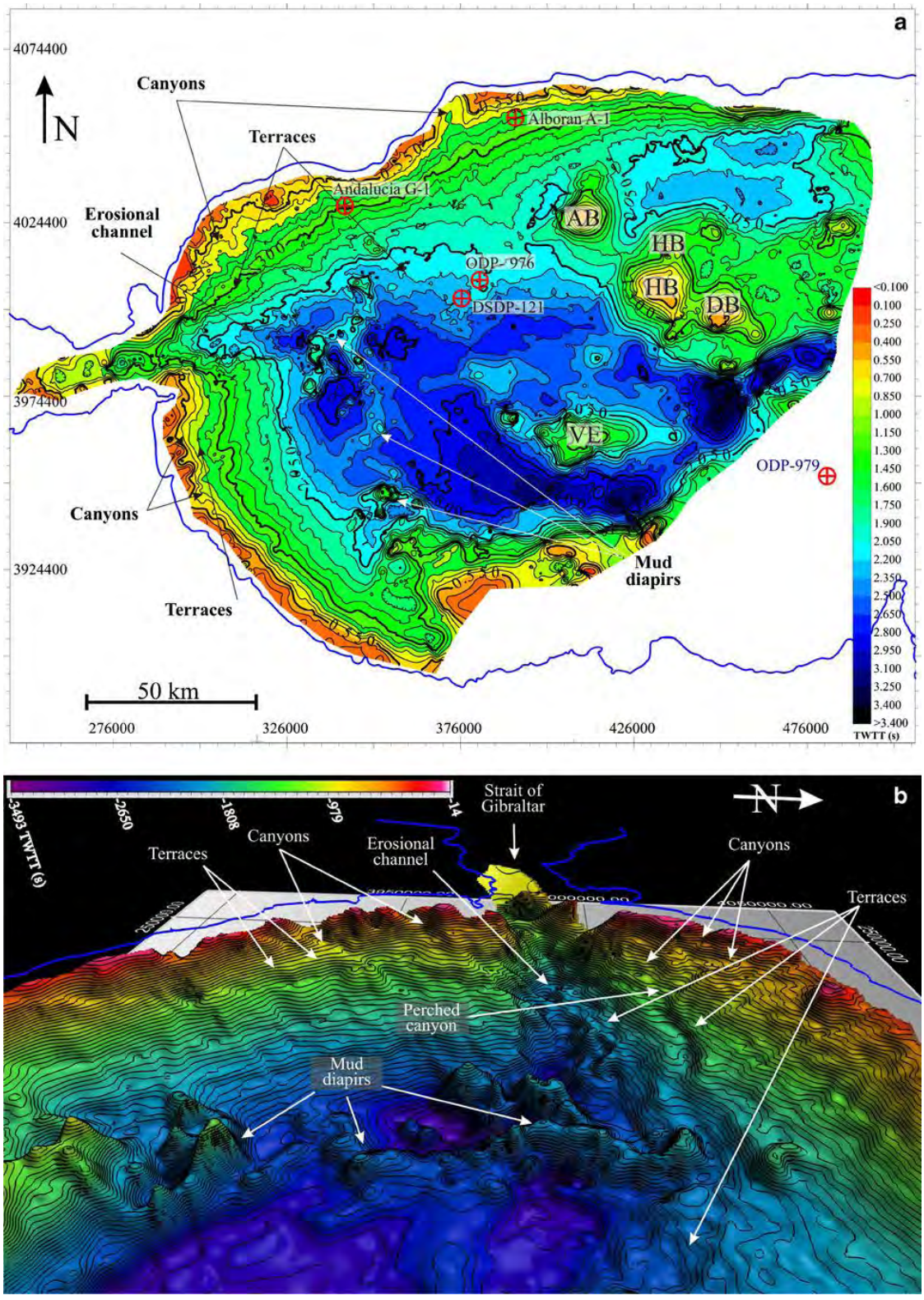

Figure 7.1-3. a) Topographic map of the Messinian surface (isobaths in seconds TWTT): AB Algarrobo Bank, DB Djibouti Bank, HB Herradura Bank, VE Vizconde de Eza High. b) Three-dimensional zoomed view of the present-day Messinian surface in the transition area between the Strait of Gibraltar and the Western Alborán Basin, showing the main morphological features related to the Zanclean flooding of the Mediterranean Sea. Vertical scale × 6 in seconds TWTT.

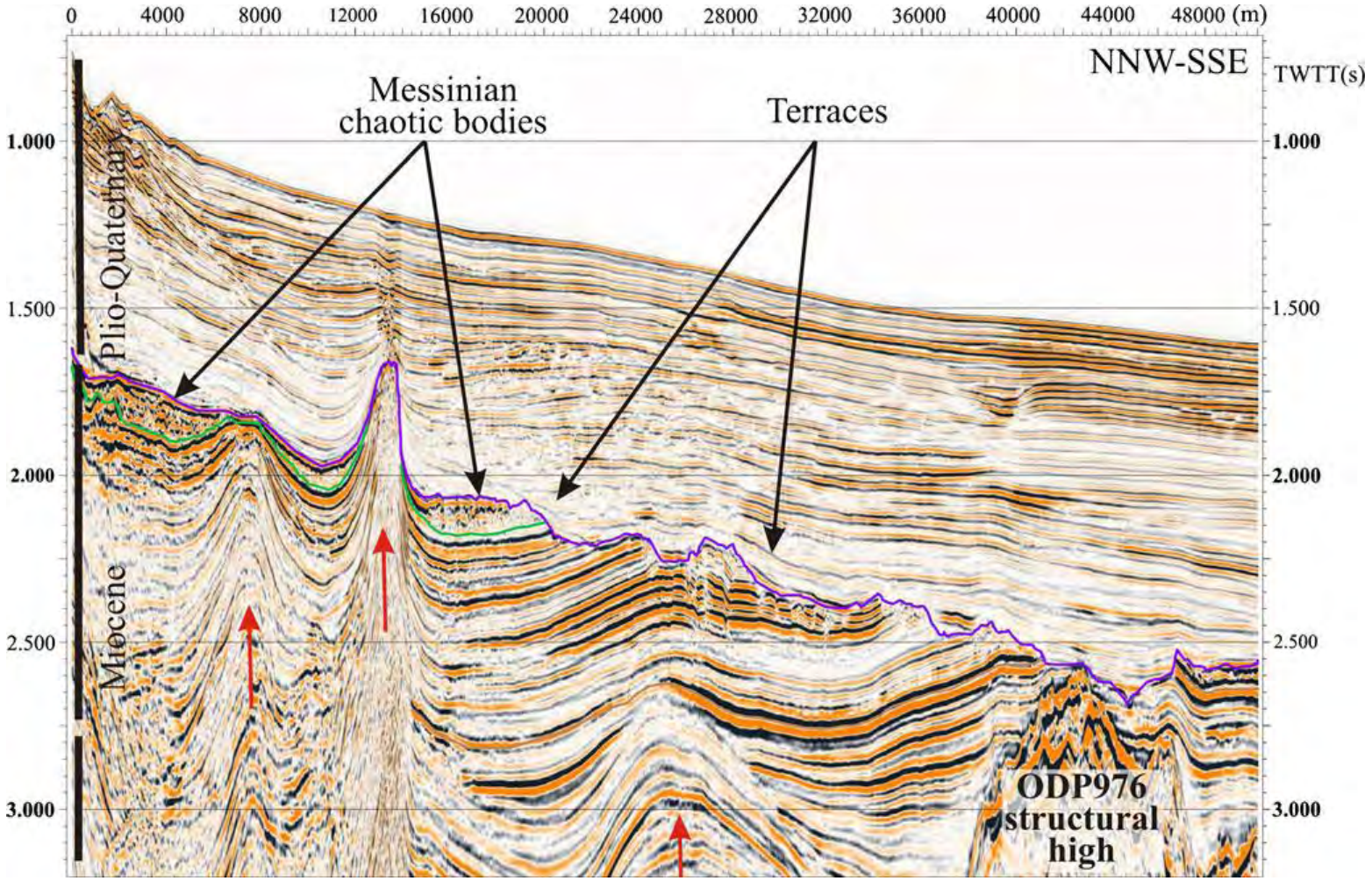

Figure 7.1-4. Multi-channel seismic profile showing the main configuration of the continental margin in the vicinity of the ODP976 high. Note the terraced slope, associated with chaotic Messinian sedimentary bodies and mud diapirism (pre- and post-Messinian). Red arrows diapirs, violet line top of Messinian surface, green line base of Messinian chaotic bodies (see Fig. 7.1-2 for profile location).

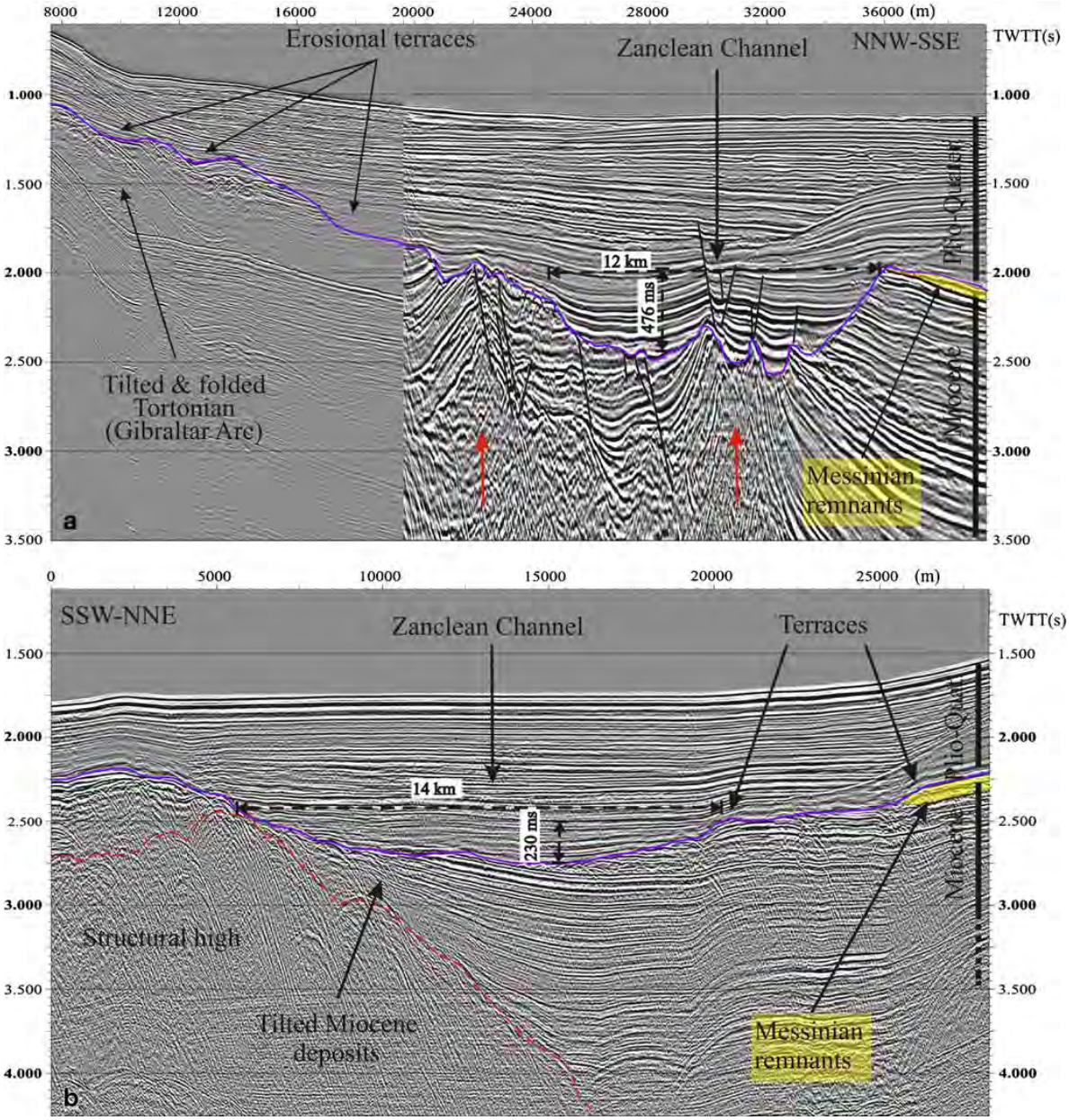

Figure 7.1-5. a) Composite single- (left) and multi-channel (right) seismic profile, showing the incised Zanclean Channel. Note the diapirism affecting the Miocene units, and the compressional structures (folding) along the Spanish margin (north). b) Multichannel seismic profile showing terraces and the Zanclean Channel in the distal reaches of the Western Alborán Basin. Note the tilted Miocene deposits against the structural high. c) Multi-channel seismic profile along the Zanclean Channel axis on the eastern side of the Strait of Gibraltar. Note the irregular erosion surface at the base of the Pliocene, and the deformed basement. Red arrows diapirs, violet lines top of Messinian surface, dashed red lines acoustic basement, black lines faults (see Fig. 7.1-2 for profile locations).

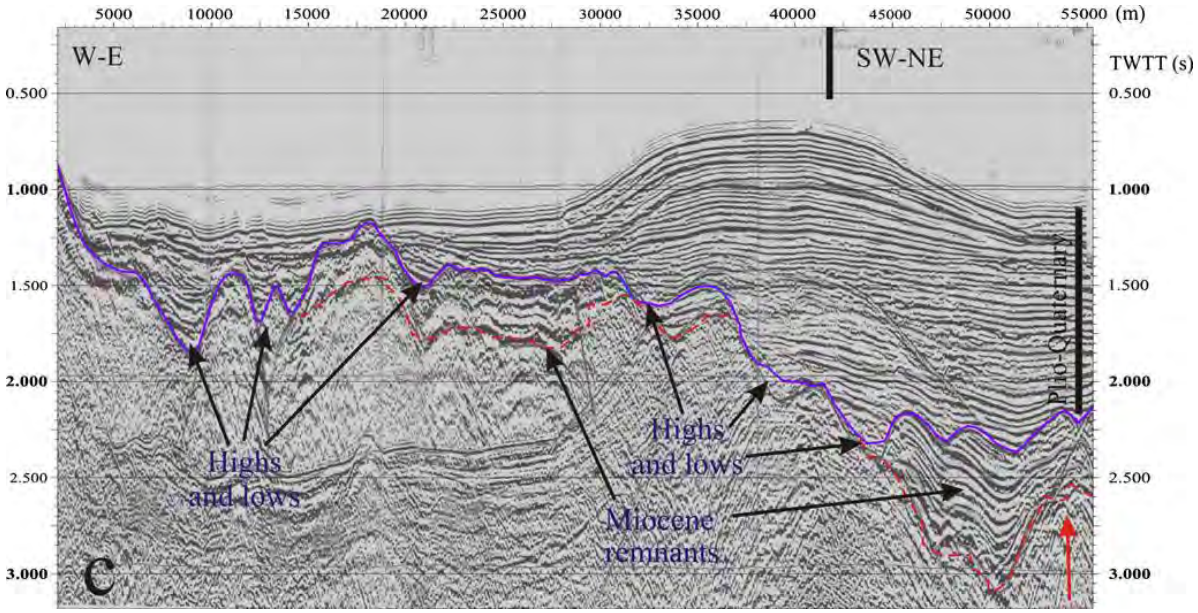

Figure 7.1-5c. (continued)

7.1.5 Morphology of the Messinian surface

Mapping of the Messinian surface has resulted in a regional morphological chart of the Alborán Sea soon after the Zanclean flooding event (Fig. 7.1-3). This surface, which covers a depth range of up to 3,300 ms (measurements include the water column), broadly depicts the main physiographic features that configured the Alborán Basin and conditioned the Zanclean flooding. The data reveal that the shape of the ancient Alborán Basin was similar to the present-day one, except for more enhanced topographic irregularities along the Spanish and Moroccan slope margins (compare Figs. 7.1-2 and 7.1-3). This is because the morphological features at that time were created mainly by the structural template, rather than by sedimentary systems as is the case today. The basin morphology can be broadly categorized into topographic highs and erosional features.

7.1.5.1 Topographic highs

Topographic highs have positive reliefs that protrude from the Messinian surface, either isolated or clustered (Figs. 7.1-3 and 7.1-6). Three types can be distinguished: diapirs, volcanic highs and structural highs.

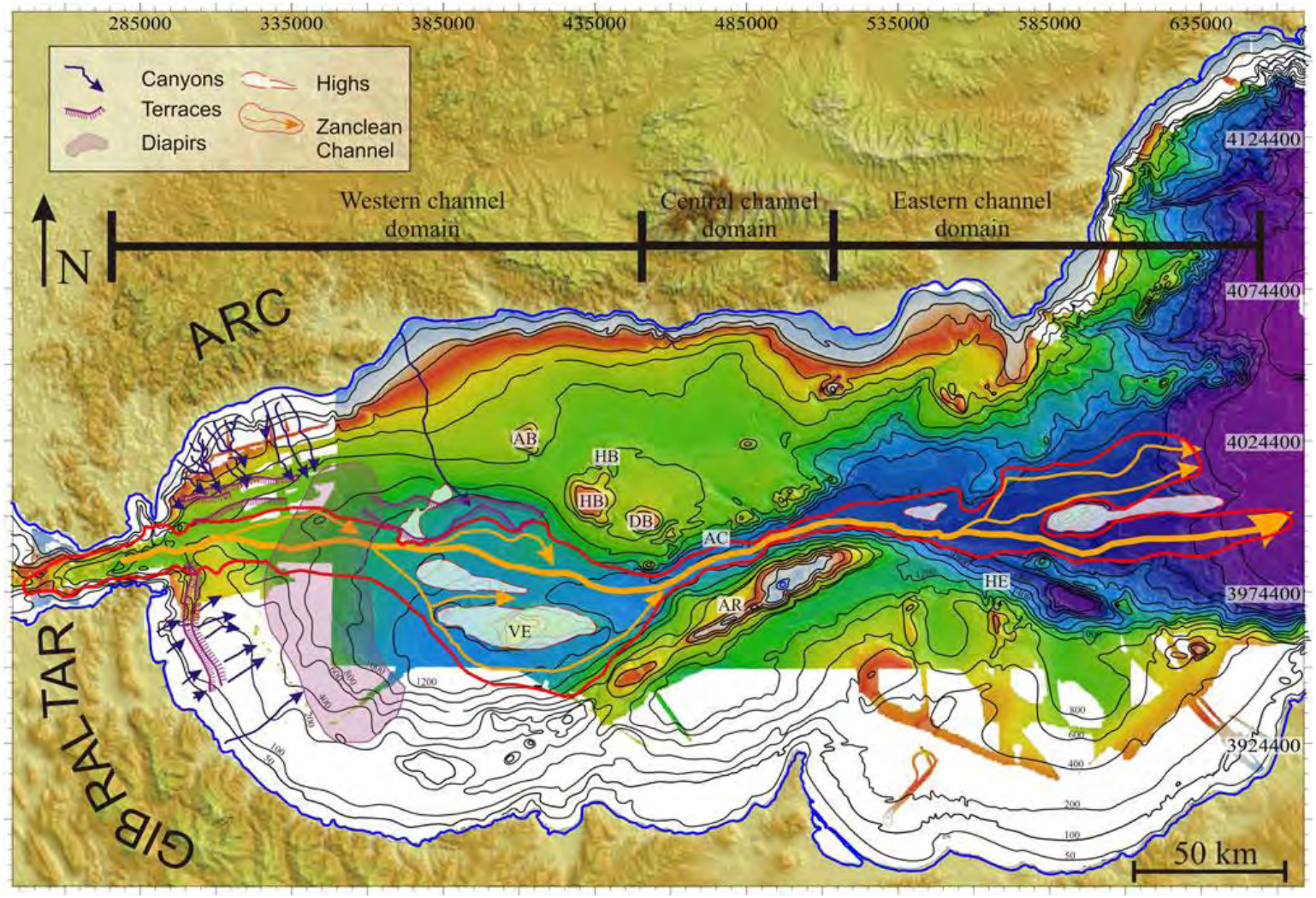

Figure 7.1-6. Present-day bathymetric map showing the locations of major highs and other morphological features: AB Algarrobo Bank, AC Alborán Channel, AR Alborán Ridge, DB Djibouti Bank, HB Herradura Bank, HE Habibas Escarpment, VE Vizconde de Eza High.

Diapirs

Diapirs occur mainly along the western side of the WAB, on the margin slope and in the deep basin sector defining a roughly arcuate field with an inverted bowl morphology that parallels the Gibraltar Arc (Figs. 7.1-3 and 7.1-6). These are mud diapirs related to overpressured sediments of Early to Middle Miocene (Jurado and Comas 1992; Talukder 2003) or even Messinian age (Pérez-Belzuz et al. 1997). On the basis of their distribution and the available seismic profiles, two different age groups were identified, one having formed prior to the MSC, the other post-MSC in Plio-Quaternary times. Diapirs emplaced prior to the MSC are located closer to the Strait of Gibraltar; the morphological expression of some is subdued, plausibly due to partial erosion during the Zanclean flooding (Fig. 7.1-5a, c). Other diapirs continued to be active or were uplifted during the Plio-Quaternary, as indicated by their association with several faults of that age (Fig. 7.1-5a). They are located to the east of the older diapirs, causing a local deformation of the Messinian surface (Fig. 7.1-4). In fact, the main mud diapir expression on the digital elevation map corresponds to the Plio-Quaternary period.

Volcanic highs

Volcanic highs are the most striking morphological features on the topographic map and dominate the present-day seafloor topography as much as they did during the Zanclean (Figs. 7.1-1 and 7.1-3a). They are largely concentrated on the north-eastern slope of the WAB in the form of a volcanic complex comprising the Djibouti Bank, Algarrobo Bank, and Herradura North and South banks. In addition, an isolated volcanic edifice, the Vizconde de Eza Bank, is located in the centre of the WAB (Figs. 7.1-1 and 7.1-3a).

Structural highs

Structural highs correspond to basement features shap-ing the Messinian surface on the slopes and in the deep sub-basins of the Alborán Sea (Figs. 7.1-1, 7.1-3 and 7.1-6). These highs, which are related to tectonic activity in the Alborán Basin (Woodside and Maldonado 1992; García-Dueñas et al. 1992; Watts el al. 1993; Martínez-García et al. 2011), are bounded by faults that have locally exhumed basement blocks (Fig. 7.1-5b). In the WAB, these comprise the ODP976 high and two unnamed highs in

the vicinity of the Vizconde de Eza Bank (Fig. 7.1-3a). It is suggested that the ODP976 high represents an outcrop exposed by erosion during the Zanclean flooding, because the M reflector truncates the Miocene deposits of which it is composed (Fig. 7.1-4). The two highs in the vicinity of the Vizconde de Eza Bank are likely also of Zanclean age, as demonstrated by the Plio-Quaternary sequence covering them and the lack of morphological expression on the present-day seafloor (Fig. 7.1-5b). Their formation is probably related to Late Miocene tectonism (Comas et al. 1992).

In the EAB, several structural highs were identified on the slopes and in the deep basin sector (Figs. 7.1-1, 7.1-6 and 7.1-7a). The most prominent is the Habibas Escarpment, which is NW-SE-aligned and outcrops on the present-day seafloor of the deep basin (Figs. 7.1-1 and 7.1-6). In addition, a number of Zanclean highs have been mapped that are buried under Plio-Quaternary sediments (Fig. 7.1-7a; Estrada et al. 1997).

7.1.5.2 Erosional features

Three major types of erosional features characterize the Messinian surface: the Zanclean Channel, several terraces, and canyons.

Zanclean Channel

This deep erosional feature, hereafter referred to as the Zanclean Channel, comprises a generally E-W-aligned, 390-km-long erosional depression that crosses the deepest parts of all three Alborán sub-basins from the Camarinal Sill in the Strait of Gibraltar (Figs. 7.1-2 and 7.1-3) to at least the transition to the Algero-Balear Basin. Seismic records show the channel to have been eroded into the Messinian Erosion Surface, being incised into Miocene deposits and subsequently filled by Pliocene–Quaternary sediments. The channel can be divided into three geographic domains based on morphological characteristics: a western domain, which extends from the Strait of Gibraltar to the easternmost end of the WAB, a central domain, which coincides with the present-day Alborán Channel, and an eastern domain that crosses the EAB.

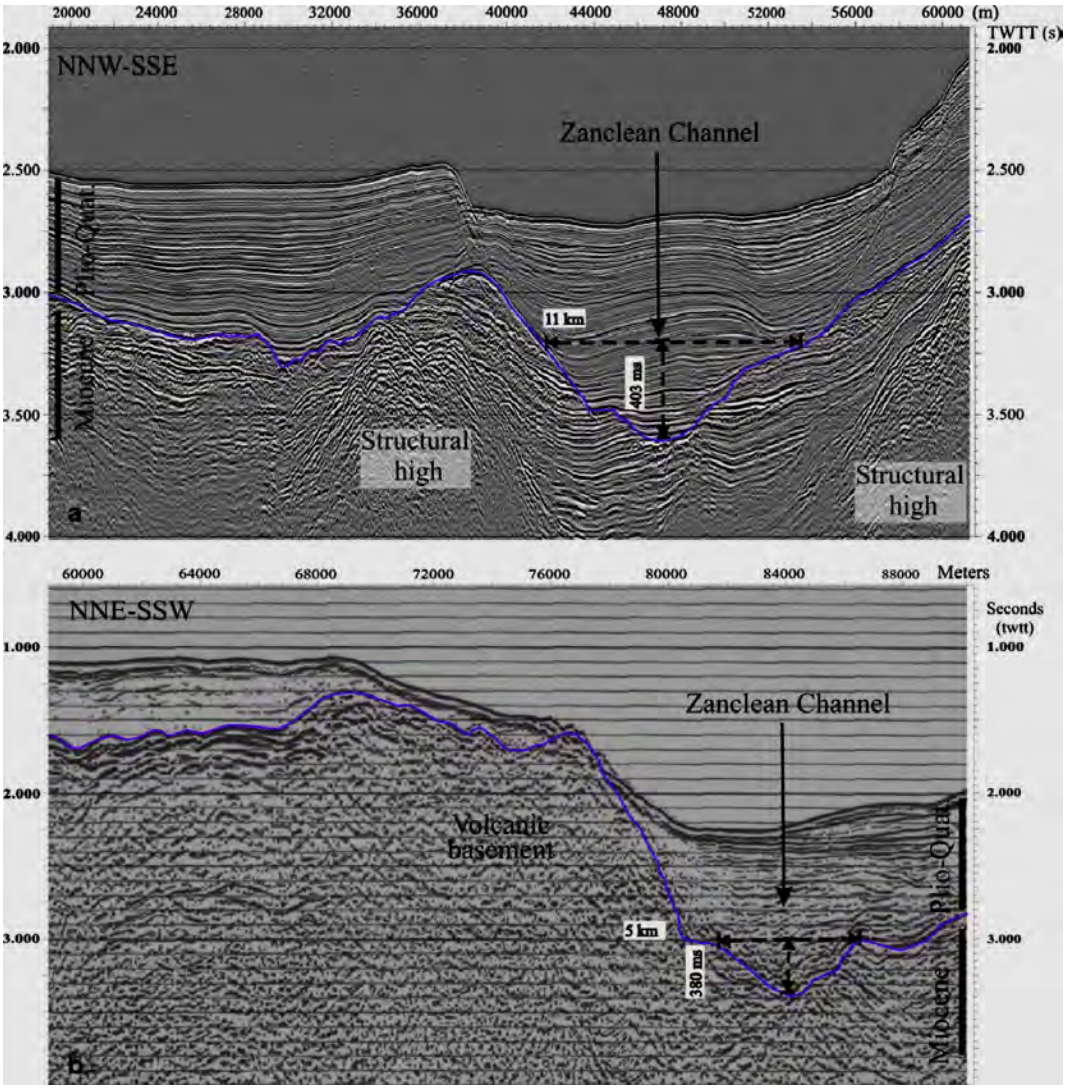

Figure 7.1-7. a) Single-channel seismic profile showing the Zanclean Channel in the easternmost part of the Alborán Basin, at the transition to the Algero-Balear Basin. b) Multi-channel seismic profile showing the Zanclean Channel in the narrow passage of the Alborán Channel. Violet lines top of Messinian surface (see Fig. 7.1-2 for profile locations).

In the western domain, the Zanclean Channel has a complex morphological configuration (Fig. 7.1-6) related to the pre-existing irregular morphology near the Strait of Gibraltar and the widespread presence of mud diapirs (Fig. 7.1-5a, c), their activity having contributed to the deformation and remoulding of the channel in Plio-Quaternary times. In this domain, the channel is 210 km long and displays an initial WSW–ENE direction in and near the Strait of Gibraltar, which changes to WNW–ESE as it enters the WAB. Along the first 80 km, the channel is deeply incised (up to 650 ms) into Miocene deposits and displays a U shape (average width 12 km; Fig. 7.1-5a) with

increasing asymmetry towards the east. At the same time the channel relief decreases towards the east from 650 ms to less than 250 ms (Fig. 7.1-5a, b). Locally, a substantially reduced relief can be explained by disturbance by mud diapirism during the Plio-Quaternary. The longitudinal profile of the channel axis is irregular and displays two minor branches along its northern side. Along the first 35 km, where the channel crosses the Strait of Gibraltar, the longitudinal profile is stepped and characterized by several highs and lows (Fig. 7.1-5c) spaced about 4 km apart and with reliefs reaching 650 ms. From 35 to 80 km the channel is more deeply incised and the axis dips towards the centre of the WAB, displaying a series of lows and highs associated with a significant reduction in relief between 65 and 87 km explainable by Plio-Quaternary diapirism.

Along the last 130 km, the incision of the Zanclean Channel decreases eastwards (relief about 100 ms) while it bends towards the ESE until connecting with the Alborán Channel close to the ODP976 high. In this section, the channel splits into a northern and a southern branch as it encounters the Vizconde de Eza High. The northern branch has locally been tilted by Plio-Quaternary tectonic activity (Fig. 7.1-5b). It is less than 7 km wide and the incision depth 100/160 ms. The southern branch is about 5 km wide and up to 110 ms in relief. The two branches converge towards the mouth of the Alborán Channel (i.e. where the central domain begins).

In the central domain, the Zanclean Channel is laterally confined by the Alborán Ridge and several topographic highs (Djibouti Bank, Herradura Northand Southbanks), andis SW-NE-aligned (Figs. 7.1-1 and 7.1-6). Although its morphological expression is partly masked by the Plio-Quaternary compressive tectonics in this domain, the data indicate that the channel gradually narrows (to about 4 km in width and 75 km in length) and deepens (to 325 ms on average; Fig. 7.1-7b).

In the eastern domain, straddling the EAB, the Zanclean Channel splits into three branches where it meets structural highs (Fig. 7.1-6). The largest incision is located to the south of the topographic highs, whereas the two smaller ones are located to the north. The main incision is 90 km long, has a U-shaped cross-section, and runs predominantly in an W–E direction parallel to the Habibas Escarpment (Figs. 7.1-1 and 7.1-6). Although some reaches of the main incision are masked by Plio-Quaternary deformation (Estrada et al. 1997), it has an estimated average relief of 245 ms and a

width of 5.8 km. In detail, its dimensions vary strongly from 143 to 403 ms in relief and from 4.5 to 8 km in width (Fig. 7.1-7a), the latter initially increasing and then decreasing towards the transition to the Algero-Balear Basin. The two minor channels are up to 200 ms deep and 4 km wide.

Terraces

Terraces have shaped the Messinian surface into a stepped profile along the margins of the WAB. Seismic records show these features to truncate Miocene deposits. They are aligned sub-parallel to the western Spanish and Moroccan margins and display variable dimensions (Figs. 7.1-3, 7.1-4, 7.1-5a, b). The Spanish terraces are located between the Strait of Gibraltar and the Herradura Bank, and the Moroccan terraces between the strait and the surroundings of Cabo Negro (Figs. 7.1-1 and 7.1-6).

The Spanish terraces are longer (up to 70 km) and higher (up to 250 ms), their main direction being WSW–ENE parallel to the Zanclean Channel (Fig. 7.1-3). Three main terraces have been identified in the present study, occupying different depths and converging westwards towards the Strait of Gibraltar. They display an arcuate shape in plan view, and their lateral continuity is affected by mud diapirism that also distorts the stepped morphology (Fig. 7.1-3). The two shallower terraces deepen eastwards from 650 and 900 ms to about 2,400 ms, and their crosssections are concave-up (up to 120 ms in height and 1.5 km in width; Fig. 7.1-5a). The seismic records reveal that the shallowest one truncates the uppermost layers of the chaotic body of Messinian age around the ODP976 high (Fig. 7.1-4). The deeper terrace (6 km in width) is characterized by a downslope-dipping step; its relief decreases eastwards from 490 ms until it essentially disappears 120 km from the Strait of Gibraltar where mud diapirs impair any identification (Figs. 7.1-5a and 7.1-6). This terrace also deepens towards the east from 1,750 to 2,300 ms.

Along the Moroccan margin, two main terraces have been identified as counterparts of the shallower Spanish terraces, being similar in size and morphology (Fig. 7.1-6).

Canyons

The Messinian surface is also incised by canyons along both the western Spanish and Moroccan margins of the WAB (Figs. 7.1-3, 7.1-6 and 7.1-8). These canyons are incised into Miocene deposits and have subsequently been filled by Plio-Quaternary sediments (Fig. 7.1-8). They are well developed along the Spanish margin between the Strait of Gibraltar and Estepona; an isolated canyon is found further east off Malaga. The upper reaches of the canyons display amphitheatre-like shapes that trace the main orientation of the Gibraltar Arc. The canyons have a relief of up to150 ms and a width of up to 9 km, their length increasing eastwards from 9 to 27 km. Downslope, the canyon dimensions decrease (by about 60 ms) and their convergent pathways are sharply interrupted by terraces (Figs. 7.1-3 and 7.1-6). The isolated canyon off Malaga follows an almost rectilinear path that can be traced for 45 km before it disappears at 2,000 ms (depth). Its width and relief vary from 15 km and 300 ms in the upper reaches to 4 km and 50 ms respectively in the distal reaches. The canyons mapped along the Moroccan margin are, by contrast, less well developed and display rectilinear pathways that can be traced to 2,000 ms depth (Fig. 7.1-6). These canyons are up to 4 km wide and 250msin relief.

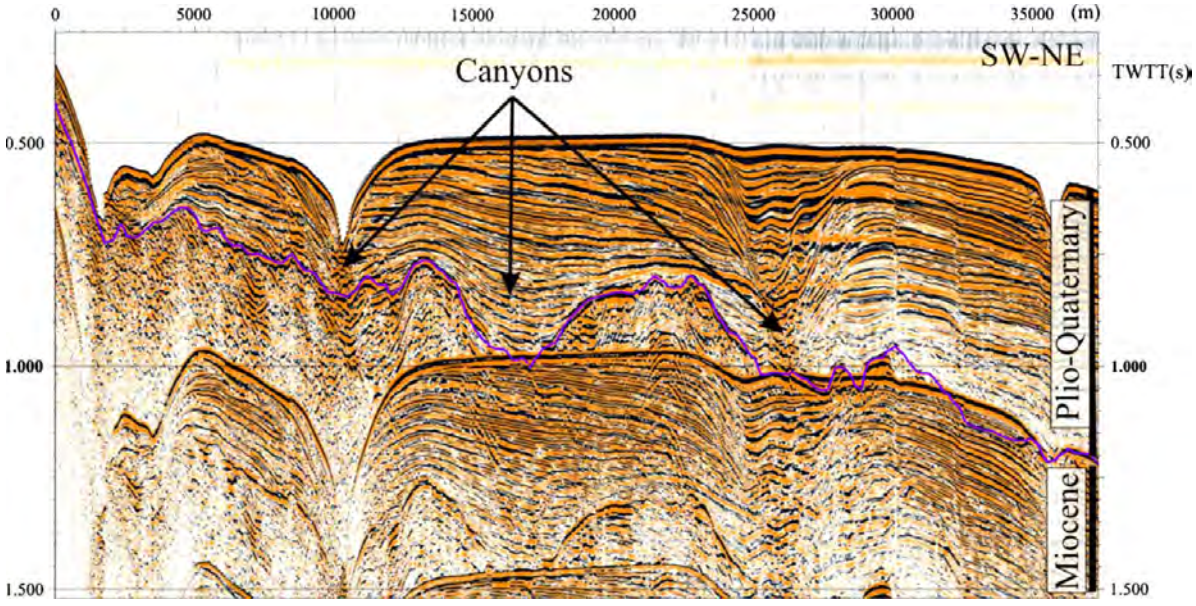

Figure 7.1-8. Single-channel seismic profile showing canyons on the Spanish continental margin near the Strait of Gibraltar. Violet lines top of Messinian surface (see Fig. 7.1-2 for profile location).

7.1.6 The Messinian surface

The palaeo-topographic map defining the Messinian surface in the Alborán Basin can be used to infer the main processes responsible for its shape. In many respects, the topography is similar to the modern configuration of the Alborán Basin due to the geological history of the Alborán Sea from the Messinian to the present.

The Messinian surface is a polygenetic product of processes active during different stages of the MSC from 5.96 Ma to the Zanclean flooding at 5.33 Ma. The superimposition of successive erosional events, subaerial desiccation, and marine influence during the Atlantic flooding has resulted in the preservation of distinct morphological features (Zanclean Channel, terraces, can-yons) of different ages. This polygenetic surface was later remoulded by various geological processes, the most important being mud diapirism that affected the area from pre-to post-Messinian times. Based on the results of the present study, mud diapirism conditioned the marginal pre-Messinian topography of the Alborán Basin in the western domain of the Zanclean Channel, whereas post-Messinian diapirism deformed and masked the original topography.

Tectonism was another process that modified the Messinian surface, particularly in the vicinity of the Gibraltar Arc where the westward emplacement of the Alborán Domain resulted in a tilting and folding of the original Messinian margin topography, at the same time uplifting the highs (Fig. 7.1-5a, c; Ercilla et al. 1992, 1994; Schoorl and Veldkamp 2003; Faccenna et al. 2004). Locally, the emplacement of structural highs masked and tilted the Messinian surface, particularly in the western channel domain (Fig. 7.1-5b).

7.1.7 Onset of Atlantic water inflow

The Zanclean Channel is inferred to have been incised by the Atlantic water masses flooding the drained Alborán Sea in a catastrophic event. Geological evidence from the Gulf of Lions suggests the occurrence of an earlier, less dramatic inflow of Atlantic water (Bache et al. 2009). However, any sedimentary deposits formed in the

Alborán Basin by that earlier inflow appear to have been completely obliterated by the subsequent catastrophic event (García-Castellanos et al. 2009).

Crossing the entire Alborán Basin, the Zanclean Channel is defined by a major erosional depression having a U-shaped cross-section along the deeper part of the WAB, and which can be traced eastwards along the Alborán Channel and the EAB up to the transition with the Algero-Balear Basin (Fig. 7.1-6). This prominent erosional feature can be explained only by a catastrophic inflow of Atlantic water when the Strait of Gibraltar reopened during the Zanclean, as there is no evidence for any link to a major canyon or river valley that could have fed the channel. Furthermore, no entrenchments of any scale are observed in the younger Plio-Quaternary deposits. These observations strongly support the contention that the Zanclean Channel was incised when the sea level was about 1,300–1,500 m lower than that of the present day (Bache et al. 2009; Urgeles et al. 2011).

The connecting valley between the Strait of Gibraltar and the channel proper is characterized by several topographic steps associated with highs and lows along the axis (Fig. 7.1-5c), their interpretation being still controversial. Three hypotheses have been invoked to explain their origin: (1) they formed by a westward migration of waterfalls, in which case the features would be the result of hydraulic jumps; (2) they formed by a combination of erosion and mud diapirism; and (3) they formed by an as yet unknown process associated with the water jet that flooded the Mediterranean Basin (Blanc 2002; García-Castellanos et al. 2009). The waterfall hypothesis has the drawback that the upstream side is smoother than the downstream one— exactly the opposite of what would be expected in a retrogressive migration of a waterfall. Whatever the origin of the topographic highs and lows, they suggest a pulsed retrogradation of a flow that was able to erode the floor. This could entail a pre-flooding period of mild Atlantic waterinflowtothe Mediterraneanbyway of small waterfalls that were partly preserved during the later Zanclean flooding event, an interpretation favouring hypothesis #2 that, in addition, postulates that the thickness of the salt deposits detected in the deep basins would have required some Atlantic water inflow prior to the flooding event (CIESM 2008). The inconclusive nature of the above discussion highlights the fact that new

insights are required to interpret the origin of these features, especially with regard to the palaeogeography during the Zanclean flooding.

7.1.8 Dynamics of the Zanclean flooding

7.1.8.1 Route, energy, and morphological control

The results of the present study convincingly demonstrate that the degree of Zanclean Channel entrenchment is highly variable across two Alborán sub-basins, suggesting variations in the erosive capacity of the inflowing Atlantic waters. In the Western Alborán Basin close to the Strait of Gibraltar, the channel incision has the highest relief, indicating that this part of the channel was more strongly impacted. The difference in elevation between the water level of the Atlantic Ocean and the Western Mediterranean during the MSC plausibly resulted in a very high flow velocity and, in turn, incision rate (García-Castellanos et al. 2009). Likewise, the natural tendency of a flow to reach an equilibrium state would have favoured erosion close to the Strait of Gibraltar. As the confinement of the channel decreased eastwards, entrenchment decreased (about 100 ms) and the channel width increased (7 km), suggesting a decrease in flow energy and erosive capacity. Here, major topographic highs (volcanoes, structural highs and mud diapirs) acted as morphological barriers diverting the flooding path, thereby inducing local variations in Atlantic flooding hydrodynamics. In the WAB, these are the Vizconde de Eza (volcanic) and ODP976 (structural) highs. The former would have caused the flood to split into a northern branch, clearly more energetic as it followed the shortest W–E route across the sub-basin, and a southern less energetic branch, as suggested by lesser incision (110 ms) into the Miocene deposits and restriction to the high edges (Figs. 7.1-5b and 7.1-6). In the vicinity of the ODP976 high, the direct impact of the Atlantic water masses evidently exhumed the partly buried high, consistent with the evidence of bay-shaped erosional zones on its eastern and western sides.

Mud diapirs would have moulded the seafloor of the WAB into inverted bowls (Pérez-Belzuz et al. 1997)that interacted with the Atlantic water masses in such a way as to expose the margin areas to stronger erosion. The diapirs also evidently configured

small basins where the Messinian chaotic wedges were trapped (Fig. 7.1-4). Locally, some diapirs were exposed during the flooding, the erosion resulting in flat tops. Active diapirism close to the Strait of Gibraltar also conditioned the morphology of the Zanclean Channel. The remnants of these diapirs suggest the existence of an antiform in front of the strait that was deeply eroded by the Atlantic flooding (Fig. 7.1-5a). This likely involved a highly energetic, non-migrating flow that, instead of being diverted by the morphological barrier, flowed straight across it at the highest point while eroding a deeper channel.

In the Alborán Channel, the Zanclean Channel would have experienced a sudden reduction in cross-section because of the structurally confined passage imposed by the volcanic Djibouti complex in the north and the Alborán Ridge in the south. However, during the Zanclean the Alborán Channel was probably wider than today, as suggested by the compressive features identified on seismic profiles and on the present-day seafloor (Woodside and Maldonado 1992; Estrada et al. 1997; Martínez-García et al. 2011). Although the precise dimensions of the Alborán Channel before the flooding event are not known, the observed increase in channel relief (from 100 to 325 ms) implies a reduction in channel width and concomitant increase in flow velocity.

In the East Alborán Basin, the flow path of the Atlantic water masses would have been strongly modulated by the Habibas Escarpment and several structural highs, as indicated by variations in Zanclean Channel width and relief. Evidence that the highest relief (403 ms) is found at the transition to the Algero-Balear Basin (Fig. 7.1-7a) would be consistent with an increased hydrological gradient between these basins.

7.1.8.2 Pulsed Atlantic water inflow into the Alborán Basin

The infilling dynamics of the Alborán Basin can be inferred from terrace formation and the preservation of canyons (subaereal in origin). Although the reconstruction of terrace formation is not straightforward, possible scenarios include an initial-stage (before) and a late-stage (after) terrace formation relative to the Zanclean Channel entrenchment. The deepest terrace (1,750–2,300 ms) was probably formed before channel entrenchment, as suggested by its deeper location and shape. Terrace

erosion would have been associated with reworking processes in the deepest part of the basin margin during initial inflow immediately before the catastrophic flooding, and the terrace subsequently preserved as a relict feature. This scenario would correspond to the initial stage of slow sea-level rise proposed by Bache et al. (2009) for the Gulf of Lions immediately before the Zanclean flooding.

The shallower terraces (600– and 900–2,400 ms) along the Spanish and Moroccan margins probably formed in response to repeated erosional events following the Zanclean Channel entrenchment, in the course of pulsed filling of the Alborán Sea when the Mediterranean was already partly refilled. The widespread occurrence of terraces on both the Spanish and Moroccan margins, their concave-up shapes paralleling the margins in continuity of the Gibraltar Arc, and their lateral changes in shape in accordance with the local morphology are all evidence in support of this interpretation. Their restricted occurrence along the margins of the WAB can be explained by the proximity to the Strait of Gibraltar, in a sector that experienced the greatest impact of the Atlantic water inflow.

Similar terraces with concave-up shapes occur on the present-day seafloor in the westernmost sector of the upper slope along the Spanish margin close to the Strait of Gibraltar. Their origin has been related to the erosional action of Atlantic water masses entering the Alborán Sea and describing an anticyclonic gyre in the Western Alborán Basin (Medialdea et al. 1994). Evidence arguing against this hypothesis is the eastward deepening of the terraces, although this could also be explained by the Plio-Quaternary tectonic deformation of the Spanish margin. In fact, several lines of stratigraphic evidence support the occurrence of differential uplifting and tilting of the Spanish margin at that time: the outcropping of Pliocene deposits, the local non-preservation of Quaternary deposits on the Spanish shelf and along the shelf break, and an unequal configuration of slope deposits that is more enhanced close to the Strait of Gibraltar (Ercilla et al. 1992, 1994; Maldonado et al. 1992). These tectonic processes—uplifting and tilting—must have favoured eastward deepening of the terraces.

Despite uncertainties regarding terrace palaeo-depth, these features may also have formed when Western Mediterranean waters reached the level of the Sicily Sill and started flooding the Eastern Mediterranean Basin (Bache et al. 2009; Just et al. 2011). In

this scenario, it is tentatively suggested that the upper terrace (600 ms) formed when the filling of the Western Mediterranean Basin reached the Sicily Sill, and that the lower terrace (900 ms) formed later when sea level dropped in the western basin due to the collapse of the Sicily Sill (similar to that of the Strait of Gibraltar; García-Castellanos et al. 2009) accompanied by water release into the Eastern Mediterranean Basin. During each of these two events the sea level would have remained constant, thereby favouring the development of wave-cut terraces in shallow waters. Recently, similar terraces have been described from two other areas (Balearic and Algerian margins) of the Western Mediterranean, these also having been related to sea-level stagnancy while the water overflowed into the Eastern Mediterranean Basin (Just et al. 2011). This hypothesis, however, would need to be supported by more morphological and sedimentary evidence from other Mediterranean basin margins.

Other factors controlling the formation of the terraces are the relative energy of the Atlantic flooding event, the topography (slope gradients), and the type and nature of the eroded deposits. Assuming that the erodibility of Miocene deposits was similar throughout the region (based on their similar seismic and sedimentary characteristics; Campillo et al. 1992; Comas et al. 1992), it is suggested that if the deepest terrace formed before the Zanclean Channel entrenchment, then this would have been when the Alborán Basin experienced the dramatic change from a subaerial to marine environment. In this scenario, the erosion caused by the Atlantic flooding event would have affected the whole deep basin. This would explain the larger width of the terrace (6 km), its deeper location (1,750–2,300 ms), and its topographic link with the Strait of Gibraltar. On the other hand, the smaller widths (ca. 1.5 km) of the shallowest terraces along both the Spanish and Moroccan margins may have been associated with a decrease in the energy of the inflowing Atlantic water, a steeper gradient of the slope margins, and/or a smaller part of the seafloor being affected by erosion due to the sea-level rise. When the Alborán Sea was partly infilled, erosion would have affected only those sections of the marginal seafloor close to the new sea level. Along steep margins, correspondingly smaller sections of the seafloor would have been affected by erosion.

The canyons identified along the Spanish margin between the Strait of Gibraltar and the ODP976 high (Figs. 7.1-3 and 7.1-8) represent morphological features that

developed in a subaerial environment when the Mediterranean Sea level was substantially lower (by ~1,500 m) during the MSC (Bache et al. 2009). Such canyons (although smaller) occur also along the Moroccan sector of the Gibraltar Arc. This contrasts with other areas of the Alborán margins where canyons are absent (except for one off Malaga). These observations suggest that canyon development was enhanced by the westward pushing of the Gibraltar Arc (Loget and Van Den Driessche 2006), which resulted in uplifting and tilting of the margin. This would imply an origin prior to the Zanclean flooding. These tectonic processes produced steep slopes that would have favoured subaereal mass-wasting processes associated with canyon formation. The courses of the canyons are interrupted by terraces, in a succession of perched thalwegs. This implies that the canyons predate the terraces, the latter linked with the Atlantic flooding. The preservation of the canyons and the lack of terraces upslope both suggest that, after the formation of the shallower terraces, the flooding of the Alborán Basin proceeded as depicted in the mathematical model of García-Castellanos et al. (2009). Based on the scenario describing the shallowest terrace formation, the flooding occurred after the sea level reached the same elevation in both the Western and Eastern Mediterranean basins, although more evidence in support of this hypothesis is required (cf. above).

7.1.9 Conclusions

In conclusion, the Messinian surface broadly depicts the main physiographic setting that configured the Alborán Basin and conditioned the Zanclean flooding. The occurrence of several submarine terraces at different depths and the development of subaerial canyons suggest several inflow events of Atlantic water into the basin. There could have been two major inflow phases of Atlantic water, one shortly before and the other during the Zanclean flooding, the latter accompanied by periods of relative sea-level stillstands that enabled terrace development. Alternatively, these features were all generated during the main flooding event and subsequent pulsed infilling of the basin.

7.1.10 References

Bache F, Olivet JL, Gorini C, Rabineau M, Baztan J, Aslanian D, Suc JP (2009). Messinian erosional and salinity crises: view from the Provence Basin (Gulf of Lions, Western Mediterranean). Earth Planet Sci Lett 286(1/2):139–157.

Balanyá JC, García-Dueñas V (1987). Les directions structurales dans le Domaine d'Alborán de part et d'autre du Détroit de Gibraltar. C R Acad Sci Paris 304:929–933.

Blanc PL (2002). The opening of the Plio-Quaternary Gibraltar Strait: assessing the size of a cataclysm. Geodinámica Acta 15(5/6):303–317.

Bourgois J, Mauffret A, Ammar A, Demnati A (1992). Multi-channel seismic data imaging of inversion tectonics of the Alborán Ridge (western Mediterranean Sea). Geo-Mar Lett 12(2/3):117–122. doi:10.1007/BF02084921.

Campillo A, Maldonado A, Mauffret A (1992). Stratigraphic and tectonic evolution of the western Alborán Sea: Late Miocene to Recent. Geo-Mar Lett 12(2/3):165–172. doi:10.1007/ BF02084928.

Chiocci FL, Ercilla G, Torres J (1997). Stratal architecture of Western Mediterranean Margins as the result of the stacking of Quaternary lowstand deposits below 'glacio-eustatic fluctuation base-level'. Sediment Geol 112:195–217.

CIESM (2008). Executive summary. Roveri M, Krijgsman W, Suc JP, Lugli S, Lofi J, Sierro FJ, Manzi V, Flecker R et al. In: Briand F (ed) The Messinian Salinity Crisis from mega-deposits to microbiology—a consensus report. CIESM Worksh Monogr 33:7–28.

Clauzon G (1978). The Messinian Var canyon (Provence, Southern France)—paleogeographic implications. Mar Geol 27:231–246.

Cloetingh S, van der Beek PA, van Rees D, Roep TB, Biermann C, Stephenson RA (1992). Flexural interaction and the dynamics of Neogene extensional basin formation in the Alborán-Betic region. Geo Mar Lett 12(2/3):66–75. doi:10.1007/BF02084914.

Comas MC, García-Dueñas V, Jurado MJ (1992). Neogene tectonic evolution of the Alborán Sea from MCS data. Geo Mar Lett 12(2/ 3):157–164. doi:10.1007/BF02084927.

Comas MC, Platt JP, Soto JI, Watts AB (1999). The origin and tectonic history of the Alborán basin: insights from Leg 161 results. In: Zahn R, Comas MC, Klaus A (eds) Proc Ocean drilling program, scientific results 161. Ocean Drilling Program, College Station, pp 555–580.

Dewey JF, Helman ML, Turco E, Hutton DHWA, Knott SD (1989). Kinematics of the Western Mediterranean. In: Coward MP, Dietrich D, Park RG (eds) Alpine tectonics. Geol Soc Lond Spec Publ 45:265–283.

Docherty CA, Banda E (1995). Evidence for the eastward migration of the Alborán Sea based on regional subsidence analysis: a case for basin formation by delamination of the subcrustal lithosphere. Tectonics 14:804–818.

Ercilla G, Alonso B (1996). Quaternary siliciclastic sequence stratigraphy of western Mediterranean passive and tectonically active margins: the role of global versus local controlling factors. In: De Batist M, Jacobs P (eds) Geology of siliciclastic shelf seas. J Geol Soc Spec Publ 117:125–137.

Ercilla G, Alonso B, Baraza J (1992). Sedimentary evolution of the northwestern Alborán Sea during the Quaternary. Geo Mar Lett 12(2/3):144–149. doi:10.1007/BF02084925.

Ercilla G, Alonso B, Baraza J (1994). Post-Calabrian sequence stratigraphy of the northwestern Alborán Sea (southwestern Mediterranean). Mar Geol 120:249–265.

Estrada F, Ercilla G, Alonso B (1997). Pliocene-Quaternary tectonic-sedimentary evolution of the NE Alborán Sea (SW Mediterranean Sea). Tectonophysics 282(1/4):423–442.

Estrada F, Ercilla G, Gorini C, Alonso B, Vázquez JT, Maldonado A, Ammar A (2010). Impact of Atlantic Waters in the Alborán Basin at the end of the Messinian Salinity Crisis: the Zanclean Flooding. Geo-Temas 11:41–42.

Faccenna C, Piromallo C, Crespo-Blanc A, Jolivet L, Rossetti F (2004). Lateral slab deformation and the origin of the western Mediterranean arcs. Tectonics 23(1):TC1012. doi:10.1029/ 2002TC001488.

Farran M (2008). IMAGE2SEGY: una aplicación informática para la conversión de imágenes de perfiles sísmicos a ficheros en formato SEG Y. Geo-Temas 10:1215–1218.

García-Castellanos D, Estrada F, Jiménez-Munt I, Gorini C, Fernández M, Vergés J, de Vicente R (2009). Catastrophic flood of the Mediterranean after the Messinian salinity crisis. Nature 462:778–782.

García-Dueñas V, Balanyá JC, Martínez-Martínez JM (1992). Miocene extensional detachments in the outcropping basement of the Northern Alborán Basin (Betics) and their tectonic implications. Geo Mar Lett 12(2/3):88–95. doi:10.1007/BF02084917.

Gargani J (2004) Modelling of the erosion in the Rhone Valley during the Messinian crisis (France). Quat Int 121:13–22.

Gargani J, Rigollet C, Scarcelli S (2010). Isostatic response and geomorphological evolution of the Nile valley during the Messinian salinity crisis. Bull Soc Géol France 181(1):19–26.

Hernández-Molina JH, Somoza L, Rey J (1994). Late Pleistocene-Holocene high-resolution sequence analysis on the Alborán Sea continental shelf. In: De Batist M, Jacobs P (eds) J Geol Soc Spec Publ 117:139–154.

Hsü KJ, Ryan WBF, Cita MB (1973). Late Miocene desiccation of the Mediterranean. Nature 242:240–244.

Huang TC, Stanley DJ (1972). Western Alborán Sea: sediment dispersal, ponding and reversal of currents. In: Stanley DJ, Kelling G, Weiler Y (eds) The Mediterranean Sea: a natural sedimentation laboratory. Dowden, Hutchinson and Ross, Stroudsburg, pp 521–559.

Jurado MJ, Comas MC (1992). Well log interpretation and seismic character of the Cenozoic sequence in the northern Alborán Sea. Geo Mar Lett 12(2/3):129–136. doi:10.1007/BF02084923.

Just J, Hübscher C, Betzler C, Lüdmann T, Reicherter K (2011). Erosion of continental margins in the Western Mediterranean due to sea-level stagnancy during the Messinian Salinity Crisis. Geo Mar Lett 31(1):51–64. doi:10.1007/s00367-010-0213-z.

Krijgsman W, Hilgen FJ, Raffi I, Sierro FJ, Wilson DS (1999). Chronology, causes and progression of the Messinian salinity crisis. Nature 400:652–655.

Lobo FJ, Maldonado A, Hernández-Molina FJ, Fernández-Salas LM, Ercilla G, Alonso B (2008). Growth patterns of a proximal terrigenous margin offshore the Guadalfeo River, northern Alborán Sea (SW Mediterranean Sea): glacio-eustatic control and disturbing tectonic factors. Mar Geophys Res 29:195–216.

Lofi J, Gorini C, Berné S, Clauzon G, Dos Reis AT, Ryan WBF, Steckler MS (2005). Erosional processes and paleo-environmental changes in the Western Gulf of Lions (SW France) during the Messinian Salinity Crisis. Mar Geol 217: 1–30.

Loget N, Van Den Driessche J (2006). On the origin of the Strait of Gibraltar. Sediment Geol 188(189):341–356.

Maillard A, Gorini C, Mauffret A, Sage F, Lofi J, Gaullier V (2006). Offshore evidence of polyphase erosion in the Valencia Basin (Northwestern Mediterranean): scenario for the Messinian Salinity Crisis. Sediment Geol 188(189):69–91.

Maldonado A, Campillo AC, Mauffret A, Alonso B, Woodside JM, Campos J (1992). Alborán Sea Late Cenozoic tectonic and stratigraphic evolution. Geo Mar Lett 12(2/3):179–186. doi:10.1007/BF02084930.

Martínez del Olmo W, Comas MC (2008). Arquitectura sismica, olistostromas y fallas extensionales en el norte de la Cuenca Oeste del mar de Alborán. Rev Soc Geol España 21(3/4).

Martínez-García P, Soto JI, Comas M (2011). Recent structures in the Alborán Ridge and Yusuf fault zones based on swath bathymetry and sub-bottom profiling: evidence of active tectonics. Geo Mar Lett 31(1):19–36. doi:10.1007/s00367-010-0212-0.

Mauffret A, Maldonado A, Campillo AC (1992). Tectonic framework of the Eastern Alborán and Western Algerian basins, Western Mediterranean. Geo Mar Lett 12(2/3):104–110. doi:10.1007/ BF02084919.

Medialdea J, Maldonado A, Alonso B, Díaz JI, Ercilla G, Farran M, Medialdea T, Vázquez T (1994). Mapa geológico de la plataforma continental española y zonas adyacentes. 1:200.000. Memoria y Hojas No. 25 y 25E. Figueres. Servicio de Publicaciones del Ministerio de Industria y Energía, Madrid.

Millot C (1999). Circulation in the Western Mediterranean Sea. J Mar Syst 20(1/4):423–442.

Montadert L, Letouzey J, Mauffret A (1978). Messinian event: seismic evidence. In: Hsü KJ, Montadert L, Bernoulli D et al (eds) Initial reports of the deep sea drilling project, vol 42, part 1. US Government Printing Office, Washington, DC, pp 1037–1050.

Mulder CJ, Parry GR (1977). Late Tertiary evolution of the Alborán Sea at the eastern entrance of the Straits of Gibraltar. In: Diju-Duval B, Montadert L (eds) Proc Int Symp the structural history of the Mediterranean Basins, October 1976, Split, Yugoslaviath edn. TECHNIP, Paris, pp 401–410.

Nelson CH (1990). Estimated post-Messinian sediment supply and sedimentation rates on the Ebro continental margin, Spain. Mar Geol 95(3/4):395–418.

Parrilla G, Kinder TH, Preller RH (1986). Deep and Intermediate Mediterranean Water in the western Alborán Sea. Deep Sea Res 33(1):55–86.

Pérez-Belzuz F (1999). Geología del Margen y Cuenca de Mar de Alborán Durante el Plio-Cuaternario: Sedimentación y Tectónica. PhD Thesis, CSIC, Universidad de Barcelona

Pérez-Belzuz F, Alonso B, Ercilla G (1997). History of mud diapirism and trigger mechanisms in the Western Alborán Sea. Tectono-physics 282(1/4):399–422.

Platt JP, Vissers RLM (1989). Extensional collapse of thickened continental lithosphere: a working hypothesis for the Alborán Sea and Gibraltar Arc. Geology 17:540–543.

Rouchy JM, Caruso A (2006). The Messinian salinity crisis in the Mediterranean Basin: a reassessment of the data and an integrated scenario. Sediment Geol 188:35–67.

Ryan WBF, Hsü KJ, Cita MB et al (eds) (1973). Initial reports of the deep sea drilling project, vol 13, parts 1/2. US Government Printing Office, Washington, DC.

Schoorl JM, Veldkamp A (2003). Late Cenozoic landscape development and its tectonic implications for the Guadalhorce valley near Álora (Southern Spain). Geomorphology 50:43–57.

Soto JI, Comas MC, de la Linde J (1996). Espesor de sedimentos en la cuenca de Alborán mediante una conversión sísmica corregida. Geogaceta 20:382–385.

Talukder AR (2003). La provincia diapírica de lodo en la Cuenca Oeste del Mar de Alborán: estructuras, génesis y evolución. PhD Thesis, University of Granada.

Tandon K, Lorenzo JM, de La Linde RJ (1998). Timing of rifting in the Alborán Sea basin—correlation of borehole (ODP Leg 161 and Andalucia A-1) to seismic reflection data: implications for basin formation. Mar Geol 144(4):275–294.

Urgeles R, Camerlenghi A, Garcia-Castellanos D, De Mol B, Garcés M, Vergés J, Haslam I, Hardman M (2011). New constraints on the Messinian sealevel drawdown from 3D seismic data of the Ebro Margin, western Mediterranean. Basin Res 23(2):123–145. doi:10.1111/j.1365-2117.2010.00477.x.

Vargas-Yañez M, Plaza F, García-Lafuente J, Sarhan T, Vargas JM, Vélez-Belchi P (2002). About the seasonal variability of the Alborán Sea circulation. J Mar Syst 35:229–248.

Vázquez JT (2001). Estructura del margen septentrional del Mar de Alborán. PhD Thesis, Universidad Complutense de Madrid.

Watts AB, Platt JP, Buhl P (1993). Tectonic evolution of the Alborán Sea Basin. Basin Res 5:153–177.

Weijermars R (1988). Neogene tectonics in the Western Mediterranean may have caused the Messinian salinity crisis and an associated glacial event. Tectonophysics 148(3/4):211–219.

Woodside JM and Maldonado A (1992). Styles of compressional neotectonics in the eastern Alborán Sea. Geo Mar Lett 12(2/ 3):111–116. doi:10.1007/BF02084920.

7.2 Megaflood modelling

Catastrophic flood of the Mediterranean after the Messinian salinity crisis

D. Garcia-Castellanos[1], F. Estrada[2], I. Jiménez-Munt[1], C. Gorini[3,4], M. Fernàndez[1], J. Vergés[1] and R. De Vicente[1]

[1]Institut de Ciències de la Terra Jaume Almera, CSIC, Sole´ i Sabarís s/n, Barcelona, Spain.

[2]Institut de Ciències del Mar, CSIC, Passg. Marítim Barceloneta, 37-49, Barcelona, Spain.

[3]Université Pierre et Marie Curie (UPMC) Paris 06, France

[4]CNRS, UMR 7193, ISTEP, F-75005, Paris, France.

Published on: Nature, 2009.

Volume 462, pages 778-782

DOI: 10.1038/nature08555

Impact Factor (JCR): 34.480 (2009), Q1 en Multidisciplinary. 1/50

ABSTRACT

The Mediterranean Sea became disconnected from the world's oceans and mostly desiccated by evaporation about 5.6 million years ago during the Messinian salinity crisis (Hsü et al., 1973; Clauzon et al., 1996; Krijgsman et al., 1999). The Atlantic waters found a way through the present Gibraltar Strait and rapidly refilled the Mediterranean 5.33 million years ago in an event known as the Zanclean flood (Blanc, 2002). The nature, abruptness and evolution of this flood remain poorly constrained (Blanc, 2002; Hsü and Ryan, 1973; Meijer and Krijgsman, 2005). Borehole and seismic data show incisions over 250 m deep on both sides of the Gibraltar Strait that have previously been attributed to fluvial erosion during the desiccation (Blanc, 2002; Campillo et al., 1992). Here we show the continuity of this 200-km-long channel across the strait and explain its morphology as the result of erosion by the flooding waters, adopting an incision model validated in mountain rivers. This model in turn allows us to estimate the duration of the flood. Although the available data are limited, our findings suggest that the feedback between water flow and incision in the early stages of flooding imply discharges of about 10^8 m^3 s^{-1} (three orders of magnitude larger than the present Amazon River) and incision rates above 0.4 m per day. Although the flood started at low water discharges that may have lasted for up to several thousand years, our results suggest that 90 per cent of the water was transferred in a short period ranging from a few months to two years. This extremely abrupt flood may have involved peak rates of sea level rise in the Mediterranean of more than ten metres per day.

7.2.1 Introduction

The main evidence for a kilometre-scale sea level drop in the Mediterranean is the excavation of canyons by the rivers flowing to the empty sea during the Messinian stage, up to 2,500 m deep in the Nile Delta (Barber, 1981) and about 1,000 m deep at the mouth of the Rhone (Clauzon, 1978). The salt accumulation in the deeper parts of the basin and the deposition of cyclic alternations between brackish and fresh-water sediment of the Lago Mare facies, combined with high-resolution biostratigraphy and astronomically-calibrated magnetostratigraphy (Clauzon et al., 1996; Krijgsman et al., 1999), indicate that total disconnection between both sides of the Betic–Rifean orogen started about 5.6 million years ago.

The Messinian salinity crisis finished 5.33 million years ago (Krijgsman et al., 1999), when the Atlantic waters found a way through the present Gibraltar Strait and refilled the Mediterranean in an event known as the Zanclean or post-Messinian flood (Blanc, 2002). There is agreement that this was triggered primarily by tectonic subsidence at the Gibraltar sill, probably related to the sinking of a lithospheric slab under the Betic–Rifean orogeny (Govers, 2009), and perhaps in combination with sill erosion (Loget and Van Den Driessche, 2006) and sea-level rise.

Outburst floods triggered by overspilling of large lakes have induced dramatic changes in surface hydrology and topography in regions as diverse as the Pleistocene Lake Bonneville (O'Connor, 1993), the Tertiary Ebro basin (García-Castellanos et al., 2003) (northeast Iberia), or the English Channel (Gupta et al., 2007), but the case of the post-Messinian flood is special because of the enormous size of both the source and the sink basins. The equilibrium level of the isolated Mediterranean during desiccation was between 1,500 m and 2,700 m below present sea level (Meijer and Krijgsman, 2005; Blanc, 2006), implying that the flooding water volume was three orders of magnitude larger than that at Lake Bonneville. Because they were based on an arbitrary evolution for the depth of the Gibraltar Strait during the flood, previous estimates of the flood duration yielded divergent values ranging between ten years (Blanc, 2002) and a few thousand years (Hsü and Ryan, 1973; Meijer and Krijgsman, 2005).

To quantify and understand the abruptness of the post-Messinian flood we needed to incorporate the dynamics of rock incision as the mechanism that progressively excavated the floodway and let ever increasing flow of Atlantic waters into the Mediterranean basin.

The present maximum depth of the Gibraltar Strait ranges between 284 m at the present Camarinal sill (the shallowest pass between the Atlantic and the Mediterranean; Fig. 7.2-1) and about 900 m at the Strait itself. Its present morphology might be affected by the strong streams between both oceanic domains and by tectonic vertical motions after flooding, rather than being an intact relict of Messinian or Zanclean incision. However, the streams did not impede deposition in the strait after the Messinian (Fig. 7.2-2a and Supplementary Fig. 7.2-S2), and therefore they cannot be responsible for the bulk of the present bathymetry. As for tectonic motions, if present at all after the Messinian, they are limited to long-wavelength isostatic or dynamic motions such as those controlling the onset (Duggen et al., 2003) and the end (Govers, 2009) of the Mediterranean isolation, because local fault deformation is minor (Loget and Van Den Driessche, 2006; Iribarren et al., 2007) (see, for example, Fig. 7.2-2b).

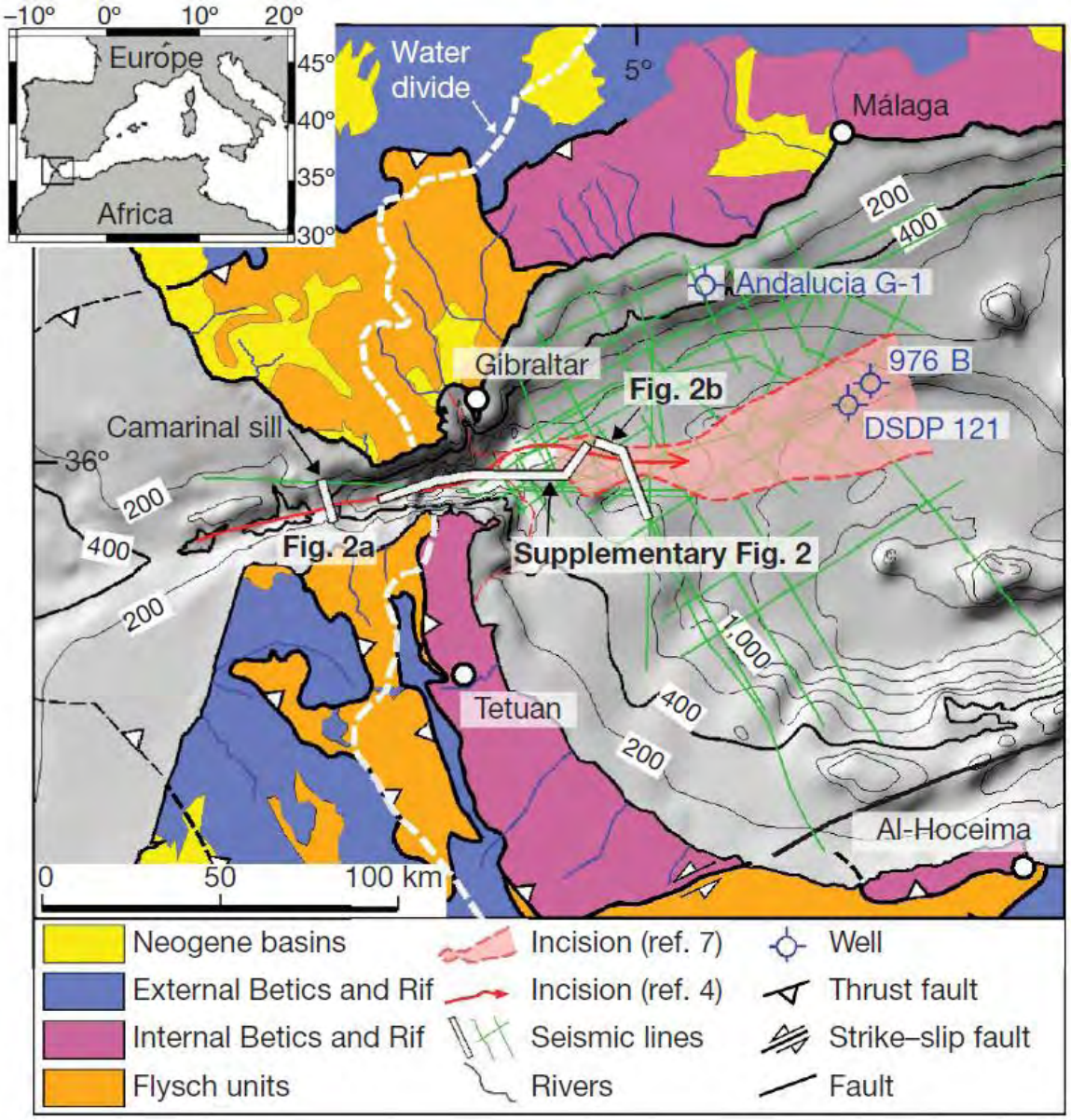

Figure 7.2-1. Geological map and bathymetry of the Gibraltar Arc region. The extent of the erosion channel is shown (after Blanc, 2002 and Campillo et al., 1992). The incision channel cuts 70 km beyond the drainage divide, which we interpret as the result of westwards retrogressive erosion during the post-Messinian flood. The interpretation of the seismic lines is correlated with the three located wells. Fault tectonic deformation has been mi nor since the Messinian. The water divide between the Atlantic and Mediterranean rivers is shown as a white dashed line.

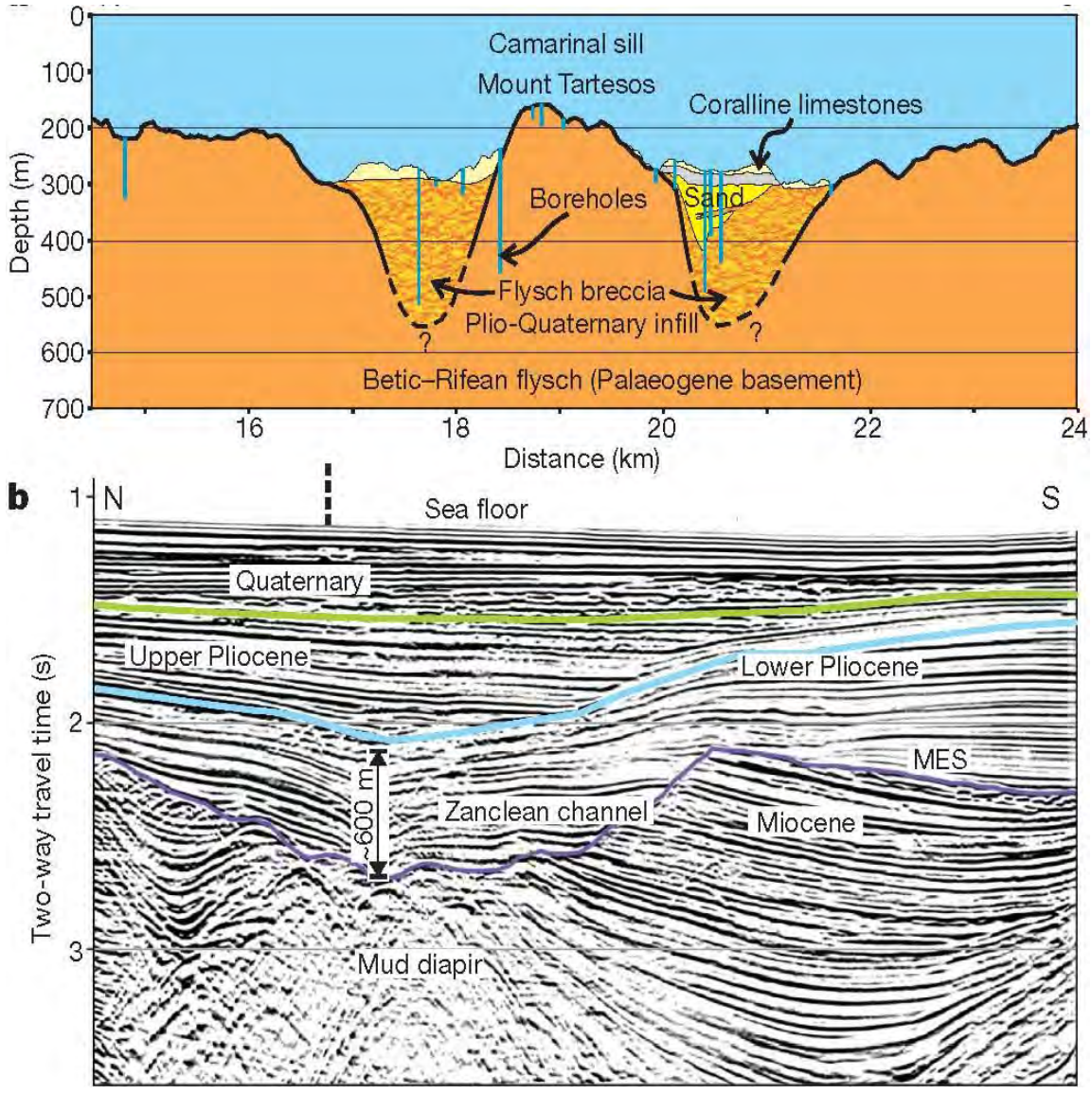

Figure 7.2-2. Evidence for an erosion channel across the Gibraltar Strait. a), Section across the Gibraltar Strait based on borehole exploration18. Flysch breccia coming from the Betic–Rifean flysch units fill an erosive trough more than 250 m deep. Whether Mount Tartesos is an autochthonous relict of the resistant flysch (Esteras et al., 2000), or a block slumped from the undermined banks of the flooding channel (Blanc, 2002) is not clear. Vertical exaggeration is 5:1. b), Multi-channel seismic profile of Conrad 828 (Watts et al., 1993; Docherty and Banda, 1995) interpreted in this work, based on correlation with the wells located in Fig. 7.2-1. The profile shows the dimensions and U-shape of the late-Messinian incision channel in the eastern side of the Gibraltar Strait related to the Zanclean flood. The asymmetry of the channel is partly due to the obliquity of the profile in its northern end (see location in Fig. 7.2-1), and partly due to differential isostatic subsidence after the flood (Govers, 2009). MES, Messinian Erosional Surface. Approximate vertical exaggeration is 4:1.

7.2.2 Methods

To use the incision around the Gibraltar Strait as a constraint for the flood velocity, we developed a one-dimensional model that accounts for the feedback between water-flow-controlled incision and sill-depth-controlled water flow. The formulation, based on previous river incision studies (Whipple and Tucker, 1999) and on hydrodynamic formulae, is detailed in the Methods. In essence, the model is based on the approach that incision rate dz_s/dt underneath a water flow is a power-law function of basal shear stress τb:

$$\frac{dz_s}{dt} = \mathrm{K}_b b(\tau b)^a \qquad (1)$$

where K_b and a are positive constants. An analytical solution of this equation coupled to slope-driven water flow shows that sill incision grows exponentially with time in the early stages of flooding, the speed of this incision being dependent on the lithological erodibility K_b and the effective slope on the Mediterranean side of the sill. For the post-Messinian flood, erosion rate doubles in timescales of ten to a hundred years, showing that feedback between incision and water flow is a key control of the timing of the flood.

The interplay between incision (as the floodgate opener) and slope reduction due to the replenishment of the Mediterranean is calculated using an explicit finite-difference time-iterative technique, starting with an initial sill depth of z_s = 1m at t =0. At each time step, water discharge is calculated based on the depth of the sill and then sill incision is calculated based on basal shear stress and effective slope S (hydrological gradient). As the Mediterranean becomes filled, *S* gradually decreases to zero. The calculated water discharge is passed from the Atlantic Ocean to the western Mediterranean basin and, if the Sicily sill (430 metres below sea level) is reached, to the eastern Mediterranean basin, accounting for a reconstructed hypsogram of the Messinian Mediterranean (after Meijer and Krijgsman, 2005).

Consider a sill at an average depth $z_s > 0$ (a positive value of depth means below initial ocean level) acting as a water gate between a source basin (the Atlantic Ocean) at level z_0 and a sink basin (the western Mediterranean basin) at level z_1 ($z_1 > z_s > z_0$). Symbols are depicted in Supplementary Fig. 7.2-1. The incision rate dz_s/dt under a water

flow is generally approached as a power-law function of basal shear stress τb (equation (1)). The unit stream power approach, including water velocity *V* as multiplying factor of τb in equation (1), has also been tested, but the predicted floods are more abrupt than those shown here because incision is more concentrated at the fastest flooding stages. River incision studies show that *a* ranges between 1 and 3 (Whipple and Tucker, 1999). For a = 1, k_b ranges between 10^{-5} and 2 X 10^{-4} m yr^{-1} Pa^{-1} (Lavé and Avouac, 2001) and ~10^{-7} m yr^{-1} Pa^{-1} (Wobus et al., 2005) for river bed incision, and is 18–40 m yr^{-1} Pa^{-1} for unconsolidated soil erosion (Elliot et al., 1989). For a = 1.5, k_b has been estimated at 8 X 10^{-6} m yr^{-1} $Pa^{-1.5}$ (Attal et al., 2008).

Shear stress at the sill can be approached as the product of water density r, the acceleration of gravity *g*, the mean water depth of the channel (z_s - z_0) and the slope of the water surface *S* (also known as hydraulic gradient):

$$\tau b = \rho g (z_s - z_0) S \qquad (2)$$

We assume that $S=H/L$, where H = z_1 - z_0 is the head loss, and length L = 100 km, which maximizes the half-width of the Betic–Rifean orogen. For a conservative estimation of *S* we impose a limit of H < 1,000 m (representative for the present depth of the Alborán Sea). We note that adopting higher slopes would result in a more abrupt flood.

To calculate the water flow over the sill and the level of the Mediterranean basins, we use an empirical relationship relating water flow speed *V* with the hydraulic gradient *S* (Manning's formula), frequently used to estimate outburst flood discharges (Gupta et al., 2007):

$$V = \frac{1}{n} R_h^{\frac{2}{3}} S \qquad (3)$$

where *V* is the average velocity (in metres per second), n = 0.05 is the roughness coefficient, and R_h is the hydraulic radius (in metres) of the strait connecting the Atlantic and the Mediterranean. The hydraulic radius is a measure of the flow efficiency of a river channel, and because channel width is significantly larger than channel depth, it can be estimated as $R_h \approx z_s - z_0$. River discharge (in cubic metres per second) can be calculated

as $Q = W\ (z_s - z_0)V$, where the W is the width of the channel expressed in metres. At each iteration we update the value of W using a relationship derived from river channel studies (Whittaker et al., 2007):

$$W = k_w Q^{aw} \qquad (4)$$

where a_w = 0.5 is an empirically determined constant (see, for example, Attal et al., 2008; Whittaker et al., 2007) and k_w = 1.2 is a value comparable to normal rivers that has been calibrated here to account for the final width of the Gibraltar Strait, assuming this coincides with the present strait width $W = 14$ km. The model predictions have a very small sensitivity to these parameters, as well as to the assumed initial width.

It is possible to solve the feedback dynamics analytically taking z_0 and S as constant (which is valid as long as head loss is not reduced by the refill of the Mediterranean):

$$\frac{dz_s(t)}{dt} = \mathrm{K}(z_s - z_0)^a \qquad (5)$$

where $K = k_b (\rho g S)^a$ for $K > 0$. The solution to equation (5) for a = 1 for the sill depth as a function of time is:

$$z_s(t) = z_s(0) + ce^{kt} \qquad (6)$$

Therefore, the sill is incised exponentially with time in the early stages of water flow, and the speed of this growth is dependent mostly on the lithological erodibility kb and the slope in the Mediterranean side S. For the post-Messinian flood, $K = 10^{-2}$ to 10^{-1} per year, indicating that erosion rate doubles in timescales of ten to a hundred years and that the feedback between incision and water flow is relevant to the timescales of the post-Messinian flood.

To study a more general scenario incorporating both the role of incision (as the mechanism excavating the water gate) and the head-loss reduction due to the

replenishment of the Mediterranean, we numerically solved equations (1) to (4) using an explicit finite-difference time-iterative technique. A time step of 0.1 days is used, starting with an initial sill depth of z_s = 1 m below the initial ocean level, taken as z_0 = 0. We note that changing the initial sill depth from 1 m to 0.1 m induces a strong delay in the reference flood (t_2 increases from 14 to 47 years; see note 4 in Supplementary Table 1), while the predicted maximum flooding rates undergo otherwise insignificant changes (the flood evolution is just shifted in time). Our model cannot determine whether this initial sill depth is related to tectonic subsidence at the Gibraltar Strait (Govers, 2009), or to global sea level rise, or to erosion of the sill (Loget and Van Den Driessche, 2006). For the Mediterranean basins we adopt initial levels of z_1 = 2,500 m (west) and z_2 = 2,700 m (east) below sea level (Meijer et al., 2004). The predicted timing of the flood does not vary substantially for a more conservative initial level of 1,500 m. Global sea level drops 9.5 m as a result of the flood, although this result uses the present global ocean hypsometry as a proxy for the one at Messinian times.

The initial geometry adopted for the flooding channel is conservative in the sense that it is chosen to find a maximum estimate for the duration of the flood. For this reason, we have adopted a low value for both the initial slope (S = 1%) and a mean incision (240 m for the examples in Fig. 7.2-3). Similarly, we have neglected other mechanisms that may have increased incision during the flood, such as cavitation (O'Connor, 1993). It is also implicitly assumed that the observed incision is due to a single flood. If an earlier flood took place, its incision across the sill should have been raised above sea level to close theMediterranean and, in order to affect our estimation of the amount of incision, should be brought below sea level again before the next flood occurred. In other words, multiple flooding could only induce an overestimation of the amount of incision in the presence of post-flood uplift and desiccation-related subsidence at the sill. These vertical sill motions are exactly the opposite of those predicted for the Messinian choking of the Mediterranean (Govers, 2009). It is therefore unlikely that the incision resulted from multiple flooding. Supplementary Fig. 7.2-3a shows the effect of the estimated total incision on the predicted duration of the flood.

7.2.3 Evidences of channel incision

The strongest evidence for a deep incision channel across the Gibraltar Strait comes from recent boreholes and from seismic data. Drilling cores related to the Africa–Europe tunnel project (Fig. 7.2-2a) show a thickness of at least 250 m of flysch breccia redeposited or slumped into a trough carved across the original flysch units (Late Cretaceous to Neogene in age) outcropping in the Iberian and Moroccan sides of the strait (Esteras et al., 2000; Pliego, 2005). A similar eastward-oriented incision is observed further to the east, in the Alborán side of the strait7 (Fig. 7.2-1). Both features have previously been interpreted as subaerial (fluvial) erosion during the Messinian desiccation (Blanc, 2002; Loget and Van Den Driessche, 2006; Esteras et al., 2000). In Fig. 7.2-2b and Supplementary Fig. 7.2-S2 we present two sample seismic profiles correlated with Ocean Drilling Program (ODP) site976 and the commercial well Andalucia G-1 (Comas et al., 1996; Tandon et al., 1998) through a large set of other publicly available seismic surveys (Fig. 7.2-1). These profiles provide evidence for the geometry of this incision and its continuity across the Gibraltar Strait along at least 200 km. As previously recognized (Esteras et al., 2000), this erosive channel is incised into Miocene deposits and filled by Pliocene–Quaternary sediments, and merges laterally with the basin-wide Messinian Erosional Surface (MES).

In areas unaffected by the widespread mud diapirism, the geometry of the incision has a U-shaped cross section with a size varying from 650 m depth by 11 km width near the strait to less than 300 m depth per 6 km in different branches of the channel further to the east. The size of this channel is not comparable to any other Messinian palaeovalley observed in the Alborán Sea, but only to canyons carved during the Messinian desiccation by the largest rivers in the Mediterranean (Barber, 1981; Clauzon, 1978). However, the U-shape of this incision (Fig. 7.2-2b) and its presence at both the eastern and western sides of the drainage divide (Fig. 7.2-1) cast doubt on its formation by subaerial fluvial erosion (typically producing V-shaped valleys) by an eastward-flowing river. Such mechanism would require a large catchment area during the Messinian, but the scarcity of tectonic deformation since that age (Loget and Van Den Driessche, 2006; Iribarren et al., 2007) suggests that the drainage divide shown in Fig. 7.2-1 has not undergone major changes. Recently, U-shapederosion channels found

in the English Channel have been attributed to a megaflood sourced in a large glacial lake in the North Sea (Gupta et al., 2007).

7.2.4 Flood modelling

We therefore postulate that the erosion channel observed in Gibraltar (Fig. 7.2-1) was excavated by the Zanclean flood. To validate this hypothesis, we calculate the timing of water flow and incision produced during the overspill of the Atlantic basin into the Mediterranean basin by combining a model of rock incision by water with hydrodynamic equations (see Methods). To calculate the flood evolution displayed in Fig. 7.2-3, we searched for combinations of the erosional parameters k_b and a that fit a final sill incision of 240 m (a mean value of observed incision in the eastern and western sides of the strait, averaged across the channel). All model runs show a long first period of very little incision owing to the reduced amount of water discharge allowed by the shallow sill depth of 1 m prescribed at the initial time (t = 0). As the Gibraltar gate is excavated growing deeper and wider, water flow and incision rate increase exponentially. This situation persists until water flow becomes limited by the rising level of the Western Mediterranean. This event is labelled as stage 1 in Fig. 7.2-3. Later, the reduction of the hydrological gradient between the Atlantic Ocean and the western Mediterranean results in reduction of flow velocity, water discharge and incision rate. As the Sicily sill is reached (stage 2), the level of the western basin (and the hydrological gradient) remains constant and the flooding water discharge is transferred to the eastern basin until this is also filled up to that level (stage 3). Afterwards, the whole Mediterranean rises synchronously while the level difference between basins, the water discharge, and the velocity decrease gradually to zero (stage 4).

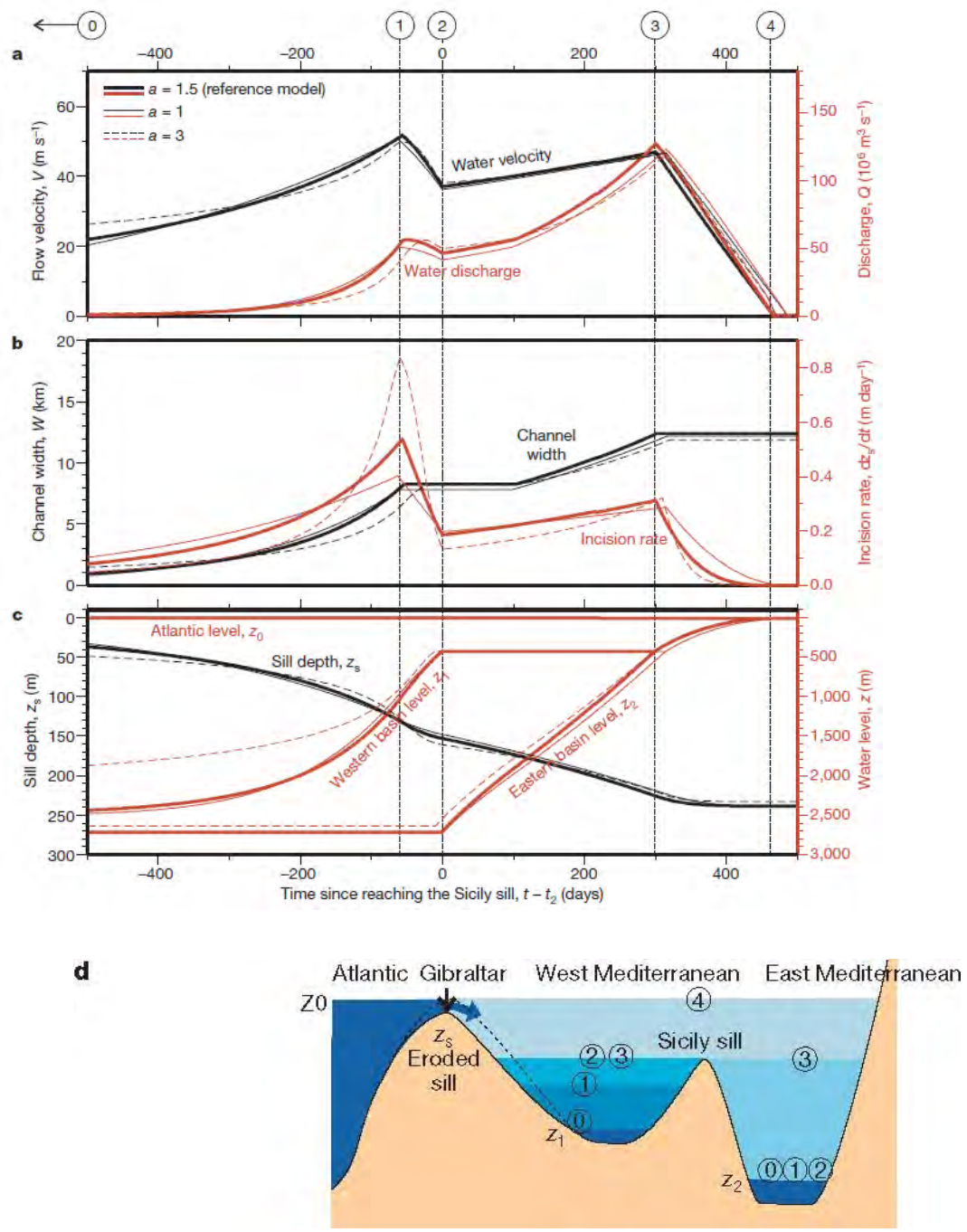

Figure 7.2-3. Evolution of three floods producing a final incision of 240 m, calculated for different exponents of the erosion law *a*.a) Water velocity and water discharge through the Gibraltar Strait; b) Channel width and incision rate; c) Sill depth (black lines) and level of the Atlantic, the Western Mediterranean, and Eastern Mediterranean (red lines). For comparison purposes, time is relative to the time when the Sicily Sill is reached *t2* (Supplementary Table 1). The three floods start with a sill depth of 1 m. Although peak discharges take much longer to arrive for large *a* values, the bulk of the water flow is concentrated in a similar amount of time. Circled numbers refer to the five stages shown in the cartoon d): (0) initial time; (1) time of maximum incision rate; (2) western Mediterranean level reaches the Sicily Sill (*t2*); (3) eastern basin level reaches the Sicily Sill; and (4) The Mediterranean becomes full.

For comparison, the three model evolutions in Fig. 7.2-3 are shown using a time relative to the instant when the western basin reaches the Sicily sill (t_2, stage 2), which roughly coincides with the time when the rate of sea level rise becomes maximum. Though the exponent of the erosional law a strongly influences t_2 (Supplementary Table 1 and Supplementary Fig. 7.2-S3), the abruptness of the flood remains relatively insensitive to a. This is shown by defining the bulk duration of the flood Δt_b as the time taken by 90% of the total water transfer. High-a, low-k_b model runs imply slow incision at the first stages and therefore a long period of water supply and basin level rise before the catastrophic flow (large t_2). A priori, this could result in a significant refill of the Mediterranean and a reduction in hydraulic gradient, diminishing the abruptness of discharge, but the results show that this occurs only for unrealistic values of the exponent $a > 3$. Within a value derived for river incision studies, Δt_b changes only from 510 days to 790 days. A complete model parameterization is available in Supplementary Fig. 7.2-S3.

7.2.5 Discussion and conclusions

The amount of incision expected during the post-Messinian flood on the basis of river incision studies (see note 2 in Supplementary Table 1) is comparable in depth and width to the erosion channel observed at the Gibraltar Strait. Using this geometry as a model constraint implies that the Zanclean flood was a catastrophic event (Fig. 7.2-3), more abrupt than previously thought (Blanc, 2002; Hsü and Ryan, 1973; Meijer and Krijgsman, 2005), and involved maximum rates of Mediterranean level rise of over 10 m per day. This abruptness has significance not only for its potential effects on ecosystems of the Mediterranean region but also for its palaeoclimatic effects, because a smaller (by two orders of magnitude) outburst flooding at Lake Agassiz has been related to a global cold period around 12,000 years ago (Broecker, 2006). The peak discharge across the Gibraltar Strait reached more than 10^8 m^3 s^{-1} at a speed of over 40 m s^{-1}, only months before flood completion, and produced maximum incision rates exceeding 0.4 m per day. For comparison, the Amazon mean discharge is only 1.5 X 10^5 m^3 s^{-1} and the Lake Missoula late glacial catastrophic flood has been estimated in 10^7 m^3 s^{-1} (O'Connor and Baker, 1992). The Messinian flood implied a dissipation of gravitational potential energy

of about 1.6 X 10^{22} *J*, similar to the heat transport along the Gulf Stream in a year, and ~4% of the kinetic energy of the K-T Chicxulub meteorite impact (Covey et al., 1994).

These estimates are consistent with the exceptionally rapid restoration of deep marine conditions recorded at the Messinian–Pliocene boundary (Rouchy and Caruso, 2006). High-resolution sedimentological studies of this boundary (Iaccarino and Bossio, 1999; Pierre et al., 2006) show a brief freshwater influence on the mineralogy, fauna and stable-isotope composition of carbonates over only 15 cm of sediment in ODP site 975. These might reflect the initial flooding period of relatively slow water flow predicted in our calculations, before stage 1. The flood evolution obtained for high values of the incision law exponent (a = 3) undergoes little sea level rise in the Mediterranean for the first few thousand years before the catastrophic flow is triggered. Future studies should determine the spatial distribution of the approximately 500 km^3 of rock eroded at the Gibraltar Strait during the flood climax.

We do not envisage the flood as a waterfall, as is often represented: instead, the geophysical data (Supplementary Fig. 7.2-S2) suggests a huge ramp, several km wide, descending from the Atlantic to the dry Mediterranean with a slope of 1% to 4%, similar to the slope of the present sea floor eastward from Gibraltar. Erosional retreat caused by the flood shifted the sill 30–80 km westwards from its Messinian location at the Gibraltar Strait and shaped the incision channel and the bulk of the strait morphology as we see them today.

Supplementary information

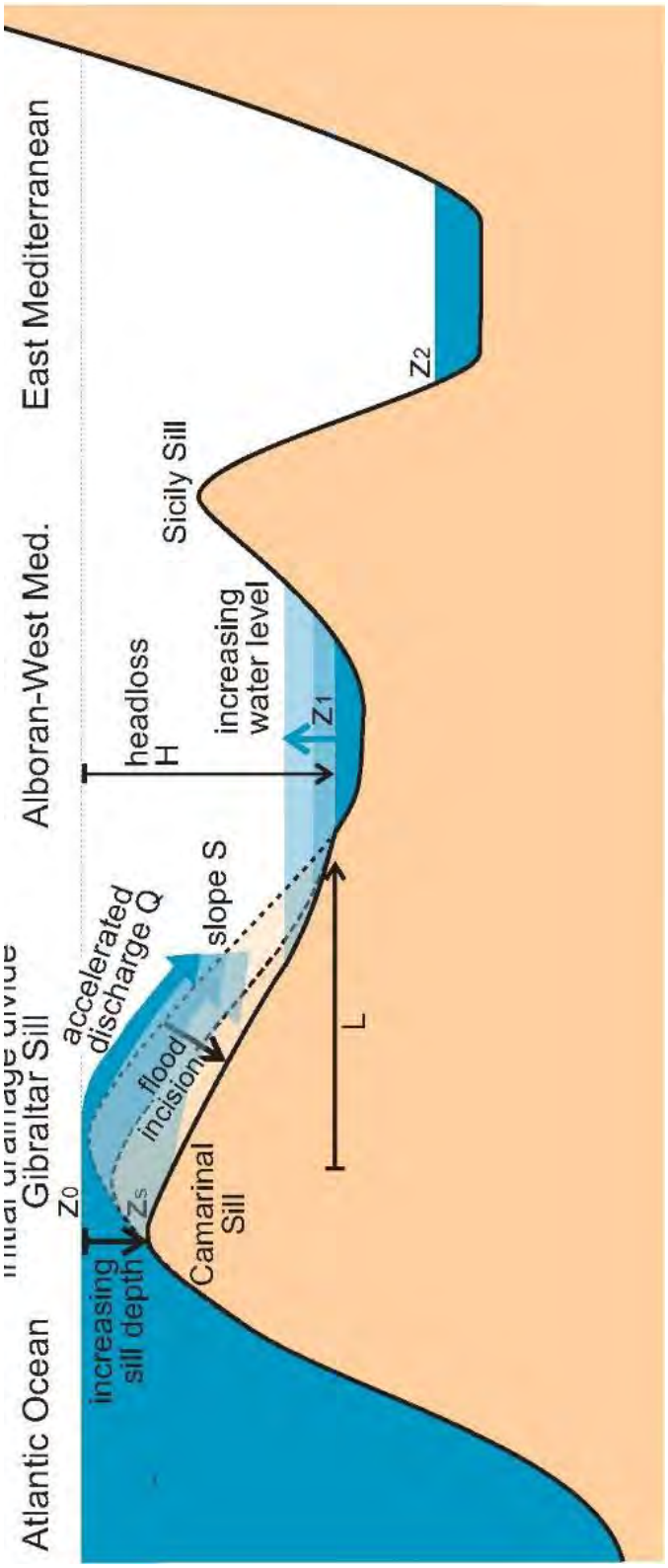

Figure 7.2-S1.- Conceptual model of feedback between water-flow shear stress and sill incision at the Gibraltar Strait. Notation is defined in the Methods. Incision at the sill is controlled by rock erodibility and water flow, which is calculated as a function of sill depth zs-z0 and head loss H. In turn, the increasing sill depth implies an exponential growth of water discharge that ends only as head loss H is reduced. The progress of the flood is determined by the total amount of incision, which allows constraining the erodibility parameters. The volumes adopted for the western and eastern Mediterranean are based on reconstructions by Meijer and Krijsgsman6. Evaporation and precipitation are not significant at the time scales of the flood.

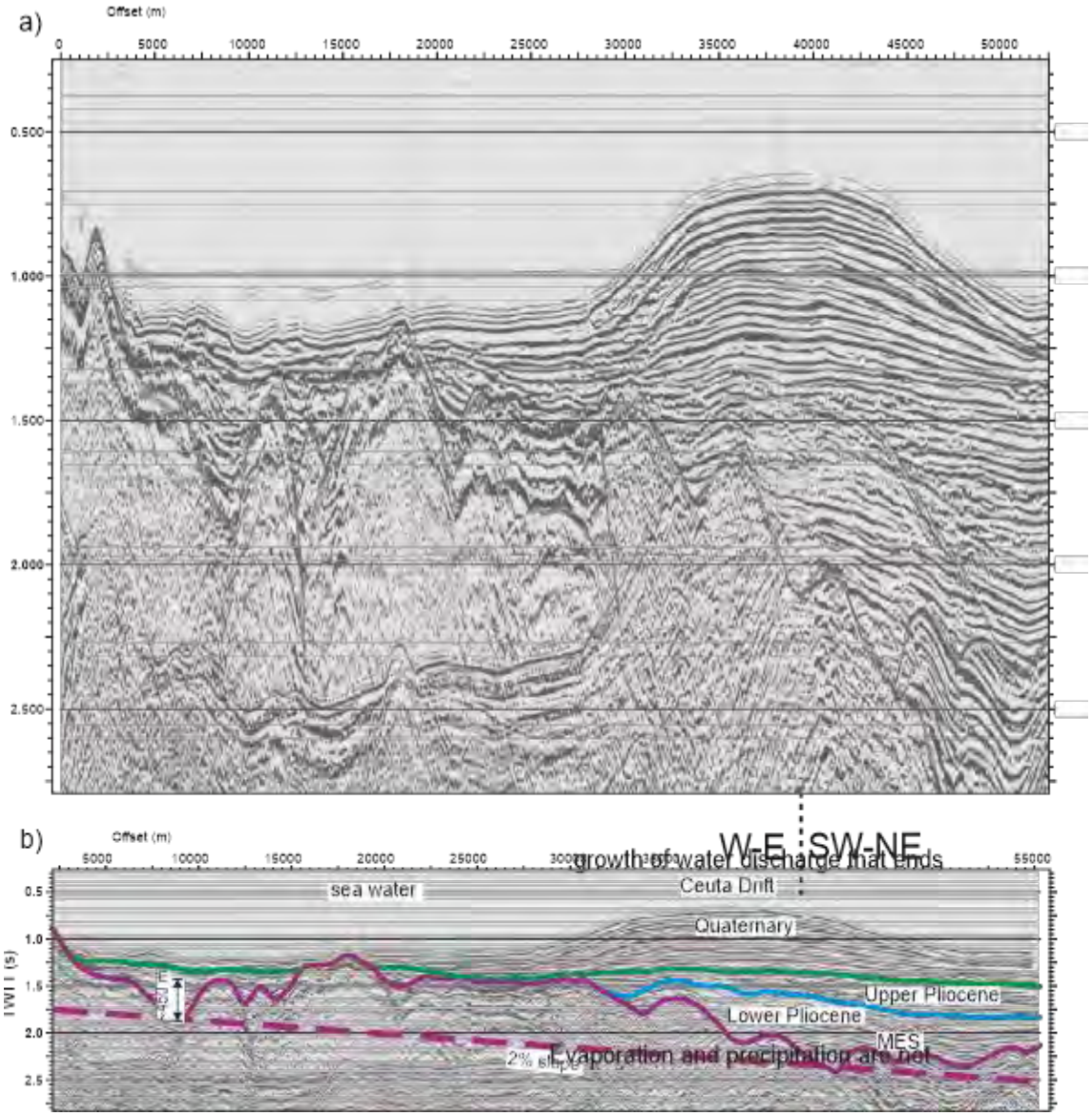

Figure 7.2-S2. Multi-channel seismic profile Conrad 829 along the Gibraltar Strait. a) Row data; b) Interpretation based on correlation with the wells located in Fig. 7.2-1. Approximate vertical exaggeration is 15:1 (a) and 5:1 (b). The vertical axis is two-way travel time of the seismic waves. The profile follows the channel path only roughly, and the offset between both induces the undulations in the MES reflector (Messinian Erosional Surface). Taking the deepest points of the western and eastern sides as indicators of the channel axis depth yields a channel slope of ca. 2%. Location in Fig. 7.2-1. The sedimentary mound is a contourite depositional system (Ceuta Drift) resulting from the interaction of the Mediterranean outflow water and sediments coming from the Moroccan margin. Most seismic lines located in Fig. 7.2-1 are available at the websites of the Instituto Geológico y Minero de España (IGME) and the Institut de Ciències del Mar (ICM-Barcelona).

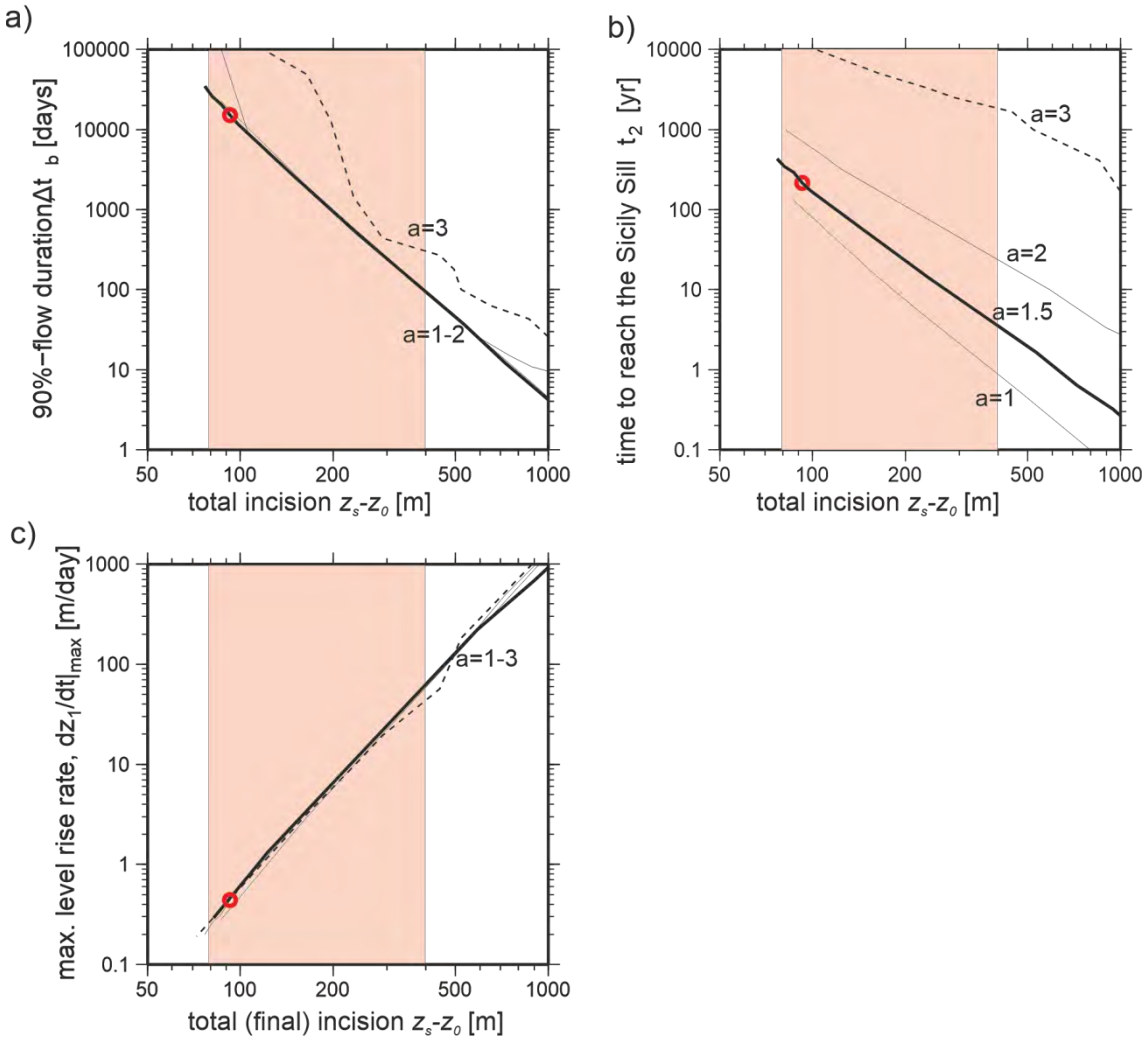

Figure 7.2-S-3. Model parameterization. Relationship between the calculated total sill erosion zs-z0 and: a) the time lapse taken by 90% of the water flow Δtb; b) the time when sea level reaches the Sicily Sill t2; and c) the maximum level rise rate dz1/dt. The values predicted for river incision parameters from Attal et al.34 are indicated with a circle. The shaded area indicates the range of incision observed, averaged across the sill in the Gibraltar area.

Table 1. Results for selected combinations of input parameters a,k_b. The reference model is indicated in bold.

Shear stress power law exponent a	Shear stress law constant k_b [m yr^{-1} Pa^{-a}]	Total incision z_s-z_0 [m]	Max. water level rise rate, dz_1/dt_{max} [m/day]	Time elapsed to reach the Sicily Sill , t_2 [years]	Max. water discharge [10^6 m^3 s^{-1}]	90% water flow completion time, Δt_b [days]
1	(1) $1.15\cdot10^{-2}$	240	10.71	4.2	123	510
1.5	**(1) $1.30\cdot10^{-4}$**	**240**	**11.84**	**14.0**	**127**	**514**
3	(1) $1.63\cdot10^{-10}$	240	10.91	3,072.0	128	790
(2) 1.5	(2) $8.00\cdot10^{-6}$	92	0.44	215.6	4.3	15100
(3) 1.5	(3) $1.30\cdot10^{-4}$	271	35.82	5.3	390	168
(4) 1.5	(4) $1.30\cdot10^{-4}$	240	11.83	47.1	127	514

(1)Erosion parameter values imposed to obtain a 240 m total incision; (2)Parameter values derived from river incision by Attal et al.[34]; (3)Same erosion parameters as in the reference model but adopting double initial slope (L=50 km); (4)Same erosion parameters as in the reference model but adopting an initial sill depth of z_s=0.1 m instead of 1 m..

7.2.6 References

Attal, M., Tucker, G. E., Whittaker, A. C., Cowie, P. A. and Roberts, G. P. Modeling fluvial incision and transient landscape evolution: Influence of dynamic channel adjustment. J. Geophys. Res. 113, F03013, doi:10.1029/2007JF000893 (2008).

Barber, P. M. Messinian subaerial erosion of the proto-Nile Delta. Mar. Geol. 44, 1981 253–272 (1981).

Blanc, P.-L. The opening of the Plio-Quaternary Gibraltar Strait: assessing the size of a cataclysm. Geodin. Acta 15, 303–317 (2002).

Blanc, P.-L. Improved modelling of the Messinian Salinity Crisis and conceptual implications. Palaeogeogr. Palaeoclimatol. Palaeoecol. 238, 349–372, doi:10.1016/ j.palaeo.2006.03.033 (2006).

Broecker, W. Was the Younger Dryas triggered by a flood? Science 312, 1146–1148 (2006).

Campillo, A., Maldonado, A. and Mauffret, A. Stratigraphic and tectonic evolution of the western Alborán sea: Late Miocene to recent. Geo-Mar. Lett. 12, 165–172 (1992).

Clauzon, G. The Messinian Var canyon (Provence, southern France): paleogeographic implications. Mar. Geol. 27, 231–246 (1978).

Clauzon, G., Suc, J.-P., Gautier, F., Berger, A. and Loutre, M.-F. Alternate interpretation of the Messinian salinity crisis: controversy resolved? Geology 24, 363–366 (1996).

Comas, M. C. et al. Volume 161. Proc. ODP Init. Rep. 161, doi:10.2973/ odp.proc.ir.161.1996 (1996).

Covey, C., Thompson, S. L., Weissman, P. R. and MacCracken, M. C. Global climatic effects of atmospheric dust from an asteroid comet impact on Earth. Glob. Planet. Change 9, 263–273 (1994).

Docherty, C. and Banda, E. in The Tertiary Basins of Spain (eds Friend, P. and Dabrio, C.) 392–398 (Cambridge University Press (1995).

Duggen, S. and Hoernle, K. v. d. Bogaard, P., Ru¨pke, L. and Phipps-Morgan, J. Deep roots of the Messinian salinity crisis. Nature 422, 602–606 (2003).

Elliot, W. J., Liebenow, A. M., Laflen, J. M. and Kohl, K. D. A compendium of soil erodibility data from WEPP cropland soil field erodibility experiments 1987 and 88. NSERL Report 3 (Ohio State University and USDA Agricultural Research Service, National Soil Erosion Research Laboratory, 1989).

Esteras, M. Izquierdo, J. Sandoval, N. G. and Bahmad, A. Evolucio´n morfolo´gica y estratigrafı´a Plio-Cuaternaria del Umbral de Camarinal (Estrecho de Gibraltar) basada en sondeos marinos. Rev. Soc. Geol. Esp. 13, 539–550 (2000).

Garcia-Castellanos, D., Vergés, J., Gaspar-Escribano, J. M. and Cloetingh, S. Interplay between tectonics, climate and fluvial transport during the Cenozoic evolution of the Ebro Basin (NE Iberia). J. Geophys. Res. 108 (B7), 2347, doi:10.1029/2002JB002073 (2003).

Govers, R. Choking the Mediterranean to dehydration: the Messinian salinity crisis. Geology 37, 167–170, doi:10.1130/G25141A.1 (2009).

Gupta, S., Collier, J. S., Palmer-Felgate, A. and Potter, G. Catastrophic flooding origin of shelf valley systems in the English Channel. Nature 448, 342–345 (2007).

Hsü, K. J., Cita, M. B. and Ryan, W. B. F. The origin of the Mediterranean environments. Init. Rep. Deep Sea Drilling Project, 13, 1203–1235 (US Government Printing Office, 1973).

Hsü, K. J., Ryan, W. B. F. and Cita, M. B. Late Miocene desiccation of the Mediterranean. Nature 242, 240–244 (1973).

Iaccarino, S. M. and Bossio, A. Paleoenvironment of uppermost Messinian sequences in the Western Mediterranean (site 974, 975, and 978). Proc. ODP Sci. Res. 161, 529–541 (1999).

Iribarren, L., Vergés, J., Camurri, F., Fullea, J. and Fernandez, M. The structure of the Atlantic-Mediterranean transition zone from the Alborán Sea to the Horseshoe Abyssal Plain (Iberia-Africa plate boundary). Mar. Geol. 243, 97–119, doi: 10.1016/ j.margeo.2007.05.011 (2007).

Krijgsman, W., Hilgen, F. J., Raffi, I., Sierro, F. J. and Wilson, D. S. Chronology, causes and progression of the Messinian salinity crisis. Nature 400, 652–655 (1999).

Lavé, J. and Avouac, J.P. Fluvial incision and tectonic uplift across the Himalayas of central Nepal. J. Geophys. Res. 106, 26561–26592, doi:10.1029/2001JB000359 (2001).

Loget, N. and Van Den Driessche, J. On the origin of the Strait of Gibraltar. Sedim. Geol. 188–189, 341–356 (2006).

Meijer, P., Th., Slingerland, R. and Wortel, M. J. R. Tectonic control on past circulation of the Mediterranean Sea: a model study of the late Miocene. Paleoceanography 19, PA1026, doi:10.1029/2003PA000956 (2004).

Meijer, P., Th. and Krijgsman, W. A quantitative analysis of the desiccation and refilling of the Mediterranean during the Messinian Salinity Crisis. Earth Planet. Sci. Lett. 240, 510–520, doi:10.1016/j.epsl.2005.09.029 (2005).

O'Connor, J. E. Hydrology, Hydraulics, and Gomorphology of the Bonneville Flood GSA Special Paper 274 1–90 (Geological Society of America, 1993).

O'Connor, J. E. and Baker, V. R. Magnitudes and implications of peak discharges from glacial Lake Missoula. Geol. Soc. Am. Bull. 104, 267–279 (1992).

Pierre, C., Caruso, A., Blanc-Valleron, M. M., Rouchy, J. M. and Orszag-Sperber, F. Reconstruction of the paleoenvironmental changes around the Miocene–Pliocene boundary along a West–East transect across the Mediterranean. Sedim. Geol. 188–189, 319–340 (2006).

Pliego, J. M. The Gibraltar Strait tunnel. An overview of the study process. Tunnelling Underground Space Technol. 20, 558–569 (2005).

Rouchy, J. M. and Caruso, A. The Messinian salinity crisis in the Mediterranean basin: a reassessment of the data and an integrated scenario. Sedim. Geol. 188–189, 35–67, doi:10.1016/j.sedgeo.2006.02.005 (2006).

Tandon, K., Lorenzo, J. M. and de La Linde Rubio, J. Timing of rifting in the Alborán Sea basin—correlation of borehole (ODP Leg 161 and Andalucia A-1) to seismic reflection data: implications for basin formation. Mar. Geol. 144, 275–294 (1998).

Watts, A. B., Platt, J. P. and Buhl, P. Tectonic evolution of the Alborán Basin. Basin Res. 5, 153–177 (1993).

Whipple, K. X. and Tucker, G. E. Dynamics of the stream-power river incision model; implications for height limits of mountain ranges, landscape response timescales, and research needs. J. Geophys. Res. B 104, 17661–17674, doi:10.1029/ 1999JB900120 (1999).

Whittaker, A. C., Cowie, P. A., Attal, M., Tucker, G. E. and Roberts, G. P. Bedrock channel adjustment to tectonic forcing: implications for predicting river incision rates. Geology 35, 103–106, doi:10.1130/G23106A.1 (2007).

Wobus,C.W.,Heimsath,A.M.,Whipple,K.X.andHodges,K.V.Activeout-of-sequence thrust faulting in the central Nepalese Himalaya. Nature 434, 1008–1011 (2005).

7.3 Integration of the mathematical model with the geomorphological evidences

ABSTRACT

The mathematical modelling of the catastrophic event that put an end to the Messinian Salinity Crisis is integrated with the geomorphological features defined on the Messinian top surface, based on the analysis of a dense net of seismic profiles surveyed in the surroundings of the Strait of Gibraltar and Alborán Sea. The mapped morphosedimentary features as terraces and great erosive channel that crosses the entire Alborán basin coupled with the five Zanclean flooding phases (0 to 4) of the mathematical model, have allowed a more precise interpretation and timing of the geological processes related to the flooding. Likewise, this integration permits quantifying the catastrophic magnitude of that flooding which had been difficult to infer from the geomorphological evidences.

7.3.1 Introduction

The study of the evolution of the relief through mathematical modelling in combination with geomorphological analysis is a very useful tool to understand the processes that have governed the relief formation. Mathematical modelling allows a continuous view in the time between original relief and the resulting morphology as well as the interaction between the parameters responsible of relief formation. In this subchapter is analysed how the flooding mathematical model fits with the geomorphological evidences obtained from the analysis of seismic profiles and bathymetric data of the catastrophic event that ended to the Messinian salinity crisis in the Mediterranean.

7.3.2 The mathematical model

The mathematical model predicts five phases in the evolution of the Zanclean flood (Fig. 7.3-1). Phase 0 corresponds to a long-term period where the reduced entry of Atlantic water, induced by the depth of 1 m established (imposed) by the mathematical model at time t = 0, generates little significant erosion. In phase 1, the Strait of Gibraltar becomes deeper and wider, exponentially increasing its erosion rate and Atlantic water flow. In phase 2, there is a reduction in the hydrological gradient between the Atlantic Ocean and the Western Mediterranean that results in a decrease in speed flow and discharge of water, as well as the rate of erosion. During this phase all the Atlantic water that enters the Strait of Gibraltar is invested in filling the Western Mediterranean Basin (Fig. 7.3-2). The Eastern Basin remains isolated from the western one due to the Sicily sill. In phase 3, the sea level reaches the threshold of Sicily and the hydrological gradient remains constant in the Western Basin, since the water that enters through the Strait of Gibraltar is transferred to the Eastern Basin, producing a rapid sea level rise in the latter. Finally, in phase 4, the sea level rises synchronously in both Mediterranean basins until it is level with the Atlantic Ocean.

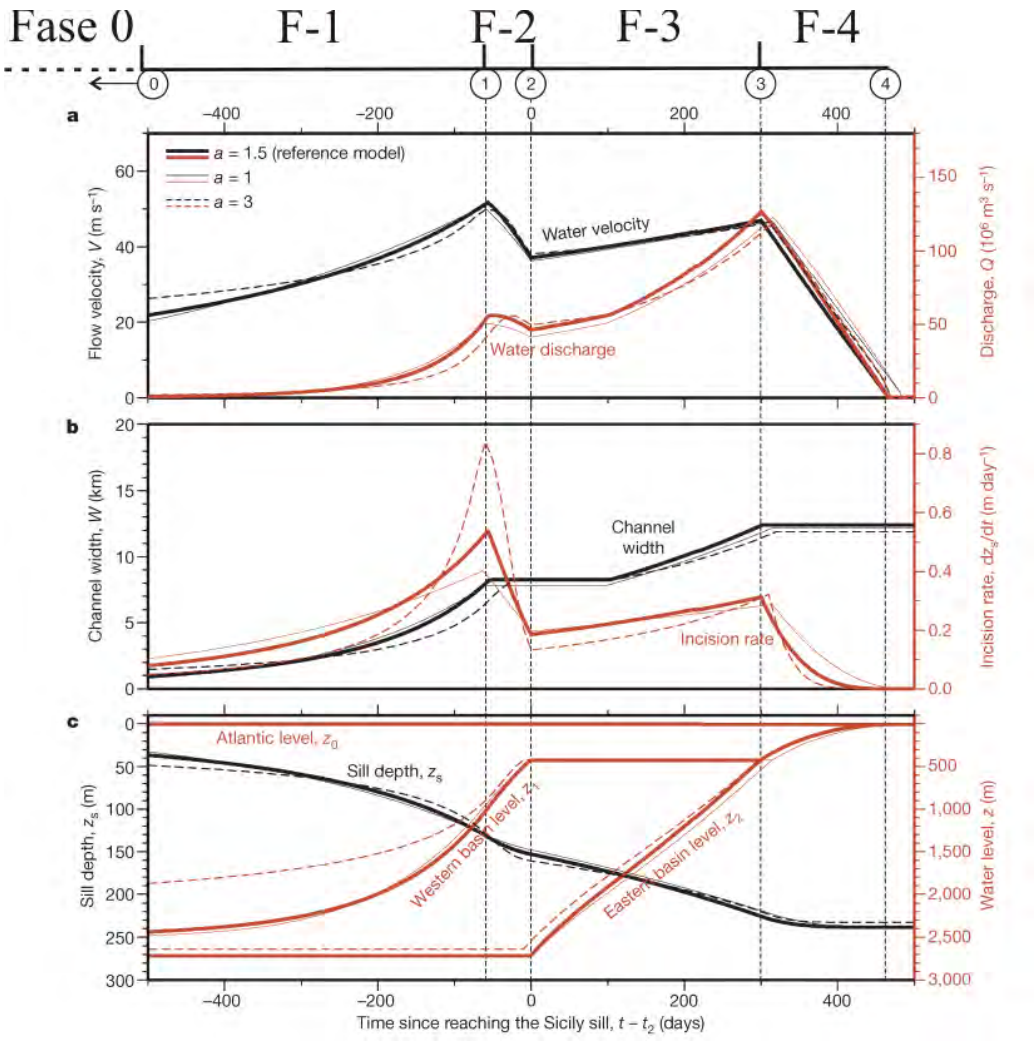

Figure 7.3-1. Mathematical model of the Zanclean flooding in the Strait of Gibraltar. a) Water velocity (black) and discharge (red). b) Channel width (black) and incisión rate (red). c) Sill depth (black) and level of the Atlantic, Western and Eastern Mediterranean (red). Modified from Garcia-Castellanos et al., (2009).

7.3.3 Geomorphological evidence

The geomorphological study of the impact of the Zanclean flood in the area of the Strait of Gibraltar and the Alborán Basin reveals the existence of a large erosive channel and the presence of several terraces.

The erosive channel originates in the Strait of Gibraltar and crosses the entire Alborán Basin from west to east through the deepest zone and along 390 km. It has a U-shaped cross section with dimensions of kilometre order, in general, decrease with distance from the Strait of Gibraltar. This erosive channel truncates the regional surface of the Messinian affecting more than 600 m in the deposits of the upper Miocene.

Moreover, it interrupts the distal part of several Messinian-age canyons developed on the Spanish continental margin near the Strait of Gibraltar.

The terraces develop in the Western Alborán Basin outside the area of influence of the erosive channel, identifying two groups located at different depths, between 650 and 2450 ms (double time) on the Iberian and African margins. The lower terraces are better developed on the Iberian margin, which was more exposed to the direct impact of the Atlantic flow. The upper terraces locate on the African and Iberian margin and developed in some cases on the chaotic deposits attributed to the salinity crisis, when these preserved. A better development of the upper terraces on the Iberian margin is also observed in this case.

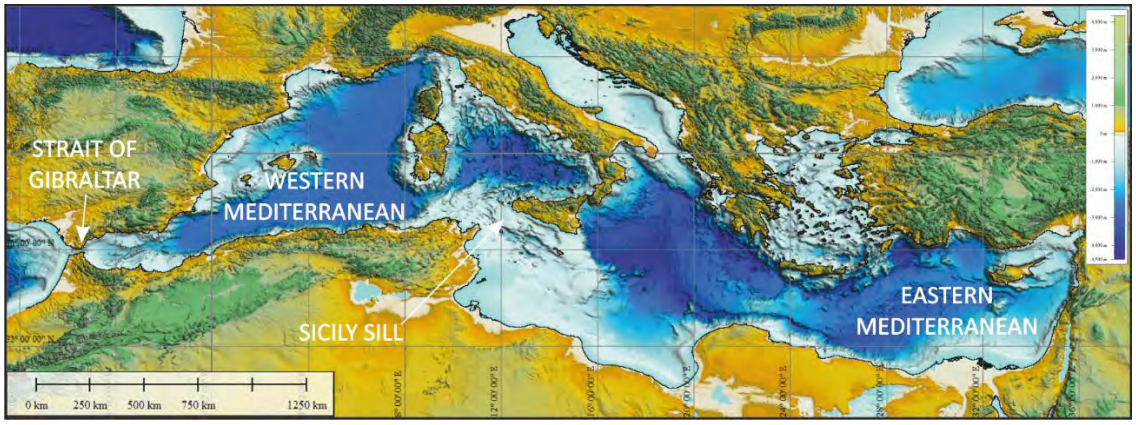

Figure 7.3-2. Topo-bathymetric map of the Mediterranean Sea showing the Eastern and Westerns basins and the location of the Sicily sill that separates them.

7.3.4 Discussion and conclusions: integration of mathematical and geological models

The different phases of the Zanclean flood, established by the mathematical model (Fig. 7.3.1) (Chapter 7.2), allow integrating both models and chronologically ordering the geomorphological elements and associating them with a specific phase of the flood. The first level of terraces, the deepest, are probably associated with phase 0 of the mathematical model, given the depth at which they develop. They would represent morphologies formed just before the great flood by a reduced watercourse and which were left hanging by the subsequent incision of the erosive channel. It is not ruled out that they may also be related to an initial stage of the flood, during phase 1, when the corridor began to impact.

The erosive channel, which crosses the entire Alborán Sea, from west to east, would be formed in phase 1 of the flood, when the impact of the Atlantic water was greater due to the marked hydraulic gradient existing between the Atlantic Ocean and the Mediterranean Basin. It probably formed in the early stages of this phase, before the reduction of the hydraulic gradient by the Mediterranean fill reduced the impact of the flood on the seabed of the Alborán Basin.

The second level of terraces, shallower, would be developed during phase 3 of the mathematical model, when the sea level temporarily stabilized upon reaching the threshold of Sicily and all the water that entered through the Strait of Gibraltar was invested in the filling of the Eastern Mediterranean Basin. These terraces present a similar development on both the African and Iberian margins, although the orientation of the Strait of Gibraltar with respect to the Iberian margin significantly favoured the development of the Iberian terraces. Recently, similar terraces have been observed in areas far from the Strait of Gibraltar such as on the Alborán Island and the Mallorca Island (Just et al., 2011). Finally, during phase 4 of the mathematical model, the connection between the Mediterranean and the rest of the world's oceans is reestablished.

The integration between the mathematical and the geomorphological model shows the great benefit of the interdisciplinary approach in general, and in particular, it allows to explain more precisely the history of the Zanclean flood in the Alborán Sea. Geological observations offer the main and necessary data to limit the variables that must be applied to the mathematical model. The numerical model allows fitting the geomorphological elements in a frame / temporal succession, and therefore to establish the evolution of the different sedimentary processes, their interaction with the environment, the paleoenvironmental variations and the history of the Zanclean flood of the Alborán Sea.

7.3.5 References

Just, J., Hübscher, C., Betzler, C., Lüdmann, T. and Reicherter, K. (2011). Geo-Marine Letters, 31, 51-64. doi: 10.1007/s00367-010-0213-z.

Chapter 8

The Zanclean megaflood of the Mediterranean – Searching for independent evidence

Daniel Garcia-Castellanos [a], Aaron Micallef [b], Ferran Estrada [c], Angelo Camerlenghi [d], Gemma Ercilla [c], Raúl Periáñez [e], José María Abril [e]

[a] Instituto de Ciencias de la Tierra Jaume Almera, ICTJA-CSIC, Barcelona, Spain

[b] Marine Geology and Seafloor Surveying, Department of Geosciences, University of Malta, Msida, MSD 2080, Malta

[c] Helmholtz Centre for Ocean Research, GEOMAR, Kiel, Germany

[d] Instituto de Ciencias del Mar, ICM-CSIC, Barcelona, Spain

[e] Istituto Nazionale di Oceanografia e di Geofisica Sperimentale (OGS), Trieste, Italy

[f] University of Sevilla, Spain

Published on: Earth-Science Reviews, 2020.

Volume 201, 103061pages 24-33

DOI: doi.org/10.1016/j.earscirev.2019.103061

Impact Factor (JCR): 12.413 (2020), Q1 en Geosciences, multidisciplinary. 5/239

ABSTRACT

About six million years ago, the Mediterranean Sea underwent a period of isolation from the ocean and widespread salt deposition known as the Messinian Salinity Crisis (MSC), allegedly leading to a kilometer-scale level drawdown by evaporation. One of the competing scenarios proposed for the termination of this environmental crisis 5.3 million years ago consists of a megaflooding event refilling the Mediterranean Sea through the Strait of Gibraltar: the Zanclean flood. The main evidence supporting this hypothesis is a nearly 390 km long and several hundred meters deep erosion channel extending from the Gulf of Cádiz (Atlantic Ocean) to the Algerian Basin (Western Mediterranean), implying the excavation of ca. 1000 km^3 of Miocene sediment and bedrock. Based on the understanding obtained from Pleistocene onshore megaflooding events and using ad-hoc hydrodynamic modeling, here we explore two predictions of the Zanclean outburst flood hypothesis: 1) The formation of similar erosion features at sills communicating sub-basins within the Mediterranean Sea, specifically at the Sicily Sill; and 2) the accumulation of the eroded materials as megaflood deposits in areas of low flow energy. Recent data show a 6-km-wide amphitheater-shaped canyon preserved at the Malta Escarpment that may represent the erosional expression of the Zanclean flood after filling the western Mediterranean and spilling into the Eastern Basin. Next to that canyon, a ~1600 km^3 accumulation of chaotic, seismically transparent sediment has been found in the Ionian Sea, compatible in age and facies with megaflood deposits. Another candidate megaflood deposit has been identified in the Alborán Sea in the form of elongated sedimentary bodies that parallel the flooding channel and are seismically characterized by chaotic and discontinuous stratified reflections, that we interpret as equivalent to gravel and boulder megabars described in terrestrial megaflood settings. Numerical model predictions show that sand deposits found at the Miocene/Pliocene (M/P) boundary in ODP sites 974 and 975 (South Balearic and Tyrrhenian seas) are consistent with suspension transport from the Strait of Gibraltar during a flooding event at a peak water discharge of ~10^8 m^3 s^{-1}.

8.1 A pre-scientific myth about the origin of the Mediterranean Sea

In his Historia Naturalis (~77 AD), Pliny the Elder reports on a legend popular among the inhabitants of southern Iberia, telling how the Mediterranean Sea was born. According to this myth, the Mediterranean Sea was deserted and cut-off from the Ocean, and it was Hercules who dug an inlet with his sword between Jebel-el-Mina (Africa) and the rock of Gibraltar (Europe). This allowed the ocean to flow into the Mediterranean Basin, where “it was before excluded”, thus “changing the face of Nature”. All through the history of western culture, a myriad of later classical writers including Galileo Galilei's Dialogues (1632) or Jacinto Verdaguer's poem Atlàntida (1876) were inspired by Pliny's account, elaborating on the scenario of a desiccated Mediterranean Sea flooded by Atlantic waters. None of these accounts linked explicitly the myth to field evidence. Even after Steno and Lyell set the principles of Geology and the Messinian stage was recognized as a pan-Mediterranean evaporitic phase in the late nineteenth century by Mayer-Eymar in 1867 (Selli, 1960), nobody linked it with Pliny's accounts, perhaps because their catastrophic nature was at odds with the principle of gradualism, a scientific pillar deeply rooted in the birth of Geology.

Gradualism was eventually challenged when Bretz (1925) and Pardee (1942) set the floor for a paradigm change in geology recognizing outburst floods of unprecedented magnitude as the main agent for landscape formation in the Scablands (Washington state, NW USA) during the Pleistocene. Bretz and Pardee described flood deposits, giant erosion coulees and giant ‘ripples’ that are today widely accepted to be the result of the catastrophic emptying of Lake Missoula in Montana, about seventeen thousand years ago (Benito, 2003).

8.1.1 The development of the Messinian Salinity Crisis theory

Only in the decade of the 1970's did the hypothesis of a flood ending a Mediterranean desiccation enter the scientific literature, when DSDP drilling confirmed large deposits of evaporites in the deepest regions of the Mediterranean Sea (Hsü et al., 1973b; Ryan et al., 1973). The question as to how did this Messinian Salinity Crisis (MSC) end emerged from the barely 15 cm M/P transition in ODP 974B (Tyrrhenian Sea; Fig. 8-

1), which meant an “abrupt palaeoceanographic change created by the re-establishment of an open-marine environment in the earliest Pliocene” (Iaccarino and Bossio, 1999). The term flood or reflooding of the Mediterranean became a common place in the scientific literature studying the MSC (Hsü et al., 1973a, b; Comas et al., 1996), although it referred vaguely to a geologically-rapid transition from evaporitic to open marine conditions. Sedimentological analysis of the drilling cores (grain-size and microfauna) cannot resolve gradual changes shorter than a few millimeters in the core (i.e., a few thousand years in duration). For example, based on DSDP sites 121-139, K. J. Hsü et al. (1973a) speculated about a refill of the Mediterranean lasting “probably less than 1000 years”. Onshore evidence for a rapid Mediterranean Sea level rise at the end of the MSC came from the abundance of Giberttype deltas in the Gulf of Lyons and the Tyrrhenian Sea (Clauzon, 1978, 1982; Breda et al., 2009) and from the abrupt transit from paleosol to foraminifera-rich, deep marine laminites in the M/P contact in Pissouri (Orszag-Sperber et al., 2000). These observations suggested that the sea level rise was rapid in sedimentological terms and that the Strait of Gibraltar was the scenario for the reconnection between the Atlantic Ocean and the Mediterranean Sea, reestablishing the normal marine conditions ca. 5.3 million years ago.

The main evidence for a restriction from the Ocean and a Mediterranean-wide environmental change is the widespread presence of gypsum deposits along the Mediterranean coast, and a 1 to 3 km thick layer of halite in the abyssal areas of the Mediterranean, generally interpreted as the result of a severe restriction of the connection to the Atlantic Ocean. This halite layer is outcropping today in Calabria and it is widely present in the subsurface of the Caltanissetta Basin in Sicily, where it is commercially exploited in salt mines, and it is conspicuous in the deep Mediterranean basins from marine seismic reflection data (Lofi, 2010, 2018). Its mass had been estimated at > 3 1018 kg (Blanc, 2000; Ryan, 2009), around 10% of the salt contained in the global ocean, but a recent study based on a dense compilation of seismic prospection surveys, estimates its volume at only 821 to 927 106 km3 of (Haq et al., 2020), ca. 4% of today's salt dissolved in the ocean.

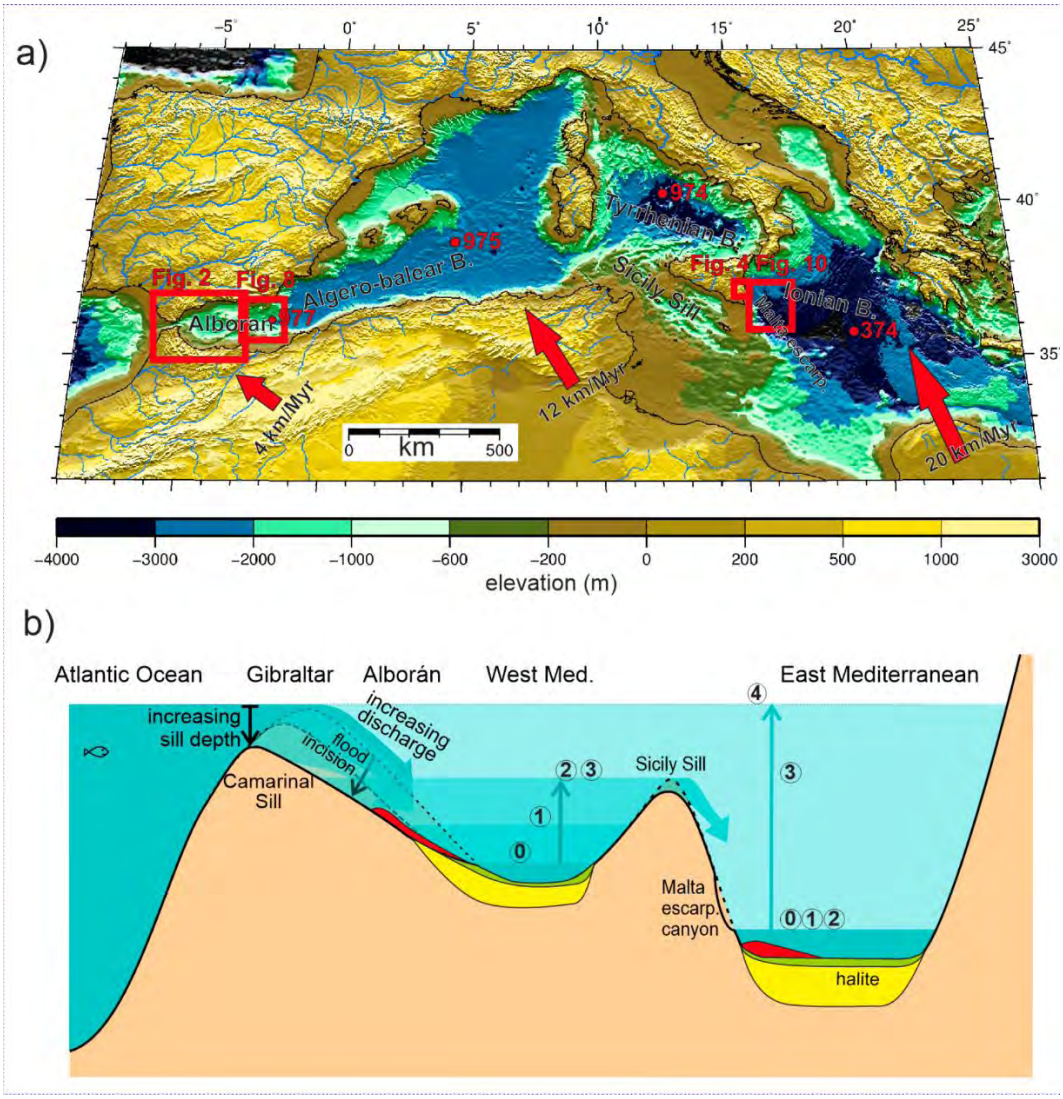

Figure 8-1. a) Topographic map of the Ionian Sea and western Mediterranean showing the location of data shown in this article. Red arrows indicate the average motion of Africa relative to Eurasia since 5.3 million years ago. Numbers in red indicate IODP/DSDP drillings mentioned in the text. b) Cartoon (not to scale) showing the timing and the flood erosional and depositional features expected in the eastern and western basins of the Mediterranean as a result of a large water input through the Gibraltar gateway, showing 5 stages: 0) Initial level before significant Atlantic inflow occurred; 1) time of maximum erosion rate at the Strait of Gibraltar; 2) the western basin level reaches the Sicily Sill. 3) eastern basin level reaches the Sicily Sill; and 4) the Mediterranean is filled to the normal oceanic level. The *mobile unit* (Messinian halite), *Lago-Mare*, and flood deposits discussed in this study are depicted in yellow, green, and red, respectively.

However, salt precipitation does not necessarily imply a desiccation. Natural salt pans do not require a level drawdown by desiccation in order to accumulate salt; a persistent but restricted connection that allows no outflow of brine but only inflow of normal saline water can lead to salt precipitation with no drawdown (e.g., today's

Garabogazköl in Turkmenistan). The main evidence actually supporting a kilometric drawdown for the Mediterranean during the late Neogene is the Mediterranean-wide Messinian Erosion Surface (MES) (Lofi, 2010, 2018) recorded in the seismic stratigraphy of the basin margins.

The Zanclean flood hypothesis is thus entangled with a wider dis cussion about the MSC: whether there was a kilometric-scale drawdown after the precipitation of the marginal primary gypsum. The Zanclean (5.33 to 3.60 million year ago) is the first stage of the Pliocene and its beginning coincides with the termination of the Messinian (last stage of the Miocene). A megaflood-like termination of the MSC requires a significant drawdown of the Mediterranean level. The occurrence of a significant drawdown of the Mediterranean during the Messinian (be it a full or a partial desiccation) is currently under strong debate and far from a consensus. Let us start summarizing the main reasons that question the kilometric drawdown scenario. A geochemical reexamination of the aforementioned drillings has questioned the shallowwater formation of the deep evaporite cores (Hardie and Lowenstein, 2004). Some studies suggest that the evaporitic deposition occurred under no substantial sea level drawdown but in a deep-basin under deep-water in a deep-basin condition, i.e., in a Mediterranean Sea filled to a level close to today's (e.g., Lugli et al., 2015; Roveri et al., 2001). This model is also supported by the homogeneity of isotopic signatures between distant synchronous gypsum deposits, suggesting a connection between the Mediterranean sub-basins and hence a high water level (García-Veigas et al., 2018).

Questioning a significant lowering of the level of the Mediterranean requires a mechanism to explain the MES alternative to subaerial exposure. The most developed such alternative mechanism so far is the hyperpycnal submarine cascading erosion (Roveri et al., 2014b), according to which the erosion of the margins resulted from sea water currents from the platforms towards the abyssal areas as a result of high density related to evaporation. As for the abrupt M/P transition, the alternative explanation to the Zanclean flood is a density-driven outpumping (Marzocchi et al., 2016) of the Mediterranean Sea. In this model, the Mediterranean level raises due to fresh water inputs from the Paratethys during the Lago-Mare stage, reconnecting and pumping it out to the denser Atlantic Ocean. Salt deposition was followed by a pan-Mediterranean

phase of sedimentation in a fresh to brackish water environment, represented by the so-called “Lago-Mare” sedimentary facies, which includes microfossils and ostracods originating from the Paratethys realm (present Carpathian and Black Sea areas) (Krijgsman et al., 2010). This deposition preceded the reestablishment of normal open marine conditions (Zanclean stage), and its presence at nearly the present sea level in outcrops in the margins around the Mediterranean Sea suggests that those fresh/brackish waters were covering a full and connected Mediterranean. However, the nature and environment of this last stage of the MSC are to date far from well understood since it also includes marine fish (Carnevale et al., 2006, 2017).

Studies that argue for a kilometer-scale drawdown (not necessarily implying a full desiccation) place it temporally either following (Escutia and Maldonado, 1992; Ryan, 2008; Estrada et al., 2011; Urgeles et al., 2011) or preceding (Bache et al., 2009, 2015) the precipitation of the 1 km of halite in the abyssal regions. Within the drawdown hypothesis, the erosional surfaces in the margins of the sea are attributed to subaerial processes such as river incision or wave erosion. Further evidence supporting is based on the relative abundance of volcanic samples dating to the MSC around the Mediterranean, which according to modeling results can be explained by the decompression of the crust due to the removal of the water column (Sternai et al., 2017).

As for the deep geodynamic causes for these changes in oceanic connectivity at the Strait of Gibraltar, computer simulations suggest that desiccation of the basin, as well as its later reflooding at the earliest Pliocene, may have been caused both by the vertical motions related to deep processes in the lithospheric mantle, namely the sink and detachment of a lithospheric slab underneath the Gibraltar Arc (Garcia-Castellanos and Villaseñor, 2011; Jiménez-Munt et al., 2019). The combination of these processes with erosion by the inflowing water at the gateway may explain the long initial stage of salt precipitation (gypsum and halite) and an extremely rapid basin refill.

The aim of the present article is to summarize recent and new stratigraphic evidence and modeling results that test the megaflood hypothesis (Garcia-Castellanos et al., 2009). The geophysical data we examine target the erosional and depositional impact of a large water flow entering the Mediterranean through the Alborán Sea and

then entering the Eastern Mediterranean over the Malta Escarpment. Be-cause such a megaflooding event would require a significant sea level drawdown in the Mediterranean, we will discuss the implications of the findings for the evolution of the MSC.

8.1.2 First models and quantifications of the Zanclean flood

The quantification of a geologically-rapid refill after the MSC was addressed specifically only in this century, first based on the geomorphology of the Strait of Gibraltar area and then based on geophysical and modeling techniques (Blanc, 2002, 2006; Garcia-Castellanos et al., 2009). According to Blanc (2002), an unprecedented stream shaped the Strait of Gibraltar after a capture of the Atlantic Ocean took place by retrogressive erosion of a river draining into the desiccated Alborán Sea (a process also known as river piracy). Based on assumptions on the size of the gateway during the Late Messinian and on collapse structures near the straits, that study concluded that the refill was cataclysmic, following an "instant breakthrough of the Atlantic waters".

Meanwhile, cores from drilling funded by the Africa–Europe tunnel project (Esteras et al., 2000) showed a > 200 m-deep erosional trough carved in the hard flysch units (Late Cretaceous to Neogene in age) outcropping around the strait. A similar eastward-oriented Pliocene incision is observed further to the east, in the Mediterranean side of the strait (Alborán Sea; Fig. 8-2). Both features had previously been interpreted as subaerial (fluvial) erosion by a forerunner stream during the Messinian sea level drawdown (Blanc, 2002; Esteras et al., 2000). However, the U-shape of the Messinian erosion surface (MES) in the Alborán Sea, the lack of a significant catchment, and the fact that this erosional channel crosses the natural drainage divide between the Atlantic and the Mediterranean (80 km in the Gulf of Cádiz and >200 km in the Alborán Basin) argue against subaerial erosion during the MSC drawdown (Garcia-Castellanos et al., 2009). Numerical modeling of this erosion channel assuming that it was excavated by the Atlantic waters overtopping the Strait of Gibraltar, led to estimations of the flood discharge of up to 100 Sv (1 Sverdrup = 10^6 m^3 s^{-1}), with a duration of 2 years or less (Garcia-Castellanos et al., 2009) (see Section 5). The initial

stages of the flood, according to that model, may have lasted up to a few thousand years before the inflow of water becomes significant relative to the Mediterranean water balance. By the time the flood overcomes lake evaporation and significantly refills the Mediterranean basin, erosion rates are predicted higher than a few mm yr^{-1}, preventing any tectonic or eustatic change from closing the seaway again and making the flooding process irreversible. This argues against the possibility of multiple flooding events (Rouchy and Martin, 1992) or against calm periods intercalated during the flood. It conflicts with the interpretation of a ravinement surface in the Gulf of Lions as the result of wave erosion during the flood (Bache et al., 2009; Estrada et al., 2011) and suggests that this might have been formed during climatically-controlled changes of lake level during the drawdown phase, similar to the wave-cut surfaces in the Malta Escarpment that will be shown below (Micallef et al., 2019). The accelerating flooding rates due to inlet erosion (Garcia-Castellanos et al., 2009) precludes the stagnation of the flooding process once the water discharge has become substantial in comparison with the water budget of the Mediterranean and has significantly risen its level.

In summary, while observations remain unclear on whether the crisis involved an important desiccation of the Mediterranean Sea (necessary condition for a catastrophic flood), models do provide some ideas on how to independently test this scenario. In this article, we summarize recent results from seismic stratigraphy and hydrological modelling assessing two predictions implied by the Zanclean flood thesis: 1) that at a few thousand cubic kilometres of rock eroded from the sills should have deposited elsewhere in the Mediterranean Sea; and 2) that flood erosion and sedimentation patterns similar to those described in Gibraltar should be found near the Sicily Sill, in the area where the flooded western Mediterranean should overspill into the eastern basin.

8.2 Flood erosion features

Apart from the ubiquitous MES discordance in the seismic sedimentary record of the Mediterranean Sea, two erosional features have so far been described that seem incompatible with subaerial exposure during the MSC drawdown or with processes

other than an unprecedented discharge of water. One is at the seaway between the Atlantic Ocean and the Mediterranean Sea, and the other at the gateway between the western and eastern Mediterranean basins.

8.2.1 Alborán Sea erosion channel

A remarkable erosive channel has been described in the deepest areas of the Messinian Erosion Surface (MES) of the Alborán Sea, particularly in the vicinity of the Strait of Gibraltar. Fig. 8-2 shows a significantly updated version of the depth to the MES in this region, based on a denser and more extended seismic reflection database relative to Estrada et al. (2011). The erosion channel is in lateral continuation with the erosional trough incised into the flysch units in the Strait of Gibraltar (Blanc, 2002; Esteras et al., 2000) and extends along 390 km with a W-E trend from the Gulf of Cádiz (Atlantic Ocean) (Garcia-Castellanos et al., 2009), crossing the deepest parts of the Alborán Sea (Figs. 8-2 and 8-3) until the Algerian Basin. This erosion channel geometry varies from 2 km width and > 200 m depth in the Atlantic side (were it dissects the basement) to > 15 km width and > 500 m depth in the Alborán Sea (were it erodes Miocene sediment). While Blanc (2002) linked the Atlantic section of this feature to the reflooding of the Mediterranean Sea, its Alborán continuation was linked to subaerial erosion by rivers during the MSC drawdown (Blanc, 2002; Campillo et al., 1992). Later investigations based on a wider geophysical database and numerical modeling lead to the alternative interpretation of an outburst flood erosion due to the breaching of the Strait of Gibraltar (Garcia-Castellanos et al., 2009; Estrada et al., 2011), after which the subsequent flood-retrogressive erosion propagated westwards, 80 km into the Atlantic domain. This hypothesis is consistent with the channel's U-shaped section, which contrasts with the V-shaped valley associated to fluvial erosion (Fig. 8-3). It also explains why this erosional feature has continuity westwards from the Strait of Gibraltar into the Gulf of Cádiz, crossing the natural divide formed by the Betic-Rif orogen.

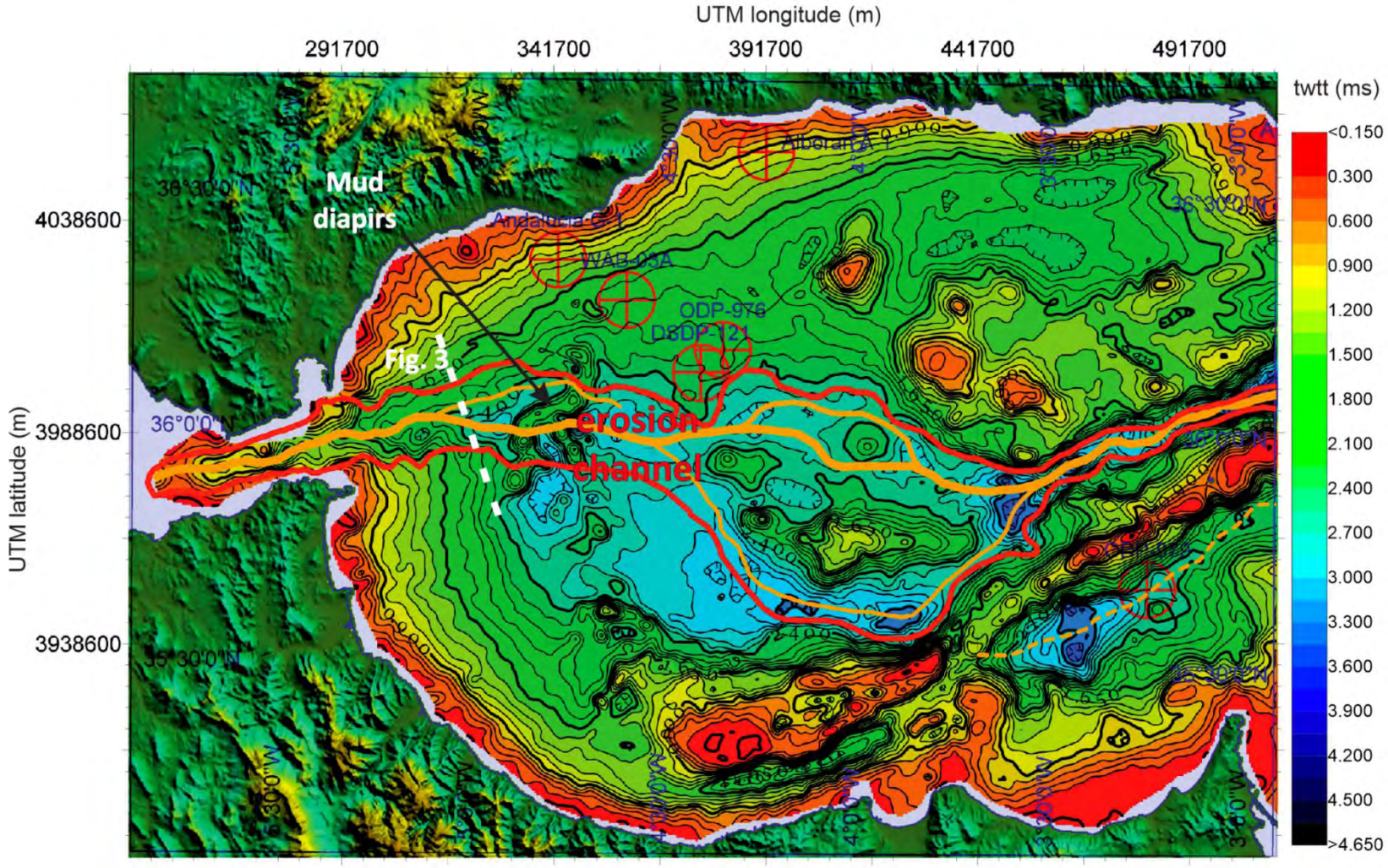

Figure 8-2. Map showing the depth to the base of Pliocene, including the Messinian Erosion surface (MES) and the erosion channel (red line) resulting from the Zanclean megaflood and the main flood paths (orange line). The MES has a polygenetic origin and represents the base of Pliocene (purple line in the seismic profiles. Contours in milliseconds, color scale bar in seconds. Updated from Estrada et al. (2011).

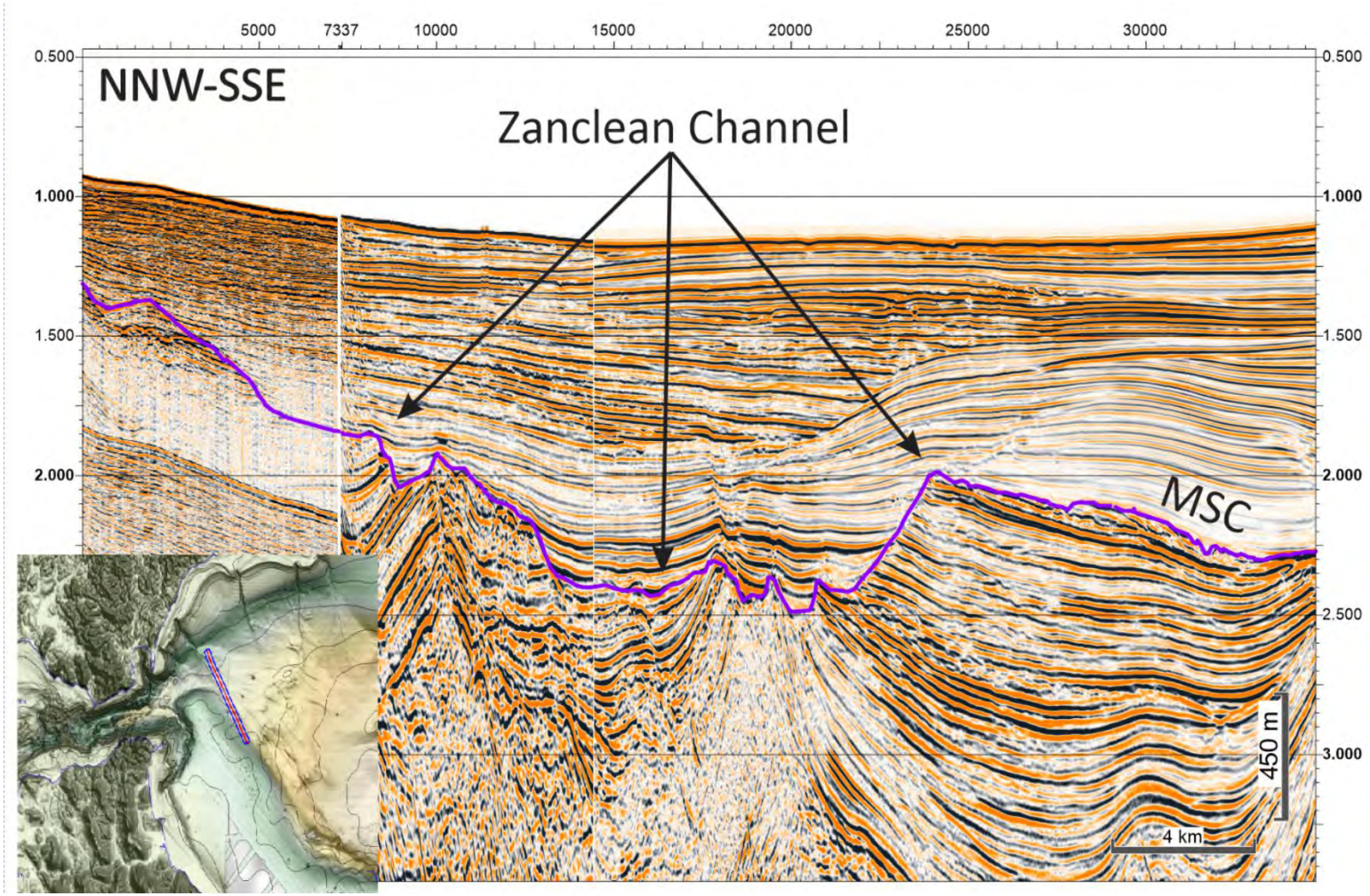

Figure 8-3. Composite seismic profile showing the Messinian erosion surface (MES; purple line) in the eastern side of the Strait of Gibraltar. Location in Fig. 8-2. This unconformity is interpreted as the erosion channel excavated into Miocene sediments at the latest MSC or earliest Pliocene. Depth in TWTT (double sound travel time in seconds). Detailed discussion and other seismic profiles in Estrada et al. (2011).

The morphological setting of the Alborán Basin is inherited from Late Neogene E-W extension coeval with African-Eurasian convergence and with volcanism (Duggen et al., 2003). As a result, the relief of the Alborán Basin was already abundant in volcanic seamounts and structural highs (Fig. 8-2). Adapting to this inherited landscape, the channel splits in two W-E branches only to merge again further to the E (Fig. 8-2). They are separated by a seamount (the Vizconde de Eza High, VdE in Fig. 8-2) that may have been a topographic obstacle during the flood. The channel incises vertically up to 600 m into the upper Miocene deposits, eroding MSC deposits that do not include the halite evaporites (Mobile Unit) found in the deeper basins of the Mediterranean. This is probably due to the shallower depth of this basin during that time (e.g., Booth-Rea et al., 2018). The channel has been subsequently deformed during the Plio-Quaternary by mud diapirism in the Western Alborán Basin and the compressional tectonism as a consequence of the ca. 4–5mm yr−1 of the ongoing convergence rate between Africa and Eurasia (Estrada et al., 2018).

8.2.2 Amphitheater-headed canyon in the Malta Escarpment

The Noto Canyon is a ca. 27 km long, 15 km wide, and 1.5 km deep geomorphic feature in the northern Malta Escarpment (SE Sicily margin; Fig. 8-4) (Micallef et al., 2018). It includes a canyon with a Ushaped cross-section carved in Mesozoic limestone. The head of this canyon has an amphitheater-shaped head, 6 km in width and 700 m high. This is very unusual for a submarine canyon and conspicuously different from the other canyons along the escarpment (Micallef et al., 2019). The strike of the Noto Canyon changes by 90° at a distance of 8 km upslope from its mouth. The canyon walls have a slope of 70°. Upslope of the Noto Canyon head, the seafloor has a gentler gradient of 7° and hosts a dendritic network of small tributary canyons. At the base of the Noto Canyon head, a sediment layer 100–200 m thick has accumulated at the bottom of the canyon (Fig. 8-4b).

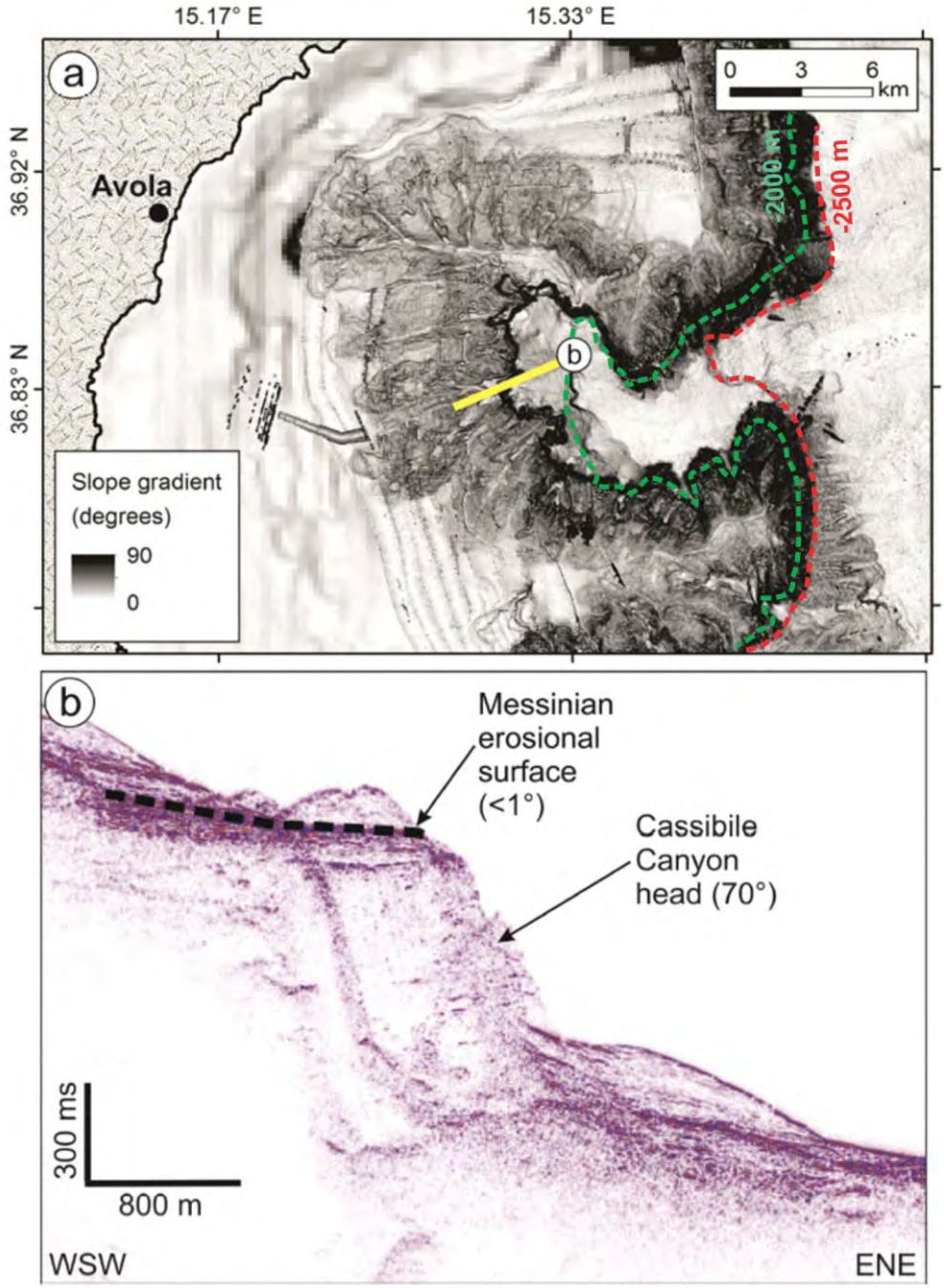

Figure 8-4. Probable gateway for the Zanclean flood into the eastern Mediterranean. (a) Shaded relief model of south-eastern Sicily showing terrestrial chaotic Zanclean deposits, and seafloor slope gradient map showing Noto Canyon. Isobaths denoted by dotted red lines. Location in Fig 8-1. (b) Seismic reflection profile CIR-07 showing Noto Canyon head and Messinian erosional surface upslope. Location in (a). The sediment resting on the acoustic basement in the right side (bottom of the canyon) is up to 200 m thick. Modified from Micallef et al. (2018).

The Noto canyon is located next to a set of massive, seismically chaotic to transparent deposits identified through multi-channel seismic reflection data in the western Ionian Basin and interpreted as a sedimentary body of up to 860 m in thickness and 1600 km3 in volume (see next section). Based on the inference that this sedimentary unit is compatible with a megaflood deposit, the Noto Canyon has been interpreted as having formed via excavation by a large subaerial flow of water caused by the overflow of the Western Mediterranean and its spilling into the Eastern Mediterranean basin during Zanclean flood (Micallef et al., 2018). However, this erosional feature is not directly dated and no stratigraphic correlation exists between its excavation and the Ionian stratigraphy and drillings.

Further to the south along the same escarpment, a series of concave slope breaks is observed at a consistent depth of 2400–2500 m below present sea level and with a total length of about 100 km (Fig. 8-5). These are interpreted as palaeoshorelines and shore platforms excavated by wave erosion related to a lowstand of the Mediterranean Sea below its present sea level (Micallef et al., 2019).

An isostatic restoration of those palaeoshorelines and shore platforms on the northern Malta Escarpment suggest an evaporative drawdown of 1800–2000 m below present sea level. While these do not directly support the occurrence of an abrupt outburst flood refilling the eastern Mediterranean, the shorelines do support a large hydraulic head available for the refilling waters pouring into the eastern basin with a flow energy comparable to, if not larger than, that at the Strait of Gibraltar.

The bottom of the Noto Canyon (2300–2600 m) is close to the depth of those shorelines and to the base of the megaflood deposit, allowing us to speculate that the canyon may have been excavated after a long period when the level of the Eastern Mediterranean remained at that level. After isostatic restoration by removing the weight of the Plio-Quaternary sediment and the water column (Micallef et al., 2019), the original depth of the base of the canyon the during the MSC would range between 1750 and 2050 m.

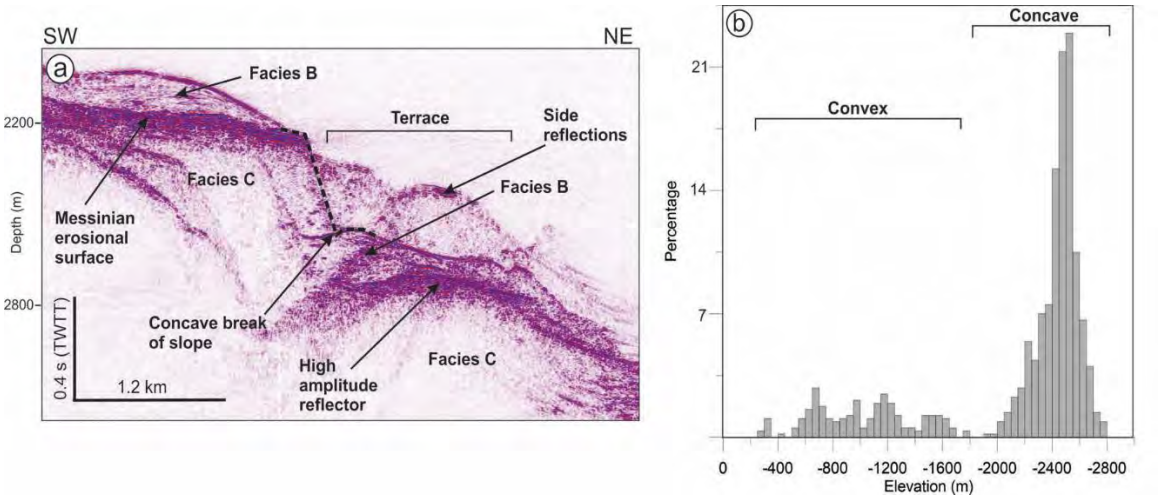

Figure 8-5. (a) Multi-channel seismic reflection profile across the Malta Escarpment intersecting the break of slope (dotted black line) and associated terrace, with the concave break of slope at the base. (Facies B=sub-parallel, convex upward reflectors; facies C=transparent facies). (b) Histogram of the depth of breaks of slope in the northern Malta Escarpment. The concave breaks are concentrated at depths of 2400-2500 mbsl. After isostatic restoration, these breaks have been interpreted as the result of wave erosion during the MSC lowstand of the Mediterranean level at -1800 to -2000 m below present sea level. Modified from (Micallef et al., 2019).

8.2.3 Hydrodynamic models for the fate of megaflooding sediment

The erosional channel that runs from the Gulf of Cádiz to the Algerian Basin (Fig. 8-2) implies the excavation of at least 1000 km^3 of Miocene sediment from the Alborán Basin and bedrock (Oligocene flysch) from the Strait of Gibraltar. The submarine threshold at today's Camarinal Sill is thought to have been incised by at least 200 m during the flood (Garcia-Castellanos et al., 2009). This number is key in constraining the peak velocity and discharge of the Zanclean flood (Fig. 8-6; Garcia-Castellanos et al., 2009; Periáñez et al., 2019). To show this, we calculate the feedback between the flow of water (calculated using Manning's equation) and the enlargement of the inlet by erosion (assumed proportional to basal shear stress). using the same algorithm as Garcia-Castellanos et al. (2009). We show two simulations of the Mediterranean refill using two values of sill rock erodability (Fig. 8-6). Although erodability ke is a still a poorly understood property of rocks and its quantification is limited by orders of magnitude of uncertainty (Garcia-Castellanos and O'Connor, 2018), the erodability value used for our reference model is constrained by the total incision of the flood, estimated at > 200 m in the present Camarinal Sill (Esteras et al., 2000), The results show that this depth of

erosion is reached only if ke >210^{-4} myr^{-1} $Pa^{-1.5}$, which in turn implies a peak water discharge close to 100 Sv (1 Sverdrup = 10^6 m^3 s^{-1}). Smaller values of erodability fail to reproduce the observed depth of the erosional trough across Camarinal and the Strait of Gibraltar.

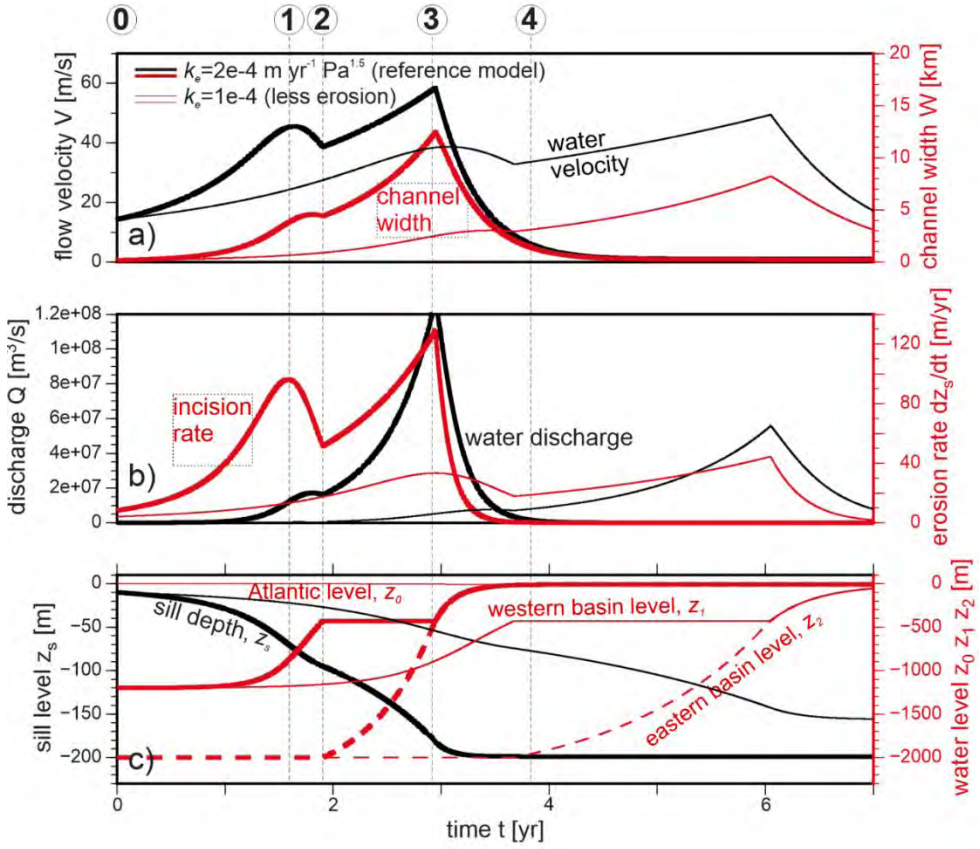

Figure 8-6. Modeling results of the evolution of the Zanclean flood based on the same methodology as in Garcia-Castellanos et al. (2009). These two simulations assume different rock erodability k_e for the Gibraltar Sill. The refill of the Mediterranean starts with a 10 m deep inflow river of oceanic water. The reference model (bold lines) erodes this sill down to -200 m below the global sea level, whereas imposing half the erodability (thin lines) leads to a sill eroded by only 155 m, less than observed in geophysical data. a) Water velocity and inflow channel width at the Strait of Gibraltar. b) Water discharge and incision rate. c) Inlet depth (black lines) and level of the Atlantic, the Western Mediterranean, and Eastern Mediterranean (red lines). The Sicily Sill is flooded after 1.9 yr in the reference model (3.6 yr in the less erodible model). Most of the water flow is concentrated within less than two years in the reference model, implying sea level rise rates of up to 10 m/day in the Mediterranean. Circled numbers and vertical dashed lines show the five stages defined in Fig. 8-1 (for the reference model only).

Nevertheless, the fate of these eroded materials has remained unknown, despite the fact that their present location might be an independent source of evidence to validate the megaflood hypothesis. A first attempt to predict the distribution of these

flood deposits has been recently performed (Periáñez et al., 2019) using a Lagrangian 2D hydrodynamic model to simulate the transport of material eroded from the Strait of Gibraltar. The transport of rock particles of variable size, either in suspension or as bed load is calculated using standard sediment transport equations. Water circulation during the flood has been estimated from a hydrodynamic model of the whole Mediterranean Sea (Abril and Periáñez, 2016) based on the assumption that the inlet was enlarged by the flow itself (Garcia-Castellanos et al., 2009). The hydrodynamic model solves the 2D depth-averaged fluid dynamic equations incorporating wetting/drying processes. The model finds the topographic lows in the exposed seafloor along which water flows (Periáñez and Abril, 2015). The numerical solution of the equations yield values for the water velocity over the model domain and modifies water depth preserving the volume of water. Sea-bed stresses over the domain due to the water current are calculated for the suspended sediment transport. The incision model used for calculating the enlargement of the Gibraltar inlet is based on an energy balance for the energy dissipated by the stream of water (when gravitational potential energy decreases) and the energy required for eroding the unit volume of substrate. This explains the erosion of the former Gibraltar isthmus and the Zanclean Channel (both the branch running through the Alborán Sea and the recessive incision channel extending to the Camarinal Sill in the Gulf of Cádiz). The approach uses as initial conditions the water level drop inferred from the Messinian shoreline reported by Urgeles et al. (2011), ca. 1200 m, and adopts the present-day bathymetry of the Mediterranean as a proxy for the Messinian hypsometry. Sediment transport is described in a Lagrangian framework both for suspended load and bed load. The transport model for suspended load includes the processes of advection (transport with the water current), diffusion (mixing due to water turbulence), and settling of particles. Settling velocity depends on the particle size. Particles are deposited once they reach the bottom if the bed stress is lower than a critical deposition stress. This critical stress depends on the particle size as well. A detailed description of the model and its parameters (particle sizes, settling velocities, critical stresses) may be seen in Periáñez et al. (2019). Bed load transport occurs when a critical velocity is exceeded that depends on the local water depth and sediment size following (Bilgili et al., 2003). Particles are assumed to travel at one-sixth of the depth averaged current (Periáñez et al., 2019).

We show the areas of preferential sediment deposition in the Mediterranean Sea depending on grain size (Fig. 8-7) for sediments eroded from the Strait of Gibraltar and precisely at the stage of peak discharge, when the sea level has risen to −170 m. Suspended load is deposited in areas sheltered from the jet of incoming water by the local topography, areas where water current abruptly decreases due to a sudden increase in water depth, and the central zone of eddies, where water current magnitudes also decrease, as well as in areas were the flow changes from more to less restricted. Thus, main deposits are predicted at both sides of the Strait of Gibraltar (i.e., both sides of the Zanclean channel), the Alborán Sea central area and its northern and southern shores during the peak discharge. Once a particle leaves the Alborán Sea, it follows two main routes, one along the African coast and the second south of the Balearic Islands and Sardinia. Particles, as they are transported with the water jet, fall according to their settling velocity and finally they are deposited on the seabed in areas of lower flow energy. The distance of these deposits to the Strait of Gibraltar increases as particle size decreases. As a consequence, very extensive deposits of mainly silt and fine sand are predicted between the Balearic Islands and Sardinia due to energy loss and deposition along a northern current jet (Fig. 8-7c to e). Only a small fraction of sediment, particularly the finer particles, reaches the eastern Mediterranean through the Sicily Sill. Long deposits may also be seen along the Algerian coast, tracing the route of the stronger southern jet (Fig. 8-7a).

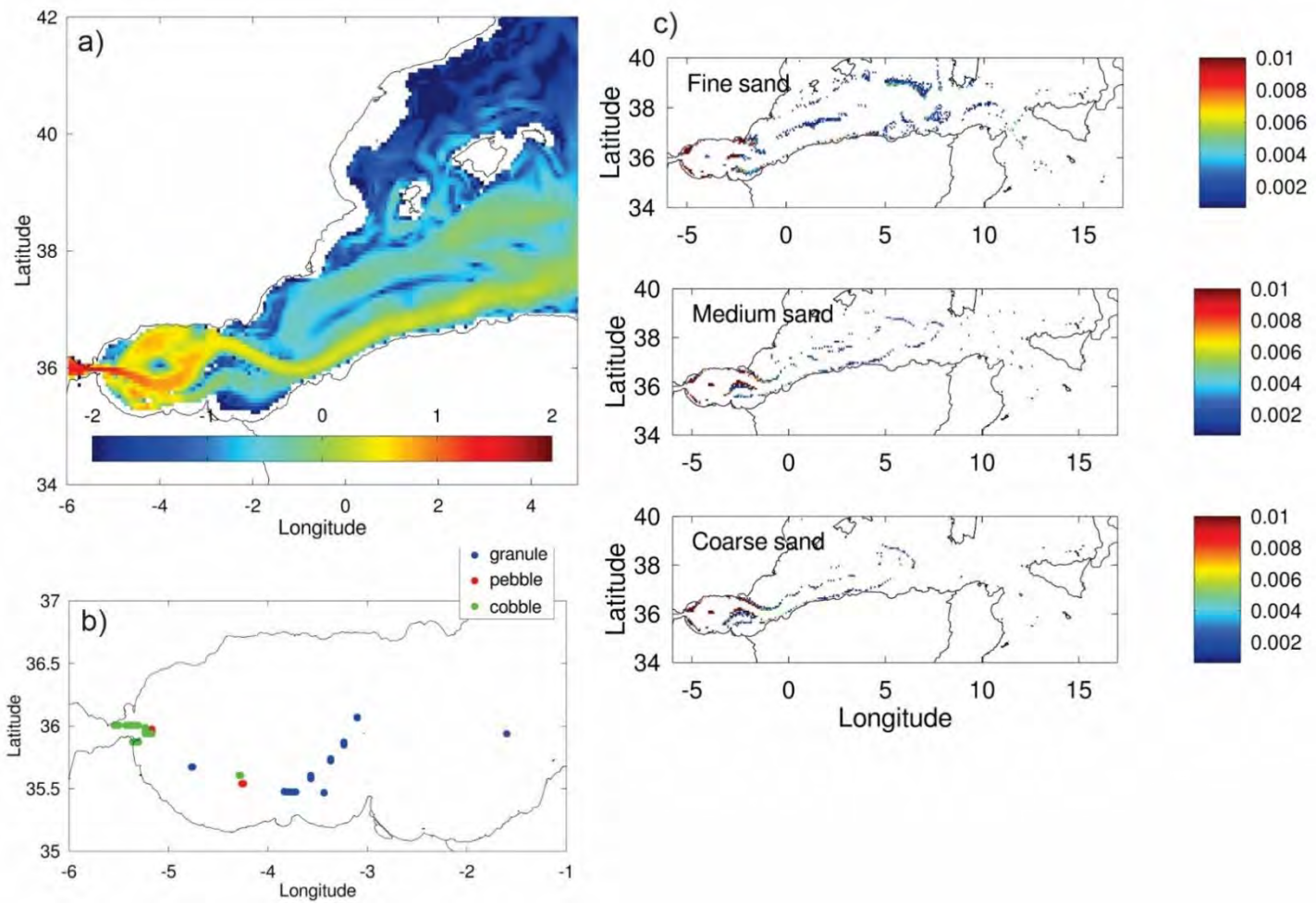

Figure 8-7. Sediment transport model results corresponding to the peak discharge of the flood. Top left: logarithm of the water velocity (m/s) in the western Mediterranean at the peak stage of flooding. Bottom left: predicted distribution of bed-load deposits fed to the flow at the Strait of Gibraltar. Right: density of suspension particles sedimented per unit area (normalized to the maximum value). A total of 20k particles are released for each grainsize of sand. Areas in white mean no grain is deposited in that location. Note the correlation between areas of deposition and areas of slow velocity. The results point to a strong concentration of most of the deposits in less than 1% of the area of the Western Mediterranean. Modified from Periáñez et al. (2019).

In contrast, sediment particles transported as bed load are deposited following the main streamlines. Deposits of very coarse sediment eroded from the Strait of Gibraltar and transported as bed load are more localized in space than sediment transported in suspension (Fig. 8-7b; Periáñez et al., 2019). In interpreting these model results, one must bear in mind that they are valid for the adopted bathymetry, which we take as the present one due to the absence of reconstructions of the Messinian paleo-bathymetry. Therefore, the relevance for the Zanclean flood is in the qualitative relationships between flow and deposition, rather than the exact location predicted for the deposits, particularly in areas of significant tectonic deformation such as the Tyrrhenian and the Alborán seas.

8.2.4 Identification of possible flood deposits in seismic reflection and borehole data

While the volume of eroded bedrock and sediment in Gibraltar and Alborán was estimated at 500 km^3 (Garcia-Castellanos et al., 2009), more recent data in Figs. 8-2 and 8-8 suggest this volume could be double that amount, since the erosional trough is now known to extend towards the east until the Algerian basin (Fig. 8-8). 1000 km^3 of sediment evenly distributed over the extent of the western Mediterranean evaporites ($4\ 10^5$ km^2) would imply a sediment layer of only 2 m, un-detectable in the available seismic stratigraphy. However, our model predictions suggest a strong localization of the flood deposits in areas of low energy (Fig. 8-7), and therefore larger size deposits are expected to be detectable in the seismic record and apparent in the core sedimentary record from drilling. Here we report new and recently published possible Zanclean flood deposits within the eastern Alborán Basin and off the Malta Escarpment based on seismic reflection profiles.

8.2.5 Possible megabar deposits in the Alborán Sea

Seismic reflection profiles show the presence of an elongated sedimentary body (Fig. 8-8C to D) associated to the erosion channel shown in Figs. 8-2 and 8-3. These deposits have contrasting seismic character with the underlying Miocene and overlying Pliocene deposits. Seismically they are characterized by chaotic, hyperbolic and discontinuous stratified facies. They form an elongated body up to 163 m thick, 35 km long and 7 km wide, located next to the main erosion channel and oriented parallel to its main trend (Fig. 8-8A). The Upper Miocene and Plio-Quaternary seismic stratigraphy of the Alborán Sea (Estrada et al., 2011; Juan et al., 2016), based on correlation with commercial, DSDP and ODP sites, indicate that this body is sandwiched between the MSC erosive surface (MES) and the Pliocene contourites deposited once the oceanic circulation was restored. The presence of these deposits occurs in the eastern Alborán basin, behind (in the lee side of) a pre-MSC volcanic edifice.

Their elongated plan-view shape, seismic facies, stratigraphic position and their orientation parallel to the flooding channel, are compatible with megabar flood deposits described for Pleistocene outburst flood scenarios such as the Altay floods (Carling et al., 2009; Herget, 2005). We propose that these deposits are related to the formation to the Zanclean erosion channel and represent possible megaflood deposits that were deposited because of the presence of a volcanic obstacle. This edifice may have acted as a topographic obstacle to the impinging flood flow, allowing the accumulation of sediments near the peak of the Zanclean flood, in the protected area at the lee side of the volcano. Similar sedimentary bars of larger grain size (boulder) have also been reported downstream the Snake River, spillway of the Bonneville flood in the Late Pleistocene (O'Connor, 1993), in areas where the flooding waters decreased in flow energy, for instance as a result of entering a less restricted topography.

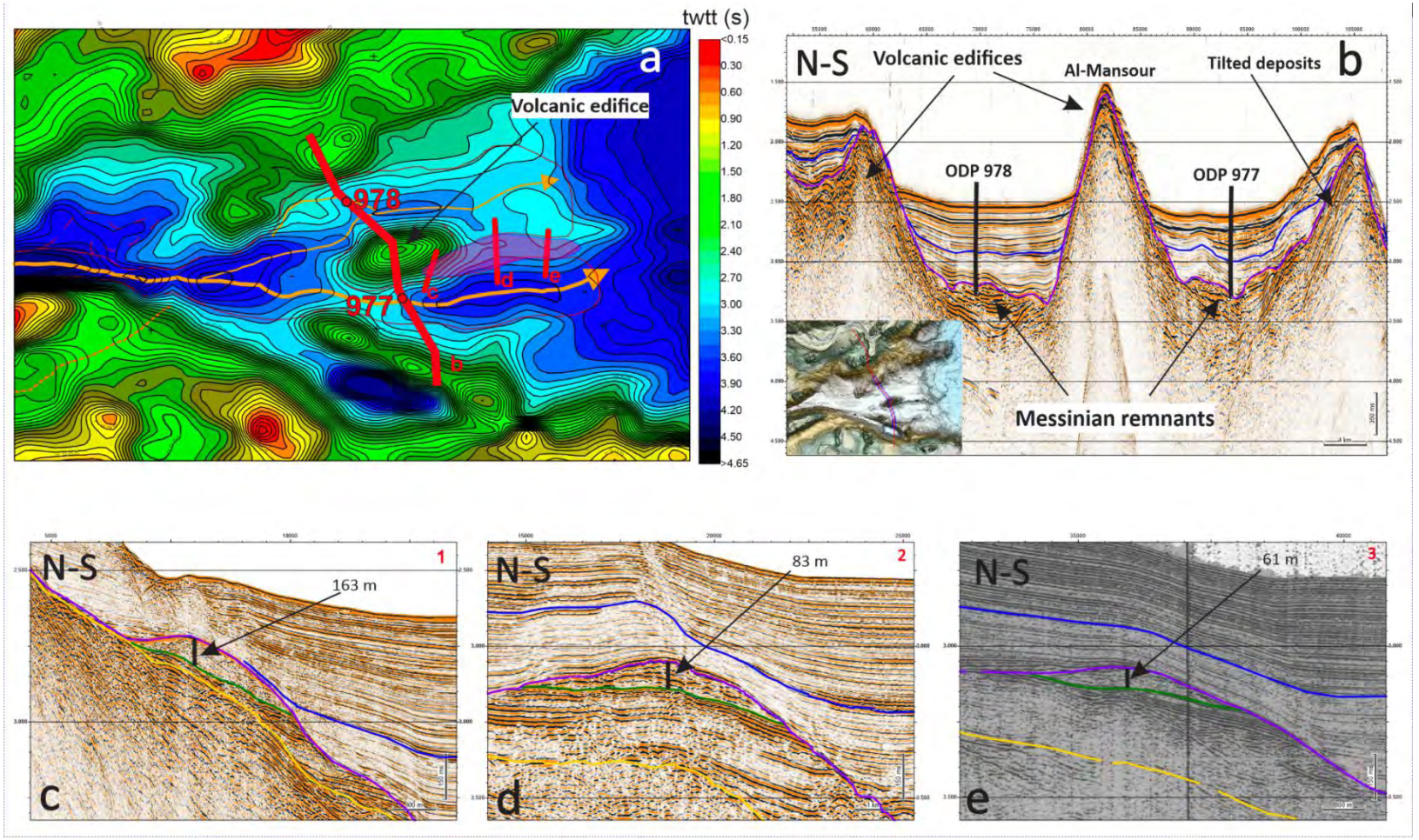

Figure 8-8. Seismic profiles showing possible megaflood deposits in the lee side of a volcanic edifice in the eastern Alborán Basin. a) Isobath map of base of the Pliocene (MES) and the main flood paths (orange lines). Location in Fig. 8-1. The shaded area maps the proposed flood megabar deposit. Contours every 150 milliseconds of double seismic travel time (TWTT), colour scale bar in seconds. b) Seismic cross-section Conrad 826 showing the two erosion channels separated by the volcanic building. Inset shows the location in a bathymetric map. c-d-e) Seismic profiles showing possible megaflood deposits in the lee side of a volcanic edifice in the eastern Alborán Basin. Legend: blue line represents base of Quaternary; The purple line marks the base of Pliocene (top Messinian); the green line is the base of hypothetical flooding deposits and the yellow line corresponds to Messinian salt deposition in the deep Algero-Balear Basin. Vertical scale in seconds (TWTT) and horizontal scale in meters.

Chaotic deposits have been reported as filling the bottom of the erosion channel in a seismic profile a few kilometers to the west of the section shown in Fig 8-7b (Periáñez et al., 2019), and interpreted as the deposition of flood-erosion products during the late stages of the flood. These are not visible in the Conrad 823 seismic line, perhaps due to the smaller thickness undetectable in the seismic record, in turn caused by a more constrained flow imposed by the seamounts in this area. However, it must be noted that ODP site 977 (Figs. 8-1 and 8-7) drilled the lowermost part of the southern and northern erosion channels, respectively, reaching partially cemented rounded gravels and sands that contained a mixed fauna of Miocene and Pliocene, interpreted as possibly related to the Zanclean reflooding (Comas et al., 1996). ODP site 978 also reported pebble-sized clasts in the equivalent stratigraphic position. Model results in Fig 8-7b predict that gravel-to-pebble-sized clasts can be dragged for a few hundreds of km at peak discharge, thus suggesting that the pebbles recovered from the drilling cores could come from the numerous volcanic sea mounts located further to the west, in the centre of the Alborán Basin.

8.2.6 Possible megaflood deposits in the Ionian Sea

Multi-channel seismic reflection data in the western Ionian Basin exhibit an acoustically chaotic to transparent body of up to 860 m in thickness and 1430–1620 km^3 in volume, covering an area of 11,000 km^2 buried at depth between 3.4 and 4.8 km below sea level (Fig. 8-9) (Micallef et al., 2018). Towards the west, this body terminates abruptly against the Malta Escarpment. Although this unit has not been drilled, its stratigraphic position is placed with confidence between the Messinian Upper Unit (UU) and the overlying 200–400 m thick Plio-Pleistocene sediment layer characterized by well-laminated, continuous reflectors. Therefore, its age is at or near the Miocene/Pliocene boundary (5.33 Ma).

The scale of this feature cannot be readily explained by collapse of the eastern margin of the Malta Escarpment. A large submarine mass movement has been discarded as a possible explanation for the origin of Unit 2 due to the lack of nearby scars of sufficient volume and the hard (limestone) lithology of the escarpment (Micallef et al.,

2018). A formation by folded Messinian upper gypsum is also discarded based on the seismic velocities measured (2.3–2.6 km/ s), which are significantly lower than the 3.1 km/ s associated with gypsum deposits. Finally, the lack of local sources of sediment (the canyons along the Malta Escarpment combined add up to only 1100 km^3 in volume), suggests that this unit may be a megaflood deposit. The seismic texture and the isopachs of the body indicate that this sedimentary unit represents highenergy deposits sourced in the W, beyond the Malta Escarpment. Its location next to the Noto amphitheater-shaped canyon (SE Sicily margin; Fig. 8-9) suggests a NW provenance of the flow, likely through the Pelagian Platform. Thus, the interpretation by Micallef et al. (2018) is that the chaotic body records deposition from a megaflood flow as the water refill of the western Mediterranean overtopped the Sicily Sill. These overtopping waters would plunge into the partially desiccated eastern Mediterranean basin, possibly at a level of −1750 to −1900 m as suggested by the wave erosion marks preserved in the escarpment, the base of the Noto Canyon, and the base of the flood deposits (Figs. 8-4, 8-5 and 8-9).

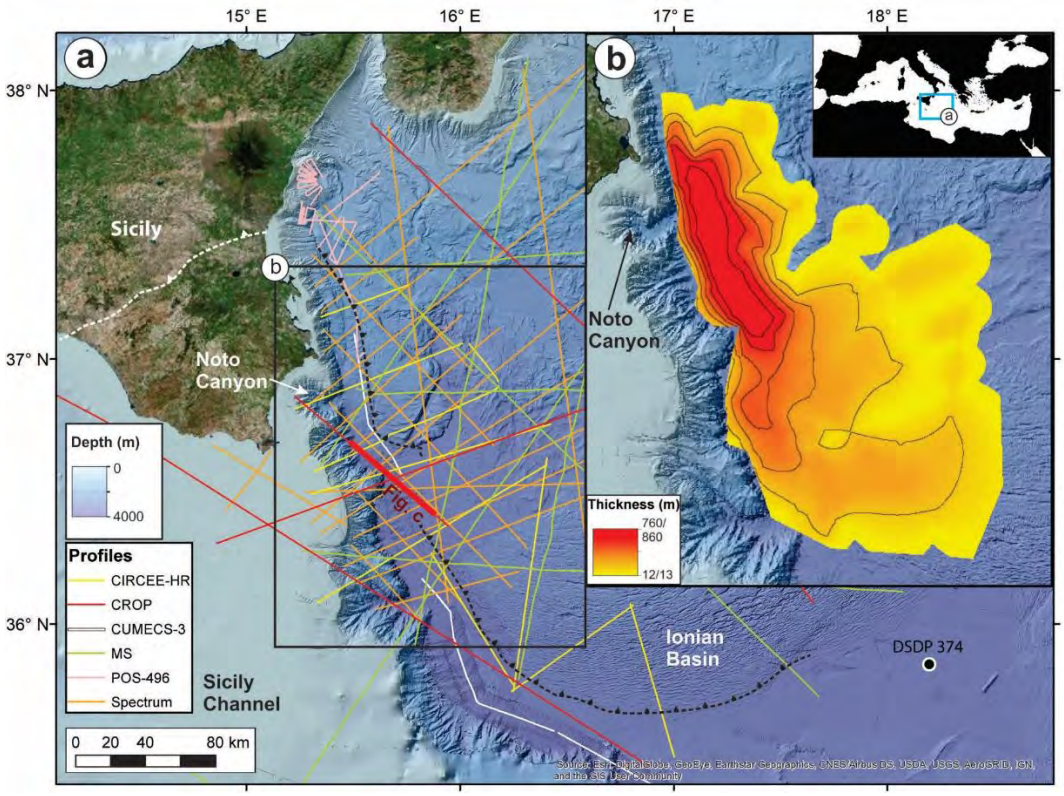

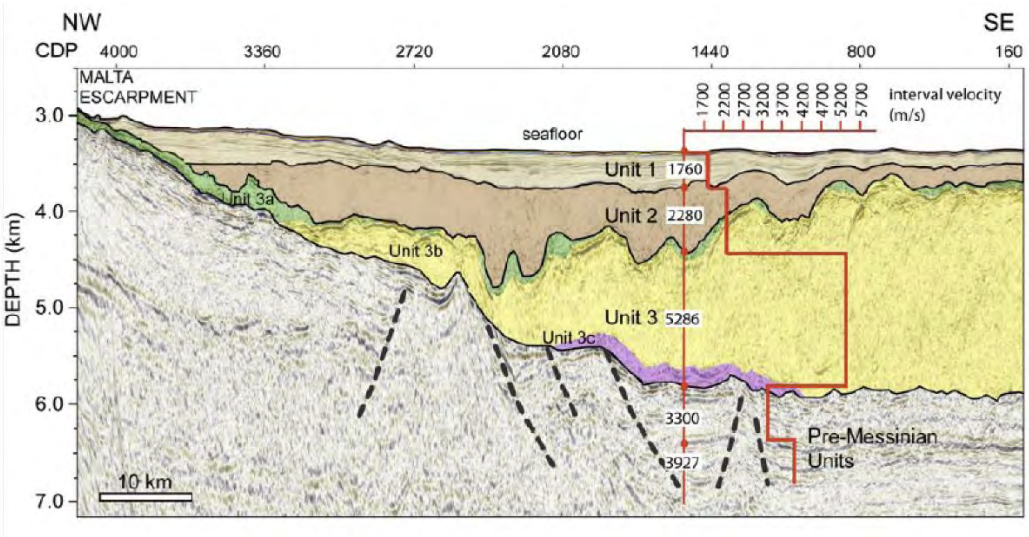

Figure 8-9. a) and b) lateral extension of the transparent unit interpreted as megaflood deposits off the Malta escarpment, next to the Noto canyon. c) Seismic stratigraphy of western Ionian Basin. Interpreted units on reflection profile CROP 21 (pre-stack depth-migrated). The red plot shows the estimated PSDM seismic velocity profile. Correlation with DSDP drilling site 374 indicates that Unit 1 corresponds to Pliocene-Quaternary pelagics, contourites and turbidites; Unit 3 correlates with MSC evaporites including a highly reflective and mostly deformed upper unit made of gypsum and marls (3a, green), and a typically reflector-less unit with a basin-fill geometry made of halite and also known as *mobile* unit (3b, yellow); a lower, highly reflective, discontinuous unit (3c, purple) has never been drilled yet but is attributed to lower gypsum or clastics. Modified from (Micallef et al., 2018).

8.3 Discussion

8.3.1 Significance for the Messinian salinity crisis

The Zanclean flood hypothesis is closely entangled to the controversy about the desiccation of the Mediterranean Sea during the Messinian salinity crisis. The occurrence and extent of this desiccation by the end of the Neogene is far from a consensus among the scientific community (e.g., Roveri et al., 2014a). The main evidence questioning a kilometric-scale drawdown right before the Pliocene is the ubiquitous presence of Lago-Mare facies (fresh to brackish water fauna that also include marine fish; Carnevale et al., 2017) during the last stage of the MSC, at elevations close to normal sea level (Orszag-Sperber, 2006). The Lago-Mare is characterized by mollusks, ostracods and/or dinoflagellate cysts of Paratethyan-type (originating from the Black Sea region) indicating a brackish sedimentary environment before the return to normal

open-marine environment across the Miocene-Pliocene boundary. The widespread presence of these sediments from southern Spain to the Levant Basin suggests that, right before the Pliocene, the Mediterranean was a single connected body of water with its level above the Sicily Sill (today at −430 m) and that its salinity was lower than the open ocean. To explain the abrupt end of the MSC without a significant drawdown that can trigger a flood, Marzocchi et al. (2016) proposed a Mediterranean-wide hydrological pump model driven by the strong salinity contrast between the Mediterranean, the Atlantic, and the Paratethys. This can explain the co-existence of dense Atlantic water influx from Gibraltar and lighter brackish water influx from the Paratethys during the Lago-Mare stage prior to the end of the MSC, all under normal sea-level conditions. Supporting this view, the ages of the Neogene marine seaways onshore the Alborán Sea suggest that the Gibraltar Strait (Krijgsman et al., 2018) may have never been fully closed (Manzi et al., 2005), questioning the idea of a completely isolated Mediterranean Sea during the MSC. In order to keep a kilometric drawdown for a period longer than a few thousands of years, a full disconnection of the marine gateways is required (Garcia-Castellanos and Villaseñor, 2011), because otherwise the inflow of water would trigger a fast erosion and reestablish the level of the Mediterranean Sea. Finally, models excluding a significant sea level drawdown explain the erosion features of the Mediterranean margins as the result of hyperpycnal density currents related to storage of high-density water due to evaporation during the MSC (Roveri et al., 2014b). A possible explanation for the intriguing Lago-Mare facies is that it post-dates the flooding. Based on outcrops near Málaga (southern Spain), Do Couto et al. (2014) suggest that the Lago-Mare sediments were deposited after the Atlantic flooding, which would then have taken place at 5.46 Ma instead of the Messinian/Zanclean boundary (5.33 Ma).

To add to these conflicting observations, recent industrial seismicreflection data-sets in the deep Ionian Sea (Sirt Basin, Libya) and in the deep Levant Basin (offshore Syria) show the existence of large fluvial sedimentary systems formed after the halite precipitation (Bowman, 2012; Madof et al., 2019). In the Levant, these fluvial systems are longer than 100 km and interpreted as fluvio-deltaic lobes resting directly atop the Messinian halite and seem coeval with the erosion of deformed salt layers (Bowman, 2012; Kartveit et al., 2019; Madof et al., 2019). These are interpreted as the result of

vast paleo-river basins draining areas of Africa and the Middle East region during the lowering of the Mediterranean Sea level. In contrast, seismic stratigraphy in the same area suggests that salt promontories formed by salt flow in the sea floor were truncated by dissolution under a deep, stratified water column, conflicting with the possibility of a seafloor exposure (Gvirtzman et al., 2017). In the absence of drill holes and age determinations, the presumed fluvial lobes are ambiguously correlated to the Lago-Mare phase, but could they alternatively predate it and predate the megaflood? The seismic stratigraphic record to date fails to answer this question so far and points to the need for scientific drilling.

The evidence shown in this chapter supports an abrupt, catastrophic refill of the Mediterranean in the form of an outburst flood caused by the overtopping of the Atlantic through a Neogene isthmus in Gibraltar (Garcia-Castellanos et al., 2009). The same mechanism has been described for tens of Pleistocene overtopping lakes that triggered outburst floods (Garcia-Castellanos and O'Connor, 2018). Such scenario requires a significantly low level in the Mediterranean Sea (hundreds of meters at least) prior to flooding, to be consistent with the erosion and flood deposits reported in the Alborán area and the Malta Escarpment. But it does not require a complete desiccation of neither of the Mediterranean sub basins.

8.3.2 Comparison to other megafloods

The Missoula floods in the Scablands region (Washington, USA) are the first studied and best-known outburst floods that have. Based on information as diverse as the elevation of ice-rafted boulders, megaripple marks, the size of mobilized blocks and 0D step-backwater and 3D hydrodynamic modeling, several tens of events of up to around 10^7 m^3 s^{-1} in discharge (O'Connor and Baker, 1992; Benito and O'Connor, 2003; Alho et al., 2010; Larsen and Lamb, 2016) have been described in this region dating between 18.5 and 15 thousand years ago (late Pleistocene).

Erosional and deposition features, including km-scale regressive erosion cliffs as the Dry Falls or the Potholes Coulee are attributed to a series of outburst events involving a water flow deeper than 100 m at speeds up to 15 m/ s. Such horseshoe-or

amphitheatershaped cliffs, frequent smoking guns for megaflooding, are similar to the Noto Canyon in the Malta Escarpment (Fig. 8-4). Such features are found widespread across the state of Washington and attributed to the Missoula floods. The Pothole coulee is ca. 2 km wide and therefore narrower than the Noto Canyon (6 km), a priori consistent with the 10 times higher peak discharge derived for the Zanclean flood (Garcia-Castellanos et al., 2009; Abril and Periáñez, 2016).

Similar amphitheater-headed valleys have been linked to megaflooding events in Idaho (Lamb et al., 2008). Because of the current impossibility to date the formation of the Noto Canyon, the only indication linking its origin to the Zanclean flood is its morphology, its location next to the possible megaflood deposits in Fig. 8-9, and the absence of other explanations for its formation (Micallef et al., 2018).

The Altay flood along the Katun River (Altay Republic, Russia) is another case scenario where discharge rates comparable to the Missoula Floods (~10 Sv) have been estimated. Here, outburst-flood sedimentary features along mountain valleys are well exposed due to tributaries of the main flooding channel that were backflooded during the events. An abundant depositional feature is megabars, equivalent to fluvial bars but two orders of magnitude larger and thought to form near the time of peak discharge of outburst floods. The concept in Fig. 8-10 is based on a gravel megabar exposure cut by a tributary river after the flooding. It shows three cycles of flood deposition separated by slack water deposits, interpreted as an indication for repeated flooding.

Accretion results from intense fallout of suspended gravels and is then rearranged by unsteady traction transport during upper stage surges. As the flood discharge wanes, cross-beds may form due ripple and dune migration during the lower stage (Carling et al., 2009). In the analogue case of the Zanclean flood, one single flooding event is envisaged. If, as proposed, the sedimentary feature shown in Fig. 8-8 corresponds to an equivalent megabar formed during the transition from high to low energy flow in the Alborán Sea, then an upward-fining sequence of mostly suspended sediment would be expected within that unit. However, the potential megabar shown in Fig. 8-8 has not been drilled so far, and the existing seismic surveys do not have enough resolution to detect grain-size changes or features like those in Fig. 8-10. Therefore, while we are unable to further check the consistency between the unit

identified in Alborán Sea and the megabars in the Altay, the morphological distribution of the sediments (elongated, parallel and next to the main channel) make it an important candidate site for future drilling to find supporting lithological evidence for the Zanclean flood deposits.

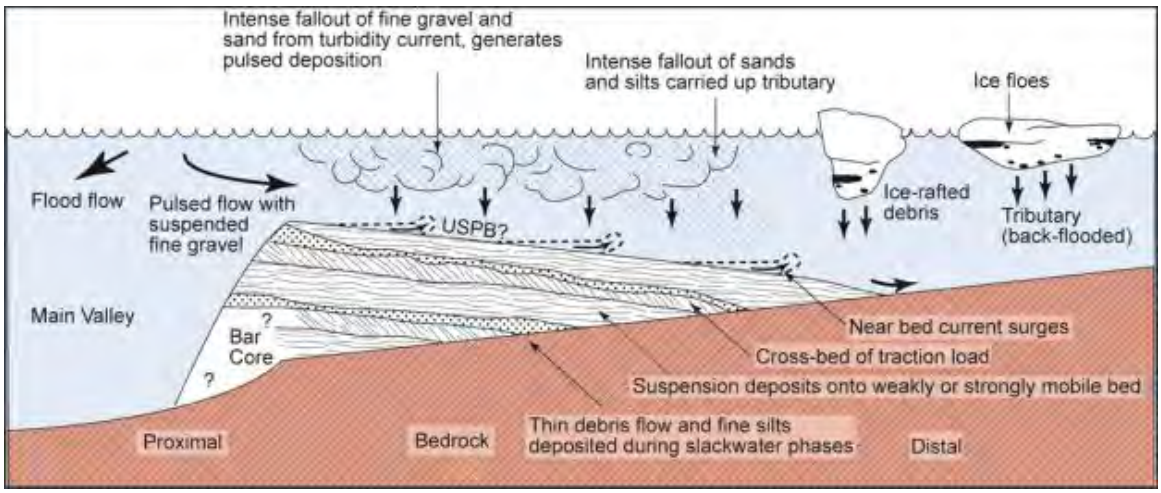

Figure 8-10. Sedimentological studies in Pleistocene continental megafloods provide a model for future assessment of the megaflood origin of the buried deposits of the Zanclean megaflood (Fig. 8-9). One frequent feature observed along the spillway of outburst floods consists of lateral megabars off- and parallel to the main flooding channel. This sedimentary facies model summarizes the depositional surfaces across a megabar along the Katun River in the Altay Mnts, were an ice-dam lake burst during the Pleistocene reached a discharge of ca. one million m3/s, with layers tilting towards the mountain side of the valley. Flood flow is directed towards the reader. The section has been exposed by incision along a tributary valley that had been backflooded during the events. Three cycles of flood deposition are visible separated by slack water silt deposits (black). For each cycle, fine gravel is deposited onto the flooded, rapidly-accreting bar surface, largely from intense fallout from suspension and is then rearranged by unsteady (surges) traction transport during upper stage flow. As flood flow wanes, cross-beds form due to bedload sheet and minor ripple and dune migration across predominantly at lower stage. A detailed correlation between these deposits and those in Fig. 8-9 will require scientific drilling. Modified from Carling et al. (2009).

8.3.3 Future search for further evidence

A fundamental peculiarity of the Zanclean flood setting relative to Pleistocene outburst floods is that, whereas its water source (the global ocean) is virtually infinite in volume, the sink (the desiccated Mediterranean Sea) is not. During the flood, the western shoreline of the western Mediterranean should raise and shift towards the Strait of Gibraltar, possibly hindering the spatial concentration of deposits.

Nevertheless, because of the large size of the Mediterranean basin, the ever-increasing flooding discharge becomes significant to the water budget only when the flood discharge becomes comparable to hydrological deficit (presently 75,000 $m^3 s^{-1}$). Therefore, future geophysical exploration of the western margin of the Algerian basin should address the presence of buried Zanclean flood deposits postulated by the hydrodynamic models.

The numerical modeling results in Fig. 8-7 provide an explanation for the 15 cm M/P transition found in ODP site 974 in the Tyrrhenian Sea (Fig. 8-1 for location) (Iaccarino and Bossio, 1999; Pierre et al., 2006) and the 2–3 cm of > 0.3 mm of terrigenous clasts (medium sand) recovered just above the M/P boundary in site 975 at the South Balearic Basin (Iaccarino and Bossio, 1999; Zahn et al., 1999) consisting of "foraminifera and calcareous nannofossils that are reworked from the early marine Messinian, while the ostracod fauna reflects the original paleoenvironment". The inflow of Atlantic waters at unprecedented discharge rates close to $10^8 m^3 s^{-1}$ (100 Sv) are proven capable of transporting medium sand and foraminifera at such distances (Fig. 8-7). In using these models for searching flood erosional and depositional features in the Alborán sea, one must consider the uncertainty induced by the use of today's bathymetry as a proxy for the paleogeography of the region. During the Messinian, most of the Tyrrhenian Sea, for instance, was still not formed by the retreat of the Calabrian Arc. In the Alborán Sea, the paleo bathymetry at the time of flooding may have been significantly different from today, since the lithosphere was younger, thinner, hotter and therefore more buoyant (Booth-Rea et al., 2018), and the compressional tectonics of the ongoing convergence between Africa and Eurasia has raised most of the Alborán Ridge during the Plioquaternary. Since the Messinian, Africa has approached Eurasia by 20 to 100 km (in the west and the east of the Mediterranean Sea, respectively), and the bathymetry has been modified by a layer of Plio-Quaternary deposits of, typically, a few hundreds of meters. The lack of good reconstructions of the bathymetric and geographic changes of the Mediterranean Sea at the time of the flooding limits a more detailed prediction of the locations ideal for future megaflood deposits exploration.

The present review shows recent independent assessments of the Zanclean megaflood hypothesis, and highlights the need for further future research in order to

test it. Seismic studies may validate it if clinoform deposits and found in the westernmost Algerian basin and dated to the end of the MSC, for example. But a more direct test may arrive from drilling the sedimentary deposits described in the Alborán basin and in the Ionian Sea. In this regard, the outcome of three drilling proposals (DEMISE, DREAM, and IMMAGE) that are currently undergoing a second round of review by IODP, will be crucial. If approved and drilled, they have the potential to decipher many of the aforementioned open scientific questions regarding the end of the Messinian salinity crisis.

8.4 Conclusions

We have summarized a set of observations that provide additional evidence to the previously identified erosional channel at the Strait of Gibraltar, supporting a megaflood of the Mediterranean basin near the limit between the Miocene and the Pliocene. Based on them, we can draw the following conclusions:

1. If the > 200 m erosion at the Strait of Gibraltar was caused by the refilling of the Mediterranean Sea, numerical modeling shows that this erosion implies a flood of an unprecedented discharge, possibly above 100 Sv ($10^8\ m^3\ s^{-1}$).

2. The amphitheater-headed Noto Canyon, off SE Sicily, is compatible with an overspill the Zanclean flood from the western to the eastern Mediterranean across the Sicily sill. The morphology of the canyon and the Malta Escarpment slope suggest a Mediterranean Sea level at the time of the flood −1750 to −1900 m lower than today.

3. A 1600 km^3 sedimentary body to the east of the Noto Canyon, laying atop the Messinian salt layer and below the Plio-Quaternary muds is compatible with a megaflood deposit delivered to the eastern basin and bringuing to an end the drawdown phase.

4. A 163 m thick, elongated sediment body of 35 × 7 km, oriented parallel to the main flood channel in the Alborán Sea and located in the lee side of a seamount, is compatible with megabars formed along the largest documented continental outburst floods.

8.5 Acknowledgements

Funding has been provided by the COST Action Medsalt CA15103, by the ETN SaltGiant (European Union funded, Horizon2020, Marie Skłodowska-Curie grant agreement No 765256 and 674899) and by the Spanish public projects MITE (CGL2014-59516) FAUCES (CMT201565461-C2-R, MINECO/FEDER) and DAMAGE (AEI/FEDER CGL201680687-R).

8.6 References

Abril, J.M., Periáñez, R., 2016. Revisiting the time scale and size of the Zanclean flood of the Mediterranean (5.33Ma) from CFD simulations. Mar. Geol. 382, 242–256. https://doi.org/10.1016/j.margeo.2016.10.008.

Alho, P., Baker, V.R., Smith, L.N., 2010. Paleohydraulic reconstruction of the largest Glacial Lake Missoula draining(s). Quat. Sci. Rev. 29, 3067–3078. https://doi.org/10.1016/j.quascirev.2010.07.015.

Bache, F., Olivet, J.L., Gorini, C., Rabineau, M., Baztan, J., Aslanian, D., Suc, J.P., 2009. Messinian erosional and salinity crises: view from the Provence Basin (Gulf of Lions, Western Mediterranean). Earth Planet. Sci. Lett. 286, 139–157.

Bache, F., Gargani, J., Suc, J.-P., Gorini, C., Rabineau, M., Popescu, S.-M., Leroux, E., Couto, D.D., Jouannic, G., Rubino, J.-L., Olivet, J.-L., Clauzon, G., Dos Reis, A.T., Aslanian, D., 2015. Messinian evaporite deposition during sea level rise in the Gulf of Lions (Western Mediterranean). Mar. Pet. Geol. 66, 262–277. https://doi.org/10.1016/j.marpetgeo.2014.12.013.

Benito, G., O'Connor, J.E., 2003. Number and size of last-glacial Missoula floods in the Columbia River valley between the Pasco Basin, Washington, and Portland. Oregon. Geol. Soc. Am. Bull. 115, 624–638. https://doi.org/10.1130/0016-7606(2003)115<0624:NASOLM>2.0.CO;2.

Bilgili, A., Swift, M.R., Lynch, D.R., Ip, J.T.C., 2003. Modeling bed-load transport of coarse sediments in the Great Bay Estuary, New Hampshire. Estuar. Coast. Shelf Sci. 58, 937–950. https://doi.org/10.1016/j.ecss.2003.07.007.

Blanc, P., 2000. Of sills and straits: a quantitative assessment of the messinian salinity crisis. Deep Sea Res. Part Oceanogr. Res. Pap. 47, 1429–1460. https://doi.org/10.1016/S0967-0637(99)00113-2.

Blanc, P.L., 2002. The opening of the Plio-Quaternary Gibraltar Strait: assessing the size of a cataclysm. Geodin. Acta 15, 303–317.

Blanc, P.L., 2006. Improved modelling of the Messinian Salinity Crisis and conceptual implications. Palaeogeogr. Palaeoclimatol. Palaeoecol. 238, 349–372.

Booth-Rea, G., Ranero, R., Grevemeyer, I.C., 2018. The Alborán volcanic-arc modulated the Messinian faunal exchange and salinity crisis. Sci. Rep. 8. https://doi.org/10.1038/s41598-018-31307-7.

Bowman, S.A., 2012. A comprehensive review of the MSC facies and their origins in the offshore Sirt Basin, Libya. Pet. Geosci. 18, 457–469. https://doi.org/10.1144/petgeo2011-070.

Breda, A., Mellere, D., Massari, F., Asioli, A., 2009. Vertically stacked Gilbert-type deltas of Ventimiglia (NW Italy): the Pliocene record of an overfilled Messinian incised valley. Sediment. Geol. 219, 58–76. https://doi.org/10.1016/j.sedgeo.2009.04.010.

Bretz, J.H., 1925. The Spokane fl ood beyond the channeled scablands. J. Geol. 33, 97–125.

Campillo, A.C., Maldonado, A., Mauffret, A., 1992. Stratigraphic and Tectonic evolution of the Western Alborán Sea late Miocene to recent. Geo-Mar. Lett. 12, 165–172.

Carling, P.A., Martini, I.P., Herget, J., Borodavko, P., Parnachov, S., 2009. Megaflood sedimentary valley fill: Altai Mountains. In: Siberia, in: Megaflooding on Earth and Mars. Cambridge University Press, Cambridge, pp. 243–264. https://doi.org/10.1017/CBO9780511635632.013.

Carnevale, G., Landini, W., Sarti, G., 2006. Mare versus Lago-mare: marine fishes and the Mediterranean environment at the end of the messinian salinity crisis. J. Geol. Soc. 163, 75–80. https://doi.org/10.1144/0016-764904-158.

Carnevale, G., Pierre, F.D., Natalicchio, M., Landini, W., 2017. Fossil Marine Fishes and the? Lago Mare? Event: has the Mediterranean ever Transformed into a Brackish lake? [WWW Document]. https://doi.org/10.1127/nos/2016/0343.

Clauzon, G., 1978. The Messinian Var canyon (Provence, southern France) - Paleogeographic implications. Mar. Geol. 27, 231–246.

Clauzon, G., 1982. Le canyon messinien du RhÃ’ne: une preuve dÃ©cisive du “desiccated deep-basin model” (HsÃ¼, Cita et Ryan, 1973). Bull Soc GÃ©ol Fr 24, 597–610.

Comas, M.C., Zahn, R., Klaus, A., 1996. Comas et al., 1996 ODP 977 Alborán ir161_07.pdf. Proceedings of the Ocean Drilling Program. Initial Reports.

Do Couto, D., Popescu, S.-M., Suc, J.-P., Melinte-Dobrinescu, M.C., Barhoun, N., Gorini, C., Jolivet, L., Poort, J., Jouannic, G., Auxietre, J.-L., 2014. Lago Mare and the Messinian Salinity Crisis: evidence from the Alborán Sea (S. Spain). Mar. Pet. Geol. 52, 57–76. https://doi.org/10.1016/j.marpetgeo.2014.01.018.

Duggen, S., Hoernie, K., Van den Bogaard, P., Rapke, L., Morgan, J.P., 2003. Deep roots of the Messinian salinity crisis. Nature 422, 602–606.

Escutia, C., Maldonado, A., 1992. Paleogeographic implications of the Messinian surface in the Valencia Trough Northwestern Mediterranean Sea. In: Banda, E., Santanach, P. (Eds.), Geology and Geophysics of the Valencia Trough. 203. Tectonophysics, Western Mediterranean, pp. 263–284.

Esteras, M., Izquierdo, J., Sandoval, N.G., Bahmad, A., 2000. Evolución morfológica y estratigráfica plio-cuaternaria del umbral de Camarinal (estrecho de Gibraltar) basada en sondeos marinos. Rev. Soc. GeolÃ3gica EspaÃ ± a 13, 539–550.

Estrada, F., Ercilla, G., Gorini, C., Alonso, B., VÃ¡zquez, J.T., GarcÃ-a-Castellanos, D., Juan, C., Maldonado, A., Ammar, A., Elabbassi, M., 2011. Impact of pulsed Atlantic water inflow into the Alborán Basin at the time of the Zanclean flooding. Geo-Mar. Lett. 31, 361–376. https://doi.org/10.1007/s00367-011-0249-8.

Estrada, F., Galindo-Zaldívar, J., Vázquez, J.T., Ercilla, G., D'Acremont, E., Alonso, B., Gorini, C., 2018. Tectonic indentation in the central Alborán Sea (westernmost Mediterranean). Terra Nova 30 (1), 24–33. https://doi.org/10.1111/ter.12304.

Garcia-Castellanos, D., O'Connor, J.E., 2018. Outburst floods provide erodability estimates consistent with long-term landscape evolution. Sci. Rep. 8. https://doi.org/10.1038/s41598-018-28981-y.

Garcia-Castellanos, D., Villaseñor, A., 2011. Messinian salinity crisis regulated by competing tectonics and erosion at the Gibraltar arc. Nature 480, 359–363.

García-Castellanos, D., Estrada, F., JimÃ©nez-Munt, I., Gorini, C., Fernández, M., VergÃ©s, J., De Vicente, R., 2009. Catastrophic flood of the Mediterranean after the Messinian salinity crisis. Nature 462, 10. December 2009. https://doi.org/10.1038/nature08555.

García-Veigas, J., Cendón, D.I., Gibert, L., Lowenstein, T.K., Artiaga, D., 2018. Geochemical indicators in Western Mediterranean Messinian evaporites: implications for the salinity crisis. Mar. Geol. 403, 197–214. https://doi.org/10.1016/j.margeo.2018.06.005.

Gvirtzman, Z., Manzi, V., Calvo, R., Gavrieli, I., Gennari, R., Lugli, S., Reghizzi, M., Roveri, M., 2017. Intra-Messinian truncation surface in the Levant Basin explained by subaqueous dissolution. Geology 45, 915–918. https://doi.org/10.1130/G39113.1.

Haq, B., Gorini, C., Baur, J., Moneron, J., Rubino, J.-L., 2020. Deep Mediterranean's Messinian evaporite giant: how much salt? Glob. Planet. Change 184, 103052. https://doi.org/10.1016/j.gloplacha.2019.103052.

Hardie, L.A., Lowenstein, T.K., 2004. Did the Mediterranean Sea Dry out during the Miocene? A reassessment of the evaporite evidence from DSDP Legs 13 and 42A Cores. J. Sediment. Res. 74, 453–461. https://doi.org/10.1306/112003740453.

Herget, J., 2005. Reconstruction of Pleistocene ice-dammed lake outburst floods in the Altai Mountains, Siberia, special papers. In: Geological Society of America, Boulder, Colo.

Hsü, K.J., Cita, M.B., Ryan, W.B.F., 1973a. The origin of the Mediterranean evaporites. Initial Rep. Deep Sea Drill. Proj. 13, 1203–1231.

Hsü, K.J., Ryan, W.B.F., Cita, M.B., 1973b. Late Miocene Desiccation of the Mediterranean. Nature 242, 240–244. https://doi.org/10.1038/242240a0.

Iaccarino, S.M., Bossio, A., 1999. Paleoenvironment of uppermost Messinian sequences in the Western Mediterranean (site 974, 975, and 978). Proc. Ocean Drill. Program Sci. Results 161, 529–541.

Jiménez-Munt, I., Torne, M., Fernàndez, J., Vergés, J., Kumar, A., Carballo, D., García-Castellanos, D., 2019. Deep seated density anomalies across the Iberia-Africa plate boundary and its topographic response. J. Geol. Res. https://doi.org/10.1029/2019JB018445.

Juan, C., Ercilla, G., Javier Hernández-Molina, F., Estrada, F., Alonso, B., Casas, D., García, M., Farran, M., Llave, E., Palomino, D., Vázquez, J.-T., Medialdea, T., Gorini, C., D'Acremont, E., El Moumni, B., Ammar, A., 2016. Seismic evidence of currentcontrolled sedimentation in the Alborán Sea during the Pliocene and Quaternary: palaeoceanographic implications. Mar. Geol. 378, 292–311. https://doi.org/10.1016/j.margeo.2016.01.006.

Kartveit, K.H., Ulsund, H.B., Johansen, S.E., 2019. Evidence of sea level drawdown at the end of the Messinian salinity crisis and seismic investigation of the Nahr menashe unit in the northern levant basin, offshore Lebanon. Basin Res. 0. https://doi.org/10.1111/bre.12347.

Krijgsman, W., Stoica, M., Vasiliev, I., Popov, V.V., 2010. Rise and fall of the Paratethys Sea during the Messinian Salinity Crisis. Earth Planet. Sci. Lett. 290, 183–191.

Krijgsman, W., Capella, W., Simon, D., Hilgen, F.J., Kouwenhoven, T.J., Meijer, P.Th., Sierro, F.J., Tulbure, M.A., van den Berg, B.C.J., van der Schee, M., Flecker, R., 2018. The Gibraltar Corridor: watergate of the Messinian Salinity Crisis. Mar. Geol. 403, 238–246. https://doi.org/10.1016/j.margeo.2018.06.008.

Lamb, M.P., Dietrich, W.E., Aciego, S.M., DePaolo, D.J., Manga, M., 2008. Formation of Box Canyon, Idaho, by megaflood: implications for seepage erosion on earth and mars. Science 320, 1067–1070.

Larsen, I.J., Lamb, M.P., 2016. Progressive incision of the channeled scablands by outburst floods. Nature 538, 229–232. https://doi.org/10.1038/nature19817.

Lofi, J., 2010. Atlas of the Messinian Salinity Crisis MSC.

Lofi, J., 2018. The Messinian Salinity Crisis MSC Markers in the Mediterranean Sea - Volume 2. Commission for the World Geological Map.

Lugli, S., Manzi, V., Roveri, M., Schreiber, B.C., 2015. The deep record of the Messinian salinity crisis: evidence of a non-desiccated Mediterranean Sea. Palaeogeogr. Palaeoclimatol. Palaeoecol. 433, 201–218. https://doi.org/10.1016/j.palaeo.2015.05.017.

Madof, A.S., Bertoni, C., Lofi, J., 2019. Discovery of vast fluvial deposits provides evidence for drawdown during the late Miocene Messinian salinity crisis. Geology 47, 171–174. https://doi.org/10.1130/G45873.1.

Manzi, V., Lugli, S., Lucchi, F.R., Roveri, M., 2005. Deep-water clastic evaporites deposition in the Messinian Adriatic foredeep (northern Apennines, Italy): did the

Mediterranean ever dry out? Sedimentology 52, 875–902. https://doi.org/10.1111/j.1365-3091.2005.00722.x.

Marzocchi, A., Flecker, R., Van Baak, C.G.C., Lunt, D.J., Krijgsman, W., 2016. Mediterranean outflow pump: an alternative mechanism for the Lago-mare and the end of the Messinian Salinity Crisis. Geology 44, 523–526. https://doi.org/10.1130/G37646.1.

Micallef, A., Camerlenghi, A., Garcia-Castellanos, D., Otero, D.C., Gutscher, M.-A., Barreca, G., Spatola, D., Facchin, L., Geletti, R., Krastel, S., Gross, F., Urlaub, M., 2018. Evidence of the Zanclean megaflood in the eastern Mediterranean Basin. Sci. Rep. 8, 1078. https://doi.org/10.1038/s41598-018-19446-3.

Micallef, A., Camerlenghi, A., Georgiopoulou, A., Garcia-Castellanos, D., Gutscher, M.-A., Lo Iacono, C., Huvenne, V.A.I., Mountjoy, J.J., Paull, C.K., Le Bas, T., Spatola, D., Facchin, L., Accettella, D., 2019. Geomorphic evolution of the Malta Escarpment and implications for the Messinian evaporative drawdown in the eastern Mediterranean Sea. Geomorphology 327, 264–283. https://doi.org/10.1016/j.geomorph.2018.11. 012.

O'Connor, J.E., 1993. Hydrology, hydraulics, and geomorphology of the Bonneville flood. Geol. Soc. Am. Spec. Pap. 274.

O'Connor, J.E., Baker, V.R., 1992. Magnitudes and implications of peak discharges from glacial Lake Missoula. Geol. Soc. Am. Bull. 104, 267–279.

Orszag-Sperber, F., 2006. Changing perspectives in the concept of "Lago-Mare" in Mediterranean late Miocene evolution. Sediment. Geol. 188–189, 259–277. https://doi.org/10.1016/j.sedgeo.2006.03.008.

Orszag-Sperber, F., Rouchy, J.-M., Blanc-Valleron, M.-M., 2000. La transition Messinien–Pliocène en Méditerranée orientale (Chypre): la période du Lago-Mare et sa signification. C. R. Acad. Sci. 331, 483–490. https://doi.org/10.1016/S1251-8050(00)01433-6.

Pardee, J.T., 1942. Unusual currents in Glacial Lake Missoula, Montana. Geol. Soc. Am. Bull. 53, 1569–1600.

Periáñez, R., Abril, J.M., 2015. Computational fluid dynamics simulations of the Zanclean catastrophic flood of the Mediterranean (5.33Ma). Palaeogeogr. Palaeoclimatol. Palaeoecol. 424, 49–60. https://doi.org/10.1016/j.palaeo.2015.02.017.

Periáñez, R., Abril, J.M., Garcia-Castellanos, D., Estrada, F., Ercilla, G., 2019. An exploratory modelling study on sediment transport during the Zanclean flood of the Mediterranean. SN Appl. Sci. 1. https://doi.org/10.1007/s42452-019-0374-y.

Pierre, C., Caruso, A., Blanc-Valleron, M.-M., Rouchy, J.M., Orzsag-Sperber, F., 2006. Reconstruction of the paleoenvironmental changes around the Miocene"Pliocene boundary along a West"East transect across the Mediterranean. Sediment. Geol. 188–189, 319–340. https://doi.org/10.1016/j.sedgeo.2006.03.011.

Rouchy, J.-M., Martin, J.-P.S., 1992. Late Miocene events in the Mediterranean as recorded by carbonate-evaporice relations. Geology 20, 629. https://doi.org/10.1130/0091-7613(1992)020<0629:LMEITM>2.3.CO;2.

Roveri, M., Bassetti, M.A., Ricci Lucchi, F., 2001. The mediterranean Messinian salinity crisis: an Apennine foredeep perspective. Sediment. Geol. 140, 201–214.

Roveri, Marco, Flecker, R., Krijgsman, W., Lofi, J., Lugli, S., Manzi, V., Sierro, F.J., Bertini, A., Camerlenghi, A., De Lange, G., Govers, R., Hilgen, F.J., Habscher, C., Meijer, P.T., Stoica, M., 2014a. The Messinian Salinity Crisis: past and future of a great challenge for marine sciences. Mar. Geol. https://doi.org/10.1016/j.margeo.2014.02.002.

Roveri, M., Manzi, V., Bergamasco, A., Falcieri, F.M., Gennari, R., Lugli, S., Schreiber, B.C., 2014b. Dense shelf water cascading and Messinian Canyons: a new scenario for the Mediterranean salinity crisis. Am. J. Sci. 314, 751–784. https://doi.org/10.2475/05.2014.03.

Ryan, W.B., 2008. Modeling the magnitude and timing of evaporative drawdown during the Messinian salinity crisis. Stratigraphy 5, 227–243.

Ryan, W.B.F., 2009. Decoding the Mediterranean salinity crisis. Sedimentology 56, 95–136. https://doi.org/10.1111/j.1365-3091.2008.01031.x.

Ryan, W.B.F., Hsu, K.J., Cita, M.B., 1973. Site 120. Initial Rep. Deep Sea Drill. Proj. 13, 19–41.

Selli, R., 1960. Il Messiniano Mayer-Eymar, 1867. Proposta di un neostratotipo. Giorn. Geol., ser. 2, 28: 1-33.

Sternai, P., Caricchi, L., Garcia-Castellanos, D., Jolivet, L., Sheldrake, T.E., Castelltort, S., 2017. Magmatic pulse driven by sea-level changes associated with the Messinian salinity crisis. Nat. Geosci. 10, 783–787. https://doi.org/10.1038/ngeo3032.

Urgeles, R., Camerlenghi, A., Garcia-Castellanos, D., De Mol, B., Garces, M., Verges, J., Haslam, I., Hardman, M., 2011. New constraints on the Messinian sealevel drawdown from 3D seismic data of the Ebro margin, western Mediterranean. Basin Res. 23, 123–145. https://doi.org/10.1111/j.1365-2117.2010.00477.x.

Proceedings of the Ocean Drilling Program, 161 Scientific results. In: Zahn, R., Comas, M.C., Klaus, A. (Eds.), Proceedings of the Ocean Drilling Program. Ocean Drilling Program, https://doi.org/10.2973/odp.proc.sr.161.1999.

PART IV

DISCUSSION AND CONCLUSIONS

Chapter 9

9.1 General discussion

The convulsive events analysed in this Thesis, i.e., the tsunami earthquake triggered by the Averroes fault and the Zanclean megaflood, provide new insights in the recognition of their products in the submarine sedimentary record, their underlying causative mechanisms, their impacts at basin scale evolution/analysis and their serious threat to society, economy, and environment. In general, earthquakes, landslides and volcanism are the examples of convulsive events mostly studied in the geological record, both offshore and onshore. But there are also unusual convulsive events that have been reported as unique case studies, such as the Chicxulub crater in the Gulf of Mexico (Fig. 9-1), produced by the impact of an asteroid 66 Ma ago (Canales-García et al., 2018); or the megaflood in the English Channel (Gupta et al., 2007) (Fig. 9-2). These unusual examples are limited in the geological record and their influence on the sedimentary record is generally poorly understood (Clifton, 1988). In the marine environment, this scarcity is accentuated by the practical inexistence of studies. This is because the difficult access to deep seafloor and sub bottom due to the technical limitation that the marine environment imposes. This fact determines that there are very few analogous reference models for comparison.

The difficulty associated with the identification of convulsive events in the marine sedimentary record, as opposed to "classic" records, lies mainly in three main factors: the magnitude of the event, understood as the energy suddenly released; the affected area/space, which varies commonly from regional to global scales; and the short duration on a geological time scale. These intrinsic properties of the convulsive events contrast with the generally more gradualist view of geological processes to which geologists are more accustomed. Sedimentary evidence of convulsive events, whether in the form of deposits or erosional surfaces, are rarely well preserved, and this fact often means that their distinctive marks in the sedimentary record are limited, or deficient, and their sedimentary processes are poorly understood, especially for events that did not occur in historical times (Clifton, 1988). All this affects the ability of geologists to recognize the effects of convulsive processes in the geological record,

mainly of those being unusual and affecting large areas, the latter hindering the correlation of their sedimentary products between basins or even within the same basin. In any case, and as Clifton (1988) says, "responsible scientific procedure dictates that we accept the most likely explanation, usually the simplest, for any phenomenon in the geologic record", and as he continues, "it is very likely that deposits resulting from a large event will be considered as part of a "typical" sedimentary sequence and given the inability to establish their origin their real significance is obscured".

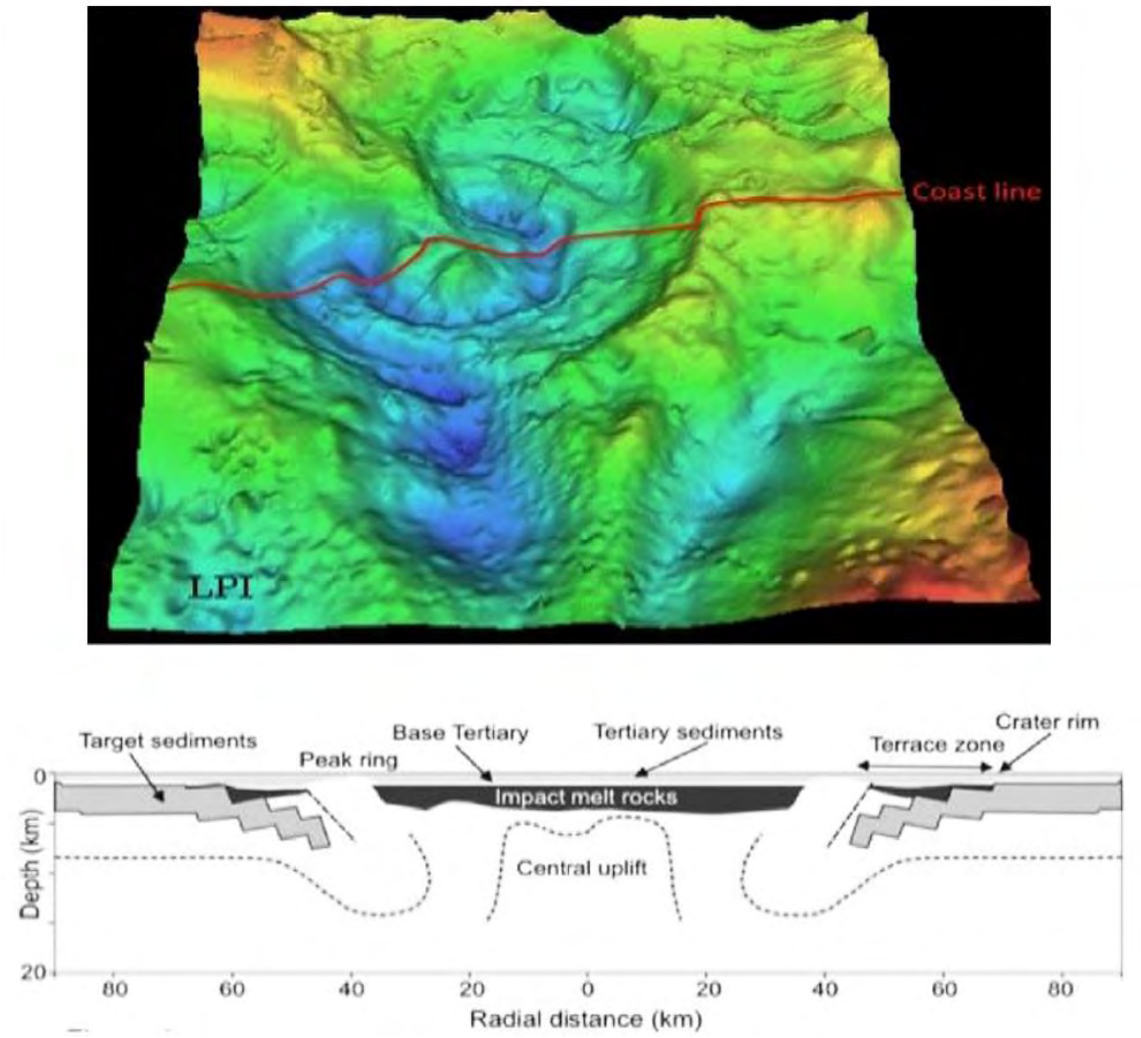

Figure 9-1. Bouguer anomaly map of Chicxulub crater; below, Schematic cross-section showing the main structural elements (Canales-García et al., 2018 and references therein).

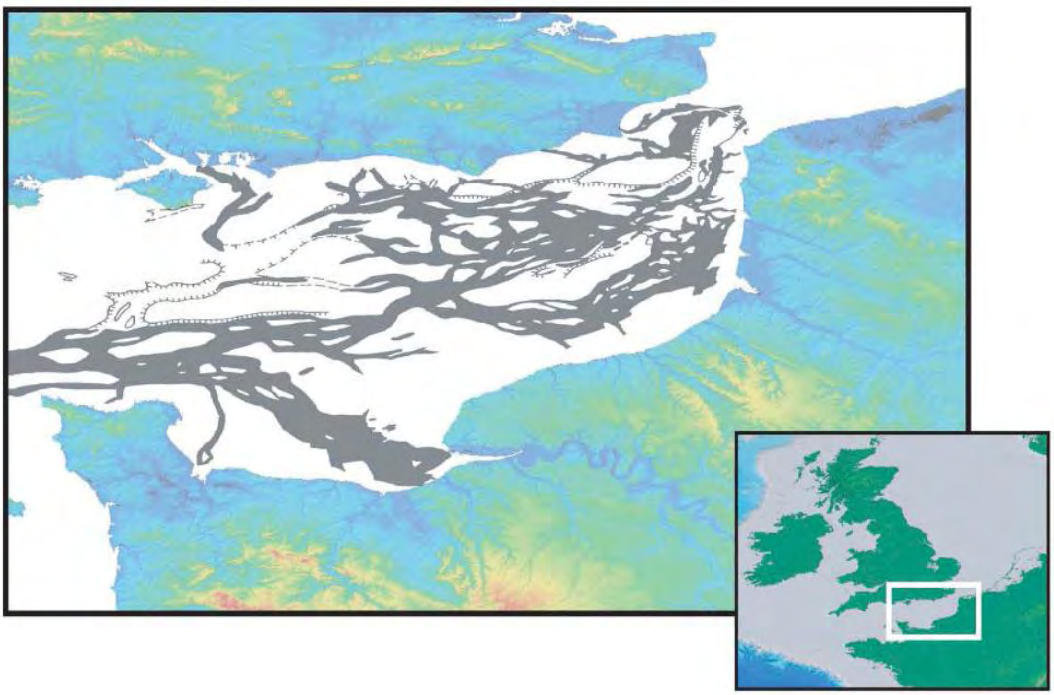

Figure 9-2. Location map and inferred distribution of palaeovalleys on the English Channel shelf (Gupta et al., 2007).

In light of the difficulty of studying convulsive events, the combination of classical geological analysis with geophysical techniques, together with mathematical modelling, has proved to be a powerful tool for their study, allowing us to investigate deeper into their mechanisms of formation, dynamics of the process, and recognition of their products in the sedimentary record. From partial geological evidences, obtained with seismic profiles and other marine research techniques, we usually have a biased and discontinuous view of the true nature of these processes, which hinders their correct identification and understanding. On the other hand, mathematical models, based on geological evidence and knowledge of the physical laws that govern those events, offer a continuous vision of them, in space and time, thus helping to better fit their geological evidences and formation contexts.

The Alborán basin is an excellent laboratory for studying convulsive events by a distinctive multidisciplinary approach bringing together long-term geological records, such as seismic profiles with different degrees of resolution and penetration, geophysical data (e.g., magnetometer, gravity and seismic data), and numerical modelling. This is because of its relatively limited extension (350x174 km) and its semi-

enclosed basinal configuration that favour the correlation and identification of geological processes in space and time. The complex tectonic dynamics and active seismicity in the context of collision between the Eurasian and Nubian (Africa) plates makes this area prone to earthquakes and sedimentary instability processes that can trigger tsunamigenic events (Amir et al., 2010, González et al., 2010; Álvarez-Gómez et al., 2011; Vázquez et al., 2012; Macías et al., 2013; Macías et al., 2015; Rodríguez et al., 2017;). In addition, the chronostratigraphy of its infilling sedimentary record is well-known, mainly the Plio-Quaternary (Ercilla et al., 1992, 2016; Alonso and Maldonado, 1992; Estrada et al., 1997; Juan et al., 2016, 2020). Likewise, the existence of a dense network of seismic profiles covering almost the entire basin makes the correlation of geological structures and their spatial/temporal relationships possible.

9.1.1 Convulsive event *versus* Catastrophism

The term convulsive event, as used in this thesis, refers to an extraordinarily energetic event of regional influence (Clifton, 1988). We agree with this author's formulation, and we think that the term convulsive event is preferable to "catastrophe". This is because catastrophe leads to the concept of disaster and carries philosophical implications. The term "convulsive" is neutral in the sense of disaster and has no doctrinal implications (Clifton, 1988). As Vera (1994) said, "the new conception of actualistic catastrophism (Hsü, 1983) has led to… the birth… of Event Stratigraphy", however this author does not reject the idea of catastrophism, although it deepens and develops the concept of event.

Another implication of the term catastrophism, in relation to the use of convulsive event, is the long nineteenth-century debate between the concept of gradualism and catastrophism that contained a strong religious charge. It is important to note that, in the 80s of the last century, and as a result of the increase in studies of catastrophic processes (Berggren and Couvering, 1984), a new debate resurfaced about the importance of catastrophic events over the "gradualists". In the late 1980s it was stated that "many sedimentologists today would agree with the assertion that the sedimentary record is largely a record of episodic events" (Clifton, 1988). This statement

is probably extrapolated to the present-day. The current tendency with respect to the concept of catastrophe refers to this type of events in terms of geological hazards, which is a more aseptic concept and in accordance with a scientific view. However, large events such as the Zanclean megaflood, or the impact of the Chicxulub crater do not easily fit into the concept of geological hazard and it is in these cases where the term "convulsive event" acquires relevance.

9.1.2 Convulsive events: megaflood *versus* tsunami

Comparing the earthquake tsunami triggered by the Averroes fault and the Zanclean megaflood, in terms of magnitude (energy released by the event), geographical area affected and duration of the convulsive process, we observe that both events present similarities and differences.

The difference between both events has to do with magnitude. The case of the earthquake tsunami, the energy released by the seismic shaking is significantly lower than the megaflood, which is equivalent to ~4% of the kinetic energy released by the Chicxulub meteorite impact (Chapter 7.2). In order to compare both processes, the energy released has been transformed into tons of explosives trinitrotoluene (TNT) (https://www.translatorscafe.com/unit-converter/es-ES/energy/1-41/).

In the case of the earthquake that triggers the tsunami, the graph in Figure 9-3 has been taken as a reference and shows that the magnitude of a given earthquake is linked to the energy released by the equivalent in kilograms of explosives. The approximate value for the earthquake is 1,800,000 t of explosives, which corresponds to a seismic magnitude MW=7 calculated for the Averroes fault (Chapter 6).

For the case of the Zanclean megaflood, a gravitational potential energy dissipation of 1.6x1022 J was calculated (Chapter 7.2) which is equivalent to 3,824,091,778,200 t of explosives. Comparing the equivalence in tons of explosives between both convulsive events, we observe that the megaflood is 6 orders of magnitude higher than the tsunami. Therefore, the magnitude of the geological consequences will be in accordance with the energy released. It should be noted that in the case of the energy released by the earthquake, the magnitude does not reflect all

the energy involved in the earthquake, since a significant part is released in the form of heat. Even so, 6 orders of magnitude difference indicate that the megaflood released relatively more energy than the tsunami.

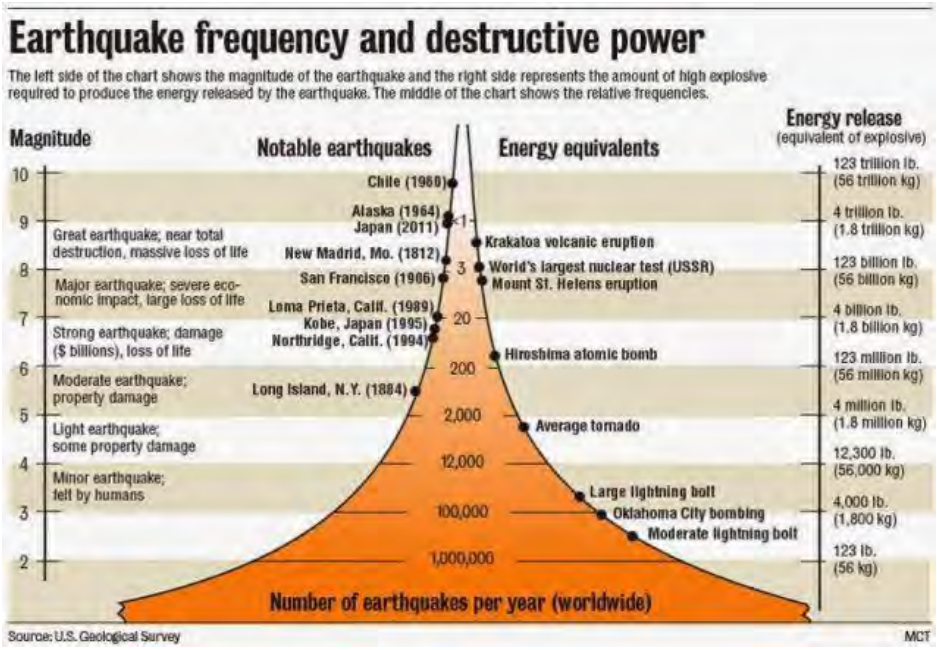

Figure 9-3. Graph comparing the magnitude of earthquakes with their equivalent of energy released by an explosive (TNT). The most relevant events and the number of annual earthquakes according to magnitude are highlighted (Source: U.S. Geological Survey).

The similarities refer to the area affected by both events. The area is similar and driven by the evolution of the Eurasia-Africa plate boundary. While the consequences of the tsunami were mostly confined to the Alborán basin, the indirect consequences of the megaflood event likely went beyond that geographical area. In fact, the oceanographic circulation at the scale of the Mediterranean basin was reactivated (Juan et al., 2016 and 2020) (Fig. 9-4). Likewise, the reconnection of the Mediterranean with the Atlantic Ocean through the Strait of Gibraltar influenced the North Atlantic circulation, mainly impacting on the Atlantic Meridional Overturning Circulation (AMOC) (Fig. 9-5) (Pérez-Asensio et al., 2012; Swingedouw et al., 2019). This is because the Mediterranean Outflow Water (MOW) is considered one of the major transporters of dense water, as well as an injection of salt and heat that has influenced not only the

oceanic circulation, but also the climate of this hemisphere (Voelker et al., 2006; Legg et al., 2009; Rogerson et al., 2012). With regard to the tsunami, its consequences on the coast are unknown due to the lack of studies. Only the evidence of tsunamites described on the Andalusian coast is known (Reicherter and Becker-Heidmann, 2008; Roig-Munar et al., 2020).

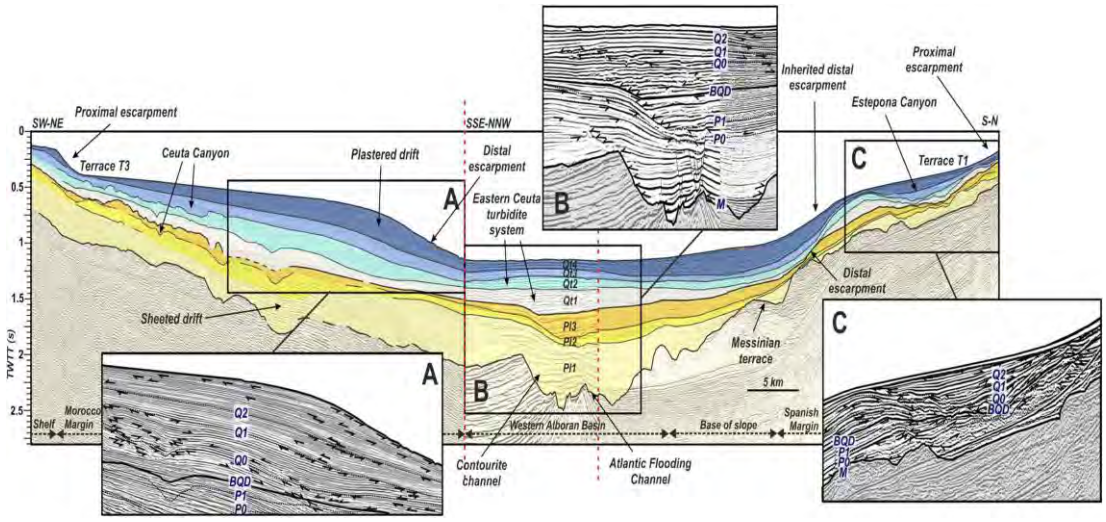

Figure 9-4. Seismic profile showing the widespread development of contourites in the Alborán Sea after the Zanclean megaflood during the Plio-Quaternary (Juan et al., 2020).

Regarding the duration of each process, it has been found that it differs significantly. In the case of the tsunami, its effects can be felt up to one hour after the event (Video 6-S1); in the case of the megaflood it has been calculated that the Mediterranean basin was filled in approximately 2 years (Fig. 7.2-3). In terms of geological time, both cases can be considered instantaneous, but there is an important difference in terms of prediction, due to the underlying mechanisms governing their occurrence. In the case of the earthquake tsunami, the sismo- and chrono-stratigraphic analysis of the Averroes fault lead to estimate a recurrence period of ~ 31,000 years. On the contrary, in the case of the Zanclean megaflood, the convulsive event is dependent of the regional space-time variations in the basin tectonism, which makes it difficult to estimate when a similar situation may occur again.

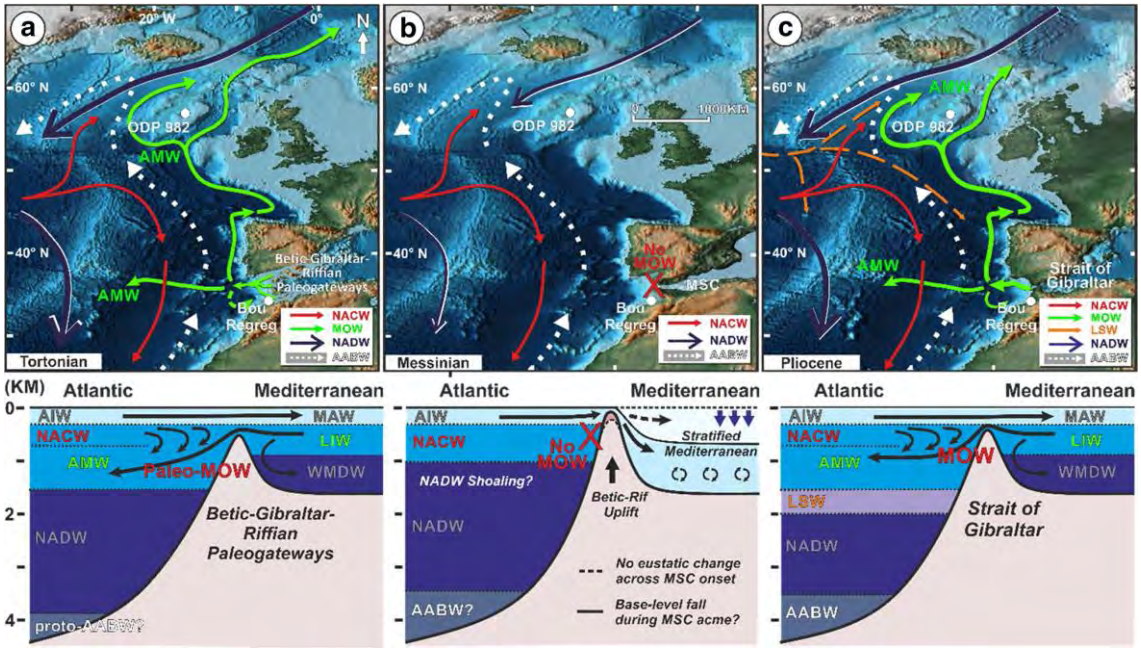

Figure 9-5. Schematic of the Mediterranean-Atlantic circulation constraint during the Tortonian (a), Messinian (b) and Pliocene (c) (Ng et al., 2021).

9.2 Geohazard implications of convulsive events in the Alborán Sea

The Alborán Sea develops in the framework of the NW-SE collision of the African and Eurasian plates with the Alborán microplate (Fig. 4-1), leading to one of the most tectonically active areas of the marine environment surrounding the Iberian Peninsula. The tectonic activity is evidenced by active sets of folds and seismic faults (Chapters 4, 5 and 6) that make the Alborán Sea an area highly prone to the development of convulsive events.

As noted in Chapter 4, most of the current deformation is concentrated in the central part of the Alborán Sea, due to a process of tectonic indentation that forms the Central Alborán Arc (Fig. 4-2). This arc determines the main features of the Trans Alborán Shear Zone (De Larouzière et al., 1988), the major seismogenic active area in the SW Mediterranean with sea-land influence that has evolved during the Neogene and Quaternary (Chapter 5). It affects the central and eastern Betic Cordillera connecting, through the continental margins of the Alborán Sea, with the Rif Cordillera (Gràcia et al., 2012; d'Acremont et al., 2014; Grevemeyer et al., 2015; Galindo-Zaldívar et al., 2022).

The tectonic indentation is produced by the collision of a spur of African continental crust that is displaced to the NNW by two major strike-slip fault systems, the NW-SE dextral Yusuf fault and the seismogenic NNE-SSW sinistral Al-Idrisi fault (Fig. 4-2). This African crustal indenter also develops a NNE-SSW and WNW-ESE conjugate strike-slip fault systems and folds (e.g., the Alborán Ridge) which generate earthquakes, earthquake tsunamis (Chapter 6) and submarine slope sedimentary instabilities (Chapter 5) (Vázquez et al., 2010; Rodríguez et al., 2017; d'Acremont et al., 2022).

In general, strike-slip faults are not considered tsunamigenic, because they do not significantly displace the seafloor. However, the analysis carried here about the NW–SE dextral Averroes Fault (chapter 6) contradicts this theory and indicates the need to investigate other strike-slip faults in similar geological frameworks. Also, tsunamigenic submarine landslides can occur (e.g., Reicherter and Hübscher, 2007; Macías et al., 2015; Rodríguez et al., 2017) including coastal ones entering the sea (e.g., Mateos et al., 2017; Harmouzi et al., 2019). Therefore, the central Alborán Sea is a key area to: i) assess the geohazard implications of the convulsive events; ii) analyse how these events can interact and their potential to generate cascading processes; and iii) understand the link between indentation and geological hazards in a land-marine transition context. Studies like this one will lead to a much greater understanding of hazardous processes, and will have significant effect on the probabilistic methods for assessing geological hazards with more robust models from which early warning systems will benefit.

Against the common social perception, hazardous processes triggered by convulsive events have impacted repeatedly on Spanish and African coasts causing damage to coastal communities and infrastructures. Prehistorical and historical cases of offshore geohazard events have been recognized in SW Mediterranean (Table 1). About 9 tsunamis impacted since 1361 (Papadopoulos et al., 2014), and also tens of historical earthquakes with offshore and nearby onshore epicentres were felt, and some with important destructive events. The seismic activity in the region continues even today (http://www.ign.es). Offshore slides, although widely spread in the SW Mediterranean margins and coastal areas, are the great unknown, in terms of frequency (Table 1, references there).

Earthquakes	Mass-movements	Tsunamis
Andalucía: about 24 historical events (e.g. 880, 1013-1014, 1406) felt or with destructive effects.	Almería after the 1522 earthquake (aprox M=5.5).	Almería: in 1522, by a submarine slide triggered by an earthquake.
Morocco: with M ≥ 6 historical earthquakes in 1660, 1682, 1792, 1847, 1848, 1887, 1899, 1916, 1926, etc	Seamounts, foot of Incrisis, Al-Idrissi and Averroes fault scarps, Ceuta drift, among others: Millennial to tens of thousands recurrences	Spanish coast-Alborán Sea triggered by earthquakes: in 1790, 1804, 1954 and tide station signal in 2016. Morocco and Algerian coasts: 1680, 1733, 1790, 1980.
	Active coastal landslides, e.g. Cantarrijan landslide (Spain); between Oued Laou and El Jebha coastline (Morocco).	

Table 1. Examples of events related to the two tectonic indentation areas of the SW Mediterranean. Earthquakes are the most frequent processes. Large amount of mass movements is observed but their recurrence is unknown. Tsunamis could be small in size but with high impact because the densely populated coastal areas. (Reicherter and Hübscher, 2007; Alvarez-Gómez et al., 2011; Alonso et al., 2014; d'Acremont et al., 2014; Buforn et al., 2017; Mateos et al., 2017; Harmouzi et al., 2019; Gràcia et al., 2019. http://iagpds.ugr.es/pages/informacion_divulgacion/Terremotos historicos; https://www.ign.es, among others).

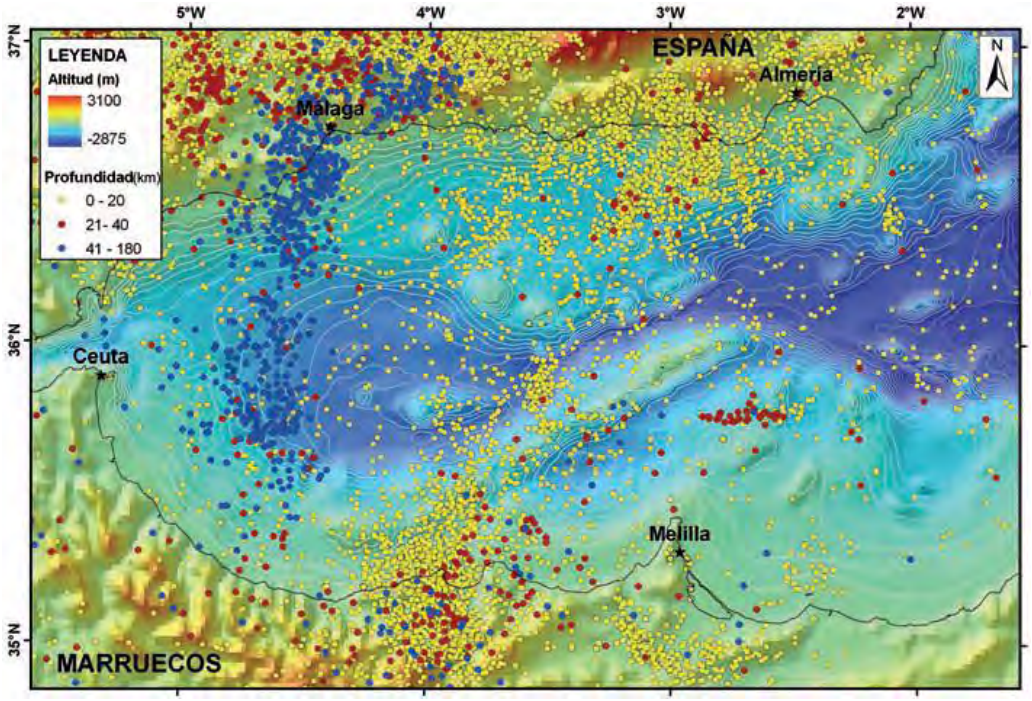

Figure 9-6. Earthquake epicentres distribution with respect to focal depth in the Alborán Sea Basin, according to the I.G.N. database updated as of September 2010, on the ETOPO topo-bathymetric database (Macías et al., 2013).

9.3 The Atlantic flooding convulsive event: what it tells us about the end of the MSC

Historically, the Messinian salinity crisis has been considered a geological event that produced the almost desiccation of the Mediterranean Sea, as consequence of the disconnection from the Atlantic Sea. Evidence of this desiccation are the evaporitic deposits up to 3 km thick in the deepest Mediterranean basins, and the regional erosion observed in the continental margins attributed to a sea level drop of about 1500 m. However, the hypothesis that there has never been such a disconnection has been gaining strength, mainly because several connection-disconnection cycles (7-8) are needed to explain the salt thickness as well as for geochemical reasons (Flecker et al., 2002). Currently, three models are proposed: deep desiccated basin (Hsu et al., 1973), deep non-dessicatted basin (Roveri et al., 2014) (Fig. 2-14), and the mixed model (Mascle and Mascle, 2019). The second hypothesis postulates that the Zanclean megaflood did not occur but there was a permanent Atlantic-Mediterranean connection, which, despite the lack of geological evidence, is located in the Strait of Gibraltar. The Alborán Basin is a key area to understand the evolution of the MSC given its proximity to the Atlantic connection. Progress made and results achieved in this thesis has led to significantly improved understanding on the impact of the convulsive event of the Zanclean megaflood in the sedimentary evolution of the Alborán Sea, and also offers important key points to the debate about the interpretation of the end of the Messinian Salinity Crisis) (Chapters 7 and 8).

The analysis of the stratigraphic architecture carried out in this Thesis with a dense network of seismic profiles, suggests that there was a disconnection and that it ended abruptly through the Zanclean Flood. The key to this statement rests in the preserved MSC deposits, their morphological features, and their chronostratigraphic relationships with the Messinian M surface, and others (Figs. 7.1-4, 7.1-5, 7.1-7 and 8-8). Typical MSC units in the Mediterranean are (Fig. 9-7): the LU (Lower Unit, with primary gypsum deposition), MU (Mobile Unit, with halite deposition) and UU (Upper Unit with lago mare facies deposition) (Lofi, 2018). On this stratigraphic basis, the MSC stratigraphy in the Alborán Sea is characterized by:

- There is a poor or lack of the typical Messinian Salinity Crisis sequence (trilogy) (Figs. 9-7 and 9-8).

- The presence of Chaotic deposits, between the LU and MU (Fig. 7.1-4). This chaotic unit is identified on the continental slope in the Málaga area and on the Moroccan coast near Melilla (Figs. 9-8 and 9-9), and results from the erosion of primary gypsum (LU) (Martínez del Olmo and Comas, 2008; Do Couto et al., 2016). Chaotic deposits are linked to the erosion caused by the 1500 m lowering of sea level.

- The lack of halite deposition, i.e. of MU (Figs. 9-7 and 9-8).

- The presence of the Lago-Mare UU mapped at the eastern end of the basin (Fig. 8-8). This unit is physically correlatable with its equivalent in the Algero-Balearic basin, where the MSC unit trilogy is well represented.

- The fact that the Messinian M surface is affected by a striking erosion in the deep basin, in the form of an E-W erosional channel crossing the entire basin (390 km long and up to 488 m deep) (Fig. 7.1-6). This channel also erodes the Chaotic unit and the UU in the easternmost Alborán (Fig. 8-8). These stratigraphic relationships suggest that the channel incision occurred at the end of the MSC and, together with their along basin trend, this indicates that the channel could be considered as being formed by the Zanclean flooding. This erosion in the deep part of the basin is in contrast with what is observed in other areas of the Mediterranean, where Messinian erosion develops mainly at the margins.

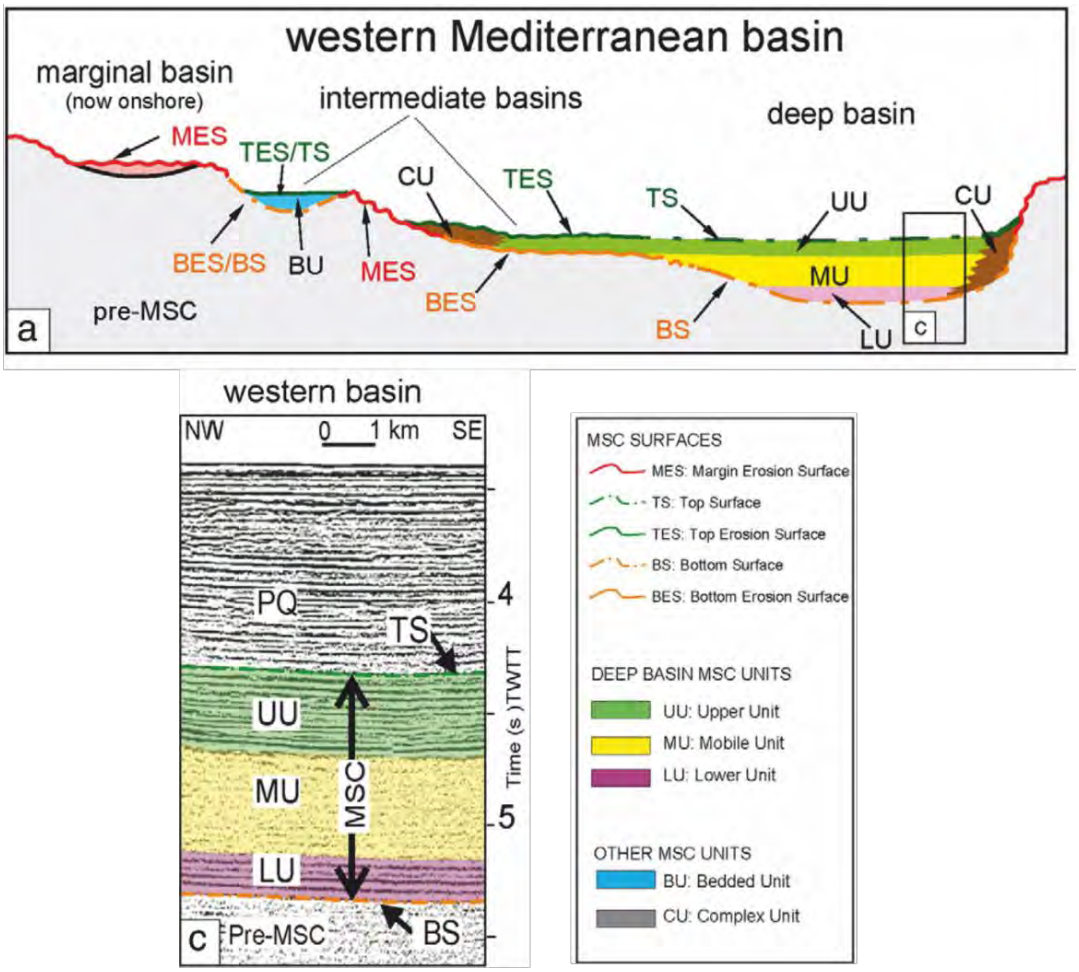

Figure 9-7. Messinian trilogy of the western Mediterranean and its relation with messinian markers (Modified from Roveri et al., 2014).

- Adjacent to the channel, along the Spanish and Moroccan margins, and close to the Strait of Gibraltar, several submarine terraces also affect the M surface at different depths, which suggests a pulsed flooding of the Alborán Basin (Figs. 7.1-6 and 9-9).

- The Messinian M surface is directly overlaid by the Plio-Quaternary contourite sequence (Fig. 9-4) (Juan et al., 2016, 2020).

- The lack of contourite deposits during the MSC. It is to be expected that if there was a permanent connection in the Strait of Gibraltar, the Mediterranean circulation

conditions were similar to those of the Plio-Quaternary, and therefore contourite deposits developed.

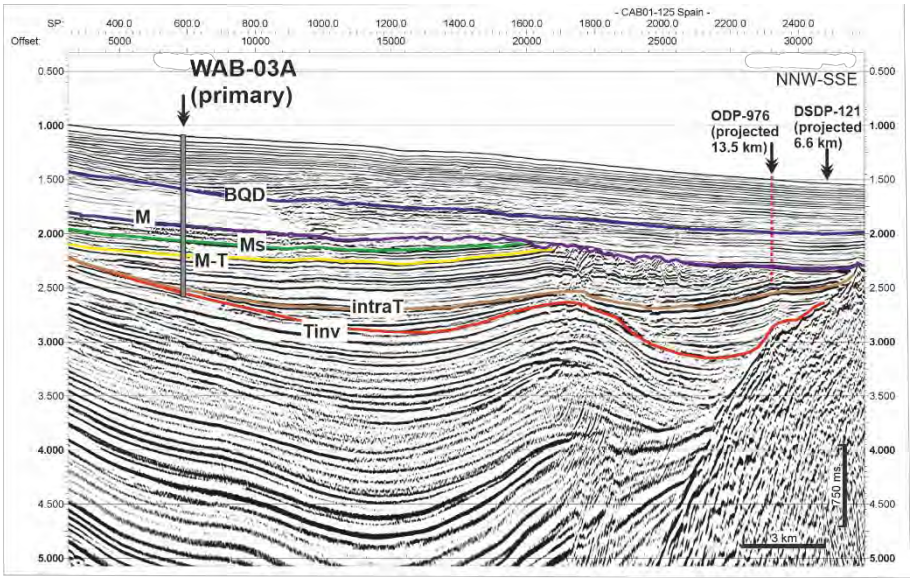

Figure 9-8. Seismic profile showing the poorly developed MSC sequence in the Alborán Sea (offshore Fuengirola). Legend: (BQD) base of Quaternary, (M) Miocene-Pliocene boundary, (Ms) base of MSC, (M-T) Messinian-Tortonian boundary, (intraT) IntraTotornian boundary and (Tinv) Tortonian inversion (Flecker et al., 2020).

All these key stratigraphic elements characterizing the MSC sedimentary record of the Alborán Sea, indicate that the Messinian M surface is clearly a polygenetic surface formed by the superimposition of repeated erosional, subaerial and desiccation processes, and marine influence during the Atlantic flooding. All this makes the Messinian M surface of the Alborán Sea unique in its sedimentological, morphological and stratigraphic characteristics in the Mediterranean Sea.

Despite all these stratigraphic evidences, several unknowns remain unsolved, pending the IODP IMMAGE proposal in the Alborán Sea (Flecker et al., 2020). What caused the opening of the Strait of Gibraltar? This is a question that currently has no clear answer. Several hypotheses related to tectonic control, sea level changes or regressive fluvial erosion have been postulated (Blanc, 2002; Loget and Van Den Driessche, 2006). Based on the geological evidence presented in this Thesis, we consider that the most plausible answer is a combination of tectonics and regressive fluvial

erosion (García-Castellanos and Villaseñor, 2011) that responds to the thickness of salts in the Mediterranean basin.

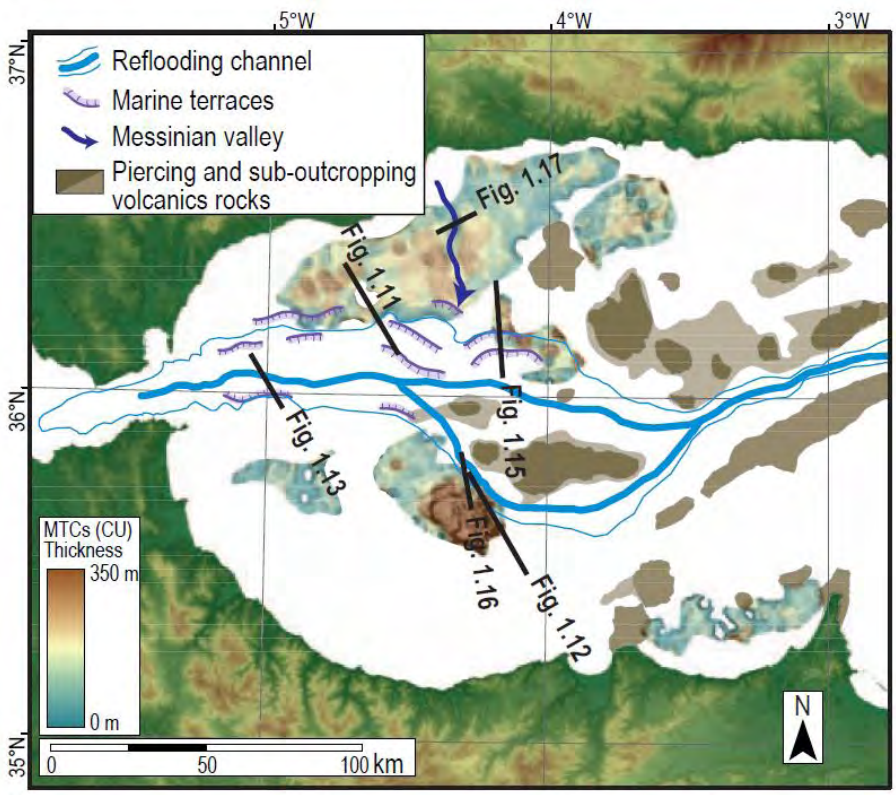

Figure 9-9. Distribution map of the Messinian chaotic deposits in the Alborán Sea (Modified from Lofi, 2018).

Chapter 10

10 CONCLUSIONS

This PhD thesis analyses two convulsive geological events, of tectonic and sedimentary-oceanographic character, that occurred in the past in the Alborán Sea: the earthquake tsunami associated with the activity of the Averroes fault and the Atlantic Zanclean megaflood. The analysis of the geology of the region allows us to deepen our knowledge of the geodynamics where both convulsive events are framed and to better understand their genesis and the geohazards associated with them. To those aims, a multidisciplinary approach based on geomorphology, geophysics, sedimentology, tectonics and mathematical modelling allowed us to reconstruct how these events developed and their consequences. On the other hand, the use of the term convulsive event *versus* catastrophe has also been analysed from a conceptual point of view, reaching the conclusion that the use of the first one is preferable since it is a more aseptic term, without philosophical connotations.

10.1 Major achievements

The main contributions of this PhD research are summarized in the following two major points:

- To understand the genesis and impact of convulsive events it is necessary to analyse the characteristics of active tectonics and associated geodynamic processes. Thus, this Ph.D. **defines for the first time the tectonic indentation model** that develops in the Alborán Sea, in the framework of the Eurasian–Nubia plate collision. This model contributes to increase the **understanding** of the **recent geodynamic** evolution of this sea. NNE–SSW sinistral and WNW–ESE dextral conjugate fault sets forming a 75° angle surround the rigid basement spur of the African plate. Northward, the **faults** decrease their transcurrent slip, becoming normal close to the tip point. The **Alborán Ridge** antiform above a detachment level was **favoured by the crustal layering**. The

indentation tectonics entails the **highest hazard** of **seismic convulsive events** of the Alborán Sea. This Ph.D. also offers new insights for the hazard assessment of these type of convulsive events, based on **imaging the growth of recent active faults** through the analysis of a seismic sequence sea bottom deformation. The results indicate that the growth of recent faults can produce potentially **higher magnitude earthquakes** than those associated to the already formed faults, thus increasing the expected earthquake convulsive events of the area.

For a deep insight on of these events, this Ph.D. assesses their potentiality to provoke another type of convulsive event in the Alborán Sea: the tsunamis. In this case, the study focused on the **Averroes strike-slip fault** tip. Its **tsunamigenic potential is modelled,** and reveals how the **tsunami waves** reach highly **populated sectors** of the **Iberian coast** with maximum arrival heights of **6 m within 21 and 35 min**. The short time elapsed between the earthquake and the arrival of the tsunami means that the **reaction time** of the **early warning systems is very short**. The characteristics of the tsunami and the high use of beaches and the Andalusian coastline in general make this area particularly prone to seismic tsunami convulsive events. The findings have broad crucial consequences for the offshore geohazards, with two major implications. One is related to the hazardous seismic faults and suggests that the **tsunamigenic potential** of **strike-slip faults** is more important than previously known, and the other is related to the **tsunami early-warning systems,** which should be considered for their **re-evaluation**.

- The **Zanclean megaflood** represents an **unusual and great convulsive event** with **sedimentary and oceanographic** implications at the **basin scale,** in the Mediterranean. This Ph. D. more accurately asserts the **chronological constraints of their features** preserved in the sedimentary record. This constrain leads to the determination that a **great flooding** occurred at the end of the Messinian, and that it **put an end to the MSC**. The key feature for this statement is the striking and large E-W channel (the **Zanclean channel**, up to 600 ms of relief and 250 km long) **eroding** the upper unit deposits (UU) that closes the **MSC trilogy**. In addition, the occurrence of post-flooding sedimentary features such as several submarine terraces at different depths, and the development of subaerial canyons, reveal that the megaflood of Atlantic water occurred in several

stages. These results are quite important because they **shed light** on the current debate about the **three models** of the **MSC**: deep desiccated basin, deep non- desiccated basin and mixed, in favour of the **desiccated basin and mixed models** because it considers both the subaereal exposure and subsequent Atlantic flooding of the Alborán Basin.

For a deep insight on the magnitude and duration of this extraordinary convulsive event, the Zanclean megaflood was **mathematically modelled**. The model determines that this convulsive event involves five phases, 0 to 5, being the **phases 2 and 3** those with **convulsive character**, due to their short duration from a geological point of view. Phase 0 corresponds to a period of long duration where the reduced inflow of Atlantic water generates little significant erosion. In phase 1, the Strait of Gibraltar becomes deeper and wider, exponentially increasing its rate of erosion and Atlantic water flow. In phase 2, there is a reduction in the hydrological gradient between the Atlantic Ocean and the western Mediterranean resulting in a decrease in the flow velocity and discharge of water, as well as a decrease in the rate of erosion. During this phase all the Atlantic water entering through the Strait of Gibraltar is reversed to refill the Western Mediterranean Basin. In phase 3, the sea level reaches the Sicily threshold and the hydrological gradient remains constant in the Western Basin, as the water entering through the Strait of Gibraltar is transferred to the Eastern Basin, producing a rapid rise in sea level in the latter. Finally, in phase 4, the sea level rises synchronously in both Mediterranean basins until it levels with the Atlantic Ocean. The estimated **time to transfer 90% of the water** to the Mediterranean basin **is two years**, causing a **sea level rise of 10 m per day**. Due to the **enormous flow** generated at the peak of the megaflood (**10^8 m^3 s^{-1}**), and the **high velocities** reached (**v=40 m s^{-1}**), it is very likely that the image of a waterfall filling the Mediterranean basin is not correct and was probably produced by a flood ramp.

10.2 Outstanding questions

The research carried out in this thesis reveals several questions not fully resolved or in the need of future research. These are relevant to the knowledge of convulsive events not only in the Alborán Sea, but also extrapolable to other areas.

For hazardous convulsive events: the generation of seismic tsunamis in the Alborán Sea still remains practically unknown. There are many potentially seismic faults to trigger tsunamis that should be mathematically modeled, especially strike-slip faults that were not previously considered as risk source. The detailed analysis of these potential sources will allow in the future a much more detailed map of the coastal areas that can be affected by tsunamis and to what degree, and thus improve early warning and mitigation plans. The aforementioned can be extrapolated to other areas located in similar tectonic frameworks.

Another important aspect for future studies would be to move further with **convulsive events in cascade**. For example, from an initial earthquake source, other earthquakes can be generated in highly stressed areas, which in turn can generate landslides that give rise to tsunamis. In this sense, the CASCADE, project presented to the Spanish "convocatoria 2021 de la Agencia Estatal de Investigación (AEI) de proyectos de investigación I+D+i PID2021" and in which I participate, (co-directed by Dr. Casas D. and Dr. Ercilla G. from ICM-CSIC and Dr. Galindo J. from UGr-IACT), will address this issue in order to improve the understanding and the impact of cascading processes in tectonic indentation areas.

As it has been seen throughout this thesis, the Alborán Sea is an area prone to the occurrence of submarine landslides, some considered to be convulsive events. This topic, that is scarcely investigated, is an extremely important element, if we wish to develop a strategy helpful for the early warning systems and mitigation measurements. A big unknown in the Alborán Sea is the development of **megaslides**, of which we have some evidences that occurred in the past, such as the Lower Pleistocene, landslide of Nerja, 35 km wide and 20 km long, with a maximum thickness of 221 m (Belzuz, 1999). The head of this landslide is located on the upper continental slope of Nerja (Málaga) at

472 m water depth and its implications in terms of geological hazards are unknown. In fact, the potential impact of an event of this magnitude could be enormous.

For the Zanclean megaflood convulsive: with regard to the Messinian salinity crisis several aspects remain unsolved: what caused the Zanclean megaflood?; what was the paleotopography of the Alborán Sea during the MSC; or what do the Messinian deposits tell us about the MSC and its influence on the global climate? To answer the question of what caused the convulsive event of the Zanclean megaflood, a more detailed analysis of the seismic stratigraphy record on both sides of the Strait of Gibraltar is required, since many of the hypotheses in the literature about its genesis are speculative due to lack of detailed studies.

To better understand the evolution of the MSC in the Mediterranean and its environmental implications, it is important to know what was the paleotopography of an area as sensitive to MSC as the Alborán Sea. Currently, we are collaborating with researchers from the GEO3BCN-CSIC Institute in the paleogeographic reconstruction of the Alborán Sea during the Messinian that will provide essential information to better understand how the MSC evolved.

The **paleoenvironmental** implications of the **MSC** and its **impact on global climate** is a topic of current debate. Marine gateways play a critical role in the exchange of water between oceans and seas that influence thermohaline circulation. The role of straits, such as the Gibraltar Strait, in mathematical climate modelling is critical because existing models use cells of a size that exceeds the dimensions of the strait itself, causing a significant bias in climate prediction. To better understand this bias, I am involved in the IMMAGE 895-ADP proposal (Flecker, 2020) that has been submitted to International Ocean Discovery Program (IODP). This proposal will carry out several drillings on both sides of the Strait of Gibraltar, in order to recover a complete record of the Atlantic-Mediterranean exchange from the Late Miocene to the present configuration.

REFERENCES

Alonso, B., Farrán, M. and Maldonado, A. (1989). Estratigrafía sísmica de alta resolución en márgenes continentales pasivos: factores de control durante el Cuaternario. Rev. Soc. Geol. Es., 2(3-4): 269-289.

Alonso, B. and Maldonado, A. (1992). Plio-Quaternary margin growth patterns in a complex tectonic setting: Northeastern Alborán Sea. Geo-Marine Letters, 12(2), 137-143.

Alonso, B., Ercilla, G., García, M., Vázquez, J. T., Juan, C., Casas, D., Estrada, F., d'Acremont, E., Gorini, C., El Moumni, B. and Farran, M. (2014). Quaternary mass-transport deposits on the North-Eastern Alborán Seamounts (SW Mediterranean Sea). In: Krastel S et al (eds) Submarine Mass Movements and their Consequences. Advances in Natural and Technological Hazards Research, vol 37. Springer, Cham, pp 561–570. https://doi.org/10.1007/978-3-319-00972-8_50

Álvarez-Gómez, J. A., Aniel-Quiroga, I., González, M., Olabarrieta, M. and Carreño, E. (2011). Scenarios for earthquake-generated tsunamis on a complex tectonic area of diffuse deformation and low velocity: The Alborán Sea, Western Mediterranean. Marine Geology, 284(1-4), 55-73.

Amir, L. and Cisternas, A. (2010). Appraisal of the 1790 Alborán Tsunami source in the west Mediterranean Sea as inferred from numerical modelling: Insights for the tsunami hazard in Algeria. In Proceedings of the 9th US National and 10th Canadian Conference on Earthquake Engineering-Compte rendu de la 9ieme Conference Nationale Americaine et 10ieme conference Canadienne de Genie Parasismique.

Anderson, A.L. and Hampton, L.D. (1974). In situ measurement of sediment acoustic properties during coring. En: Deep-Sea Sediments, Physical and Mechanical Properties, Tomo 2, 497 pp.

Bache, F., Popescu, S. M., Rabineau, M., Gorini, C., Suc, J. P., Clauzon, G., Olivet, J. L., Rubino, J. L., Melinte-Dobrinescu, M. C., Estrada, F., Londeix, L., Armijo, R., Meyer, B., Jolivet, L Jouannic, G., Leroux, E., Aslanian, D., Baztan, J., Dos Reis, A. T., Mocochain, L., Dumurdžanov, N., Zagorchev, I., Lesić, V., Tomić, D., Çağatay, M. N., Brun, J. P., Sokoutis, D., Csato, I., Ucarkus G. and Çakir, Z. (2011). A two-step process for the reflooding of the mediterranean after the messinian salinity crisis. A two-step process for the reflooding of the Mediterranean after the Messinian Salinity Crisis. Basin Research n° 23 pp. 1-29. doi: 10.1111/j.1365-2117.2011.00521.x.

Baker, V.R. (2020). Global Megaflood Paleohydrology. In: Herget, J., Fontana, A. (eds) Palaeohydrology. Geography of the Physical Environment. Springer, Cham. https://doi.org/10.1007/978-3-030-23315-0_1

Belzuz, F. P. (1999). Geología del Margen y Cuenca del Mar de Alborán Durante el Plio-Cuaternario: sedimentación y Tectónica (Doctoral dissertation, Universitat de Barcelona).

Berggren, W. A. and Van Couvering, J. A. 1984, Catastrophes and earth history: Princeton, New Jersey, Princeton University Press, 464 p.

Blanc, P. L. (2002). The opening of the Plio-Quaternary Gibraltar Strait: assessing the size of a cataclysm. Geodinamica acta, 15(5-6), 303-317.

Bourgois, J., Mauffret, A., Ammar, A. and Demnati, A. (1992). Multi-channel seismic data imaging of inversion tectonics of the Alborán Ridge (western Mediterranean Sea). Geo-Marine Letters, v.12, p.117-122.

Bouye, Ch. (1983). Etude des corrélations entre la réponse sismique haute résolution de quelques types de dépots meubles et leurs caracteristiques sédimentologiques. These d'Etat, Univ.Perpignan, 163 pp.

Brown, L.F. and Fisher, W.L. (1980). Seismic stratigraphy interpretation and petroleum exploration. Am. Ass. Petrol. Geol., Contin, Ed., Course Note Ser., 16, 125 pp.

Bryant, E. (2008). The underrated hazard. Springer.

Buforn, E., Udías, A. and Colombás, M.A. (1988). Seismicity, source mechanisms and tectonics of the Azores-Gibraltar plate boundary. Tectonophysics 152 (1-2): 89-118.

Buforn, E., Pro, C., de Galdeano, C. S., Cantavella, J. V., Cesca, S., Caldeira, B., ... and Mattesini, M. (2017). The 2016 south Alborán earthquake (Mw= 6.4): A reactivation of the Ibero-Maghrebian region?. Tectonophysics, 712, 704-715.

Canales-García, I., Urrutia-Fucugauchi, J. and Aguayo-Camargo, E. (2018). Seismic imaging and attribute analysis of Chicxulub crater central sector, Yucatan platform, Gulf of Mexico. Geologica Acta: an international earth science journal, 16(2), 215-235.

Carporzen, L., Gilder, S. A. and Hart, R. J. (2005). Palaeomagnetism of the Vredefort meteorite crater and implications for craters on Mars. Nature, 435(7039), 198-201.

Chalouan, A., Saji, R., Michard, A. and Bally, A.W. (1997). Neogene tectonic evolution of the southwestern Alborán basin as inferred from seismic data off Morocco. AAPG Bulletin-American Association of Petroleum Geologists, v.81, p.1161-1184.

CIESM (2008) The Messinian Salinity Crisis from me–ge–deposits to microbiology: a consensus report. In: Briand F (eds) CIESM workshop monographs, vol 33, Monaco, p 168.

Clauzon, G. (1982). Le canyon messinien du Rhone; une preuve decive du "desiccated deep-basin model" (Hsü, Cita and Ryan, 1973). Bull. Soc. Geol. Fr. 7 (3), 597-610.

Clifton, H. E. (1985). Journal Volume: 17; Conference: 98. annual meeting of the Geological Society of America, Orlando, FL, USA, 28 Oct 1985.

Clifton, H. E. (Ed.). (1988). Sedimentologic consequences of convulsive geologic events (Vol. 229). Geological Society of America.

Collins, G. S. and Wünnemann, K. (2005). How big was the Chesapeake Bay impact? Insight from numerical modeling. Geology, 33(12), 925-928.

Comas, M.C., García-Dueñas, V. and Jurado, M.J. (1992). Neogene tectonic evolution of the Alborán Sea from MCS data. Geo-Mar. Lett., 12, 2, 157-164.

Comas, M.C., Platt, J.P., Soto, J.I. and Watts, A.B. (1999). The origin and tectonic history of the Alborán basin: insights from leg 161 results. Ocean Drill. Progr., 161, 555-580.

Crespo-Blanc, A. (1995). Interference pattern of extensional fault systems: a case study of the Miocene rifting of the Alborán basement (north of Sierra Nevada, Betic chain). J. Struct. Geol., 17, 11, 1559-1569.

d'Acremont, E., Gutscher, M. A., Rabaute, A., de Lépinay, B. M., Lafosse, M., Poort, J., ... and Gorini, C. (2014). High-resolution imagery of active faulting offshore Al Hoceima, Northern Morocco. Tectonophysics, 632, 160-166.

d'Acremont, E., Lafuerza, S., Rabaute, A., Lafosse, M., Castelot, M. J., Gorini, C., Alonso, B., Ercilla, G., Vazquez, J. T., Vandorpe, T., Juan, C., Migeon, S., Ceramicola, S., Lopez-González, N., Rodríguez, M., El Moumni, B., Benmarha, O. and Ammar, A. (2022). Distribution and origin of submarine landslides in the active margin of the southern Alborán Sea (Western Mediterranean Sea). Marine Geology, 106739.

De Larouzière, F. D., Bolze, J., Bordet, P., Hernandez, J., Montenat, C. and d'Estevou, P. O. (1988). The Betic segment of the lithospheric Trans-Alborán shear zone during the Late Miocene. Tectonophysics, 152(1-2), 41-52.

De Mets, C., Laffaldano, G. and Merkouriev, S. (2015). High-resolution Neogene and quaternary estimates of Nubia-Eurasia-North America plate motion. Geophysical Journal International 203 (1):416-427.

Dimova L., Raykova R., Pagnoni G., Armigliato A. and Tinti S. (2021). Modelling a Composite Tsunami Scenario for Karpathos Island (Aegean Sea). In: Dobrinkova N., Gadzhev G. (eds) Environmental Protection and Disaster Risks. EnviroRISK 2020. Studies in Systems, Decision and Control, vol 361. Springer, Cham. https://doi.org/10.1007/978-3-030-70190-1_19.

Do Couto, D. (2014). Evolution géodynamique de la Mer d'Alborán par l'étude des bassins sédimentaires (Doctoral dissertation, Paris 6).

Do Couto, D., Gorini, C., Jolivet, L., Lebret, N., Augier, R., Gumiaux, C., ... and Auxietre, J. L. (2016). Tectonic and stratigraphic evolution of the Western Alborán Sea Basin in the last 25 Myrs. Tectonophysics, 677, 280-311.

Duggen, S., Hoernle, K., van den Bogaard, P. and Harris, C. (2004). Magmatic evolution of the Alborán region: The role of subduction in forming the western Mediterranean and causing the Messinian salinity crisis. Earth Planet. Sci. Lett., 218, 91-108.

Dypvik, H., Gudlaugsson, S. T., Tsikalas, F., Attrep Jr, M., Ferrell Jr, R. E., Krinsley, D. H., ... and Nagy, J. (1996). Mjølnir structure: An impact crater in the Barents Sea. Geology, 24(9), 779-782.

Ercilla, G., Alonso, B. and Baraza, J. (1992). Sedimentary evolution of the northwestern Alborán Sea during the Quaternary. Geo-Marine Letters, 12(2-3), 144-149.

Ercilla, G., Juan, C., Hernandez-Molina, F. J., Bruno, M., Estrada, F., Alonso, B., ... and Ammar, A. (2016). Significance of bottom currents in deep-sea morphodynamics: an example from the Alborán Sea. Marine Geology, 378, 157-170.

Ercilla, G., Casas, D., Alonso, B., Casalbore, D., Galindo-Zaldívar, J., García-Gil, S., ... and Yenes, M. (2021). Offshore geological hazards: charting the course of progress and future directions. In Oceans (Vol. 2, No. 2, pp. 393-428). Multidisciplinary Digital Publishing Institute.

Estrada, F., Ercilla, G., and Alonso, B. (1997). Pliocene-Quaternary tectonic-sedimentary evolution of the NE Alborán Sea (SW Mediterranean Sea). Tectonophysics, 282(1-4), 423-442.

Faccenna, C., Piromallo, C., Crespo-Blanc, A., Jolivet, L., and Rossetti, F. (2004). Lateral slab deformation and the origin of the western Mediterranean arcs. Tectonics, 23(1).

Flecker, R., de Villiers, S., Ellam, R.M., (2002). Modelling the effect of evaporation on the salinity –$^{87}Sr/^{86}Sr$ relationship in modern and ancient marginal–marine systems: the Mediterranean Messinian Salinity Crisis. Earth Planet. Sci. Lett. 203 (1), 221–233.

Flecker, R., Hernández-Molina, J., Estrada, F. and Ercilla, G (2020). Safety Review Report for IMMAGE 895-ADP Investigating Miocene Mediterranean-Atlantic Gateway Exchange.

Galdeano, A., Andreoli, M. A. G., and Hart, R. J. (2008). Magnetic imaging of the Vredefort Dome: Implications for the size and geometry of the Vredefort Crater. Large Meteorite Impacts and Planetary Evolution IV, 1423, 3051.

Galindo-Zaldivar, J., Gil, A.J., Sanz de Galdeano, C., Lacy, M.C., García-Armenteros, J.A., Ruano, P., Ruiz, A.M., Martínez-Martos, M. y Alfaro, P. (2015). Active shallow extension in central and eastern Betic Cordillera from CGPS data. Tectonophysics 663:290-301.

Galindo-Zaldívar, J., Ercilla, G., Estrada, F., Catalán, M., d'Acremont, E., Azzouz, O., Casas, D., Chourak, M., Vázquez, J.T., Chalouan, A., Sanz de Galdeano, C., Benmakhlouf, M., Gorini, C., Alonso, B., Palomino, D., Rengel, J.A. y Gil, A.J. (2018). Imaging the Growth of Recent Faults: The Case of 2016-2017 Seismic Sequence Sea Bottom Deformation in the Alborán Sea (Western Mediterranean). Tectonics 37 (8):2513-2530.

Galindo-Zaldívar, J., Gil, A.J., Tendero, V., Borque, M.J., Ercilla, G., González-Castillo, L., Sánchez-Alzola, A., Lacy, M.C., Estrada, F., Avilés, M., Alfaro, P., Madarieta-Txurruka, A., Chacón, F. (2022). The Campo de Dalias GNSS network unveils the interaction between roll-back and indentation tectonics in the Gibraltar Arc. Sensors, 22, 2128. https://doi.org/10.3390/s22062128.

García-Castellanos, D., and Villaseñor, A. (2011). Messinian salinity crisis regulated by competing tectonics and erosion at the Gibraltar arc. Nature, 480(7377), 359-363.

Gibert, L., Scott, G. R., Montoya, P., Ruiz-Sánchez, F. J., Morales, J., Luque, L., ... and Lería, M. (2013). Evidence for an African-Iberian mammal dispersal during the pre-evaporitic Messinian. Geology, 41(6), 691-694.

Goldfinger, C., Nelson, C. H., Morey, A. E., Johnson, J. E., Patton, J. R., Karabanov, E. B., ... and Vallier, T. (2012). Turbidite event history—Methods and implications for Holocene paleoseismicity of the Cascadia subduction zone (No. 1661-F). US Geological Survey.

González, M., Medina, R., Olabarrieta, M. and Otero, L. (2010). Tsunami hazard assessment on the Southern Coast of Spain. Turkish Journal of Earth Sciences, 19(3), 351-366.

González-Castillo, L., Galindo-Zaldivar, J., de Lacy, M., Borque, M., Martinez-Moreno, F., García-Armenteros, J. and Gil, A. (2015). Active rollback in the Gibraltar Arc: Evidences from CGPS data in the western Betic Cordillera. Tectonophysics, 663, 310–321. https://doi.org/10.1016/j.tecto.2015.03.010.

Gràcia, E., Bartolome, R., Lo Iacono, C., Moreno, X., Stich, D., Martínez-Diaz, J. J., Bozzano, G., Martínez-Loriente, S., Perea, H., Diez, S., Masana, E., Dañobeitia, J. J., Tello, O., Sanz, J. L., Carreño, E. and EVENT-SHELF Team (2012). Acoustic and seismic imaging of the Adra Fault (NE Alborán Sea): in search of the source of the 1910 Adra earthquake, Nat. Hazards Earth Syst. Sci., 12, 3255–3267, https://doi.org/10.5194/nhess-12-3255-2012, 2012.

Gràcia, E., Grevemeyer, I., Bartolomé, R., Perea, H., Martínez-Loriente, S., Gómez De La Peña, L., ... and Ranero, C. R. (2019). Earthquake crisis unveils the growth of an incipient continental fault system. Nature communications, 10(1), 1-12.

Grevemeyer, I., Gràcia, E., Villaseñor, A., Leuchters, W. and Watts, A. B. (2015). Seismicity and active tectonics in the Alborán Sea, Western Mediterranean: Constraints from an offshore-onshore seismological network and swath bathymetry data. Journal of Geophysical Research: Solid Earth, 120(12), 8348-8365.

Gulick, S. P. S., Christeson, G. L., Barton, P. J., Grieve, R. A. F., Morgan, J. V. and Urrutia-Fucugauchi, J. (2013). Geophysical characterization of the Chicxulub impact crater. Reviews of Geophysics, 51(1), 31-52.

Gupta, S., Collier, J. S., Palmer-Felgate, A. and Potter, G. (2007). Catastrophic flooding origin of shelf valley systems in the English Channel. Nature, 448(7151), 342-345.

Gutscher, M.A., Malod, J., Réhault, J.P., Contrucci, I., Klingelhoefer, F., Mendes-Victor, L. and Spakman, W. (2002). Evidence for active subduction beneath Gibraltar. Geology 30: 1071-1074.

Gutscher, M. A., Dominguez, S., Westbrook, G. K., Le Roy, P., Rosas, F., Duarte, J. C., et al. (2012). The Gibraltar subduction: A decade of new geophysical data. Tectonophysics, 574–575, 72–91. https://doi.org/10.1016/j.tecto.2012.08.038.

Haq, B., Gorini, C., Baur, J., Moneron, J. and Rubino, J. L. (2020). Deep Mediterranean's Messinian evaporite giant: How much salt?. Global and Planetary Change, 184, 103052.

Harmouzi, H., Nefeslioglu, H. A., Rouai, M., Sezer, E. A., Dekayir, A. and Gokceoglu, C. (2019). Landslide susceptibility mapping of the Mediterranean coastal zone of Morocco between Oued Laou and El Jebha using artificial neural networks (ANN). Arabian Journal of Geosciences, 12(22), 1-18.

Herget, J., Agatova, A. R., Carling, P. A. and Nepop, R. K. (2020). Altai megafloods—The temporal context. Earth-Science Reviews, 200, 102995.

Hsu, K. J. (1972). Origin of saline giants: a critical review after the discovery of the Mediterranean evaporite. Earth-Science Reviews, 8(4), 371-396.

Hsü, K.J., Ryan, W.B.F. and Cita, M.B. (1973). Late Miocene desiccation of the Mediterranean. Nature 242 (5395), 240–244.

Hsü, K.J. (1983): Actualistic Catastrophism. Adress of the retiring President of the International Association of Sedimentologisl. Sedimentology, 30 (1), 3-9.

Jolivet, L., Augier, R., Robin, C., Suc, J.P. and Rouchy, J.M. (2006). Lithospheric-scale geodynamic context of the Messinian salinity crisis. Sedim. Geol., 188-189, 9-33.

Juan, C., Ercilla, G., Hernández-Molina, F. J., Estrada, F., Alonso, B., Casas, D., ... and Ammar, A. (2016). Seismic evidence of current-controlled sedimentation in the Alborán Sea during the Pliocene and Quaternary: Palaeoceanographic implications. Marine Geology, 378, 292-311.

Juan, C., Ercilla, G., Estrada, F., Alonso, B., Casas, D., Vázquez, J. T., ... and Valencia, J. (2020). Multiple factors controlling the deep marine sedimentation of the Alborán Sea (SW Mediterranean) after the Zanclean Atlantic Mega-flood. Marine Geology, 423, 106138.

Jurado, M. J. and Comas, M. C. (1992). Well log interpretation and seismic character of the Cenozoic sequence in the northern Alboran Sea. Geo-Marine Letters, 12(2), 129-136.

Krijgsman, W., Capella, W., Simon, D., Hilgen, F. J., Kouwenhoven, T. J., Meijer, P. T., ... and Flecker, R. (2018). The Gibraltar corridor: Watergate of the Messinian salinity crisis. Marine Geology, 403, 238-246.

Latter, J. H. (1981). Tsunamis of volcanic origin: summary of causes, with particular reference to Krakatoa, 1883. Bulletin volcanologique, 44(3), 467-490.

Legg, S., Briegleb, B., Chang, Y., Chassignet, E. P., Danabasoglu, G., Ezer, T., ... and Yang, J. (2009). Improving oceanic overflow representation in climate models: the gravity current entrainment climate process team. Bulletin of the American Meteorological Society, 90(5), 657-670.

Leenhardt, O. (1972). Le Sondage Sismique Continui. Mass et Cie (Ed.), 164 pp.

Lis Mancilla, F. D., Stich, D., Berrocoso, M., Martín, R., Morales, J., Fernandez-Ros, A., et al. (2013). Delamination in the Betic Range: Deep structure, seismicity, and GPS motion. Geology, 41(3), 307–310.

Lofi, J. (2018). Seismic Atlas of the Messinian Salinity Crisis markers in the Mediterranean Sea-Volume 2 (Vol. 181, pp. 1-72). Société Géologique de France.

Loget, N. and Van Den Driessche, J. (2006). On the origin of the Strait of Gibraltar. Sedimentary Geology, 188, 341-356.

Macías, J., Fernández-Salas, L. M., González-Vida, J. M., Vázquez, J. T., Castro, M. J., Bárcenas, P., ... and Parés, C. M. (2013). Deslizamientos submarinos y tsunamis en el Mar de Alborán. Un ejemplo de modelización numérica. Instituto Español de Oceanografía, temas de Oceanografía 7.

Macías, J., Vázquez, J. T., Fernández-Salas, L. M., González-Vida, J. M., Bárcenas, P., Castro, M. J., ... and Alonso, B. (2015). The Al-Borani submarine landslide and associated tsunami. A modelling approach. Marine Geology, 361, 79-95.

Mader, C. L. (2001). Modeling the 1755 Lisbon tsunami. Science of Tsunami Hazards, 19(2), 93-98.

Maleika, W., Koziarski, M. and Forczmański, P. (2018). A multiresolution grid structure applied to seafloor shape modeling. ISPRS International Journal of Geo-Information, 7(3), 119.

Martínez del Olmo, W. and Comas, M. C. (2008). Arquitectura sísmica, olistostromas y fallas extensionales en el norte de la cuenca oeste del Mar de Alborán. Revista de la Sociedad Geológica de España, 21(3-4), 151-167.

Martínez-García, P., Soto, J. I. and Comas, M. (2011). Recent structures in the Alborán Ridge and Yusuf fault zones based on swath bathymetry and sub-bottom profiling: evidence of active tectonics. Geo-Marine Letters, 31(1), 19-36.

Martínez-García, P., Comas, M., Soto, I., J., Lonergan, L. and Watts, B. A. (2013). Strike-slip tectonics and basin inversion in the Western Mediterranean: the Post-Messinian evolution of the Alborán Sea. Basin Research, v.25, p.361-387.

Masaitis, V. L. (2006). Review of the Barringer crater studies and views on the crater's origin. Solar System Research, 40(6), 500-512.

Mascle, G. and Mascle, J. (2019). The Messinian salinity legacy: 50 years later. Mediterranean Geoscience Reviews, 1(1), 5-15.

Mateos, R. M., Azañón, J. M., Roldán, F. J., Notti, D., Pérez-Peña, V., Galve, J. P., ... and Fernández-Chacón, F. (2017). The combined use of PSInSAR and UAV photogrammetry techniques for the analysis of the kinematics of a coastal landslide affecting an urban area (SE Spain). Landslides, 14(2), 743-754.

Mauffret, A., Maldonado, A. and Campillo, A.C. (1992). Tectonic framework of the eastern Alborán and western Algerian basins, western Mediterranean. Geo-Mar. Lett., 12, 2, 104-110.

Mauffret, A., Ammar, A., Gorini, C. and Jabour, N. (2007). The Alborán Sea (Western Mediterranean) revisited with a view from the Moroccan Margin. Terra Nova, v.19, p.195-203.

McCoy, F. W. and Heiken, G. (2000). Tsunami generated by the Late Bronze age eruption of Thera (Santorini), Greece. Pure and Applied Geophysics, 157(6), 1227-1256.

Miall, A.D. (2016). Stratigraphy: A Modern Synthesis. Springer Cham. 433 pp.

Miller, D. J. (1960) Giant waves in Lituya Bay, Alaska. United States Geological Survey Professional Paper 354-C, pp. 51–86.

Mitchum, R.M. and Vail, P.R. (1977). Seismic stratigraphy and global changes of sea level, par! 7: seismic stratigrapby interpretation. En: Payton C.E., (Ed.), Seismic Startigrapby Applications to Hydrocarbon Exploration, Am. Ass. Petrol. Oeol." Memoir, 26: 135-163.

Mitchum, R.M., Vail, P.R. and Thompson, S. (1977). Seismic stratigraphy and global changes of sea level, part 2: the depositional sequence as a basic unit for stratigraphic analysis. In: Seismic Stratigraphy - Applications to Hydrocarbon Exploration. In: Payton, C.E., (Ed.), Am. Ass. Petrol. Geol., Memoir 26: 53-62.

Ng, Z. L., Hernández-Molina, F. J., Duarte, D., Sierro, F. J., Ledesma, S., Rogerson, M., ... and Manar, M. (2021). Latest Miocene restriction of the Mediterranean Outflow Water: a perspective from the Gulf of Cádiz. Geo-Marine Letters, 41(2), 1-17. https://doi.org/10.1007/s00367-021-00693-9.

O'connor, J. E., Baker, V. R., Waitt, R. B., Smith, L. N., Cannon, C. M., George, D. L. and Denlinger, R. P. (2020). The Missoula and Bonneville floods—A review of ice-age megafloods in the Columbia River basin. Earth-Science Reviews, 208, 103181.

Ormö, J. and Oms, O. (2013). La formación de cráteres de impacto. Un proceso fundamental en el Sistema Solar. Enseñanza de las Ciencias de la Tierra, 21(3), 310-310.

Osinski, G. R., Bunch, T. E., Flemming, R. L., Buitenhuis, E. and Wittke, J. H. (2015). Impact melt-and projectile-bearing ejecta at Barringer Crater, Arizona. Earth and Planetary Science Letters, 432, 283-292.

Papadopoulos, G. A., Gràcia, E., Urgeles, R., Sallares, V., De Martini, P. M., Pantosti, D., ... and Papageorgiou, A. (2014). Historical and pre-historical tsunamis in the Mediterranean and its connected seas: Geological signatures, generation mechanisms and coastal impacts. Marine Geology, 354, 81-109.

Pedrera, A., Ruiz-Constán, A., Galindo-Zaldívar, J., Chalouan, A., Sanz de Galdeano, C., Marín-Lechado, C., … and González-Castillo, L. (2011). Is there an active subduction beneath the Gibraltar orogenic arc? Constraints from Pliocene to present-day stress field. Journal of Geodynamics, 52(2), 83–96. https://doi.org/10.1016/j.jog.2010.12.003.

Pedrinaci, E. (1992). Catastrofismo versus actualismo. Implicaciones didácticas. Enseñanza de las ciencias: revista de investigación y experiencias didácticas, 216-222.

Pérez-Asensio, J. N., Aguirre, J., Schmiedl, G. and Civis, J. (2012). Impact of restriction of the Atlantic-Mediterranean gateway on the Mediterranean Outflow Water and eastern Atlantic circulation during the Messinian. Paleoceanography, 27(3).

Pérez-Belzuz, F., Alonso, B. and Ercilla G. (1997). History of mud diapirism and trigger mechanisms in the Western Alborán Sea. Tectonophysics, v.282, p.399-422.

Pérez-Torrado, F. J., Paris, R., Cabrera, M. C., Schneider, J. L., Wassmer, P., Carracedo, J. C., ... and Santana, F. (2006). Tsunami deposits related to flank collapse in oceanic volcanoes: The Agaete Valley evidence, Gran Canaria, Canary Islands. Marine Geology, 227(1-2), 135-149.

Perouse, E., Vernant, P., Chery, J., Reilinger, R. and McClusky, S. (2010). Active surface deformation and sublithospheric processes in the western Mediterranean constrained by numerical models. Geology, v.38(9), p.823-826.

Piper, D.J.W., Cochonat, P. and Morrison, M. L. (1999). The sequence of events around the epicentre of the 1929 Grand Banks earthquake: initiation of debris flows and turbidity current inferred from sidescan sonar. Sedimentology 46, 79–97.

Range, M. M., Arbic, B. K., Johnson, B. C., Moore Jr, T. C., Adcroft, A., Ansong, J. K., ... and Scotese, C. (2018). The Chicxulub Impact Produced a Powerful Global Tsunami. In AGU Fall Meeting Abstracts (Vol. 2018, pp. PP53B-07).

Ratzov, G., Cattaneo, A., Babonneau, N., Déverchère, J., Yelles, K., Bracene, R. and Courboulex, F. (2015). Holocene turbidites record earthquake supercycles at a slow-rate plate boundary. Geology, 43(4), 331-334.

Reicherter, K. and Hübscher, C. (2007). Evidence for a seafloor rupture of the Carboneras Fault Zone (southern Spain): Relation to the 1522 Almería earthquake?. Journal of Seismology, 11(1), 15-26.

Reicherter, K. and Becker-Heidmann, P. (2008). Tsunamites in lagunas: remains of the 1522 Almería earthquake (western Mediterranean). In 2nd International Tsunami Field Symposium IGCP Project (Vol. 495, pp. 127-129).

Rodríguez, M., Maleuvre, C., Jollivet-Castelot, M., d'Acremont, E., Rabaute, A., Lafosse, M., ... and Gorini, C. (2017). Tsunamigenic submarine landslides along the Xauen–Tofiño banks in the Alborán Sea (Western Mediterranean Sea). Geophysical Journal International, 209(1), 266-281.

Rogerson, M., Rohling, E. J., Bigg, G. R. and Ramirez, J. (2012). Paleoceanography of the Atlantic-Mediterranean exchange: overview and first quantitative assessment of climatic forcing. Reviews of Geophysics, 50(2).

Roig-Munar, F. X., Martín-Prieto, J. Á., Rodríguez-Perea, A., Gelabert, B. and Manuel, J. (2020). Revisión de los depósitos de tsunamis, bloques y tsunamitas, en las costas del mediterráneo occidental. Revista de la Sociedad Geológica de España, 33, 2.

Roveri, M., Flecker, R., Krijgsman, W., Lofi, J., Lugli, S., Manzi, V. ... and Stoica, M. (2014). The Messinian Salinity Crisis: past and future of a great challenge for marine sciences. Marine Geology, 352, 25-58.

Roveri, M., Manzi, V., Bergamasco, A., Falcieri, F.M., Gennari, R., Lugli, S. and Schreiber, B.C. (2014). Dense shelf water cascading and Messinian canyons: a new scenario for the Mediterranean salinity crisis. Am. J. Sci. 314 (3), 751-784.

Ruiz-Constán, A., Galindo-Zaldívar, J., Pedrera, A., Celerier, B. and Marín-Lechado, C. (2011). Stress distribution at the transition from subduction to continental collision (northwestern and central Betic Cordillera). Geochemistry, Geophysics, Geosystems, 12(12).

Ryan, W. B. (1978). Messinian badlands on the southeastern margin of the Mediterranean Sea. Marine Geology, 27(3-4), 349-363.

Ryan, W. B., Pitman, W. C., Sotiropoulos, A. and Haxby, W. F. (1999). El diluvio universal: nuevos descubrimientos científicos de un acontecimiento que cambió la historia. Editorial Debate.

Sassa, S., Grilli, S. T., Tappin, D. R., Sassa, K., Karnawati, D., Gusiakov, V. K. and Løvholt, F. (2022). Understanding and reducing the disaster risk of landslide-induced tsunamis: a short summary of the panel discussion in the World Tsunami Awareness Day Special Event of the Fifth World Landslide Forum. Landslides, 19(2), 533-535.

Satake, K., Smith, J. R. and Shinozaki, K. (2002). Three-dimensional reconstruction and tsunami model of the Nuuanu and Wailau giant landslides, Hawaii. GEOPHYSICAL MONOGRAPH-AMERICAN GEOPHYSICAL UNION, 128, 333-346.

Sautkin, A., Talukder, A.R., Comas, M.C., Soto, J.I. and Alekseev, A. (2003). Mud volcanoes in the Alborán Sea: evidence from micropaleontological and geophysical data. Marine Geology, v.195, p.237-261.

Seber, D., Barazangi, M., Ibenbrahim, A. and Demnati, A. (1996). Geophysical evidence for lithospheric delamination beneath the Alboran Sea and Rif–Betic mountains. Nature, 379(6568), 785–790.

Selli, R. (1954). Il Bacino dei Metauro. Giorn. Geol, 24(2).

Shopov, Y., Tsankov, L., Georgiev, L. N., Damyanova, A., Damyanov, Y., Marinova, E., ... and Krouse, H. P. R. (1996). Speleothem luminescence proxy records of annual rainfall in the past. Evidences for "The Deluge" in Speleothems. In Extended abstracts of Int. Conference on "Climatic Change-the Karst Record (pp. 1-4).

Somoza, L., Medialdea, T., León, R., Ercilla, G., Tomás Vázquez, J., Farran, M., Hernández-Molina, J., González, J., Juan, C. and Fernández-Puga, M.C. (2012). Structure of mud volcano systems and pockmarks in the region of the Ceuta Contourite Depositional System (Western Alborán Sea). Marine Geology, v.332-334, p.4-26.

Soto, J.I., Fernández-Ibáñez, F., Talukder, A.R. and Martínez-García, P. (2010). Miocene shale tectonics in the Alborán Sea (western Mediterranean). In: Wood, L., (Ed), Shale tectonics. AAPG Memoir 93, p.119-144.

Spakman, W., Chertova, M. V., van den Berg, A. and van Hinsbergen, D. J. J. (2018). Puzzling features of western Mediterranean tectonics explained by slab dragging. Nature Geoscience, 11(3), 211–216. https://doi.org/10.1038/s41561-018-0066-z.

Stewart, S. A. and Allen, P. J. (2005). 3D seismic reflection mapping of the Silverpit multi-ringed crater, North Sea. Geological Society of America Bulletin, 117(3-4), 354-368.

Swingedouw, D., Colin, C., Eynaud, F., Ayache, M. and Zaragosi, S. (2019). Impact of freshwater release in the Mediterranean Sea on the North Atlantic climate. Climate Dynamics, 53(7), 3893-3915.

Vail, P.M., Mitebum, R.M.Jr. and Tbompson, S. (1977). Seismic stratigraphy and global ehanges of sea level, part 4: global eycles of relative changes of sea level. En: Seismie Stratigraphy-Aplieations to Hydrocarbon Exploration. Am. Ass. Pe/ro/. Ceo/., Memoir, 26: 63-8 1.

Vázquez, J. T., Bárcenas, P., Palomino, D., Alonso, B., Ercilla, G., Díaz Del Río, V., ... and Sayago-Gil, M. (2010). Sedimentary instabilities along the southwestern slope of the

Alborán ridge (SW Mediterranean). Rapports Commission Internationale pour l'Exploration Scientifique de la Mer Méditerranée, 39, 76.

Vázquez, J. T., Gascón, P. B., Macías, J., Salas, L. M. F., del Rio, V. D., González, J. M. and Castro, M. J. (2012). Tsunamis generados por deslizamientos submarinos en el Mar de Alborán: Simulación de un posible tsunami a partir del sistema de movimientos en masa Al-Borani. Geotemas (Madrid), (13), 1761-1764.

Vera Torres, J. A. (1994). Estratigrafía: principios y métodos. Madrid: Editorial Rueda.

Vissers, R.L.M., Platt, J.P. and van der Wal, D. (1995). Late orogenic extension of the Betic Cordillera and the Alborán Domain: A lithospheric view. Tectonics, v.14, p.786-803.

Voelker, A. H., Lebreiro, S. M., Schönfeld, J., Cacho, I., Erlenkeuser, H. and Abrantes, F. (2006). Mediterranean outflow strengthening during northern hemisphere coolings: a salt source for the glacial Atlantic?. Earth and Planetary Science Letters, 245(1-2), 39-55.

Waitt, R. B., Atwater, B. F., Lehnigk, K., Larsen, I. J., Bjornstad, B. N., Hanson, M. A. and O'Connor, J. E. (2021). Upper Grand Coulee: New views of a channeled scabland megafloods enigma.

Watts, A.B., Platt, J.P. and Buhl, P. 1993. Tectonic evolution of the Alborán Sea basin. Basin Res., 5, 153-177.

Weijermars, R., Roep, T.B., Van den Eeckhout, B., Postma, G. and Kleverlaan, K. (1985). Uplift history of a Betic fold nappe inferred from Neogene-Quaternary sedimentation and tectonics (in the Sierra Alhamilla and Almeria, Sorbas and Tabernas Basins of the Betic Cordilleras, SE Spain). Geologie en Mijnbouw, v.64, p.397-411.